LRFD CALIBRATION OF BRIDGE FOUNDATIONS SUBJECTED TO SCOUR AND RISK ANALYSIS

A Dissertation

by

CONGPU YAO

Submitted to the Office of Graduate Studies of
Texas A&M University
in partial fulfillment of the requirements for the degree of

DOCTOR OF PHILOSOPHY

Approved by:

Chair of Committee,	Jean-Louis Briaud
Committee Members,	Paolo Gardoni
	Stefan Hurlebaus
	Mark E. Everett
Head of Department,	John Niedzwecki

May 2013

Major Subject: Civil Engineering

ABSTRACT

Bridge scour is the loss of soil by erosion due to water flowing around bridge supports. Scour has been the number one cause of bridge collapse in the United States with an average rate of 22 bridges collapsing each year. This dissertation addresses three topics related to bridge scour. First, three sets of databases are used to quantify the statistical parameters associated with the scatter between the predicted and measured scour depth as well as the probability that a deterministically predicted scour depth will be exceeded. The analysis results from these databases will also be used to provide the bias factors in the scour depth predictions in practice. In the second part of the dissertation, these statistical parameters are used to develop a reliability-based Load and Resistance Factor Design (LRFD) for shallow and deep foundations subjected to scour. The goal is to provide a design procedure for the bridge foundations, where the reliability of the foundation is the same with or without scour. For shallow foundations, the key of the design issue is the location of the foundation depth and the probability that the scour depth will exceed the foundation depth. Therefore, for shallow foundations, the proposed LRFD calibration is based on the probability of exceedance of the predicted scour depth. However for deep foundations, the key of the design issue is the resistance factor associated with the axial capacity of a pile. Hence, the proposed LRFD calibration for deep foundations is based on a reliability analysis using First-Order Reliability Method (FORM). The dissertation is broadened in the third part by analyzing

the risk associated with bridge scour, where the risk is defined as the probability of failure times the value of the consequences. In the third part, the risk associated with bridge scour is compared to risks associated with other engineering structures as well. Target values of acceptable risk are recommended as part of the conclusions.

The outcome of the research will modify the current "AASHTO LRFD Bridge Design Specifications" developed by the American Association of State Highway and Transportation Officials (AASHTO) and help the practitioners design foundations of bridges over rivers for a uniform probability of failure in the case of scour. The risk of bridge scour is also quantified in the dissertation, and compared with common societal risks and civil engineering risks. It will help engineers understand the risk level associated with bridge scour.

DEDICATION

To my parents for bringing me into this beautiful world and teaching me the wisdom of life

ACKNOWLEDGEMENTS

I would like to express my heartfelt gratitude to my academic advisor and Committee Chair, Dr. Jean-Louis Briaud. It has been a true blessing to be able to study under Dr. Briaud's supervision. Not only did I receive financial support through the whole PhD study from him, but also I learned from him an active and humorous attitude towards life, a hard-working spirit, and dedication in physical exercise. Dr. Briaud is always available to students whenever we need his advice. He has helped me go through a lot of difficult times in the research. Without his guidance, support and encouragement, this dissertation would not have been accomplished. I would like to thank him heartfully.

I also would like to thank Dr. Paolo Gardoni for his dedication and valuable guidance during my research. He is such a quick, smart and knowledgeable professor that he could always figure out what I was trying to express during our weekly conference call. His knowledge in reliability field really inspired me. It has been my privilege to be able to work with him on this research topic, and I really appreciate his help.

Great appreciation also goes to my other two committee members, Dr. Stefan Hurlebaus and Dr. Mark E. Everett, for serving on my committee. I really appreciate their advice and help during the preparation of this dissertation draft.

I owe a lot of thanks to Dr. Vahid Bisadi, who provided me with great advice and help on understanding reliability theory. His kindness and helpful advice is very much appreciated.

I would like to thank Winchell Auyeung and Michael Sullivan from New York State Department of Transportation (NYSDOT) for providing the NYSDOT Database. The database was used in Section 6 of the dissertation to quantify the bridge scour risk. Mr. Auyeung's great help and patience with my detailed questions regarding the items in the database is very much appreciated.

I also appreciate colleague-and-friend Negin Yousefpour's help on studying the Florida Department of Transportation (FDOT) Unknown Foundation Bridges Database. It has been a pleasant experience to share the same office with her for two years.

I owe thanks to Dr. Seung Jae Oh for providing the Bridge Pier Scour Database, which involves the deterministic pier scour depth predictions of more than 500 data points.

I would also like to acknowledge Dr. Andrzej Nowak at the University of Nebraska-Lincoln for the conference call with me discussing the Load and Resistance Factor Design (LRFD) in Structural Engineering field.

I would also like to thank all the professors and staff in our department for their help and assistance during my PhD study. Special thanks go to Ms. Theresa Taeger for her great help on printing the dissertation draft and on taking care of the paperwork for me while I was not around. I would also like to thank Ms. Maxine Williams for her great assistance and help during my PhD study. I would like to acknowledge our laboratory manager Mr. Mike Linger for his great help and encouragement during my PhD study. It has been a great experience to be able to work with him in the laboratory for two years.

Great appreciation goes to Mr. Mike Downey at Texas A&M University for proofreading the whole dissertation.

I also would like to thank the support and encouragement from all my friends. It is their consistent encouragement that helped me go through the whole PhD study. Great thanks go to Dr. Yi Dong, Dr. Qian Li and Dr. Xi Cui for their enormous support, understanding and precious long-term friendship. Particularly I would like to acknowledge their help and advice on the format of the dissertation in the draft preparation process. Thanks go to Dr. Chin Leung, Dr. Deeyvid Saez, Ghassan Akrouch, Xin Guo and Yunhuang Zhang for being true friends in need for the last five years. I would like also to acknowledge my friends-and-co-workers Colin Darby and Dr. Hrishikesh Sharma for bringing me pleasant research experience. I would also like to acknowledge Stacey Tucker, Dr. Xingnian Chen, Amir Hessami, Ryan Dalton, Vishal Dantal, and Ajay Shastri for their support and help.

I would like to thank my brother Dr. Conglun Yao and sister-in-law Ms. Duoduo Liu for their support and love. Special thanks go to my brother for growing up with me and sharing his personal opinion on the PhD and work with me.

Finally, I would like to show my great gratitude to my dear parents, Mr. Zengmin Yao and Ms. Rongxiang Jing, for their constant love and unconditional support. Without their encouragement and love, this dissertation would not have been finished. I would like to thank both of them for teaching me the wisdom of life and providing me the courage to face difficult times in life. This dissertation is dedicated to my parents.

TABLE OF CONTENTS

Page

LIST OF FIGURES

Page

LIST OF TABLES

Page

1 INTRODUCTION

1.1 PROBLEM STATEMENT

1.1.1 Scour

Bridge scour is the erosion of soil around the bridge foundations due to flowing water. It usually happens in sands or cohesive soils. The following information is paraphrased according to the study performed by Briaud (2006). "According to the Federal Highway Administration (FHWA), there are approximately 600,000 bridges in the states, 500,000 of which are over water. The States Department of Transportation (DOT) has evaluated nearly all their bridges for scour over the last 15 years. The evaluation shows that 25,000 out of 500,000 bridges are defined as scour critical bridges (5%). In addition to these 25,000 scour-critical bridges, 100,000 bridges have unknown foundations." (Briaud 2006, p. 3). It means it is hard to predict the performance of those 100,000 bridges with unknown foundations in the case of scour.

The following information is paraphrased from the presentation provided by Sullivan (2005b).

"A scour critical bridge is defined to be one with an abutment or pier foundation which is unstable due to observed, calculated, or assessed scour.

FHWA defines different levels of scour critical bridges:

'3'— bridge is scour critical; the bridge foundations are determined to be unstable due to assessed or calculated scour conditions;

‘2’— bridge is scour critical; field review indicates that excessive scour has occurred under bridge foundations;

‘1’— bridge is scour critical; field review indicates that the failure of piers or abutments is imminent; bridge is closed to traffic;

‘0’— bridge is scour critical; bridge has already failed and is closed to traffic;

‘7’— countermeasures have been adopted to mitigate any existing scour problem and to reduce the risk of failure during a flood event;

‘U’—bridge with ‘unknown’ foundations that has not been evaluated for scour.”

1.1.2 Schoharie Creek Bridge Failure Study

1.1.2.1 Bridge Information

On April 5, 1987, the Schoharie Creek Bridge fell. Ten people died in this event. The bridge was built over the Schoharie Creek in Montgomery Country near Amsterdam, New York. It was an east-west direction with a four-lane highway. The design speed limit was set to be 90 km/h. The bridge was 165 m long with four lanes. The section of piers is shown in Figure 1-1. The plan of the bridge is shown in Figure 1-2.

The bridge was opened to the public in 1954. During its lifetime, there were more than twenty floods in history (Resource Consultants, Inc. and Colorado State University 1987). The floods in 1955 and 1987 were the biggest ones in near history (Govindasamy 2009).

After the event, many sources did studies of the cause of the bridge failure on the behalf of the National Transportation Safety Board (NTSB). This section is about the summary of the investigation based on the literature (Resource Consultants, Inc. and

Colorado State University 1987; Wiss, Janney, Elstner Associates, Inc. and Mueser Rutledge Consulting Engineers 1987; National Transportation Safety Board 1987).

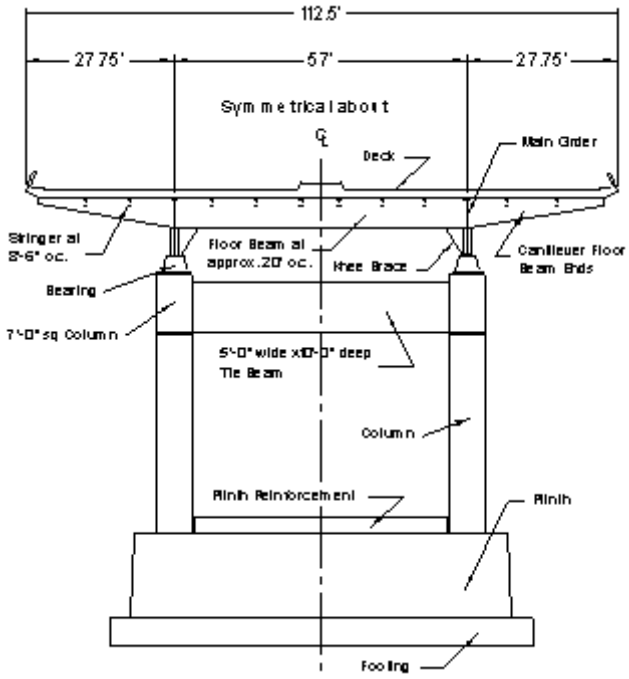

Figure 1-1. Pier Section of Schoharie Creek Bridge (National Transportation Safety Board 1987).

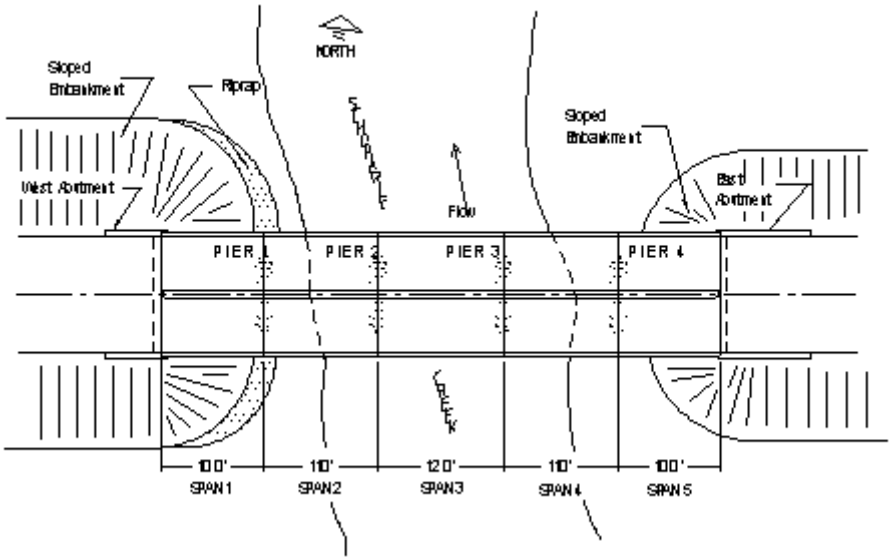

Figure 1-2. Schematic Plan of Bridge (National Transportation Safety Board 1987).

1.1.2.2 Site Geology

The Schoharie Creek delta lies close to the low seismic activity in the south central portion of New York State and moderate seismicity to the north and east. There was no earthquake when the bridge collapsed.

Wiss, Janney, Elstner Associates, Inc. and Mueser Rutledge Consulting Engineers (1987) states that "bedrock is made up of shale and limestone sedimentary formations beneath an overburden of glacial and alluvial soils" in the investigation report (p. 3.2). The footings of the piers of the bridge were built on the ice contact stratified drift. It was finely laminated. The soil under Pier 3 in Figure 1-2 was a mixture of dense sand, silt and gravel, which were well graded. The abutment was a mixture of gray and brown sandy silt with some gravel.

1.1.2.3 Flood History

The flood of April 5, 1987 was caused by heavy rains on April 4 and 5. The flood had a 70-year return frequency, and records showed that the maximum discharge was 1,838 m^3/s. The flood in 1955 had a 100-year return frequency. The flood in 1955 caused vertical cracks on a plinth of the bridge; however, the bridge did not collapse at that time.

1.1.2.4 Failure Analysis

Based on the investigation performed by different parties, the main reason of the collapse of the bridge was the severe erosion in the soil under the footings (National Transportation Safety Board 1987). The flood in 1987 was the direct cause of the failure. However, the inappropriate riprap placement contributed to the bridge failure as well. Besides the inappropriate riprap placement, the ambiguous plan and construction, inadequate inspection, and lack of structural redundancy also contributed to the failure. After the bridge wreckage was removed, the scour patterns were revealed by investigators. The maximum depth of scour was about 2.7 m below the footing of Pier 3.

1.1.3 Bridge Scour Current Study

The collapse of Schoharie Creek Bridge is a wake-up call for all the parties in the civil engineering field, especially in the geotechnical engineering field. Research has shown that bridge scour is the number one cause of bridge failure in the United States, accounting for about 58% of all failures (Briaud 2006). Figure 1-3 shows the possible causes of bridge failure based on the data collected from 1966 to 2005, which are

construction failure, concrete failure, deterioration of material, earthquakes, natural disasters, steel fatigue, fire disasters, overload failure, collision failure, hydraulic failure and miscellaneous failure. Among all the possible causes of bridge failure, hydraulic failure (scour failure) accounts for 58%.

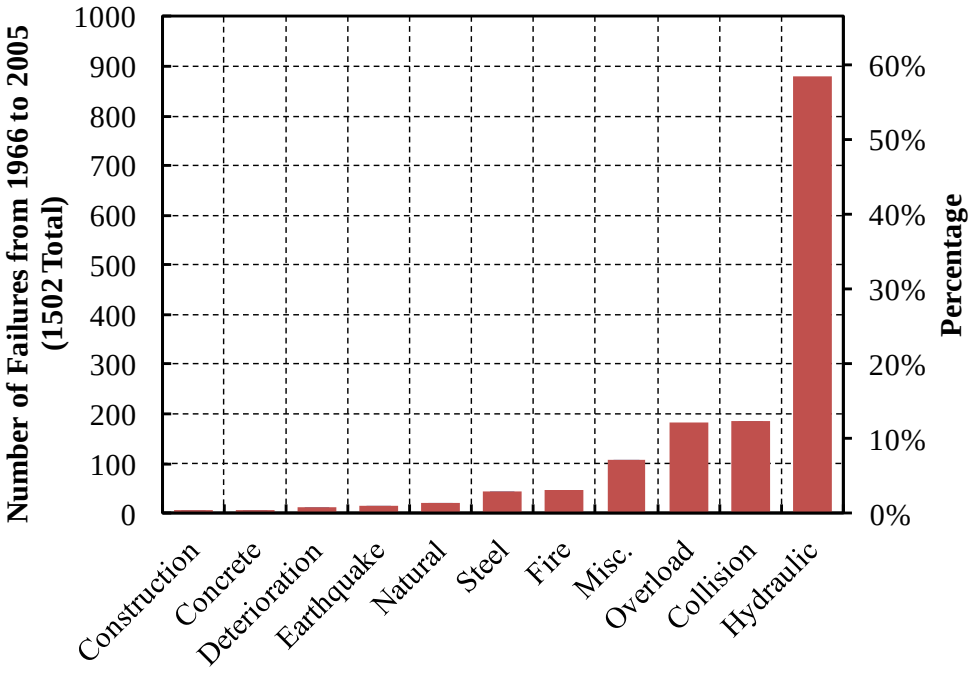

Figure 1-3. Causes of Bridge Failure (1966–2005) (after Briaud 2006).

After the failure of the Schoharie Creek Bridge, FHWA requested all State DOTs evaluate their bridges for scour and subsequently develop a plan of action for different bridge categories requiring attention (Briaud 2006). Briaud (2006) states "Shortly thereafter, the American Association of State Highway and Transportation Officials (AASHTO) set aside funds to perform research at the national level and at the state level.

It is estimated that over the last decade about 20 million dollars have been invested on scour research in the United States. This research has helped develop guidelines such as the popular HEC series (Hydraulic Engineering Circulars). These guidelines have been updated regularly sometimes as often as every 5 years." (p. 3). Figure 1-4 shows that the rate of bridge scour failure has decreased significantly over the last 10 years after more research involved.

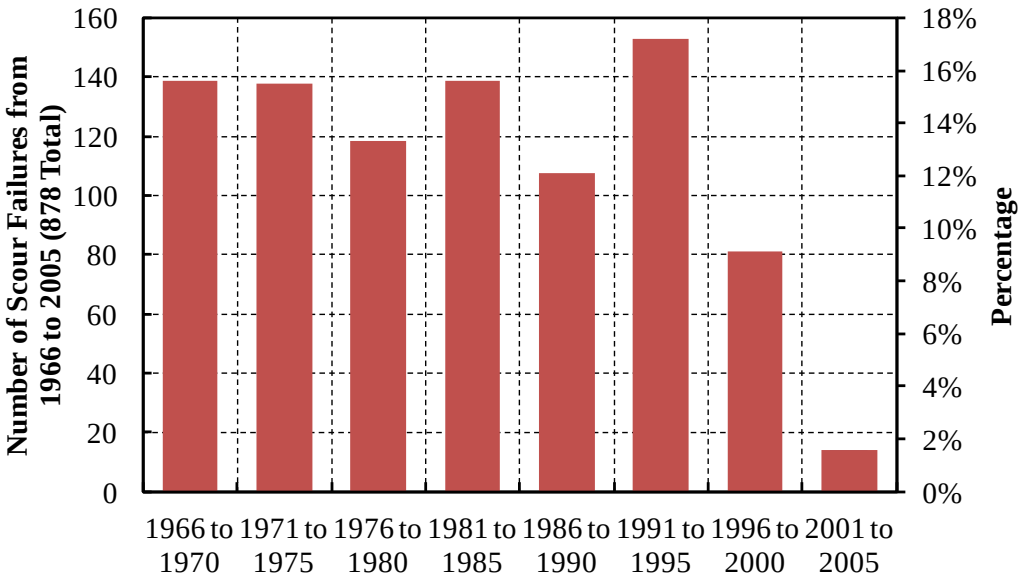

Figure 1-4. Scour Failures from 1966 to 2005(after Briaud 2006).

1.1.4 Bridge Failure Modes due to Scour (Briaud et al. 2011b)

There are four typical bridge failure modes due to scour: a big scour hole, settlement and rotation of the pier, loss of the deck, and loss of the pier. After studying 35 cases of bridge failures due to scour, researchers at Texas A&M University concluded that

settlement and rotation of the pier and big scour hole are the top two most common occurrences.

1.1.4.1 Failure Mode 1: A Big Scour Hole

Figure 1-5 shows the first failure mode: a big scour hole. In this mode, a bridge does not actually fail, but the foundation of the bridge is greatly weakened due the scour hole generated around it.

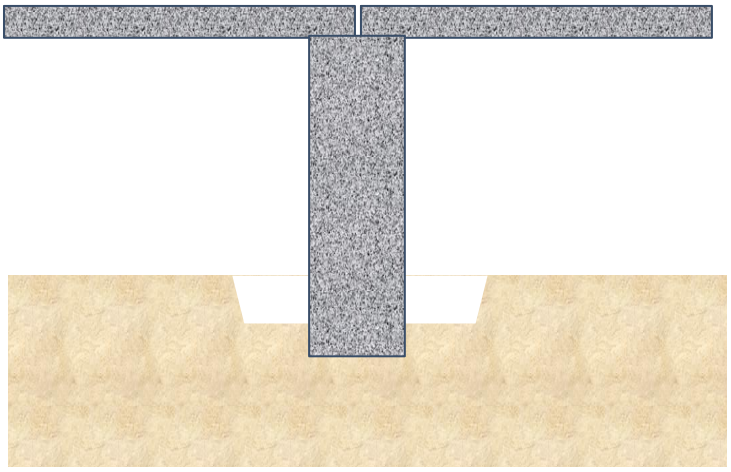

Figure 1-5. Bridge Failure Mode 1: A Big Scour Hole, 26 Percent Observed Occurrence.

Among the 35 bridge failure cases, 9 bridges "failed" in the first mode (26%). Figure 1-6 shows four examples of bridge failure due to big scour hole.

(a)

(b)

(c)

(d)

Figure 1-6. Generation of a Big Scour Hole: (a) Case 1, (b) Case 2, (c) Case 3, and (d) Case 4 (Briaud personal communication August 3, 2010).

1.1.4.2 Failure Mode 2: Settlement and Rotation of the Pier

Figure 1-7 shows the second failure mode: settlement and rotation of the pier. In this mode, a bridge fails due to the excessive settlement or rotation of the pier. Excessive settlement of the pier will generate excessive tilt of the bridge deck, which is very

common for bridge failure (Figure 1-7a). The rotation of the pier will also cause bridge failure (Figure 1-7b).

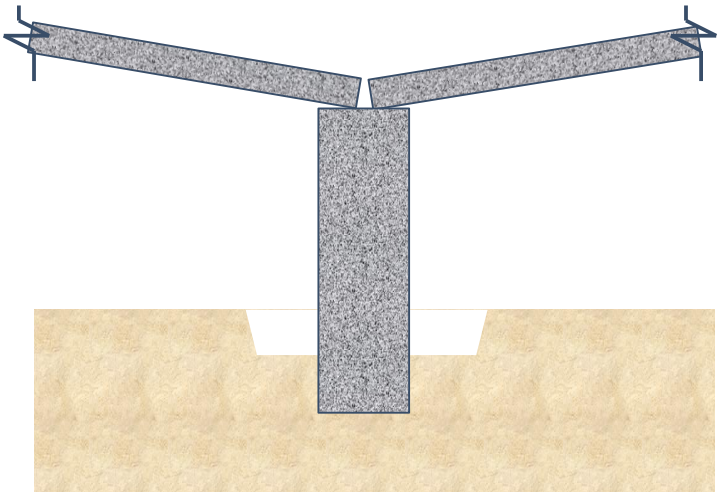

(a)

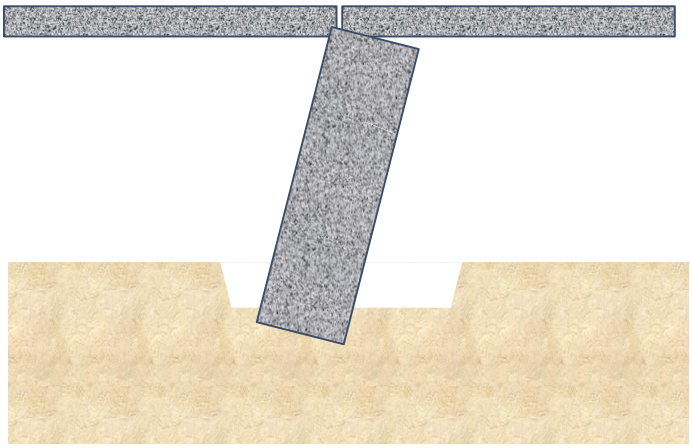

(b)

Figure 1-7. Bridge Failure Mode 2: Settlement and Rotation of the Pier, 37 Percent Observed Occurrence: (a) Settlement of the Pier and (b) Rotation of the Pier.

Among the 35 bridge failure cases, 13 bridges failed in the second mode (37%). Figure 1-8 shows the examples of the bridge failure due to settlement of the pier. Figure 1-9 shows the examples of the bridge failure due to rotation of the pier.

(a) **(b)**

Figure 1-8. Settlement of the Pier: (a) Case 1 and (b) Case 2 (Briaud, personal communication, August 3, 2010).

(a) **(b)**

Figure 1-9. Rotation of the Pier: (a) Case 1 and (b) Case 2 (Briaud, personal communication, August 3, 2010).

1.1.4.3 Failure Mode 3: Loss of the Deck

Figure 1-10 shows the third failure mode: loss of the deck. One possible reason for loss of the deck is that the settlement of the pier is so large that the deck moves out of the pier support, and it falls down. Another possible reason for loss of the deck is that the rotation of the pier is very large. The possibility of this type of failure can be reduced by increasing the width of the support (Figure 1-11).

Among the 35 bridge failure cases, 5 bridges failed in the third mode (14%). Figure 1-12 shows the examples of the bridge failure in the third failure mode.

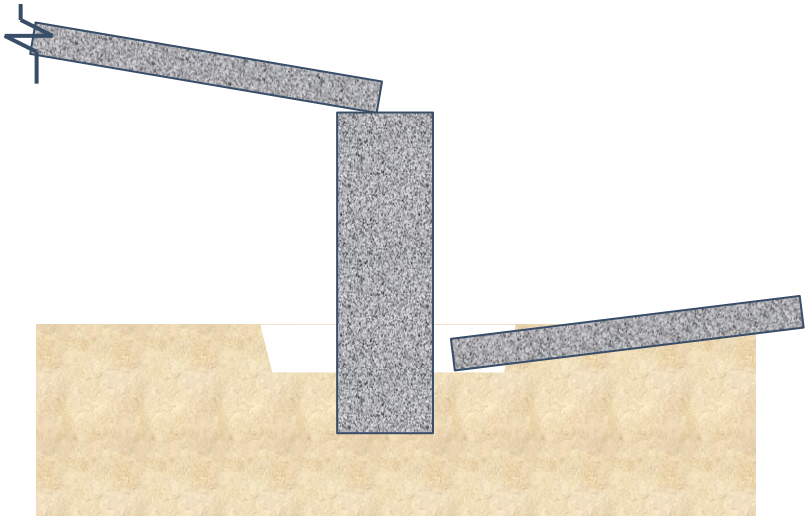

Figure 1-10. Failure Mode 3: Loss of the Deck, 14 Percent Observed Occurrence.

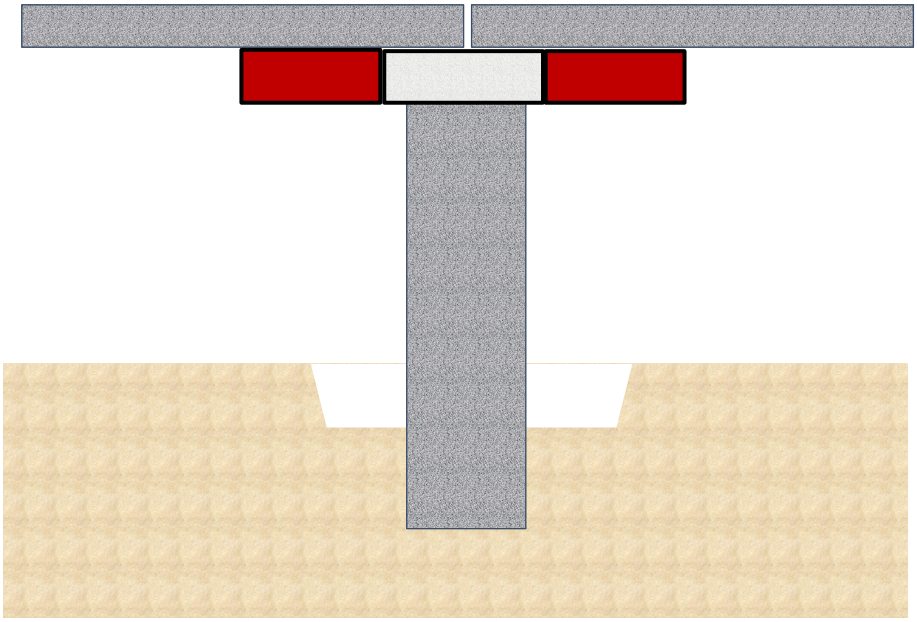

Figure 1-11. One Solution for Decreasing the Risk of Collapse.

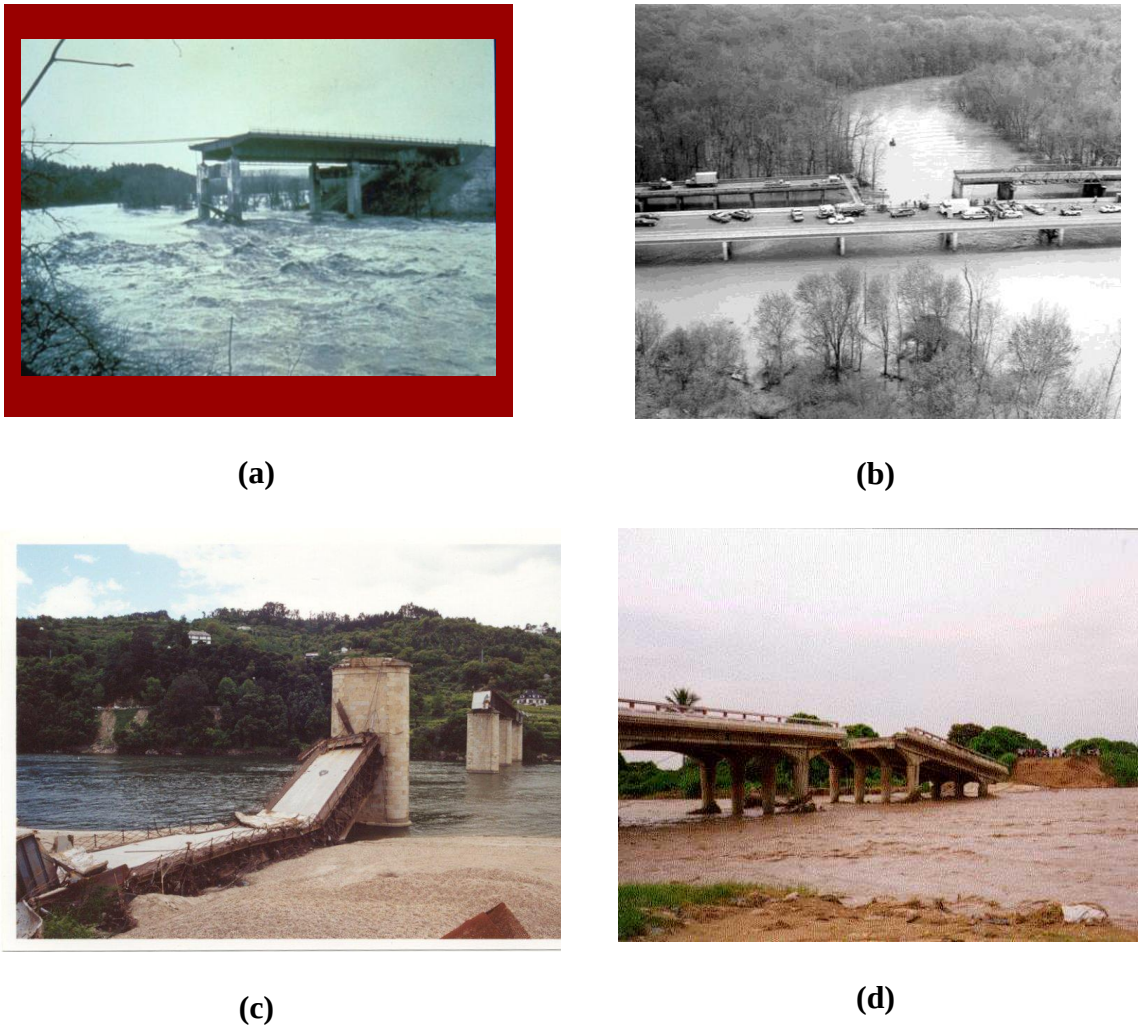

(a) **(b)**

(c) **(d)**

Figure 1-12. Loss of the Deck: (a) Case 1, (b) Case 2, (c) Case 3, and (d) Case 4 (Briaud, personal communication, August 3, 2010).

1.1.4.4 Failure Mode 4: Loss of the Pier

Figure 1-13 shows the fourth failure mode: loss of the pier. Among the 35 bridge failure cases, 8 bridges failed in the third mode (23%). Figure 1-14 shows a bridge failure process captured by two photos. Figure 1-14a shows the rotation of the pier before it

falls down, while Figure 1-14b shows the falling down of the pier. Figure 1-15 shows two more examples of bridge failure due to loss of the pier.

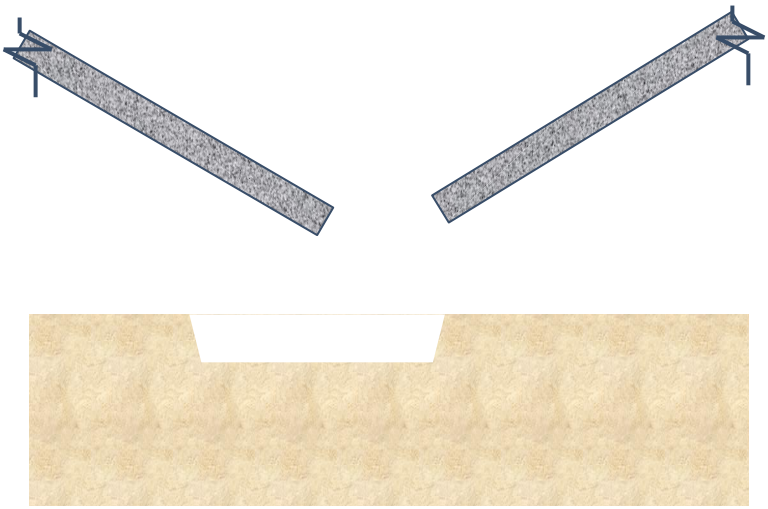

Figure 1-13. Failure Mode 4: Loss of the Pier, 23 Percent Observed Occurrence.

(a) **(b)**

Figure 1-14. Case of Loss of the Pier: (a) Rotation of the Pier and (b) Loss of the Pier (Briaud, personal communication, August 3, 2010).

(a) **(b)**

Figure 1-15. Loss of the Pier: (a) Case 1 and (b) Case 2 (Briaud, personal communication, August 3, 2010).

1.1.5 Bridge Design

The instrumentation and real-time monitoring of bridge scour could give officials ample warning before bridge failure and reduce the loss of failure significantly. But the most effective way of reducing the loss is to take into account the effect of scour in the bridge foundation design. The current bridge design code does not consider the scour effect, which makes the revision of the code urgent.

In 1931, AASHTO first introduced the Standard Specifications for Highway Bridges (Hueste et al. 2006). From 1931 to 1970, the Allowable Stress Design (ASD) philosophy was applied in the bridge design (AASHTO 2002). Afterwards, the Load Factor Design (LFD) philosophy was incorporated in the specifications.

In ASD, a global safety factor is used in the design process. ASD treats each load on the structures as equal from the point of view of statistical variability, which is not the case. Some combinations of loads are more likely to occur than others. Equation 1-1 shows the concept of ASD.

$$\Sigma Q_i < R_n / FS \tag{1-1}$$

where Q_i = a load; R_n = resistance of the element or the structure; FS = factor of safety.

LFD was introduced to "take into account the variability of loads by using different multipliers for dead load, live load, wind and other loads to a limited extent", for example, a load combination involving 130% of the dead load combined with the 217% of the live load (Kulicki 2012). These methodologies provide the desirable level of safety for bridge designs, but do not ensure uniformity in the level of safety for various bridge types and configurations. Equation 1-2 shows the concept of LFD.

$$\Sigma \gamma_i Q_i < \varphi R \tag{1-2}$$

where γ_i = a load factor; Q_i = a load; R = resistance; φ = strength reduction factor.

After 1994, Load and Resistance Factor Design (LRFD) (AASHTO 1994) was prompted in bridge design in order to perform the uniform safety level for all the components of bridges. The uniformity is made possible using improved design techniques based on probability and reliability theories. One such technique is reliability-based design, which accounts for the inherent variability or uncertainty of the loads and resistance to provide an acceptable and uniform level of safety in the design (Hueste et al. 2006). The first edition of the AASHTO LRFD Bridge Design Specifications was published in 1994, after which four more editions were published. In

recent years, all the states are trying to replace the ASD with LRFD in bridge design (Hueste et al. 2006). The advantages of LRFD are in three aspects: firstly, "it accounts for variability in both resistance and load"; secondly, "it achieves relatively uniform levels of safety based on the strength of soil and rock for different limit states and foundation types"; thirdly, "it provides more consistent levels of safety in the superstructure and substructure as both of them are designed using the same loads for target probabilities of failure" (Montana Department of Transportation, [MDOT] 2013, p. 16.2-10; Kulicki 2012). The shortcomings of LRFD are that "the method for developing the load factor and resistance factor to meet individual situations requires availability of statistical data and the probabilistic design algorithms"; "resistance factors vary with design methods and are site-specific"; and the LRFD is a combination of probability-based design and engineering judgment (MDOT 2013, p. 16.2-10; Kulicki 2012). Equation 1-3 shows the concept of LRFD.

$$\Sigma\gamma_i Q_{ni} < \phi_i R_{ni} \tag{1-3}$$

where γ_i = a load factor; Q_{ni} = a nominal load; R_{ni} = a nominal resistance; φ_i = a resistance factor.

AASHTO code (2007) provides LRFD calibration for deep foundation and shallow foundation without considering scour. The research in this dissertation is focused on revising the AASHTO code for both types of foundations in case of scour events. Once the updated resistance factors for bridge foundations in the case of scour have been provided, the bridge design will be more reasonable and more economical. For a given target reliability index, β_T, the bridge design will provide a uniform

probability of failure for all components. The target reliability index is related to the probability of failure but not equal to the probability of failure.

1.1.6 Bridge Scour Risk

The reliability-based design of bridge foundations leads to another question: How safe is enough for our design? This is a very promising topic in civil engineering: risk analysis. Risk is defined as the probability of failure times the value of the consequence (Equation 1-4).

$$Risk = POF \times C \tag{1-4}$$

The risk associated with bridge scour is another emphasis in the dissertation.

1.2 OBJECTIVES

The objectives of the research are to provide a LRFD calibration of foundation design in case of bridge scour and to analyze the risk associated with bridge scour. The objectives are divided into three parts:

- Develop a probabilistic approach for prediction of scour depth;
- Develop a reliability-based LRFD calibration of bridge foundations in the case of scour;
- Quantify bridge scour risks.

1.2.1 Objective 1: Develop a Probabilistic Approach for Prediction of Scour Depth

Currently there are two frequently used equations to predict the scour depth: HEC-18 Sand and HEC-18 Clay. Both equations are deterministic methods, which do not

consider the uncertainty associated with the scour process. The proposed probabilistic model will take into account the material uncertainty, the model uncertainty, and the measurement error during the scour depth prediction based on those two methods. The proposed probabilistic model will provide sufficient statistical parameters (mean value of scour depth, coefficient of variation of scour depth) for the LRFD calibration of bridge scour. It provides the information about the probability of exceedance for a predicted scour depth.

1.2.2 Objective 2: Develop a Reliability-Based LRFD Calibration of Bridge Foundations in the Case of Scour

The LRFD calibration of bridge scour will provide an updated resistance factor regarding scour. It will improve the performance of the current AASHTO code. Normally the bridge database should be built up, and the statistical parameters (bias factor and coefficient of variation) of loads and resistance would be obtained. After performing the reliability analysis, the load factor and resistance factor will be determined. The current AASHTO LRFD code has determined the load factor and resistance factor based on a reasonable target reliability index (β=2.33 for a redundant system, and β=3 for a non-redundant system). Here, a redundant system means the foundation having five or more piles per pile cap. A non-redundant system means the foundation having four or less piles per pile cap. Following the current AASHTO LRFD code, the proposed research will adopt the same load factors for live load and dead load, and modify the resistance factor considering scour effect in order to meet the same target reliability index.

1.2.3 Objective 3: Quantify Scour Risk for Bridges

The New York State Department of Transportation (NYSDOT) Bridge Failure Database and the Florida Department of Transportation (FDOT) Unknown Foundation Bridge Database will be analyzed to determine the risk of scour quantitatively. The annual probability of scour failure, the corresponding dollar loss, and fatalities will be analyzed; therefore the risk of scour will be quantified from the point of view of dollar loss and fatalities. The scour risk is also compared with other events, i.e. plane crashes, car accidents, dam failures, etc. The research will help the practitioners to be aware of the risk that they are facing when they are performing bridge design.

1.3 SIGNIFICANCE OF RESEARCH

Engineers will be able to design bridge foundations on the basis of a probability of exceeding a chosen scour depth. The outcome of the research will modify the current AASHTO LRFD code and help the practitioners design foundations of bridges over rivers for a uniform probability of failure. This design will be more reasonable and economical compared to the present practice. The risk of bridge scour is also quantified in the research. It will help engineers understand the risk level associated with bridge scour.

1.4 RESEARCH APPROACH

This dissertation addresses three topics related to bridge scour. First, a set of bridge pier scour databases (both full-scaled and experimental) are used to quantify the statistical parameters associated with the scatter between the predicted and measured scour depth

as well as the probability that a deterministically predicted scour depth will be exceeded. These databases are also used to give the bias factors in current predictions. In the second part, these statistical parameters are used to develop a reliability-based load and resistance factor design for shallow and deep foundations subjected to scour. The goal is to provide a design procedure where the reliability of the foundation is the same with or without scour. Reliability only addresses the probability of success and therefore of failure. The discussion is broadened in the third part by using the concept of risk defined as the probability of failure times the value of the consequences. In the third part, the risk associated with bridge scour is quantified and compared to risks associated with other engineering structures. Target values of acceptable risk are recommended as part of the conclusions.

1.5 ORGANIZATION OF DISSERTATION

The whole dissertation is organized into seven sections.

The first section is the introduction, including the problem statement, the significance of the research, and the objectives of the research.

The second section is the literature review, covering the fundamentals of scour, the deterministic and probabilistic pier scour depth prediction models in practice, the LRFD calibration in civil engineering, and the scour risk study.

The third section is the proposed probability-based pier scour depth prediction model for three databases. In this section, different types of uncertainties in the prediction model are discussed. The methodology of computing the probabilistic pier scour depth is introduced in this section. The Landers-Mueller full-scale Database

(1996), the TAMU Database (Gudavalli 1997; Li 2002), and the Froehlich full-scale Database (1988) are analyzed in this section. The different methods to compute critical velocity are also analyzed in this section since critical velocity is an important parameter in the HEC-18 Clay method. The author would like to see if the different values of critical velocity would affect the probabilistic scour depth prediction model, and hence affect the LRFD calibration in Sections 4 and 5.

According to the results obtained from Section 3, Section 4 proposes the LRFD calibration for shallow foundations in the case of scour. It is based on the probability of exceeding the measured scour depth. The target probability of exceedance is defined to be 0.001 for shallow foundations. The results from these three databases will provide a global safety factor in predicting the scour depth in the probabilistic format. In this section, the normal and lognormal distribution fitting analysis is also conducted to compare the results from Section 3.

Section 5 is the LRFD calibration for deep foundations in the case of scour. For deep foundations, the issue is the correction of resistance factor φ associated with the axial capacity of a pile in the case of scour. The proposed LRFD calibration in the dissertation is based on a reliability analysis using First-Order Reliability Method (FORM). In this section, the author first duplicates the LRFD calibration for the deep foundation design from the pioneers in the case of no scour, then revises the resistance factor taking into consideration of scour effect. The detailed calibration procedure is listed in the dissertation. Several case studies have been shown to explain the calibration methodology.

Section 6 is the extension of the dissertation. Previous sections discuss the probability of failure; hence, Section 6 discusses the risk by taking into consideration both probability of failure and consequences. First of all, common societal risks and engineering risks are discussed, including risk related to dam failure, foundation failure, cancer, car accident, plane crash, etc. Then two databases (New York State Department of Transportation Bridge Failure Database and Florida Department of Transportation Unknown Foundation Bridge Database) are used to quantify the risk of bridge failure, and used to locate the scour risk in the F-N Chart, where F means frequencies and N means consequences. Other societal risks and engineering risks are also located in the F-N Chart. The target values of acceptable risk are recommended in the conclusion.

Section 7 is the conclusion of the dissertation. The recommendations for future research are also proposed.

2 LITERATURE REVIEW

Since the research is involved bridge scour, Load and Resistance Factor Design (LRFD) and risk, the literature review in this section will cover several topics: scour, deterministic scour depth prediction, probabilistic scour depth prediction, LRFD calibration, and scour risk.

2.1 SCOUR

2.1.1 Scour Type

Bridge scour is the erosion of soils beneath or around the bridge due to flowing water. Based on the soil profile under the bridge, scour can be divided into scour in coarse-grained soils and scour in fine-grained soils. Based on the location where scour occurs, scour is divided into general scour and local scour. General scour is the aggradation or degradation of the riverbed without obstacles. "Aggradation is the gradual and general accumulation of sediments on the river bottom" (Briaud et al. 2004, p. 1). "Degradation is the gradual and general removal of sediments from the riverbed" (Briaud et al. 2004, p. 1). Local scour is the scour which occurs around piers and abutments of bridges in the path of the water flow. It includes pier scour, abutment scour, and contraction scour. Pier scour is the erosion of the soil around the pier foundations. Abutment scour is the loss of soil around an abutment which connects a bridge to an embankment. Contraction scour is caused by narrowing of the river channel, which is mostly due to approach embankments for a bridge (Yao et al. 2011). Figure 2-1 shows the definition of pier scour, abutment scour, and contraction scour.

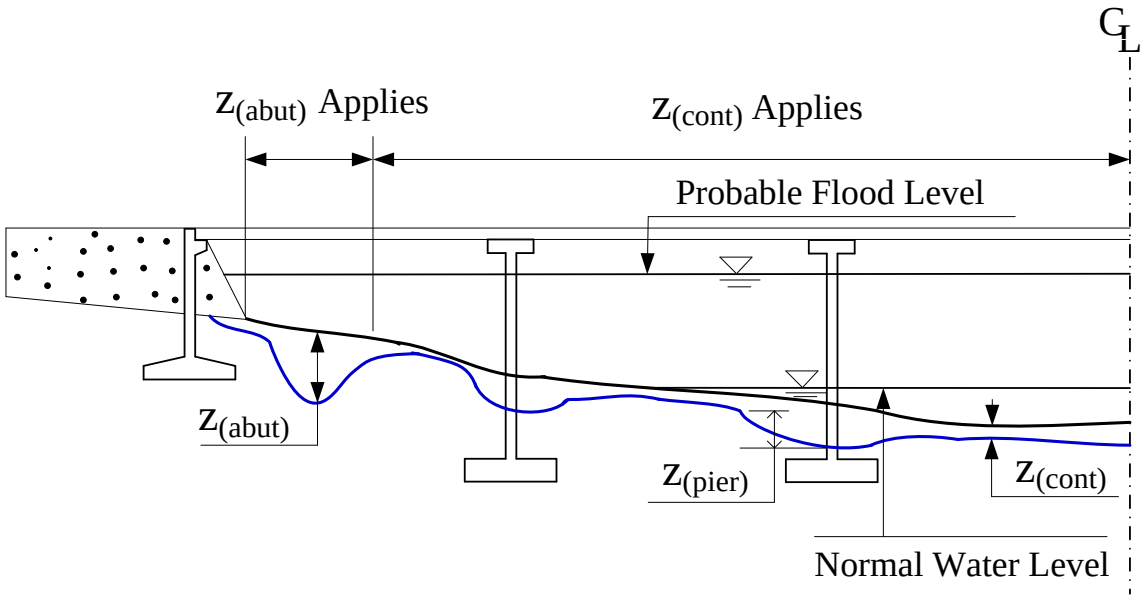

Figure 2-1. Pier Scour, Abutment Scour and Contraction Scour (after Briaud 2013).

2.1.2 Erodibility

Erodibility is a relationship between the velocity of water and corresponding erosion rate experienced by the soils (Briaud et al. 2004). It is not a specific number or index, because water velocity always changes with time, and it is hard to find a proper index to describe the erosion condition in erosion-resistant soils as well as erosion-sensitive soil. Therefore, erodibility is defined as a relationship between parameters rather than an index.

The Erosion Function Apparatus (EFA) is a machine developed by Dr. Jean-Louis Briaud's research team to testify the erodibility of soils (Briaud et al. 2001). The EFA figure is shown in Figure 2-2. Firstly, the soil sample is put into a Shelby tube and pushed into the EFA. Before running the flow, the soil sample is pushed 1mm into

the flow. With water flowing through the surface of the soil sample, erosion develops. How long it takes to erode 1 mm of soil is recorded. Then the water velocity is increased to repeat the erosion test several times. The results, consisting of the erosion rate ($\dot{Z}$) versus the shear stress (τ) curve and the erosion rate ($\dot{Z}$) versus velocity (v) curve, represent the erodibility of the soil sample.

Figure 2-2. Erosion Function Apparatus (Briaud 2008).

In cohesionless soils (sands and gravels), the critical shear stress has been empirically related to the median grain size D_{50} (Briaud et al. 2001). For cohesionless soils, one flood is probably long enough to develop the maximum scour depth. For

cohesive soils, the factors influencing the erodibility are water content, soil unit weight, plasticity index, undrained shear strength, chemical composition and so on. For rock, the factors influencing the erodibility are joint spacing, rock minerals, and so on.

2.1.3 Critical Shear Stress and Critical Velocity

In erosion studies, there are two very important parameters: critical shear stress, τ_c, and critical velocity, V_c. When the shear stress in the soil is lower than the critical shear stress τ_c, the erosion does not occur. When the water velocity is lower than the critical velocity V_c, the erosion does not occur. The advantage of using shear stress to specify critical conditions is that one quantity suffices whereas if velocity is used. one must also report the depth or the position at which the velocity is observed (White 1940).

The erosion mechanism for coarse-grained soils and fine-grained soils is different. For coarse-grained soils, there are two possible mechanisms: sliding and rolling (Briaud et al. 2001). White (1940) proposed Equation 2-1 to calculate the critical shear stress in the sand.

$$\tau_c = 0.18(\gamma_s - \gamma)D_{50}\tan\theta \tag{2-1}$$

where τ_c = critical shear stress, γ_s = unit weight of soil particles, γ = unit weight of water, D_{50} = the diameter for 50% finer by weight, and θ = the angle of repose of top layer of grains in the fluid.

Critical shear stress also can be determined using Shield's coefficient (Equation 2-2) (Shields 1936).

$$\tau_c = K_s(\gamma_s - \gamma)D_{50} \tag{2-2}$$

where K_s = Shields coefficient, varying from 0.03 to 0.1 (Vanoni 1975), γ_s = the unit weight of soil particles, γ = the unit weight of water, D_{50} = the diameter for 50% finer by weight.

Briaud et al. (1999) performed EFA tests on different sands, and proposed a simple relationship between critical shear stress, τ_c , and median grain size, D_{50}:

$$\tau_c(\mathrm{N/m^2}) \simeq D_{50}(\mathrm{mm}) \tag{2-3}$$

However, for fine-grained soils, the relationship between critical shear stress, τ_c ,and median grain size, D_{50}, is not easy to define.

Briaud (2008) analyzed the data from erosion tests on New Orleans Levee samples (Independent Levee Investigation Team 2006), TAMU data (Briaud et al. 2001), data from Vanoni (1975) and White (1940), and plotted the data in critical shear stress versus median grain size plots. The author retrieved most of the data, and reproduced the result (Figure 2-3). Note that the critical shear stress was read from the erodibility figures at the 1mm/h erosion rate.

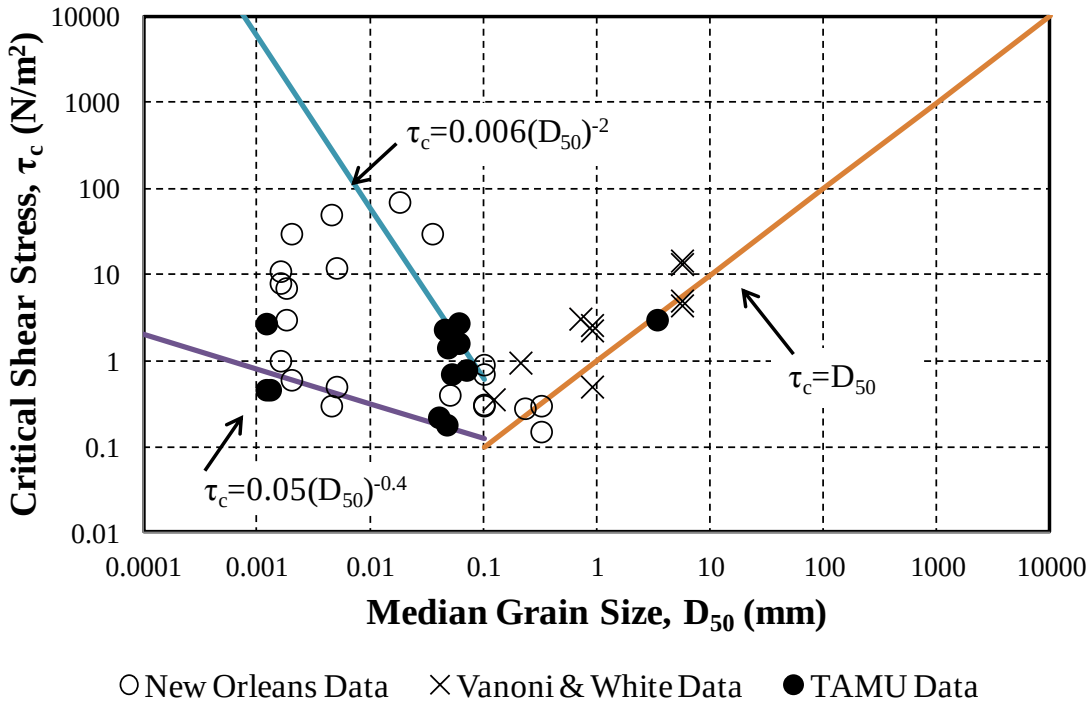

Figure 2-3. Critical Shear Stress versus Median Grain Size (after Briaud 2008).

There are plenty of studies trying to reveal the relationship between the critical velocity and critical shear stress. Equation 2-4 is widely accepted, which was proposed by White (1940).

$$V_c = \sqrt{\tau_c / \rho} \tag{2-4}$$

where V_c = the critical velocity, τ_c = the critical shear stress, and ρ = the mass density of the soil particles.

Another popular method to calculate the critical velocity of the bed material is related to Shield's coefficient, K_s, median grain size, D_{50}, water depth, y_1, and Manning's coefficient, n (Richardson and Davis 2001). The Equation 2-5 is shown below.

$$V_c(\text{m/s}) = \sqrt{\frac{\tau_c(\text{Pa}) y_1(\text{m})^{0.33}}{\rho(\text{kg/m}^3) g(\text{N/kg}) n^2}} \quad (2\text{-}5)$$

where V_c = critical velocity (in the unit of m/s), τ_c = critical shear stress (in the unit of N/m^2), y_1 = water depth (in the unit of m), ρ = density of water (in the unit of kg/m^3), g = acceleration due to gravity (in the unit of N/kg), n = Manning's coefficient.

The critical shear stress can be obtained by using Equation 2-2, hence, the critical velocity is calculated as:

$$V_c = \frac{K_s^{1/2}(G_s - 1) D_{50}^{1/2} y_1^{1/3}}{n} \quad (2\text{-}6)$$

where $K_s = 0.039$, G_s (i.e. specific gravity of bed material) = 2.65, $n = 0.041(D_{50})^{1/6}$. Note that here D_{50} is in the unit of m. The Manning's coefficient n is revised using Strickler's relation ($n = 0.034 D_{50}^{1/6}$). Richardson and Davis (2001) recommended that use of effective mean bed material size (D_m) instead of D_{50} ($D_m = 1.25 D_{50}$); hence the equation to calculate n becomes "$n = 0.041(D_{50})^{1/6}$," ($0.041 = 0.034 \times 1.25$). Equation 2-6 will be rewritten to be Equation 2-7.

$$V_c(\text{m/s}) = 6.19 y_1(\text{m})^{1/6} D_{50}(\text{m})^{1/3} \quad (2\text{-}7)$$

where V_c = critical velocity (in the unit of m/s), y_1 = water depth (in the unit of m), and D_{50} = the diameter for 50% finer by weight (in the unit of m).

Briaud (2008) did research on the critical velocity in the scour process, and proposed Equation 2-8 to calculate the critical velocity for coarse-grained soils.

$$V_c(\text{m/s}) = 0.35(D_{50}(\text{mm}))^{0.45} \quad (2\text{-}8)$$

However, it is not easy to come up with the simple relationship between V_c and D_{50} for fine-grained soils.

Briaud (2008) analyzed the data from erosion tests on New Orleans Levee samples (Independent Levee Investigation Team 2006), TAMU data (Briaud et al. 2001), data from Vanoni (1975) and White (1940), and plotted the data in critical velocity versus mean grain size plots. The author retrieved most of the data, and reproduced the result (Figure 2-4). Note that the critical velocity was read from the erodibility figures at the 1mm/h erosion rate.

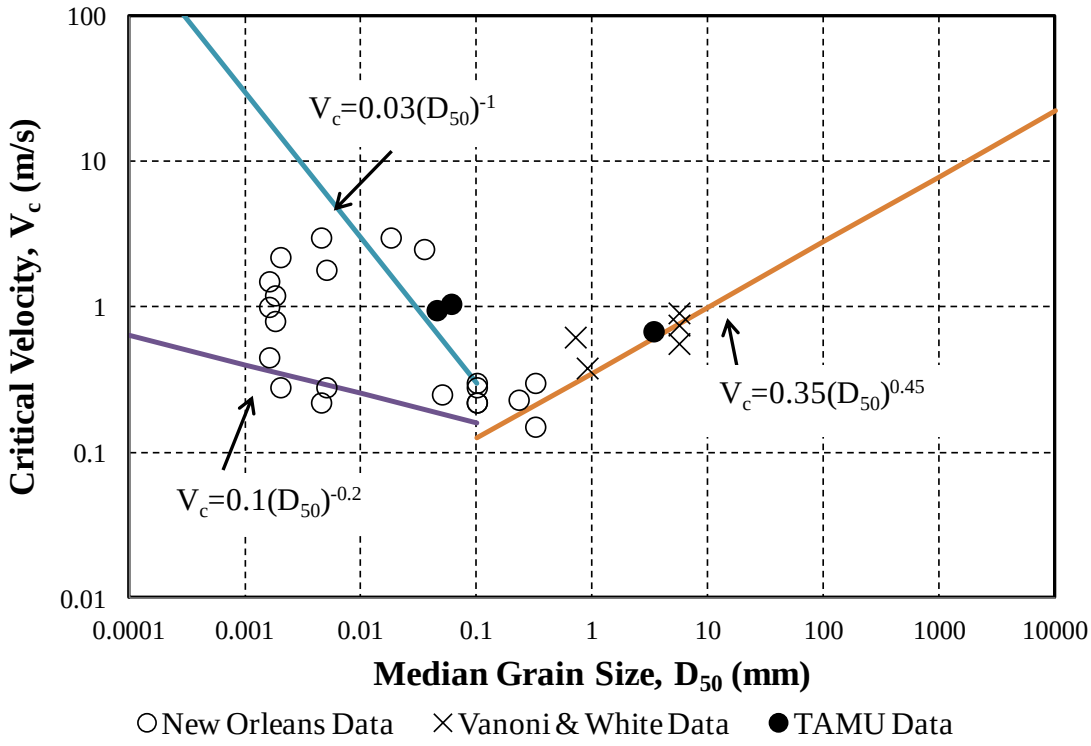

Figure 2-4. Critical Velocity versus Median Grain Size (after Briaud, 2008).

In the prediction of scour depth, the critical velocity and critical shear stress are very important parameters. The author will address this issue in more detail in Section 3.

2.2 DETERMINISTIC PIER SCOUR DEPTH PREDICTION METHODS

Currently most of the scour depth prediction models (pier scour, abutment scour and contraction scour) are deterministic. They do not consider the uncertainties in the soil condition, flowing condition, and model itself. Two common methods of prediction for pier scour depth are described in Hydraulic Engineering Circular No. 18 (HEC-18) (Arneson et al. 2012; Briaud et al. 2012). One of these methods applies when the soil is sand; it was developed at Colorado State University and is called HEC-18 Sand. The other one applies when the soil is clay. It was developed at Texas A&M University and is called HEC-18 Clay.

2.2.1 HEC-18 Sand (Briaud et al. 2012)

HEC-18 Sand recommends the use of simple equations for pier scour depth, contraction scour depth, and abutment scour depth. These equations are based on flume tests performed on fine sand and later compared to field measurements (Briaud et al. 2012; Yao et al. 2011). No soil parameters are shown in those equations. The basic assumption that all soils behave like fine sands was made. These equations have been shown on average to be very conservative with very few cases where the predicted depths were smaller than the measured depths in the field. Equation 2-9 is the formula to calculate the maximum pier scour depth using HEC-18 Sand:

$$\frac{Z_{\max}}{a} = 2.0 \times K_1 \times K_2 \times K_3 (\frac{y_1}{a})^{0.35} Fr^{0.43} \quad (2\text{-}9)$$

where $Z_{\max}$ = the deterministic prediction of the maximum scour depth, y_1 = the upstream water depth, a = the effective pier width, Fr = the Froude number upstream of the pier;

$Fr = V_1 / \sqrt{gy_1}$, V_1 = average upstream water velocity, g = acceleration due to gravity, and K_1, K_2, and K_3 = correction factors for the pier shape, angle of attack, and bed configuration, respectively.

The correction factor, K_1, is 1.1 for square nose pier, 0.9 for sharp nose pier, and 1 for other cases (round nose, circular cylinder, group of cylinders).

The correction factor, K_2, for angle of attack of the flow, θ, is calculated using the following Equation 2-10:

$$K_2 = (\cos\theta + L/a \sin\theta)^{0.65} \quad (2\text{-}10)$$

where L = the length of pier (m), θ = the skew angle of flow ( ), and a = the width of pier (m). Note that if L/a is larger than 12, L/a = 12 is the maximum.

Table 2-1 shows the values of K_3 for different bed conditions.

Table 2-1. Increase in Equilibrium Pier Scour Depths, K_3, for Bed Condition (Arneson et al, 2012).

Bed Condition	Dune Height (ft)	K_3
Clear-Water Scour	N/A	1.1
Plane bed and Antidune flow	N/A	1.1
Small Dunes	10>H≥2	1.1
Medium Dunes	30>H≥10	1.2 to 1.1
Large Dunes	H≥30	1.3

2.2.2 HEC-18 Clay (Briaud et al. 2012)

In 2012, HEC-18 Clay was incorporated in HEC-18 (Arneson et al. 2012) to predict the maximum and final scour depth in fine grained soils. A distinction is made between the

maximum scour depth, the scour depth reached when a velocity is applied for an infinite time, and the final scour depth, the scour depth reached when a velocity or a velocity hydrograph is applied for a finite time (Briaud et al. 2012; Yao et al. 2011). It is widely accepted that HEC-18 Clay method is applicable for scour in cohesive soils. Equation 2-11 shows the equation to predict the maximum scour depth using HEC-18 Clay:

$$\frac{Z_{\max}}{a'} = 2.2K_w K_1 K_L K_{sp}(2.6Fr - Fr_c)^{0.7} \quad (2\text{-}11)$$

where $Z_{\max}$ = the deterministic prediction of maximum scour depth, a' = the projected pier width perpendicular to the flow direction, Fr = the pier Froude Number based on the approach velocity V_1 and pier width a', $Fr = V_1/\sqrt{ga'}$, Fr_c = the critical pier Froude Number based on critical velocity V_c and pier width a', $Fr_c = V_c/\sqrt{ga'}$, the critical velocity can be obtained by running soil erosion tests (Briaud 2008), K_w, K_1, K_L, and K_{sp} = correction factors for shallow water effect, pier shape, aspect ratio of a rectangular pier, and pier spacing, respectively (Briaud et al. 2011a). Figure 2-5 shows the definition of the pier parameters.

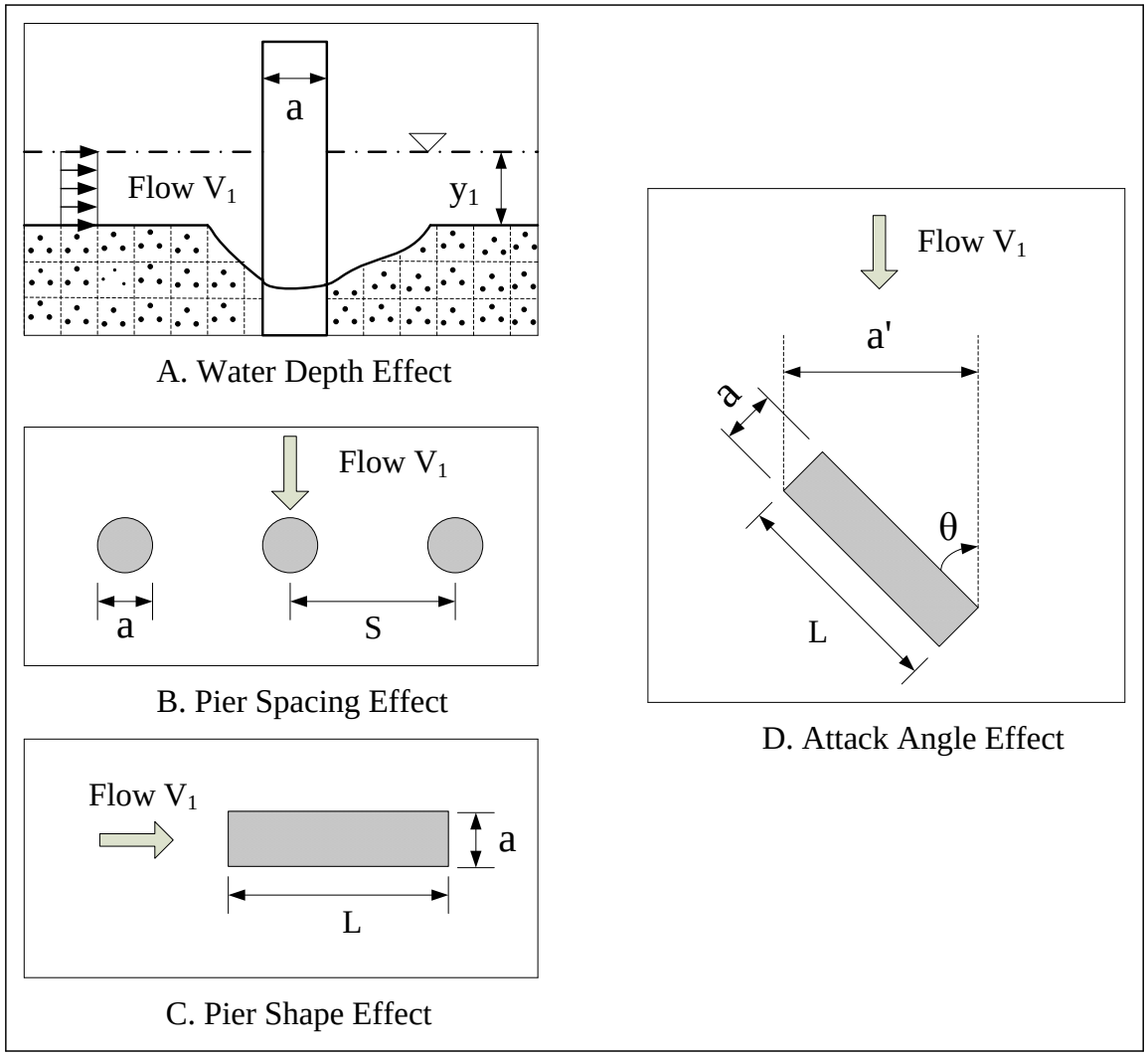

Figure 2-5. Definition of Pier Parameters (after Briaud et al. 2011a, p. 15).

The projected pier width, *a'*, is given by:

$$a' = a(\cos\theta + L/a \sin\theta) \tag{2-12}$$

The water depth influence factor, K_w, corrects for the shallow water effect, which is given in:

$$K_w = \begin{cases} 0.89\left(\frac{y_1}{a'}\right)^{0.33} & \text{, for } \frac{y_1}{a'} < 1.43 \\ 1.0 & \text{, else} \end{cases} \tag{2-13}$$

The pier shape influence factor, K_1, has the same definition as in HEC-18 Sand method. The aspect ratio influence factor, K_L, is defined to be 1 in any case. The pier spacing influence factor, K_{sp}, is given in:

$$K_{sp} = \begin{cases} 2.9\left(\frac{S}{a'}\right)^{-0.91} & \text{, for } \frac{S}{a'} < 3.42 \\ 1.0 & \text{, else} \end{cases} \tag{2-14}$$

where S = the pier spacing, and a' = the projected width. Equation 2-14 indicates that piers spaced more than 3.42 times the projected pier width from each other do not increase the scour depth at the pier.

In cohesive soils, one flood may not generate the maximum scour depth, and hence the final scour depth is of more interest. Figure 2-6 shows the relationship between the final scour depth and the maximum scour depth in cohesive soils. The hyperbola is used to describe the development of scour depth with time. Equation 2-15 shows the numerical solution to final scour depth.

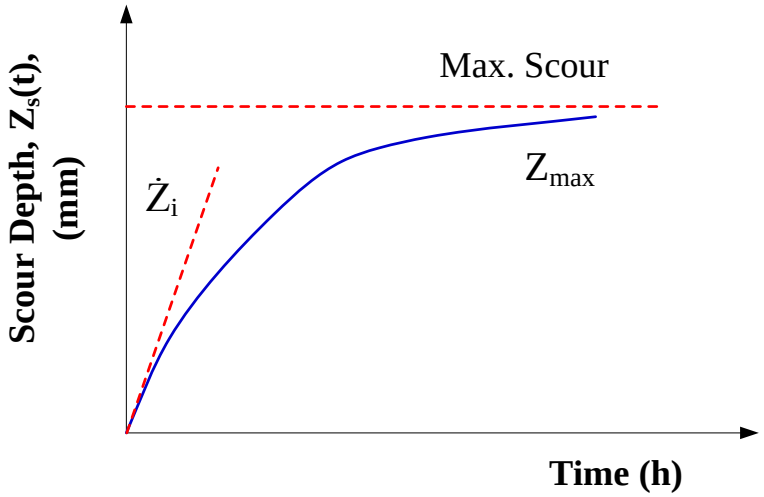

Figure 2-6. Final Scour Depth.

$$Z_s(t)(\text{mm}) = \frac{t(h)}{\frac{1}{\dot{Z}_i(\text{mm/h})} + \frac{t(h)}{Z_{\max}(\text{mm})}}\ , \qquad (2\text{-}15)$$

where $Z_s(t)$ = the final scour depth (in the unit of mm), t = the time that scour develops (in the unit of h), $\dot{Z}_i$ = the initial scour rate (in the unit of mm/h), Z_{max} is the maximum scour depth (in the unit of mm).

HEC-18 Sand and HEC-18 Clay methods are the most popular pier scour depth prediction methods; therefore, the proposed research will be based on these two deterministic models and aim to propose corresponding probability-based scour depth prediction models for pier scour.

2.3 PROBABILISTIC PIER SCOUR DEPTH PREDICTION MODELS

Research on probabilistic scour depth prediction is limited. This section shows the summary of the research from Johnson (1992), Johnson and Dock (1998), Brandimarte et al. (2006), Briaud et al. (2007), and Bolduc et al. (2008).

2.3.1 Johnson (1992)

Johnson (1992) developed a reliability-based pier scour estimate. A probabilistic model was proposed to predict pier scour depth under the condition that the bridge was assumed to fail if the scour depth reached the bottom of the pier. The best fit model was used to predict the pier scour depth for a bridge in the paper. One hundred and thirty laboratory data from University of Auckland (Chee 1982; Chiew 1984) were used to calibrate the four parameters in the model:

$$D_s = c_1 y \left(\frac{b}{y}\right)^{c_2} Fr^{c_3} \sigma^{c_4} \tag{2-16}$$

where D_s = the scour depth measured from the average channel bed to the bottom of the scour hole, y = the flow depth just upstream of the pier, Fr = the upstream Froude number ($Fr = V / \sqrt{gy}$, where V = the approach flow velocity), b = the pier width, σ = sediment gradation (i.e. d_{84}/d_{50}), and c_1, c_2, c_3 and c_4 are factors which need to be determined using the experimental data. Instead of regression analysis, a nonlinear least-squares algorithm was used to calibrate these factors. The final model was shown below:

$$D_s = 2.02 y \left(\frac{b}{y}\right)^{0.98} Fr^{0.21} \sigma^{-0.24} \tag{2-17}$$

The failure was defined as the scour depth reached the bottom of the pier footing; therefore, the safety margin was defined as:

$$M = D_p - D_s \tag{2-18}$$

where D_p = the depth from the average bed level to the bottom of the footing. Hence,

$$M = D_p - \lambda(2.02)y\left(\frac{b}{y}\right)^{0.98} Fr^{0.21}\sigma^{-0.24} \tag{2-19}$$

where λ = the model correction factor, i.e. the ratio of the observed scour depth to the scour depth predicted by Equation 2-17.

The probability of failure was calculated using the Monte Carlo Simulation for several values of safety factor in Johnson (1992). Note that the safety factor is the ratio of the pier footing depth over the scour depth. The result is shown in Figure 2-7.

Using the nonlinear least-squares numerical optimization algorithm, the safety factor (SF) was calculated using:

$$\mathrm{SF} = 1.88 - 1.06P_f{}^{0.212} \tag{2-20}$$

Where P_f = the probability of failure.

Hence, for a probability of failure as 10^{-4}, the safety factor is calculated to be 1.73. Therefore, the probabilistic pier footing depth should be calculated to be:

$$D_p = 1.73 \times 2.02y\left(\frac{b}{y}\right)^{0.98} Fr^{0.21}\sigma^{-0.24} = 3.49y\left(\frac{b}{y}\right)^{0.98} Fr^{0.21}\sigma^{-0.24} \tag{2-21}$$

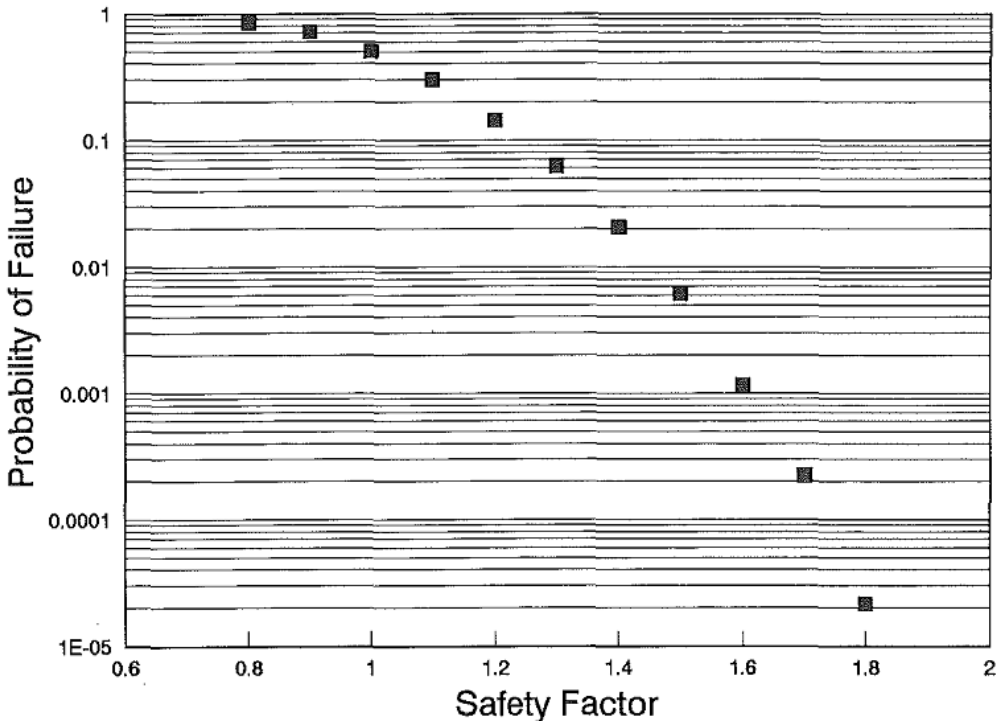

Figure 2-7. Probability of Failure as a Function of Safety Factor (Johnson 1992).

2.3.2 Johnson and Dock (1998)

Johnson and Dock (1998) developed a probabilistic bridge scour estimates. Model uncertainty, hydraulic uncertainty, and parameter uncertainty were considered in the model. For model uncertainty, the results were obtained from small-scale laboratory tests, and extrapolated to the prototype scale. The results of model uncertainty can be incorporated into an equation using a model correction or bias factor. The uncertainty about the flow depth and velocity were due to the limited and unrecorded data. The parameter uncertainty was caused from an inability to accurately assess parameters and model coefficients in the scour prediction equation. The Monte Carlo Simulation was

adopted to generate random samples of the parameters in a deterministic scour depth prediction equation based on specified coefficients of variation and distributions.

Johnson and Dock (1998) took Bonner Bridge in North Carolina as an example to compute the probabilistic scour depth prediction model. The probability distribution function of effective pier width, flow velocity, flow depth, model correction factor, and factors for attack angle and bed condition was assumed. One thousand simulation cycles were performed to compute the probabilistic scour depth distribution. In the model, the failure was defined as the point at which the scour reaches the bottom of the piles, no matter whether there was actually collapse of the structure or not.

2.3.3 Brandimarte et al. (2006)

Brandimarte et al. (2006) proposed the stochastic approach to predict pier scour in cohesive soils. The stochastic model was coupled with a scour model to determine the development of pier scour during the bridge lifespan in cohesive soils. The paper aimed to estimate the probability that a given scour depth is reached in the lifetime of the bridge and estimated the risk of failure associated with different design values of scour depth and bridge lifetime. A Monte Carlo simulation was used to generate the probability distribution of scour depth for different lift span bridges.

2.3.4 Briaud et al. (2007)

Briaud et al. (2007) presented a site specific method to estimate the probability that a certain scour depth will be exceeded during the life of a bridge. In this paper, only the uncertainty of a hydrograph was discussed; hence no uncertainty of other input

parameters was involved in the model. Briaud et al. (2007) proposed a probabilistic methodology to compute the final scour depth of bridges in a cumulative density function curve. Thousands of equally likely hydrograph distributions were generated, and corresponding final scour depths were computed in a distribution. The final scour depth distribution provides the probability that a chosen scour depth will be exceeded. Note that a simple approach, the Q100-Q500 approach and the advanced approach were presented respectively in the paper. The advanced approach was developed by adopting the Brandimarte et al. (2006) method to generate the stochastic hydrological model and compute the probability of exceedance for a given scour depth.

2.3.5 Bolduc et al. (2008)

Bolduc et al. (2008) has done analysis on several pier scour databases to develop probabilistic prediction models accounting for the estimated bias in the deterministic models and for the model uncertainty. The scour database included the Landers and Mueller Database (1996), the Gudavalli Database (1997), and the Kwak Database (2000). However, only circular piers in these databases were considered in this paper. The deterministic pier scour depth prediction model used in Bolduc et al. (2008) is updated by Arneson et al. (2012) and incorporated in the latest version of HEC-18 Series. The model proposed by Bolduc et al. (2008) only considers the parameter uncertainty and model uncertainty while not taking into account the measurement error and hydraulic uncertainty.

This dissertation mainly uses the methodology proposed in Bolduc et al. (2008) to compute the probabilistic pier scour depth for three databases: the Landers and

Mueller Database (1996), the TAMU Database (Gudavalli 1997; Li 2002), and the Froehlich Database (1988). All types of pier shape will be taken into consideration in the probabilistic scour depth prediction model. The updated deterministic pier scour depth prediction model is used in the dissertation.

2.4 LRFD CALIBRATION IN CIVIL ENGINEERING

Engineers in Europe are pioneers in the limit states design and reliability-based design (Kulicki 2012). Kulicki (2012) gave a summary of the history of developing a probability-based limit states bridge design specification. In the paper, Kulicki states that "In 1979, the first edition of the Ontario Highway Bridge Design Code (OHBDC) (Ontario Ministry of Transportation 1991) was released to the design community as North America's first calibrated, reliability-based limit states bridge specification." In 1986, a group of bridge engineers initiated a project 20-7/31 "Development of Comprehensive Bridge Specifications and Commentary." After the project, NCHRP 12-33 "Development of a Comprehensive Bridge Specification and Commentary" was initiated in order to develop Load and Resistance Factor Design Specifications for bridges (Kulicki 2012). The author will give the summary of Nowak (1995; 1999) and Paikowsky (2004) in the following section as they are the most important references the author used in this research.

2.4.1 Nowak (1995; 1999)

Nowak (1995; 1999) gave the LRFD calibration of bridge structures using an iterative procedure. The author summarizes the approach below:

A. Selection of representative bridges.

About 200 representative bridges in the United States were chosen in Nowak (1995; 1999) in order to obtain the statistical database for load and resistance parameters. The live load was modeled by using truck survey and Weigh-In-Motion (WIM) technology. A numerical simulation was used to simulate the bridge dynamic behavior. The resistance was modeled by using statistical data, performing material tests, component tests, and field measurements.

B. Development of load and resistance models.

In the model, the loads were treated as normal distribution variables, while the resistance was treated as a log-normal distribution variable.

C. Development of the reliability analysis procedure.

Structural performance was measured in terms of reliability. Reliability was measured in terms of the reliability index, β. The reliability index was calculated by using an iterative procedure. The limit state function g can be written as $g=R-Q$. Here, R represents resistance, Q represents load effect. Q is taken as a normal random variable, while R is taken as a lognormal random variable.

If $g>0$ the structure is safe, otherwise it fails. The probability of failure P_f is calculated as $P_f = \text{Prob}(R-Q<0) = \text{Prob}(g<0)$. The reliability index β is defined as a function of P_f: $\beta = -\Phi^{-1}(P_f)$. Here, ϕ^{-1} is the inverse standard normal distribution function (Nowak 1995; 1999).

The reliability analysis was performed using an iterative method based on normal approximations to non-normal distributions at the design point. The design point is

defined to be the point of the maximum probability on the failure surface or the minimum distance point on the limit state surface (Haldar and Mahadevan 2000, p. 199).

The reliability index β can be obtained:

$$\beta = \frac{R_n \lambda_n (1 - k\delta_R)[1 - \ln(1 - k\delta_R)] - m_Q}{\sqrt{[R_n \delta_R \lambda_R (1 - k\delta_R)]^2 + \sigma_Q^2}} \tag{2-22}$$

where R_n = nominal value of resistance; λ_R = bias factor of R_n; $\lambda_R = m_R / R_n$, δ_R = coefficient of variation of R_n; m_Q = mean load; σ_Q = standard deviation of load; k=2.

D. Selection of the target reliability index.

The target reliability index β_T was selected to provide a consistent and uniform safety margin for all structures. The target reliability index was chosen to be 3.5 in Nowak (1999), which was proven to be adequate for structural engineering.

E. Calculation of factors.

The load factors, γ, are calculated so that the factored loads have a predetermined probability of exceedance. Resistance factors, φ, are calculated so that the structural reliability is matching the target value, β_T.

The load factors, γ_i, can be obtained by:

$$\gamma_i = \lambda_i (1 + k\delta_i) \tag{2-23}$$

where in practice k is usually 2, which corresponds to a 98% probability of not being exceeded for the nominal value (Orr and Breysse 2008); δ_i = the coefficient of variation of loads; λ_i = bias factor of loads.

The proposed LRFD code is shown:

$$\varphi R > 1.25D + 1.5D_A + \gamma_L (1 + I)L \tag{2-24}$$

where D_A = dead load due to asphalt; I = dynamic load ratio of dynamic deflection to static deflection, usually 0.33 (applied to truck portion of the live load only); D = dead load, except effect of asphalt; L = live load effect (HS20-44); γ_L = live load factor, 1.6 and 1.7 are considered. The target reliability index was selected to be 3.5, which corresponds to 0.02% probability of failure. Resistance factor φ = 1 for prestressed-concrete girders and moment; resistance factor φ = 0.95 for steel girders, moment and shear; resistance factor φ = 0.9 for reinforced-concrete T-beams and moment; resistance factor φ = 0.85 for reinforced-concrete, prestressed-concrete and shear.

2.4.2 Paikowsky (2004)

Based on Nowak's work, Paikowsky (2004) implemented the calibration procedure to geotechnical engineering, and developed the resistance factor for driven pile and drilled shaft foundations. The load factors and the statistical parameters remained the same as in NCHRP Report 368 (Nowak 1999), which are shown in Table 2-2. The difference here is that in NCHRP 507 (Paikowsky 2004), the loads were taken as lognormal distributions, while in NCHRP 368 (Nowak 1999), the loads were taken as normal distributions.

Table 2-2. Load Factors and Statistical Parameters (after Nowak 1999).

γ_{LL}=1.75	λ_{LL}=1.15	COV_{LL}=0.2
γ_{DL}=1.25	λ_{DL}=1.05	COV_{DL}=0.1

For a given value of reliability index β, probability distributions of load variables, and the coefficient of variation for the resistance, compute the mean resistance R using First-Order Reliability Method (FORM). The resistance factor φ is computed as:

$$\varphi = \frac{\sum_{i=1}^{n} \gamma_i \mu_{Li}}{\mu_R} \tag{2-25}$$

where γ_i = a load factor; μ_{Li} = mean value of the load; μ_{R} = mean value of resistance; n = the number of load variables.

The proposed target reliability indices for structures based on NCHRP Report 507 (Paikowsky 2004) is shown in Table 2-3.

Table 2-3. Target Reliability Indices by Structural Type (Paikowsky 2004).

Structural Type	Target Reliability Level β_T
Metal structures for buildings (dead, live and snow loads)	3
Metal structures for buildings (dead, live and winds loads)	2.5
Metal structures for buildings (dead, live, snow and earthquake loads)	1.75
Metal connections for buildings (dead, live and snow loads)	4 to 4.5
Reinforced concrete for buildings (dead, live and snow loads) --ductile failure --brittle failure	 3 3.5

Note: β_T values are for structural members designed for 50 years of service.

Moses and Verma (1987) suggested the reliability index in calibrating bridge codes. Assuming that the bridge span is less than 30.5 m, β_T is 2.5 to 2.7 for redundant bridges, while β_T is 3.5 for non-redundant bridges.

NCHRP Report 507 (Paikowsky 2004) recommends that β_T is 2.33 for a redundant system, while 3 for a non-redundant system. The probability of failure is 0.01 when β_T =2.33; the probability of failure is 0.001 when β_T =3.

NCHRP Report 507 (Paikowsky 2004) listed the recommended resistance factors regarding different target reliability index values at different soil conditions and design methods for both drilled shafts and driven piles. The current AASHTO code (2007) follows Paikowsky (2004)'s work.

NCHRP Report 507 (Paikowsky 2004) also compared the resistance factors calculated using First Order Second Moment (FOSM) and FORM (Figure 2-8). The FOSM method is described below (assume *R*, *Q*, are following Lognormal Distributions):

$$\frac{\bar{R}}{\bar{Q}} = \frac{\lambda_R FS\left(\frac{Q_D}{Q_L}+1\right)}{\lambda_D \frac{Q_D}{Q_L}+\lambda_L} \tag{2-26}$$

$$\beta = \frac{\ln\left(\frac{\lambda_R FS\left(\frac{Q_D}{Q_L}+1\right)}{\lambda_D\left(\frac{Q_D}{Q_L}\right)+\lambda_L}\sqrt{\frac{1+\delta_D^2+\delta_L^2}{1+\delta_R^2}}\right)}{\sqrt{\ln[(1+\delta_R^2)(1+\delta_D^2+\delta_L^2)]}} \tag{2-27}$$

Given $\gamma_D Q_D + \gamma_L Q_L = \varphi FS(Q_D + Q_L)$,

$$\varphi = \frac{\lambda_R \left(\frac{\gamma_D Q_D}{Q_L} + \gamma_L \right) \sqrt{\frac{1+\delta_D^2+\delta_L^2}{1+\delta_R^2}}}{\left(\lambda_D \frac{Q_D}{Q_L} + \lambda_L \right) \exp[\beta_T \sqrt{\ln[(1+\delta_R^2)(1+\delta_D^2+\delta_L^2)]}]} \quad (2\text{-}28)$$

$\frac{Q_D}{Q_L}$ is relatively not sensitive to φ; in NCHRP Report 507 (Paikowsky 2004; Zhang 2008), $\frac{Q_D}{Q_L}$ usually equals to 2.

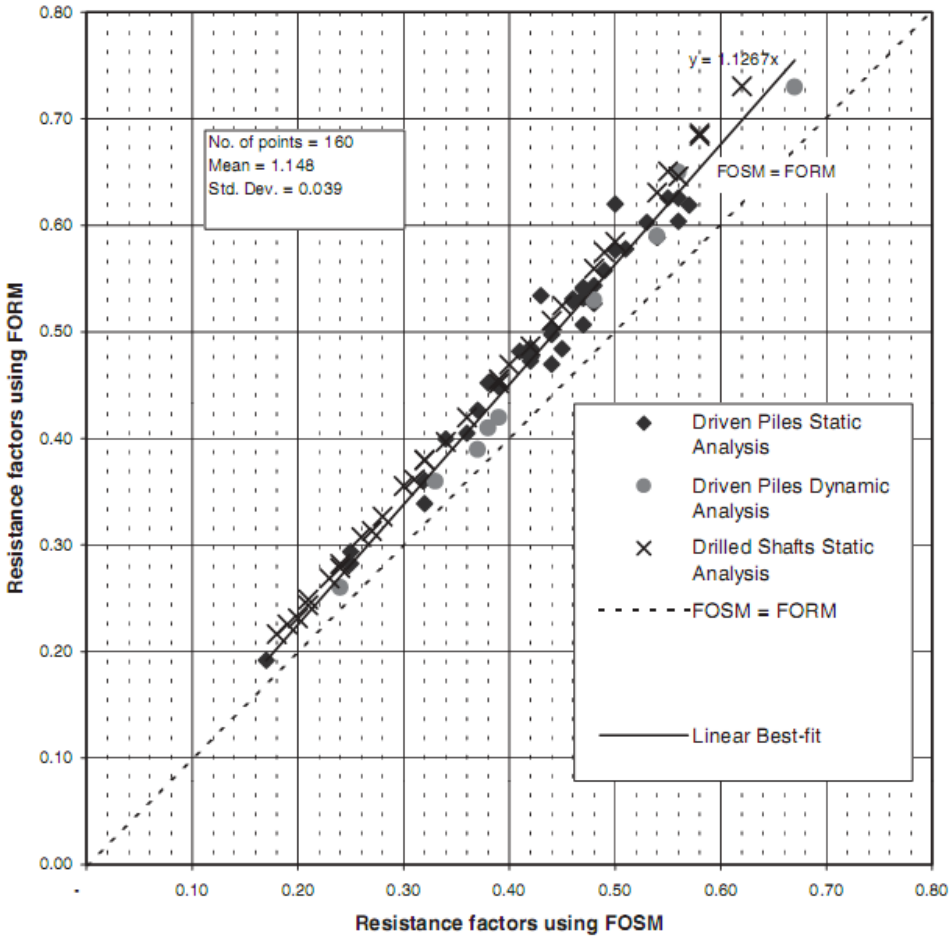

Figure 2-8. Comparison between Resistance Factors Obtained Using FOSM vs. FORM for a Target Reliability Index β_T = 2.33 (Paikowsky, 2004).

Note that Figure 2-8 shows that FORM results are 10% higher than FOSM.

2.5 SCOUR RISK STUDY

The definition of risk is the product of the probability of occurrence times the value of the consequences. The probability of exceedance is the probability that an event will be exceeded.

Figure 2-9 shows the risk in various fields of engineering (Baecher and Christian 2003).

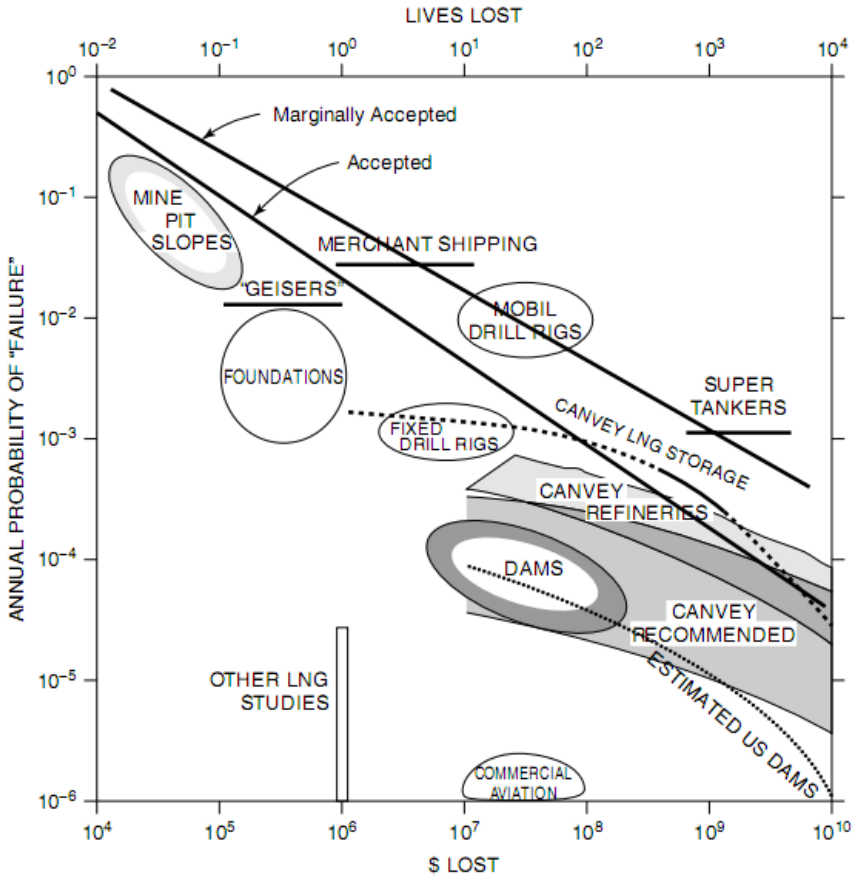

Figure 2-9. Risk in Various Fields of Engineering (Baecher and Christian 2003).

Figure 2-9 shows the annual probability of failure on the vertical axis and the value of the consequence on the horizontal axes. Two horizontal axes are presented: one for economic loss in dollars (lower axis) and one for fatalities (upper axis) (Briaud et al. 2012). The bubbles in the diagram show what risk is associated with various civil engineering structures.

The author gives a summary of the work from Elias (1994) and Stein and Sedmera (2006) in this section.

2.5.1 Elias (1994)

Elias (1994) proposed a method to calculate the risk of bridge scour, which was recorded in the FHWA Report "Strategies for Managing Unknown Bridge Foundations." In the report, a risk model was proposed to quantify the risk of bridges with unknown foundations by taking into consideration the probability of failure and consequences of potential failures. The model included the correction factors for bridge types and foundation types, which were subjective. Cost was calculated in three parts: rebuilding cost, running cost, and time cost:

$$C = C_1WL + C_2DAd + [C_3O(1-T/100) + C_4T/100]DAd/S \qquad (2\text{-}29)$$

where C_1 = unit rebuilding cost, W = bridge width, L = bridge length, C_2 = cost of running vehicle, D = detour length, A = Average Daily Traffic (ADT), d = duration of detour, C_3 = value of time per adult in passenger car, O = average occupancy rate, T = average daily truck traffic, percent of ADT, C_4 = value of time for truck, and S = average detour speed.

The probability of scour failure is estimated based on four parameters: waterway adequacy (NBI Item 71), functional classification (NBI Item 26), substructure condition (NBI Item 60), and channel protection (NBI Item 61). The probabilities of failure are a function of the scour vulnerability of a bridge and the overtopping frequency, i.e. PoF = f (scour vulnerability, overtopping frequency) (Briaud et al. 2012). Scour vulnerability, a rating of the potential for damage or failure due to a scour event, is a function of the Substructure Condition (NBI Item 60) and the Channel Protection Rating (NBI Item 61). Overtopping frequency is a measure of the likelihood of a scour producing event at the bridge. This is a function of the Waterway Adequacy (NBI Item 71) and the Functional Class (NBI Item 26).

In Elias (1994), the annual probability of overtopping was estimated using the return periods of floods specified for each overtopping frequency. The probability of failure for bridges had to be revised according to the bridge age before the final probability of failure was achieved.

2.5.2 Stein and Sedmera (2006)

HYRISK is a software application for estimating scour failure risks and bridge sites and calculator for planning scour countermeasures (Pearson et al. 2002). It was based on the FHWA Report "Strategies for Managing Unknown Bridge Foundations," and developed by the FHWA in 2002 (Pearson et al. 2002).

Stuart Stein and Karsten Sedmera at GKY & Associates applied the HYRISK method to quantify the risk of scour at bridges with unknown foundations in 2006 (Stein

and Sedmera 2006). The guidelines showed how to collect data, estimate risk of failure, and use risk in a structured approach to select an appropriate management plan.

In Stein and Sedmera (2006), the survey among 25 states showed that the annual average probability of bridge scour failure is 33/161,000=0.000205, or about 1 in 5000 per year. The results calculated from HYRISK turned out to be 60,511 failures per year. Due to the inconsistency between the survey and calculation results from HYRISK, the original HYRISK failure probabilities were scaled down to a level to match the survey results.

The cost of fatalities was incorporated in the equation of calculating the cost of bridge failure:

$$Cost = \{C_1 eWL\}_1 + \{[C_2(1-\frac{T}{100}) + C_3\frac{T}{100}]DAd + [C_4 O(1-\frac{T}{100}) + C_5\frac{T}{100}]\frac{DAd}{S}\}_2 + \{C_6 X\}_3 \qquad (2\text{-}30)$$

where, *Cost* = the total cost of bridge failure ($), C_1 = the unit building cost ($/m^2), e = the cost multiplier for early replacement based on Average Daily Traffic (ADT), W = the bridge width (m), L = the bridge length (m), C_2 = the cost of operating a running automobile ($0.28/km), T = the average daily truck traffic (percentage of ADT), D = the detour length (km), A = the Average Daily Traffic (ADT), d = the duration of the detour based on ADT (days), C_3 = the cost of operating a running truck ($0.808/km), C_4 = the value of time per adult in a passenger car ($/h), O = the average occupancy rate (1.63 usually), C_5 = the value of time for a truck ($22.01/h), S = the average detour speed (65km/h), C_6 = the cost for each life loss (typically $500,000), X = the number of fatalities from the failure. Note that the first part in the equation (subscript as 1) is the cost of replacing the bridge, the second part in the equation (subscript as 2) is the detour

cost and the time cost due to bridge failure, and the last term (subscript as 3) is the cost of fatalities. The factors in the equation are subjective, and should be adjusted using local experience.

The author of this dissertation uses the concept of calculating risk in the following sections.

3 THE PROBABILITY-BASED SCOUR DEPTH PREDICTION MODELS

3.1 INTRODUCTION

This section aims at establishing the probability-based pier scour depth prediction model. In order to achieve this goal, three pier scour databases were analyzed in this section, including the Landers and Mueller Database (1996), the TAMU Database (Gudavalli 1997; Li 2002), and the Froehlich Database (1988).

3.2 UNCERTAINTIES IN THE PREDICTION MODEL

There are two types of uncertainties in the reliability analysis: aleatory uncertainty and epistemic uncertainty. The aleatory uncertainty is inherent randomness, which means it is irreducible. It is the variability naturally inherent to a physical phenomenon, such as that in material properties and loads (Gardoni 2010). The epistemic uncertainty includes statistical uncertainty, measurement error, model error, and human error. The epistemic uncertainty is reducible. The statistical uncertainty arises in the process of estimating inherent variability and is due to lack of data. This type of uncertainty can be reduced through data accumulation. Measurement error can be reduced by improving the precision of equipment. Model error is the error inherent in the mathematical models used to describe complex physical phenomena. This type of error can be reduced by using more refined and more accurate models. Human error is the unavoidable process of making errors in the design, construction and operation of equipment by human beings. This type of error can be reduced by use of closer attention and management.

In the scour prediction model, there are several types of uncertainties involved, which will be described below.

3.2.1 Hydraulic Uncertainties

Hydraulic uncertainty includes the uncertainty of flow depth and velocity. The uncertainty is greater if there are fewer measureable data available. The hydraulic uncertainty is dependent on the accuracy of measurement and equipment. It is a type of epistemic uncertainty and therefore is reducible.

3.2.2 Hydrologic Uncertainties

Hydrologic uncertainty arises in the accuracy of prediction of Q100 and Q500. It is epistemic uncertainty and can be reduced by more accurate prediction models of floods. The hydrologic uncertainties can also be reduced by better analysis of flood history.

3.2.3 Geotechnical Uncertainties

Geotechnical uncertainty arises in the process of prediction or definition of erodibility, erosion rate and critical velocity. There are many factors affecting the erodibility of soils.

In cohesionless soils (sand and gravels), the critical shear stress has been empirically related to the mean grain size D_{50} (Briaud et al. 2001). For cohesionless soils, one flood is probably long enough to develop the maximum scour depth. For cohesive soils, the factors influencing erodibility are water content, soil unit weight, plasticity index, undrained shear strength, chemical composition and so on. For rock, the factors influencing erodibility are joint spacing, rock minerals and so on.

The determination of the erosion rate will cause uncertainty as well. It depends on the parameter of roughness, which is a very subjective estimate during the scour process.

In erosion studies, there are two very important parameters: critical shear stress, τ_c, and critical velocity, V_c. When the shear stress in the soil is lower than critical shear stress τ_c, the erosion does not occur. When the water velocity is lower than the critical velocity V_c, the erosion does not occur. The geotechnical uncertainty arises in the process of defining the critical velocity and critical shear stress.

3.2.4 Structural Uncertainties

Structural uncertainty exists in the process of identifying the geometry of bridge and angle of attack. However, usually we assume the geometry of bridge is a certain parameter. Therefore, in this model, the structural uncertainties are not included.

3.2.5 Model Uncertainty

The model uncertainty is the error inherent in the mathematical models used to describe complex physical phenomena. In this case, it means the error in the scour depth prediction model. In this dissertation, the author is using the mathematical model revised by Bolduc et al. (2008). The model uncertainty is included in two factors: θ and e. Here, θ is to account for the bias inherent in the model, while e is to account for the model error. The detailed explanation is shown in Section 3.4.

3.3 PIER SCOUR DATABASE SUMMARY

Databases are extremely important in reliability analysis. Databases have been collected and organized in Excel spreadsheets over the past 20 years at Texas A&M University. The pier scour databases include the following:

1. USGS Landers and Mueller Database (Landers and Mueller 1996): full scale field data on pier scour in the United States with approximately 380 points all in cohesionless soils.

2. TAMU Database (Gudavalli 1997; Li 2002): large scale laboratory data for pier scour in cohesive soils with a total of 73 data points.

3. Froehlich Database (Froehlich 1988): full scale field data for pier scour in both cohesionless and cohesive soils with about 79 points.

This section is the analysis of these three databases with the aim of establishing the probabilistic scour depth prediction model for these databases. This is also a necessary first step in the development of a load and resistance factor design for pile foundations subjected to scour.

3.3.1 Summary of USGS Landers and Mueller Database

The Landers and Mueller Database (1996) includes more than 380 field measurements of local scour around bridge piers, which were taken at 56 bridges in 14 states through cooperative agreements involving the U.S. Geological Survey, the Federal Highway Administration, and several state highway agencies. The Landers and Mueller database recorded the soil type, pier shape, pier length and width, skew angle, velocity and D_{50}, D_{84}, scour depth for each bridge case. Here, D_{50} is the diameter for 50% finer by weight,

and D_{84} is the diameter for 84% finer by weight. Both of the two parameters are important indices for soil. In most of the cases in the database, the soil is cohesionless. The pier shape varies from sharp, round, square to cylindrical. The flow velocity varies from 0.15 m/s to 4.5 m/s. The pier dimension changes from 0.3 m to 4.5 m.

3.3.2 Summary of TAMU Database

The TAMU database records the scour experiments mainly performed in clay by Gudavalli (1997) and Li (2002).

Gudavalli (1997) performed a series of flume experiments in the condition of different soils, water depths, flow velocities and pier sizes. In the experiments, the piers were cylindrical, with diameter of 25 mm, 75 mm, 150 mm, and 210 mm. Two types of flumes, 0.45 m and 1.5 m wide, were used in the experiments. Four types of soils were involved in the experiments: porcelain, bentonite, armstone, and sand. Porcelain is a low plasticity clay; bentonite is a high plasticity clay; armstone is a mixture of clay and sand; and sand is cohesionless (Gudavalli 1997; Oh 2009).

Li (2002) performed a series of flume tests to carry out a systematic investigation on complex pier scour and contraction scour. In the tests regarding pier scour, different attack angles, different pier dimensions, and two types of porcelain clay were considered to test the influence of those factoring in the process of prediction of scour depth.

The TAMU Database includes scour results out of 73 experiments in total. The database lists the water depth, the pier dimension, the attack angle, the water velocity, the pier spacing and the maximum scour depth for each experiment.

3.3.3 Summary of Froehlich Database

The Froehlich Database records the full scale field data for pier scour with 79 data points. The data were from published and unpublished sources collected by Froehlich in 1988, which recorded oversea and domestic scour measurement data between the years of 1950 to 1980 (Froehlich 1988). "The scour depths were measured using sonic depth finders, sounding weights, and sounding rods, and were considered to be reasonably accurate" (Froehlich 1988). The Froehlich Database recorded the scour depth, type of pier (round-nosed, sharp nosed, and square-nosed), pier dimension, approach flow velocity, attack angle, and the median diameter of soil for each case. Based on the D_{50} values of the soil materials in those scour cases, the Froehlich Database recorded both sand and clay.

3.4 METHODOLOGY

3.4.1 Proposed Probabilistic Model

The deterministic pier scour depth prediction model has been introduced in Section 2.2 in this dissertation.

The probabilistic model is developed based on the deterministic HEC-18 Sand and HEC-18 Clay models, with a factor θ to account for the bias inherent in the model and a factor e for the model error. The unbiased prediction is formulated as Equation 3-1:

$$Z_{\text{unb}} = \theta_{\text{unb}} Z_{\text{det}} e\,, \tag{3-1}$$

where Z_{unb} = the unbiased scour depth, θ_{unb} = the unknown correction factor needed for the predicted value to match the measured value on the average, Z_{det} = the deterministic scour depth prediction according to HEC-18 Sand or HEC-18 Clay, e = the error term which describes the error in the model. Following Gardoni et al. (2002) and Bolduc el al. (2008), a logarithmic transformation of Equation 3-2 is shown as:

$$\ln Z_{unb} = \ln \theta_{unb} + \ln Z_{det} + \ln e \tag{3-2}$$

$$\text{or, } \zeta(\mathbf{x}, \boldsymbol{\Theta}) = \Gamma_{\zeta} + \hat{\zeta}(\mathbf{x}) + \sigma_{\zeta}\varepsilon \tag{3-3}$$

where $\zeta = \ln(Z_{unb})$, $\mathbf{x}$ is the data set of predicted scour depth Z_{det}, $\Theta = (\Gamma_{\zeta}, \sigma_{\zeta})$ = the set of unknown model parameters, with $\Gamma_{\zeta} = \ln(\theta_{unb})$, $\hat{\zeta} = \ln(Z_{det})$, $\sigma_{\zeta}\varepsilon$ = the random error in the model, ε = a random variable with zero mean and unit variance, and σ_{ζ} = the standard deviation of the model error. The logarithmic transformation is used to satisfy the following assumptions (a) the model variance σ_{ζ}^2 is independent of $\mathbf{x}$ (homoskedasticity assumption), and (b) ε has the normal distribution (normality assumption). The maximum likelihood and Bayesian approach are used to determine $\Theta = (\Gamma_{\zeta}, \sigma_{\zeta})$.

The probabilistic value Z_{prob} is related to the deterministic value Z_{det} by the following:

$$Z_{prob} = \theta(PoE) \cdot Z_{det} \tag{3-4}$$

where θ(PoE) = a correction factor, function of the probability of exceedance. Note that $\theta(0.5)$ is θ_{unb}, the bias factor to apply to the mean predicted value to obtain the mean measured value.

3.4.2 Check of the Model-QQ Plot

In order to check whether the mathematical model proposed in this section is adaptable for our case, the Quantile-Quantile plot is done based on the Landers and Mueller Database using HEC18 Clay method.

In the proposed probabilistic model (Equation 3-2), ε is following normal distribution with zero mean and unit variance. Rewrite Equation 3-2 to obtain Equation 3-5:

$$\frac{\ln Z_{\text{measured}} - \ln Z_{\text{det}} - \ln \theta_{\text{unb}}}{\sigma_{\zeta}} = \varepsilon \tag{3-5}$$

Hence, if the model is reasonable, the left side of Equation 3-5 should follow normal distribution. Note that ε is a random variable with zero mean and unit variance. Figure 3-1 shows the Q-Q plot of the sample data (left side of Equation 3-5) versus standard normal data using the Landers and Mueller Database.

Figure 3-1 shows that the sample data follows normal distribution. Therefore, the proposed probabilistic model works perfectly in this case.

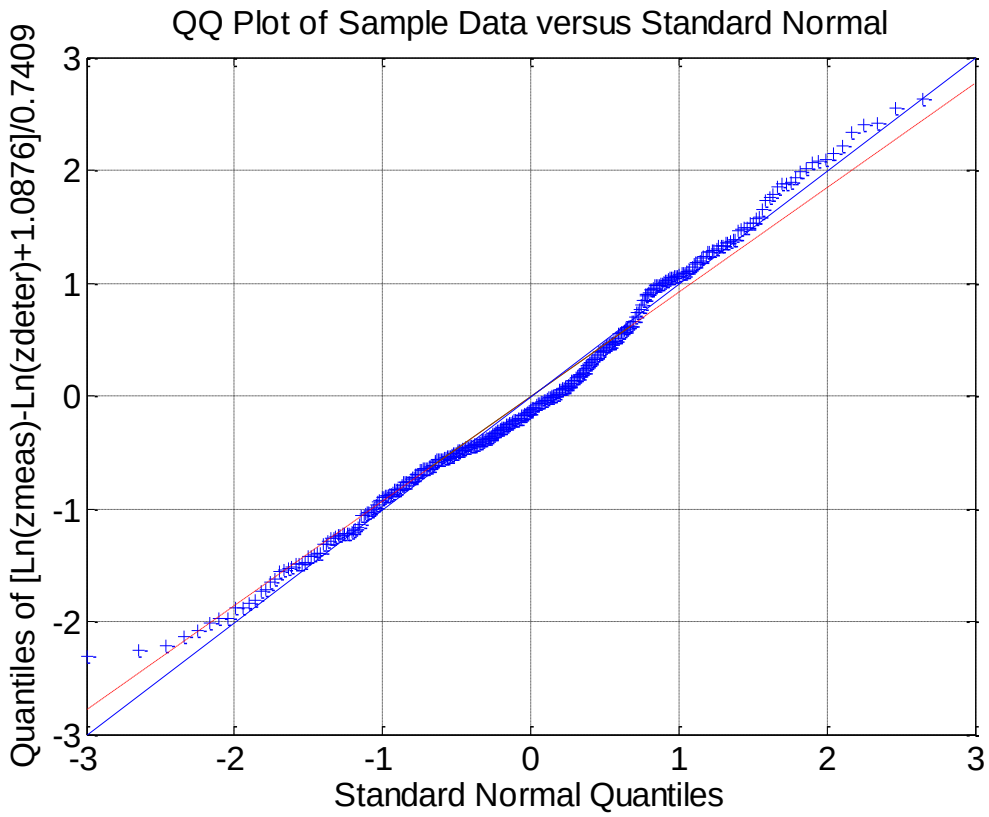

Figure 3-1. Q-Q Plot of Sample Data vs. Standard Normal Data Using Landers-Mueller Database.

Figure 3-2 shows the Q-Q plot of the sample data considering measurement errors versus stand normal data. It shows that the sample data considering measurement errors also follows normal distribution. Therefore, the proposed model is reasonable.

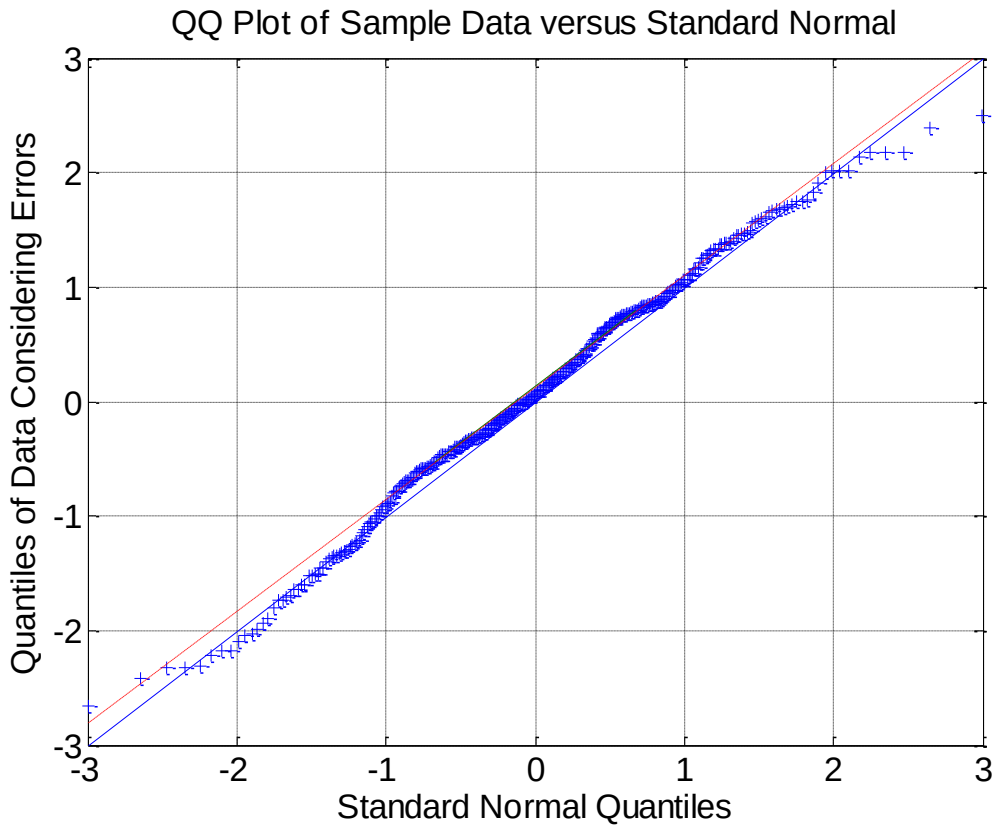

Figure 3-2. Q-Q Plot of Sample Data Considering Measurement Errors vs. Standard Normal Data Using Landers-Mueller Database.

3.4.3 Other Comparable Models

The author also tested whether the current model is the best one. Here the Landers and Mueller Database was used in the HEC-18 Clay method. This section will show four different probabilistic models in order to compare them with the proposed model.

3.4.3.1 Model 1: Two Parameters

Instead of using Equation 3-3, the author used Equation 3-6 to compute the probabilistic scour depth.

$$\zeta_1(\mathbf{x},\boldsymbol{\Theta}) = \theta_{\zeta 1} + \theta_{\zeta 2}\zeta(\mathbf{x}) + \sigma_\zeta \varepsilon \tag{3-6}$$

where $\theta_{\zeta 1}$ and $\theta_{\zeta 2}$ are the two parameters that needed to be calibrated in the model. Definitions of other parameters are the same as before. $\zeta_1 = \ln(Z_{unb})$, $\hat{\zeta} = \ln(Z_{det})$, $\sigma_\zeta \varepsilon$ = the random error in the model, ε = a random variable with zero mean and unit variance, and σ_ζ = the standard deviation of the model error.

The unbiased scour depth could be calculated using:

$$Z_{unb} = e^{\theta_{\zeta 1}} \cdot Z_{det}{}^{\theta_{\zeta 2}} \tag{3-7}$$

Table 3-1 shows the results of Model 1.

Table 3-1. Statistical Parameter Results of Model 1.

Parameter	Mean	Standard Deviation	Correlation Coefficient		
			$\theta_{\zeta 1}$	$\theta_{\zeta 2}$	σ_ζ
$\theta_{\zeta 1}$	-0.6031	0.0415	1	-0.4596	0.0173
$\theta_{\zeta 2}$	0.3942	0.0373	-0.4596	1	-0.0207
σ_ζ	0.6799	0.0255	0.0173	-0.0207	1

Hence, the unbiased pier scour depth is calculated below:

$$\zeta_1 = -0.6031 + 0.3942\xi + 0.6799\varepsilon \tag{3-8}$$

$$Z_{unb} = e^{\theta_{\zeta 1}} \cdot Z_{det}{}^{\theta_{\zeta 2}} = e^{-0.6031} \cdot Z_{det}{}^{0.3942} = 0.5471 \cdot Z_{det}{}^{0.3942} \tag{3-9}$$

Figure 3-3 shows the deterministic prediction of maximum scour depth for HEC-18 Clay using Landers-Mueller Database.

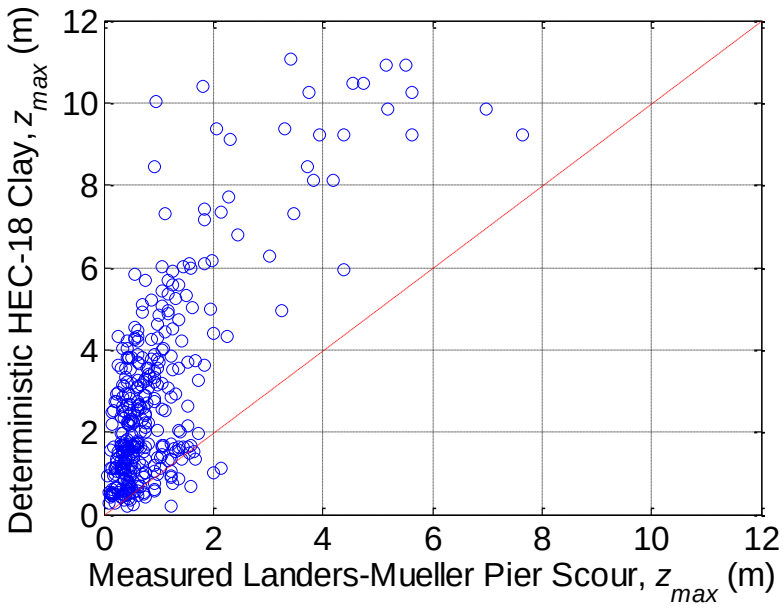

Figure 3-3. Deterministic Prediction of Maximum Scour Depth for HEC-18 Clay Using Landers-Mueller Database.

Figure 3-4 shows the unbiased prediction of maximum scour depth for HEC-18 Clay using Landers-Mueller Database based on the results from Model 1. From the results, we can conclude that the Mean Absolute Percentage Error (MAPE) is 62.4%. The unbiased value is "bent" towards X axis. It shows that Model 1 is not ideal for our problem.

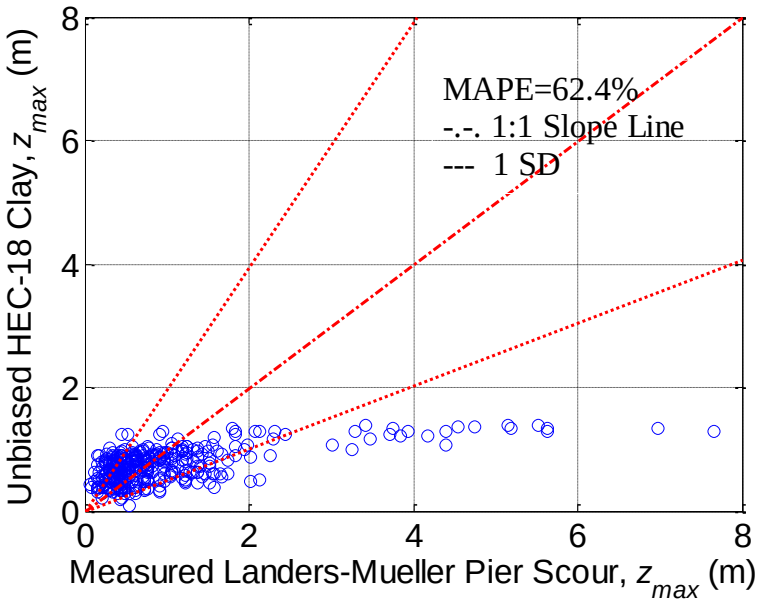

Figure 3-4. Unbiased Prediction of Maximum Scour Depth for HEC-18 Clay Using Landers-Mueller Database (1 SD, 68% confidence interval)-Model 1.

3.4.3.2 Model 2: Two Parameter

Instead of using Equation 3-3, the author used Equation 3-10 to compute the probabilistic scour depth.

$$\zeta_2(\mathbf{x},\boldsymbol{\Theta}) = \theta_{\zeta 1} + \ln(Z_{\text{det}} + \theta_{\zeta 2}) + \sigma_\zeta \varepsilon \tag{3-10}$$

where $\theta_{\zeta 1}$ and $\theta_{\zeta 2}$ are the two parameters needed to be calibrated in the model. Definitions of other parameters are the same as previous sections. $\zeta_2 = \ln(Z_{\text{unb}})$, $\sigma_\zeta \varepsilon$ = the random error in the model, ε = a random variable with zero mean and unit variance, and σ_ζ = the standard deviation of the model error.

The unbiased scour depth could be calculated using:

$$Z_{\text{unb}} = e^{\theta_{\zeta 1}} \cdot (Z_{\text{det}} + \theta_{\zeta 2}) \tag{3-11}$$

Table 3-2 shows the results of Model 2.

Table 3-2. Statistical Parameter Results of Model 2.

Parameter	Mean	Standard Deviation	Correlation Coefficient		
			$\theta_{\zeta 1}$	$\theta_{\zeta 2}$	σ_{ζ}
$\theta_{\zeta 1}$	-1.8397	0.0880	1	-0.9228	0.0084
$\theta_{\zeta 2}$	2.0835	0.3177	-0.9228	1	-0.0028
σ_{ζ}	0.6347	0.0234	0.0084	-0.0028	1

Hence, the unbiased pier scour depth is calculated below:

$$\zeta_2 = -1.8397 + \ln(Z_{\text{det}} + 2.0835) + 0.6347\varepsilon \tag{3-12}$$

$$Z_{\text{unb}} = e^{\theta_{\zeta 1}} \cdot (Z_{\text{det}} + \theta_{\zeta 2}) = e^{-1.8397} \cdot (Z_{\text{det}} + 2.0835) = 0.1589 \cdot (Z_{\text{det}} + 2.0835) \tag{3-13}$$

Figure 3-5 shows the unbiased prediction of maximum scour depth for HEC-18 Clay using Landers-Mueller Database based on the results from Model 2. From the results, we can conclude that the Mean Absolute Percentage Error (MAPE) is 58.1%. The unbiased value is "bent" towards X axis. It shows that Model 2 is not ideal for our problem.

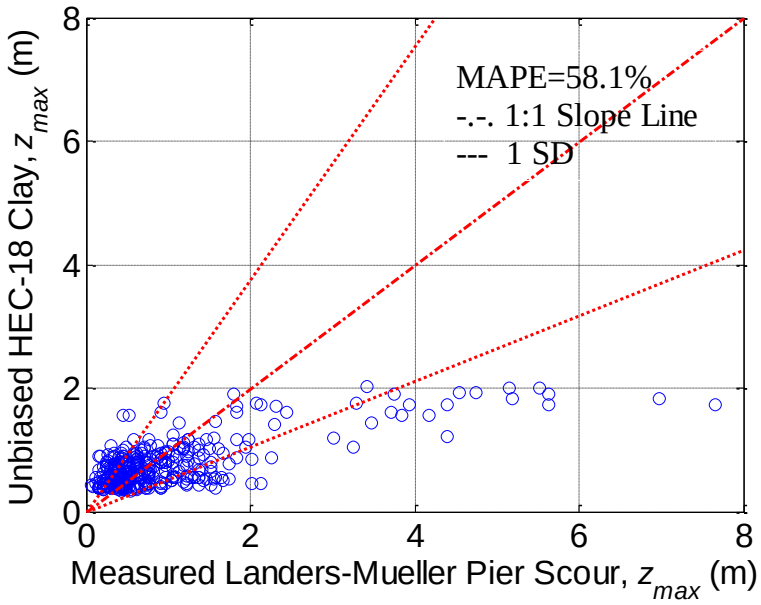

Figure 3-5. Unbiased Prediction of Maximum Scour Depth for HEC-18 Clay Using Landers-Mueller Database (1 SD, 68% confidence interval)-Model 2.

3.4.3.3 Model 3: One Parameter

Instead of using Equation 3-3, the author used Equation 3-14 to compute the probabilistic scour depth.

$$\zeta_3(\mathbf{x},\boldsymbol{\Theta}) = \ln(Z_{\text{det}} + \theta_{\zeta 1}) + \sigma_\zeta \varepsilon \tag{3-14}$$

where $\theta_{\zeta 1}$ is the parameter needed to be calibrated in the model. Definitions of other parameters are the same as before. ζ_3 = ln(Z_{unb}), $\sigma_\zeta \varepsilon$ = the random error in the model, ε = a random variable with zero mean and unit variance, and σ_ζ = the standard deviation of the model error.

The unbiased scour depth could be calculated using:

$$Z_{\text{unb}} = Z_{\text{det}} + \theta_{\zeta 1} \tag{3-15}$$

Table 3-3 shows the results of Model 3.

Table 3-3. Statistical Parameter Results of Model 3.

Parameter	Mean	Standard Deviation	Correlation Coefficient	
			$\theta_{\zeta 1}$	σ_ζ
$\theta_{\zeta 1}$	0.0243	0.0183	1	0.0512
σ_ζ	1.3085	0.0468	0.0512	1

Hence, the unbiased pier scour depth is calculated below:

$$\zeta_3 = \ln(Z_{\text{det}} + 0.0243) + 1.3085\varepsilon \tag{3-16}$$

$$Z_{\text{unb}} = Z_{\text{det}} + \theta_{\zeta 1} = Z_{\text{det}} + 0.0243 \tag{3-17}$$

Figure 3-6 shows the unbiased prediction of maximum scour depth for the HEC-18 Clay using the Landers-Mueller Database based on the results from Model 3. From the results, we can conclude that the Mean Absolute Percentage Error (MAPE) is 279%. Considering the huge error, it is not a good model either.

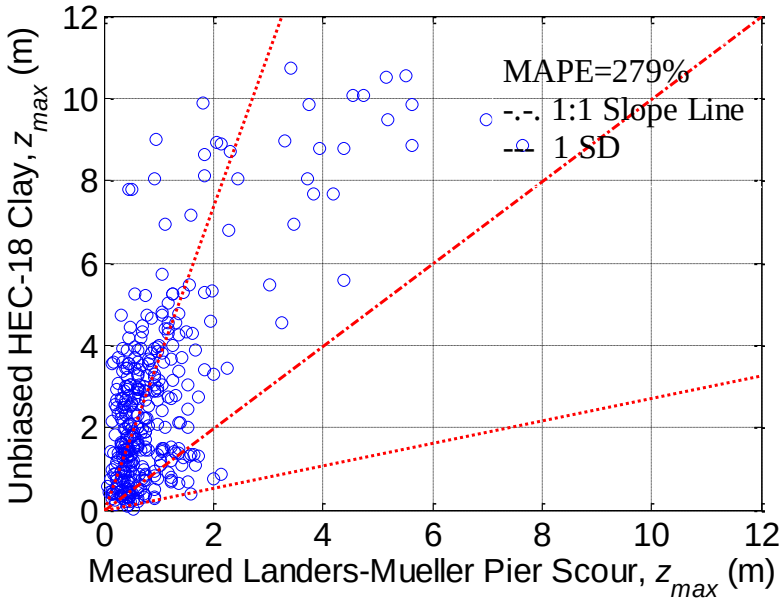

Figure 3-6. Unbiased Prediction of Maximum Scour Depth for HEC-18 Clay Using Landers-Mueller Database (1 SD, 68% confidence interval)-Model 3.

3.4.3.4 Model 4: Three Parameters

Instead of using Equation 3-3, the author used Equation 3-18 to compute the probabilistic scour depth.

$$\zeta_4(\mathbf{x},\boldsymbol{\Theta}) = \theta_{\zeta 1} + \theta_{\zeta 2} \cdot \ln(Z_{\text{det}} + \theta_{\zeta 3}) + \sigma_\zeta \varepsilon \tag{3-18}$$

where $\theta_{\zeta 1}, \theta_{\zeta 2}, \theta_{\zeta 3}$ are the parameters needed to be calibrated in the model. Definitions of other parameters are the same as before. ζ_4 = $\ln(Z_{\text{unb}})$, $\sigma_\zeta \varepsilon$ = the random error in the model, ε = a random variable with zero mean and unit variance, and σ_ζ = the standard deviation of the model error.

The unbiased scour depth could be calculated using:

$$Z_{\text{unb}} = e^{\theta_{\zeta 1}} \cdot (Z_{\text{det}} + \theta_{\zeta 3})^{\theta_{\zeta 2}} \tag{3-19}$$

Table 3-4 shows the results of Model 4.

Table 3-4. Statistical Parameter Results of Model 4.

Parameter	Mean	Standard Deviation	Correlation Coefficient			
			$\theta_{\zeta 1}$	$\theta_{\zeta 2}$	$\theta_{\zeta 3}$	σ_{ζ}
$\theta_{\zeta 1}$	-153.5156	6.8426	1	-0.9802	-0.5972	-0.2852
$\theta_{\zeta 2}$	30.9172	1.2243	-0.9802	1	0.4265	0.2726
$\theta_{\zeta 3}$	138.9562	6.8292	-0.5972	0.4265	1	0.2006
σ_{ζ}	0.6076	0.0004	-0.2852	0.2726	0.2006	1

Hence, the unbiased pier scour depth is calculated below:

$$\zeta_4 = -153.5156 + 30.9172 \times \ln(Z_{\text{det}} + 138.9562) + 0.6076\varepsilon \tag{3-20}$$

$$\begin{aligned} Z_{\text{unb}} &= e^{\theta_{\zeta 1}} \cdot (Z_{\text{det}} + \theta_{\zeta 3})^{\theta_{\zeta 2}} = e^{-153.5156} \cdot (Z_{\text{det}} + 138.9562)^{30.9172} \\ &= 2.1e-67 \cdot (Z_{\text{det}} + 138.9562)^{30.9172} \end{aligned} \tag{3-21}$$

Figure 3-7 shows the unbiased prediction of maximum scour depth for the HEC-18 Clay using the Landers-Mueller Database based on the results from Model 4. From the results, we can conclude that the Mean Absolute Percentage Error (MAPE) is 55.2%. Comparing it with the results obtained from the proposed probabilistic model, the author found that the MAPE was not improved significantly in Model 4, and Model 4 was much more complicated than the proposed model.

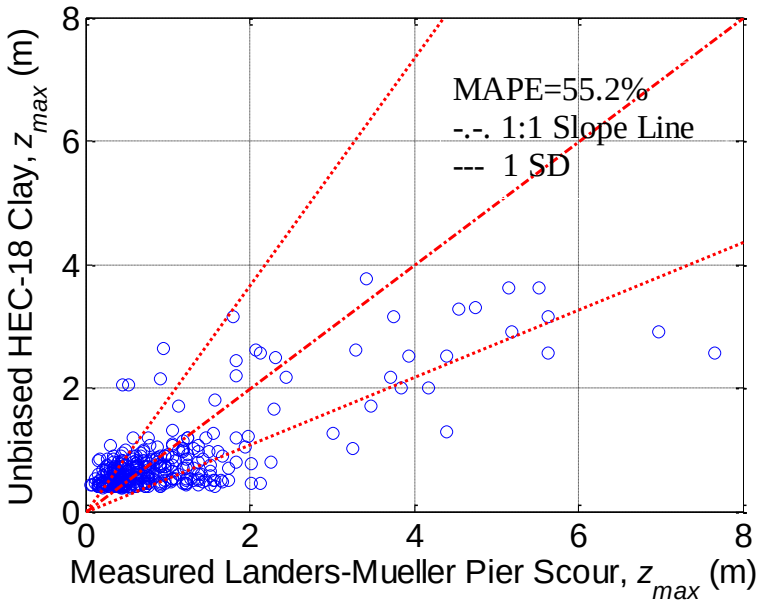

Figure 3-7. Unbiased Prediction of Maximum Scour Depth for HEC-18 Clay Using Landers-Mueller Database (1 SD, 68% confidence interval)-Model 4.

Based on the study in this section, the author concluded that the proposed probabilistic scour depth prediction model is the best fit for our problem. The author also computed the probabilistic scour depth using the HEC-18 Sand method for the Landers-Mueller Database based on the previous four models, and obtained the same conclusion that the proposed model is the best.

3.4.4 Conclusion on the Model Study

According to the analysis in Section 3.4.1, 3.4.2, and 3.4.3, the proposed probabilistic model is the best one. The following section will provide the calculation results for the three databases using the proposed model.

3.5 PROBABILISTIC MODEL RESULTS

3.5.1 Probabilistic Model Results of Landers and Mueller Database

3.5.1.1 Full Database

The whole database was analyzed below to find the probabilistic scour depth parameters. Note that since the Landers-Mueller database is cohesionless soils, in the HEC-18 Clay deterministic scour depth equation, the critical velocity was calculated using Equation 3-22 (Briaud 2008).

$$V_c(\text{m/s}) = 0.35(D_{50}(\text{mm}))^{0.45} \tag{3-22}$$

where, V_c = critical velocity (in the unit of m/s), and D_{50} = the diameter for 50% finer by weight (in the unit of mm).

Since critical velocity is very crucial during the scour depth prediction process, the author did research on this part. As mentioned in Section 2.1.3, the critical velocity can be calculated using:

$$V_c(\text{m/s}) = \sqrt{\frac{\tau_c(\text{Pa})y_1(\text{m})^{0.33}}{\rho(\text{kg/m}^3)g(\text{N/kg})n^2}} \tag{3-23}$$

where V_c = critical velocity (in the unit of m/s), τ_c = critical shear stress (in the unit of N/m^2), y_1 = water depth (in the unit of m), ρ = density of water (in the unit of kg/m^3), g = acceleration due to gravity (in the unit of N/kg), n = Manning's coefficient. Critical shear stress can be calculated using:

$$\tau_c = K_s(\gamma_s - \gamma)D_{50} \tag{3-24}$$

where K_s = Shields coefficient, varying from 0.03 to 0.1 (Vanoni 1975), γ_s = the unit weight of soil particles, γ = the unit weight of water, D_{50} = the diameter for 50% finer by weight. Note that the exact equation to compute Shield's coefficient is shown below:

$$K_s = 0.105(S^*)^{-0.3} + 0.045(e^{-35(S^*)^{-0.59}}) \tag{3-25}$$

$$S^* = \frac{\sqrt{1.65 \times 9810 \times D_{50}{}^3}}{10^{-6}} \tag{3-26}$$

Note that D_{50} is in the unit of m.

Figure 3-8 shows the computed critical shear stress based on Shield's Coefficient versus mean grain size. Regression analysis shows that the critical shear stress is following a linear relationship with D_{50}:

$$\tau_c(\mathrm{N/m^2}) = 0.745 D_{50}(\mathrm{mm}) \tag{3-27}$$

Note that Briaud et al. (1999) performed EFA tests on different sands, and found out a relative simple relationship between critical shear stress τ_c and D_{50}:

$$\tau_c(\mathrm{N/m^2}) \simeq D_{50}(\mathrm{mm}) \tag{3-28}$$

It is concluded that for the Landers-Mueller Database, the critical shear stress (Pa) is about ¾ of the median grain size (mm).

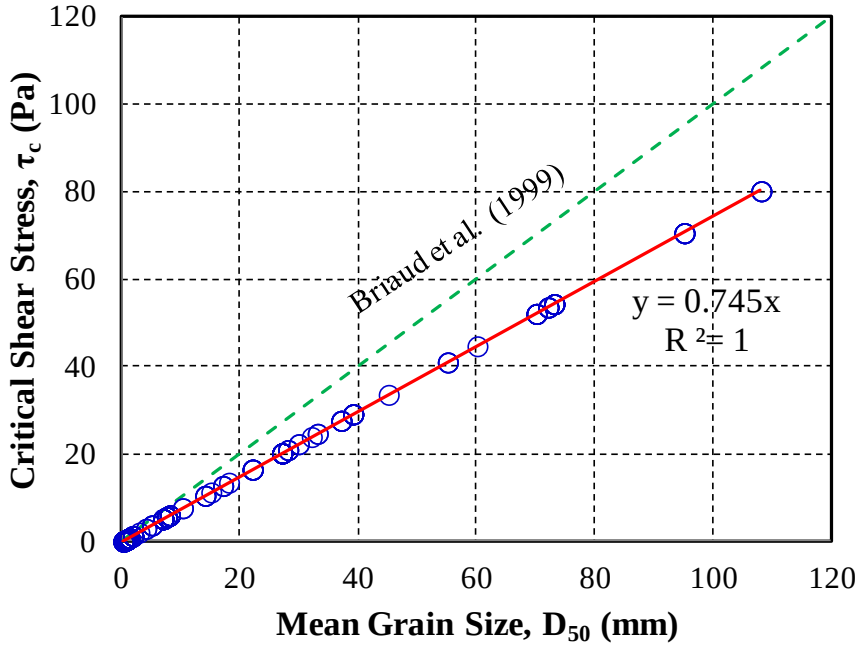

Figure 3-8. Critical Shear Stress Computed Using Shields Coefficient vs. Mean Grain Size-Landers-Mueller Database.

Figure 3-9 shows the relationship between critical velocity and mean grain size for the Landers-Mueller Database using different approaches. Note that the critical velocity computed using Equation 3-23 is marked as V_{c*} in the figure, while the critical velocity computed using Equation 3-22 is marked as V_{c_Briaud}.

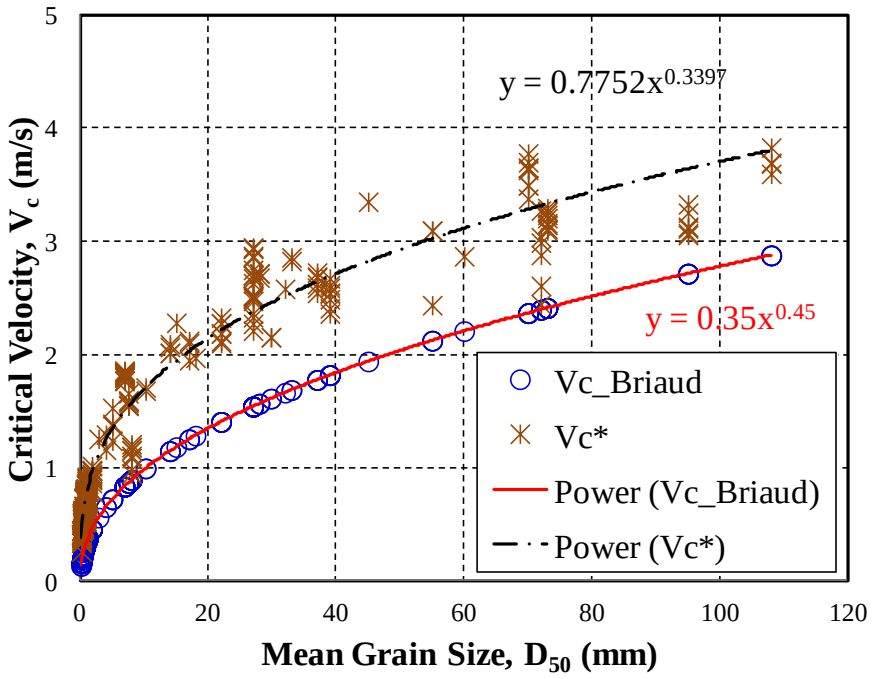

Figure 3-9. Critical Velocity vs. Mean Grain Size for Landers-Mueller Database Using Different Approaches.

The regression analysis based on V_{c*} shows the relationship between critical velocity and D_{50} :

$$V_c(\text{m/s}) = 0.78(D_{50}(\text{mm}))^{0.34} \tag{3-29}$$

Figure 3-10 shows the deterministic maximum scour depth using V_{c_Briaud} and V_{c*} respectively in the HEC-18 Clay method. From the figure, we can see that the scour depth computed using V_{c_Briaud} is more conservative. Hence, in the following analysis, the deterministic scour depth for the Landers-Mueller Database is computed using $V_{c\_Briaud.}$

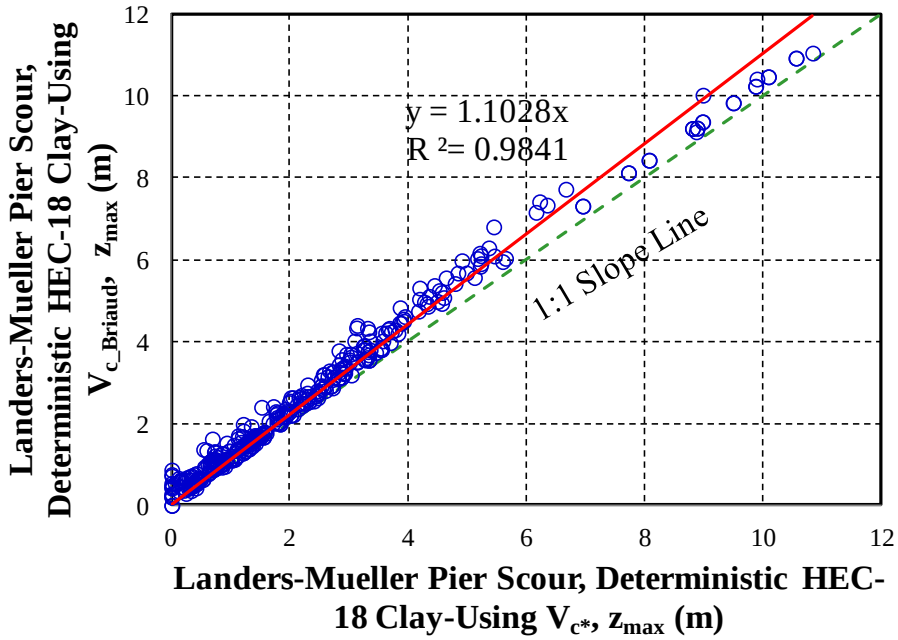

Figure 3-10. Deterministic HEC-18 Clay Using V_{c_Briaud} and V_{c*} Respectively-Landers-Mueller Database.

HEC-18 Sand Results

Table 3-5 shows the calculated parameters for the HEC-18 Sand method using the Bayesian approach, which will be the inputs for the LRFD calibration of bridge scour depth.

Table 3-5. HEC-18 Sand Calculated Results for Landers-Mueller Database.

Parameter	Mean	Standard Deviation	Correlation Coefficient	
			Γ_ζ	σ_ζ
Γ_ζ	-1.1778	0.0210	1	-0.3658
σ_ζ	0.6787	0.0273	-0.3658	1

Figure 3-11 shows the scatter plot of the predicted maximum scour depth using HEC-18 Sand against the measured scour depth in the Landers-Mueller Database. From Figure 3-11, it is clear that the prediction is conservative as most of the data points are above the 1:1 line. The correction factor θ_{unb} is determined to be 0.307; in other words, on the average the prediction is about 3.3 times larger than the measured values. The regression analysis result is shown in Figure 3-12. It can be seen that the HEC-18 Sand method is about 3.26 times larger than the measured value.

Figure 3-13 is obtained from Figure 3-11 after applying the correction factor 0.307 to all predicted values. As such, Figure 3-13 shows the unbiased prediction of maximum scour depth for the HEC-18 Sand and for the Landers and Mueller Database. The Mean Absolute Percentage Error (MAPE) is 63.6%, which means the absolute difference percentage between the unbiased prediction value and the measured scour depth is 63.5%. The R-square value is 0.30. Note that Figure 3-13 also shows the 1 Standard Deviation (68% confidence interval) and the 1.96 Standard Deviation (95% confidence interval) beyond the 1:1 slope line. Most of the unbiased data fall into the 95% confidence interval.

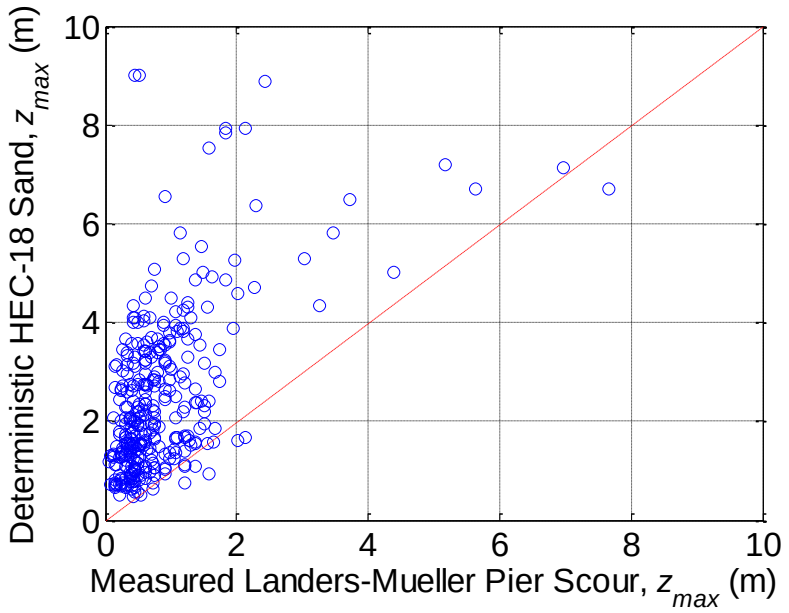

Figure 3-11. Deterministic Prediction of Maximum Scour Depth for HEC-18 Sand Using Landers-Mueller Database.

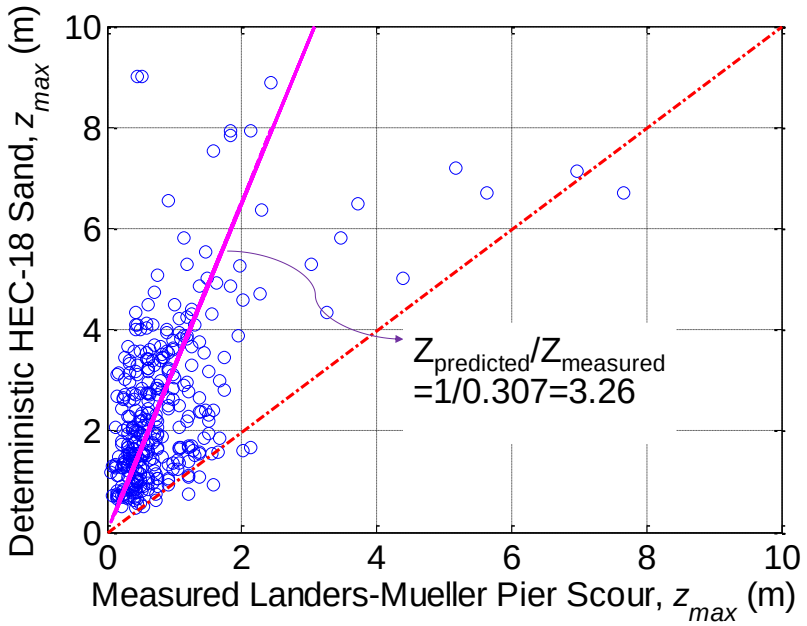

Figure 3-12. Deterministic Prediction of Maximum Scour Depth for HEC-18 Sand Using Landers-Mueller Database-Regression Analysis.

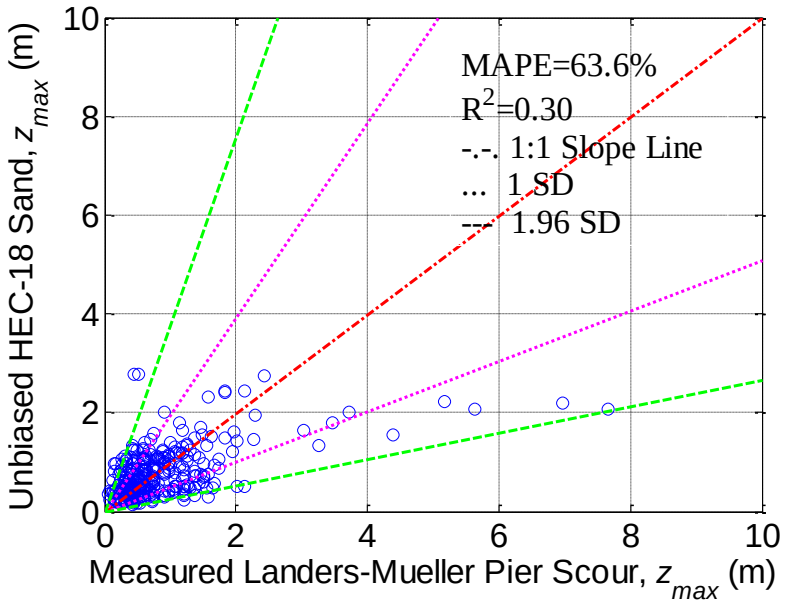

Figure 3-13. Unbiased Prediction of Maximum Scour Depth for HEC-18 Sand Using Landers-Mueller Database (1 SD, 68% Confidence Interval; 1.96 SD, 95% Confidence Interval).

The probability of exceedance (PoE) curve can be obtained following the procedure below.

1. Multiply the deterministic scour depth values by a factor θ_z. Note that θ_z is changing from 0 till 4.

2. Count the number of data points representing the probabilistic scour depth below 1:1 slope line.

3. Compute the percentage of the data points falling below 1:1 slope line, which represents PoE.

4. Plot the PoE versus factor θ_z.

Figure 3-14 and Figure 3-15 show the PoE curve for the HEC-18 Sand using the Landers-Mueller Database in an algorithm scale and a semilog scale respectively.

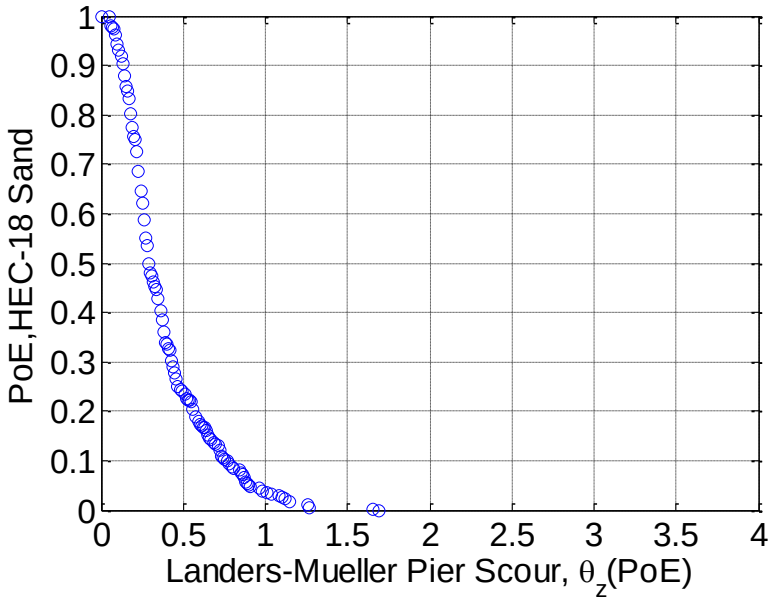

Figure 3-14. Probability of Exceedance Curve for HEC-18 Sand Using Landers-Mueller Database in an Algorithm Scale.

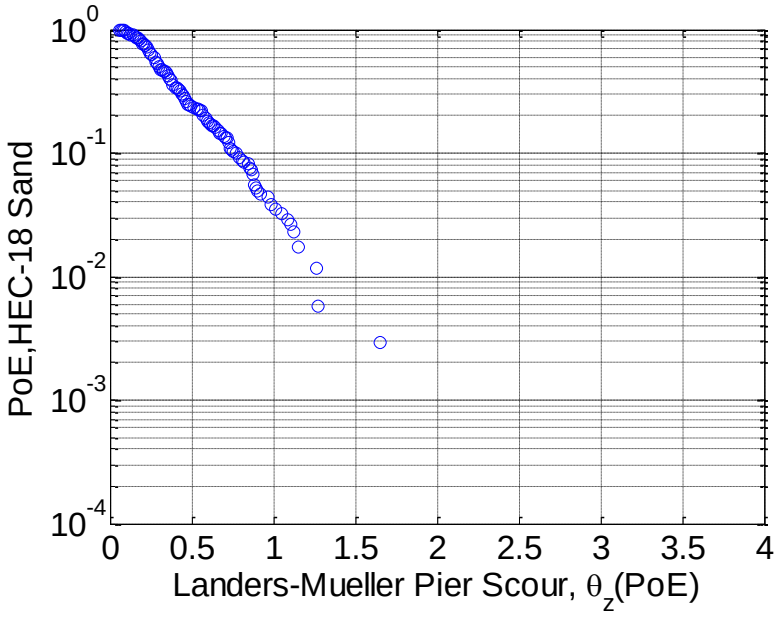

Figure 3-15. Probability of Exceedance Curve for HEC-18 Sand Using Landers-Mueller Database in a Semilog Scale.

Figure 3-16 shows the PoE curve with extension line for the HEC-18 Sand using the Landers-Mueller Database in a semilog scale. From the figure, it can be seen that there is 3.3% of chances that the HEC-18 Sand prediction is smaller than the measured depth. The target value will be explained in Section 4.

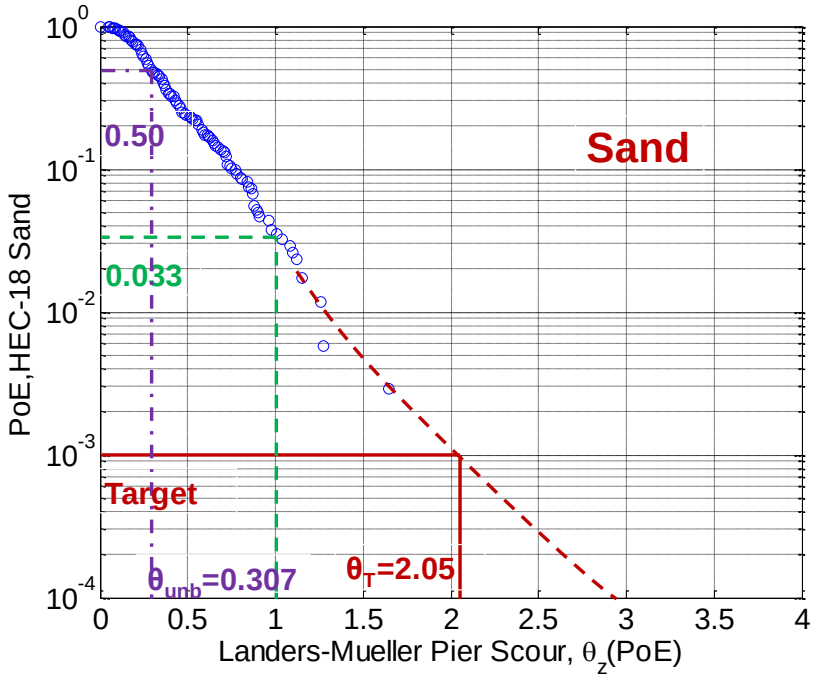

Figure 3-16. Probability of Exceedance Curve with Extension for HEC-18 Sand Using Landers-Mueller Database in a Semilog Scale.

Measurement Error

If measurement error is considered, the value of σ_ζ will be reduced. For the HEC-18 Sand method, Equation 3-30 shows the logarithm transformation of deterministic scour depth. Equations 3-31 and 3-32 show the derivative of $\ln(Z_{det})$ respective to V_1 and y_1.

$$\begin{aligned}\hat{\zeta} &= \ln[2.0\times K_1\times K_2\times K_3\times K_4\times a^{0.65}\times y_1^{0.35}\times(\frac{V_1}{\sqrt{g\times y_1}})^{0.43}]\\ &= \ln[2.0\times K_1\times K_2\times K_3\times K_4\times a^{0.65}\times V_1^{0.43}\times y_1^{0.35-\frac{0.43}{2}}\times g^{-\frac{0.43}{2}}]\\ &= \ln[2.0\times K_1\times K_2\times K_3\times K_4\times a^{0.65}\times V_1^{0.43}\times y_1^{0.135}\times g^{-0.215}]\end{aligned} \quad (3\text{-}30)$$

$$\frac{\partial \hat{\zeta}}{\partial V_1} = \frac{\partial \ln(2K_1K_2K_3K_4 g^{-0.215} a^{0.65} V_1^{0.43} y_1^{0.135})}{\partial V_1}$$
$$= \frac{\partial(\ln(2K_1K_2K_3K_4 g^{-0.215} a^{0.65}) + 0.43\ln(V_1) + 0.135\ln(y_1))}{\partial V_1} \quad (3\text{-}31)$$
$$= \frac{0.43}{V_1}$$

$$\frac{\partial \hat{\zeta}}{\partial y_1} = \frac{\partial \ln(2K_1K_2K_3K_4 g^{-0.215} a^{0.65} V_1^{0.43} y_1^{0.135})}{\partial y_1}$$
$$= \frac{\partial(\ln(2K_1K_2K_3K_4 g^{-0.215} a^{0.65}) + 0.43\ln(V_1) + 0.135\ln(y_1))}{\partial y_1} \quad (3\text{-}32)$$
$$= \frac{0.135}{y_1}$$

Table 3-6 shows the estimated statistical parameters for those variables. The updated results considering measurement errors are shown in Table 3-7.

Table 3-6. Estimated Statistical Parameters for Variables-HEC-18 Sand.

Parameters	y_1	V_1	$\zeta_{measured}$
Standard Deviation	0.3m	0.5 m/s, 0.3 m/s	1.8 Ln(m)

Table 3-7. Updated σ Considering Measurement Errors-HEC-18 Sand.

σ of V_1	0.5 m/s	0.3 m/s
Γ_ζ	-1.4117	-1.3988
σ	0.0000	0.0000

From Table 3-7, we get the conclusion that all the uncertainties have been considered in the measurement error, while the model error is 0.

HEC-18 Clay Results

Table 3-8 shows the calculated parameters for the HEC-18 Clay method, which will be the inputs for the LRFD calibration of bridge scour depth.

Table 3-8. HEC-18 Clay Calculated Results for Landers-Mueller Database.

Parameter	Mean	Standard Deviation	Correlation Coefficient	
			Γ_ζ	σ_ζ
Γ_ζ	-1.0870	0.0253	1	-0.3583
σ_ζ	0.7450	0.0294	-0.3583	1

Figure 3-17 shows the scatter plot of the predicted maximum scour depth using HEC-18 Clay against the measured scour depth in the Landers-Mueller Database. From Figure 3-17, it is clear that the prediction is conservative as most of the data points are above the 1:1 line. The correction factor θ_{unb} is determined to be 0.337; in other words, on the average the prediction is about 3 times larger than the measured values. Figure 3-18 shows the regression analysis results. It can be seen that the HEC-18 Clay method is about 3 times larger than the measured value.

Figure 3-19 is obtained from Figure 3-17 after applying the correction factor 0.337 to all predicted values. As such, Figure 3-19 shows the unbiased prediction of maximum scour depth for the HEC-18 Clay and for the Landers and Mueller Database. The Mean Absolute Percentage Error (MAPE) is 66.2%, which means that the error on any prediction is on average + or – 66.2%. For example if the prediction is 10 m, then the measured value is expected to be between 3.4 m and 16.6 m. The R-square value is

0.56. Note that Figure 3-19 also shows the 1 Standard Deviation (68% confidence interval) and the 1.96 Standard Deviation (95% confidence interval) beyond the 1:1 slope line. Most of the unbiased data fall into the 95% confidence interval.

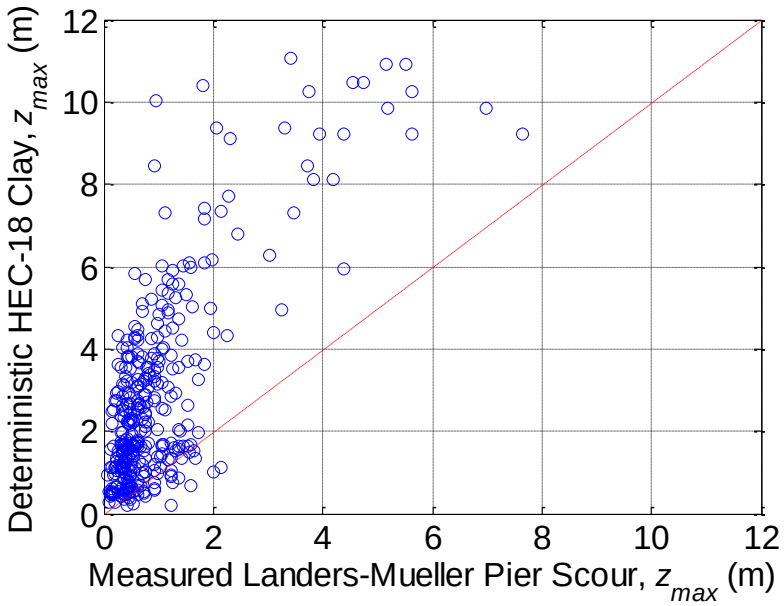

Figure 3-17. Deterministic Prediction of Maximum Scour Depth for HEC-18 Clay Using Landers-Mueller Database.

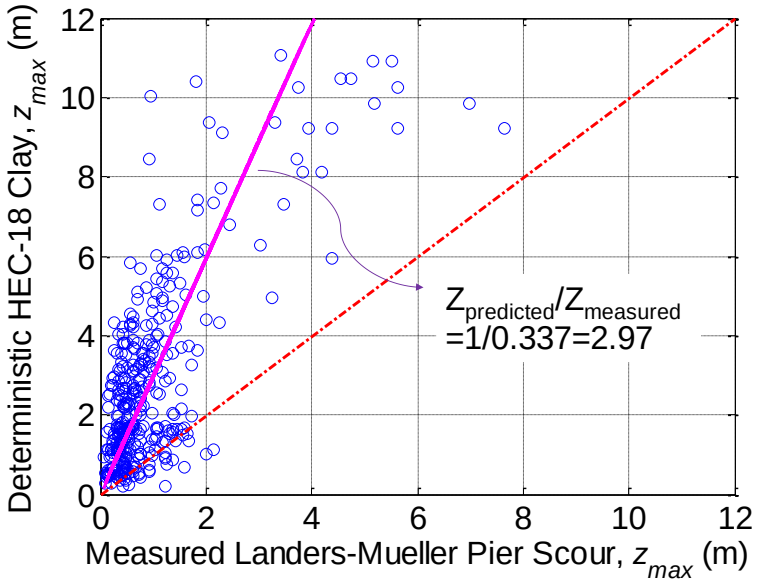

Figure 3-18. Deterministic Prediction of Maximum Scour Depth for HEC-18 Clay Using Landers-Mueller Database-Regression Analysis.

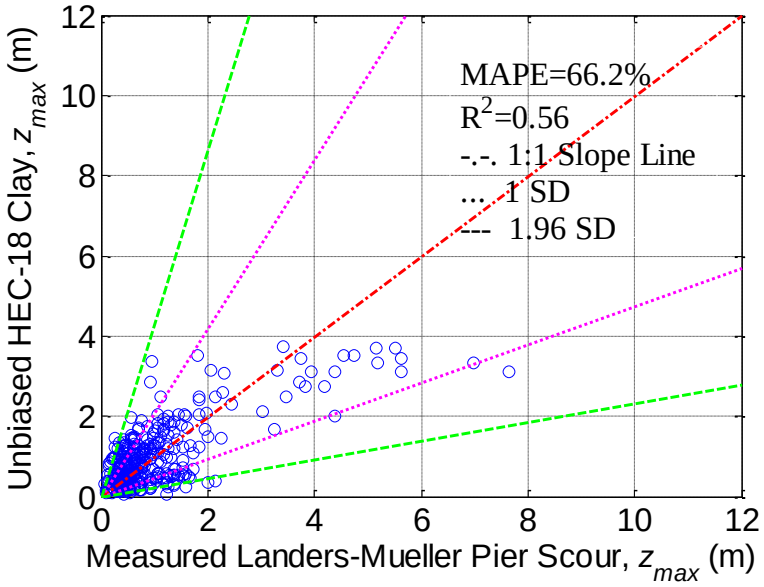

Figure 3-19. Unbiased Prediction of Maximum Scour Depth for HEC-18 Clay Using Landers-Mueller Database (1 SD, 68% Confidence Interval; 1.96 SD, 95% Confidence Interval).

PoE results are shown in Figure 3-20 and Figure 3-21.

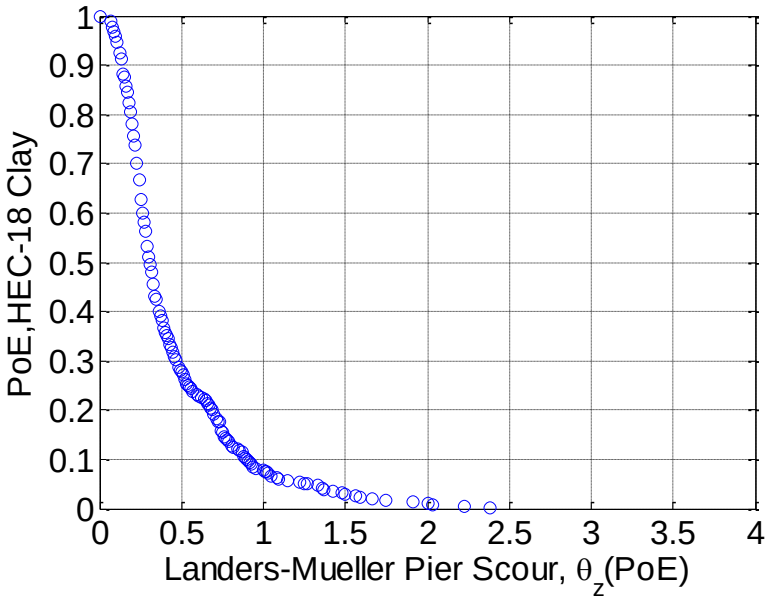

Figure 3-20. Probability of Exceedance Curve for HEC-18 Clay Using Landers-Mueller Database in an Algorithm Scale.

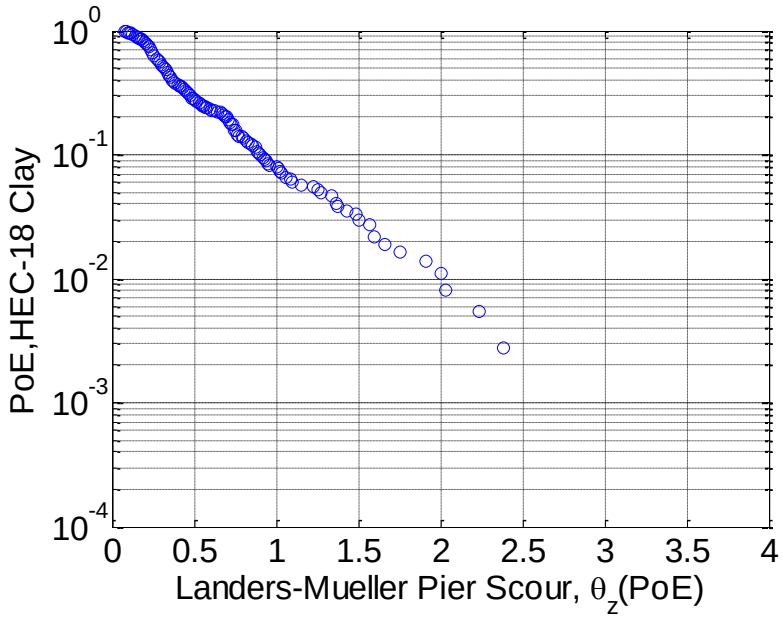

Figure 3-21. Probability of Exceedance Curve for HEC-18 Clay Using Landers-Mueller Database in a Semilog Scale.

Figure 3-22 shows the PoE curve with extension line for the HEC-18 Clay using the Landers-Mueller Database in a semilog scale. From the figure, it can be seen that there is a 7% chance that the HEC-18 Clay prediction is smaller than the measured depth. The target value will be explained in Section 4.

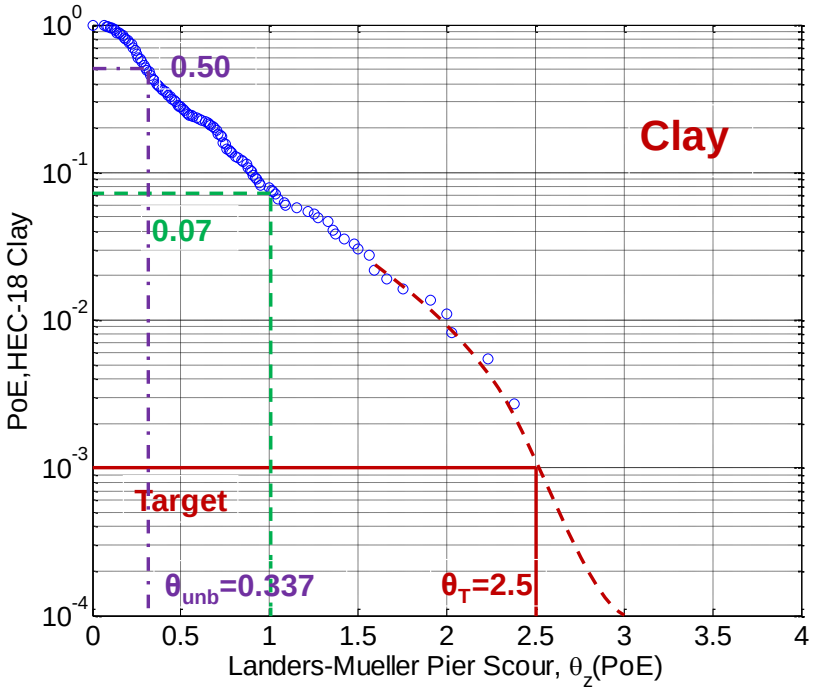

Figure 3-22. Probability of Exceedance Curve with Extension for HEC-18 Clay Using Landers-Mueller Database in a Semilog Scale.

Measurement Error

If measurement error is considered, the value of σ_ζ will be reduced. For the HEC-18 Clay method, Equation 3-33 shows the logarithm transformation of deterministic scour depth. Equations 3-34 and 3-35 show the derivative of $\ln(Z_{det})$ respective to V_1 and y_1.

$$\hat{\zeta} = \ln[2.2 \times a' \times K_w \times K_1 \times K_{sp} \times (2.6\frac{V_1}{\sqrt{ga'}} - \frac{V_c}{\sqrt{ga'}})^{0.7}] \qquad (3\text{-}33)$$

$$\frac{\partial \hat{\zeta}}{\partial V_1} = \frac{2.2a'K_1K_wK_{sp} \times 0.7 \times (2.6\frac{V_1}{\sqrt{ga'}} - \frac{V_c}{\sqrt{ga'}})^{-0.3} \times \frac{2.6}{\sqrt{ga'}}}{2.2a'K_1K_wK_{sp}(2.6\frac{V_1}{\sqrt{ga'}} - \frac{V_c}{\sqrt{ga'}})^{0.7}}$$

$$= \frac{\frac{1.82}{\sqrt{ga'}}}{(2.6\frac{V_1}{\sqrt{ga'}} - \frac{V_c}{\sqrt{ga'}})} = \frac{0.581}{\sqrt{a'} \times (0.83\frac{V_1}{\sqrt{a'}} - 0.319\frac{V_c}{\sqrt{a'}})} \quad (3\text{-}34)$$

$$\frac{\partial \hat{\zeta}}{\partial V_c} = \frac{2.2a'K_1K_wK_{sp} \times 0.7 \times (2.6\frac{V_1}{\sqrt{ga'}} - \frac{V_c}{\sqrt{ga'}})^{-0.3} \times \frac{(-1)}{\sqrt{ga'}}}{2.2a'K_1K_wK_{sp}(2.6\frac{V_1}{\sqrt{ga'}} - \frac{V_c}{\sqrt{ga'}})^{0.7}}$$

$$= \frac{\frac{(-0.7)}{\sqrt{ga'}}}{(2.6\frac{V_1}{\sqrt{ga'}} - \frac{V_c}{\sqrt{ga'}})} = \frac{-0.223}{\sqrt{a'} \times (0.83\frac{V_1}{\sqrt{a'}} - 0.319\frac{V_c}{\sqrt{a'}})} \quad (3\text{-}35)$$

Here, y_1 is incorporated into the parameter K_w (Equations 3-36 and 3-37):

$$K_w = \begin{cases} 0.89(\frac{y_1}{a'})^{0.33} & , for\ \frac{y_1}{a'} < 1.43 \\ 1.0 & , else \end{cases} \quad (3\text{-}36)$$

$$\frac{\partial \hat{\zeta}}{\partial y_1} = \begin{cases} \frac{\partial(0.33(\ln(y_1) - \ln(a')))}{\partial y_1} = \frac{0.33}{y_1} & , for\ \frac{y_1}{a'} < 1.43 \\ 0 & , else \end{cases} \quad (3\text{-}37)$$

Assume Z_{max} follows the lognormal distribution with 0.1m mean and 0.5m standard deviation (i.e. $\mu_Z = 0.1\,m$, $\sigma_Z = 0.5\,m$).

Given:

$f_Z(z) = \frac{1}{\sqrt{2\pi}(\zeta z)} e^{-\frac{(\ln(z)-\lambda)^2}{2\zeta^2}}$, Note that ζ and λ are the parameters for lognormal distribution here.

$$\zeta^2 = \ln(1+(\frac{\sigma_Z}{\mu_Z})^2) = \ln(1+(\frac{0.5}{0.1})^2) = 3.26,$$

$$\zeta = 1.8,$$

$$\lambda = \ln \mu_Z - \tfrac{1}{2}\zeta^2 = \ln 0.1 - \tfrac{1}{2}\times 3.26 = -3.9,$$

Therefore,

$$Z_{\max} \sim LN(-3.9, 3.26)$$

Estimated standard deviation for y_1, V_1, V_c, and $\zeta_{measured}$ is shown in Table 3-9. Table 3-10 shows the results.

Table 3-9. Estimated Statistical Parameters for Variables-HEC-18 Clay.

Parameters	y_1	V_1	V_c	$\zeta_{measured}$
Standard Deviation	0.3m	0.5 m/s, 0.3 m/s	0.23m/s	1.8 Ln(m)

Table 3-10. Updated σ Considering Measurement Error-HEC-18 Clay.

σ of V_1	0.5 m/s	0.3 m/s
Γ_ζ	-1.3786	-1.3288
σ	0.0000	0.0000

From Table 3-10, we get the conclusion that all the uncertainties have been considered in the measurement error, while the model error is 0.

3.5.1.2 Scour Depth > 2m

Usually people do not worry too much when the scour depth is less than 2m; hence the author analyzed the Landers-Mueller Database when the measured scour depth is larger than 2m.

HEC-18 Sand Results

Figure 3-23 shows the regression analysis for the HEC-18 Sand method for the Landers-Mueller Database when the measured scour depth is larger than 2m. It can be seen that the HEC-18 Sand method is about 1.74 times larger than the measured value.

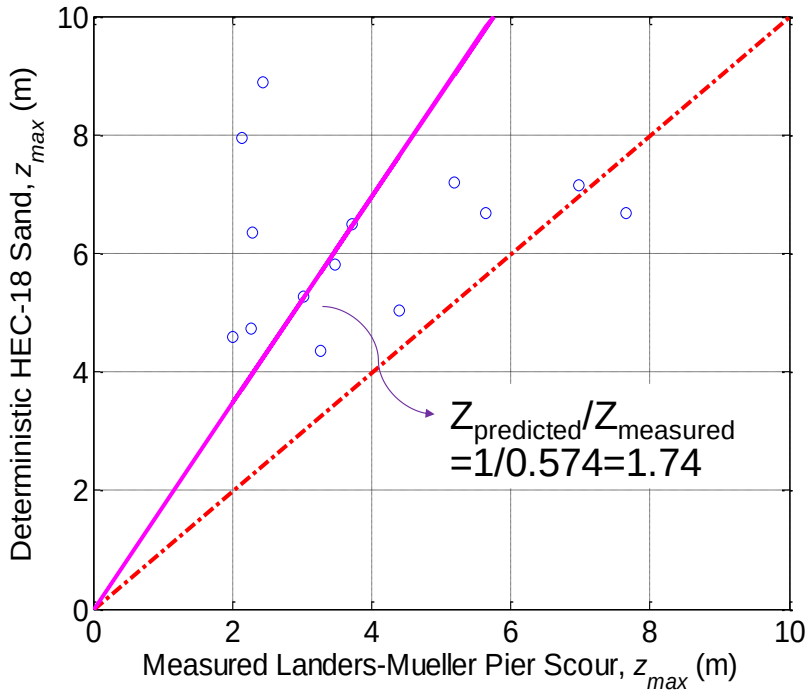

Figure 3-23. Deterministic Prediction of Maximum Scour Depth for HEC-18 Sand Using Landers-Mueller Database - $Z_{measured}$ > 2m, Regression Analysis.

The PoE curve is shown in Figure 3-24. From the figure, it can be seen that there is an 8% chance that the HEC-18 Sand prediction is smaller than the measured depth when the measured scour depth is larger than 2m. The target value will be explained in Section 4. Figure 3-25 shows the PoE curve by 1m and 2m as well.

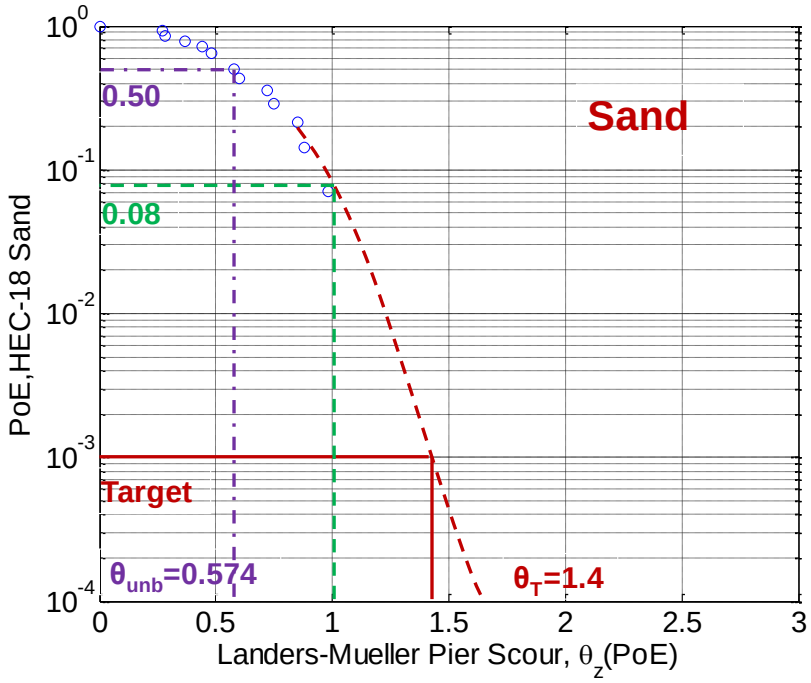

Figure 3-24. Probability of Exceedance Curve with Extension for HEC-18 Sand Using Landers-Mueller Database in a Semilog Scale - $Z_{measured}$ > 2m.

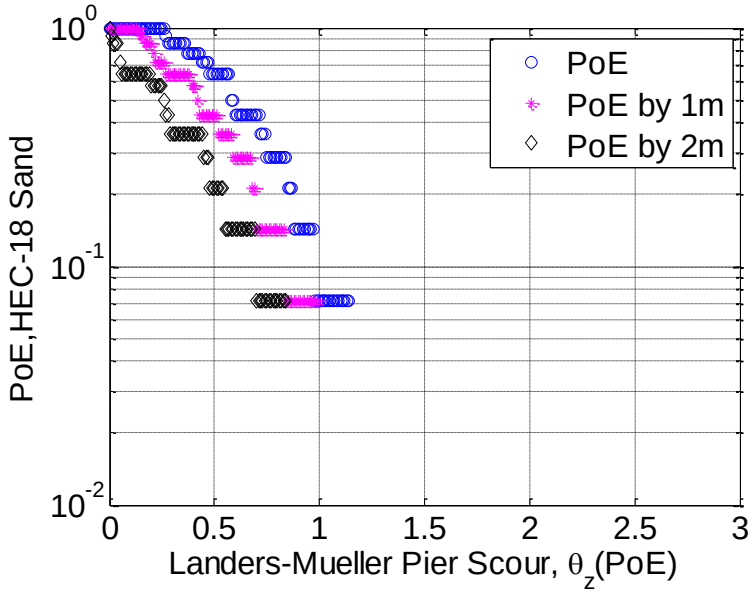

Figure 3-25. PoE Curve for HEC-18 Sand ($Z_{measured}$ > 2m).

HEC-18 Clay Results

Figure 3-26 shows the regression analysis for the HEC-18 Clay method for the Landers-Mueller Database when the measured scour depth is larger than 2m. It can be seen that the HEC-18 Clay method is about 2.22 times larger than the measured value.

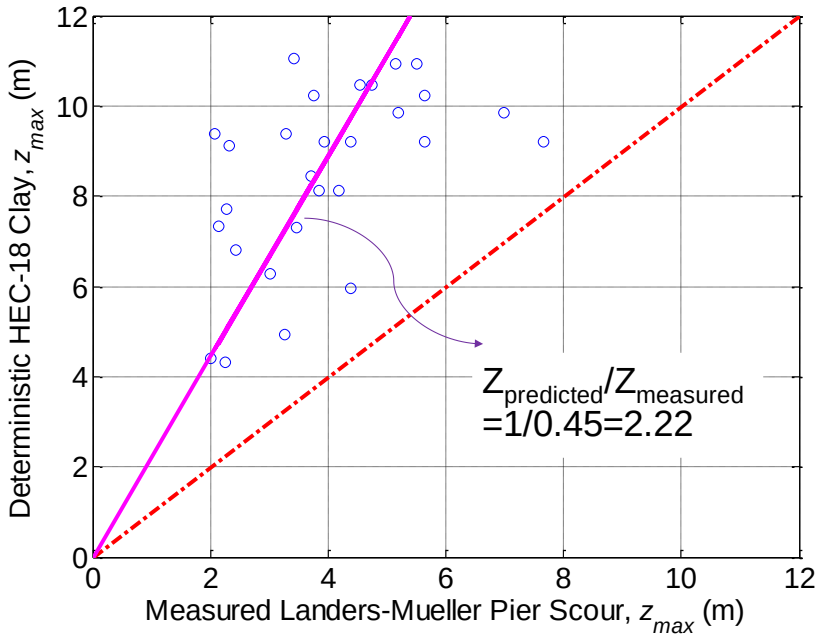

Figure 3-26. Deterministic Prediction of Maximum Scour Depth for HEC-18 Clay Using Landers-Mueller Database - $Z_{measured}$ > 2m, Regression Analysis.

The PoE curve is shown in Figure 3-27. From the figure, it can be seen that there is a 0.7% chance that the HEC-18 Clay prediction is smaller than the measured depth when the measured scour depth is larger than 2m. The target value will be explained in Section 4. Figure 3-28 shows the PoE curve by 1m and 2m as well.

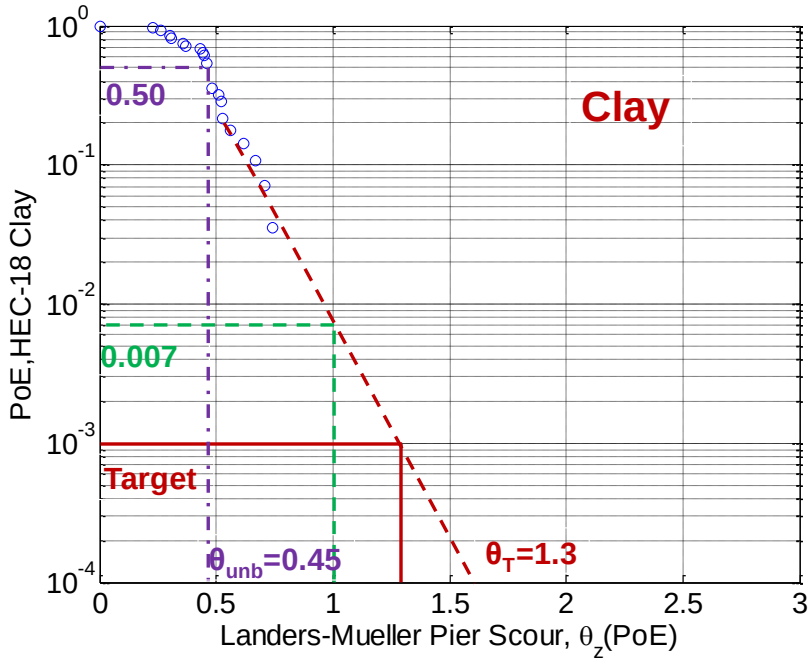

Figure 3-27. Probability of Exceedance Curve with Extension for HEC-18 Clay Using Landers-Mueller Database in a Semilog Scale - $Z_{measured}$ > 2m.

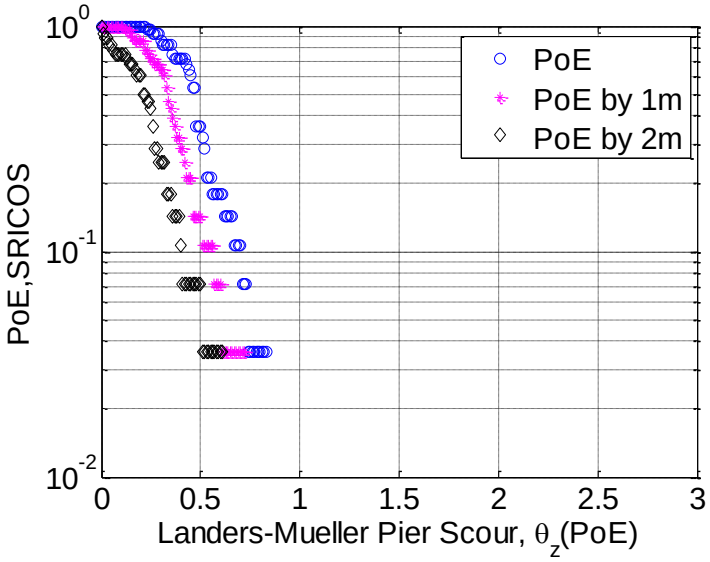

Figure 3-28. PoE Curve for HEC-18 Clay ($Z_{measured}$ > 2m).

3.5.1.3 Scour Depth < 2m

Correspondingly, the data related to $Z_{measured}$ > 2m are also analyzed.

HEC-18 Sand Results

Figure 3-29 shows the regression analysis for the HEC-18 Sand method for the Landers-Mueller Database when the measured scour depth is less than 2m. It can be seen that the HEC-18 Sand method is about 3.3 times larger than the measured value.

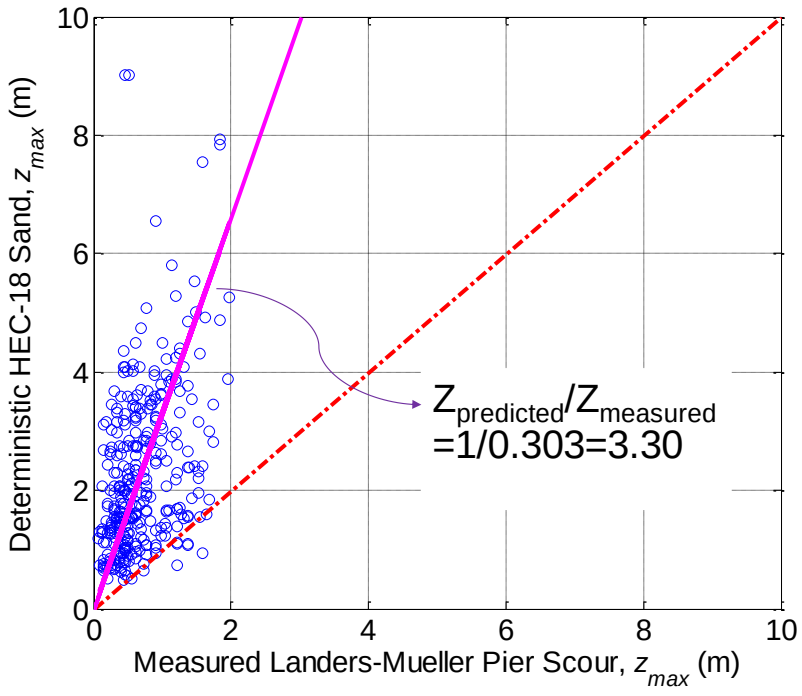

Figure 3-29. Deterministic Prediction of Maximum Scour Depth for HEC-18 Sand Using Landers-Mueller Database - $Z_{measured}$ < 2m, Regression Analysis.

The PoE curve is shown in Figure 3-30. From the figure, it can be seen that there is a 2.6% chance that the HEC-18 Sand prediction is smaller than the measured depth

when the measured scour depth is less than 2m. The target value will be explained in Section 4.

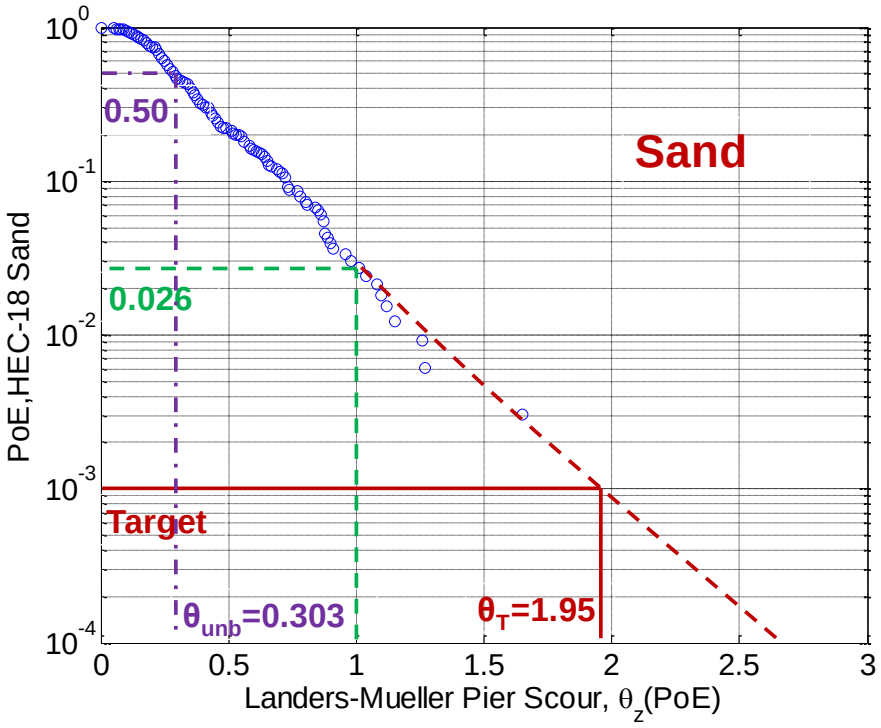

Figure 3-30. Probability of Exceedance Curve with Extension for HEC-18 Sand Using Landers-Mueller Database in a Semilog Scale - $Z_{measured}$ < 2m.

HEC-18 Clay Results

Figure 3-31 shows the regression analysis for the HEC-18 Clay method for the Landers-Mueller Database when the measured scour depth is less than 2m. It can be seen that the HEC-18 Clay method is about 3.08 times larger than the measured value.

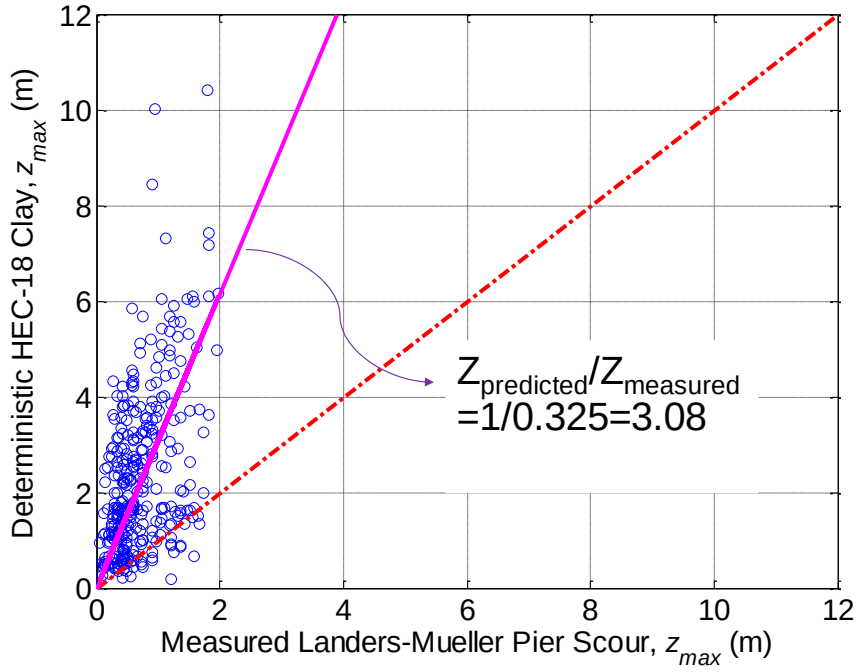

Figure 3-31. Deterministic Prediction of Maximum Scour Depth for HEC-18 Clay Using Landers-Mueller Database - $Z_{measured}$ < 2m, Regression Analysis.

The PoE curve is shown in Figure 3-32. From the figure, it can be seen that there is a 7% chance that the HEC-18 Clay prediction is smaller than the measured depth when the measured scour depth is smaller than 2m. The target value will be explained in Section 4.

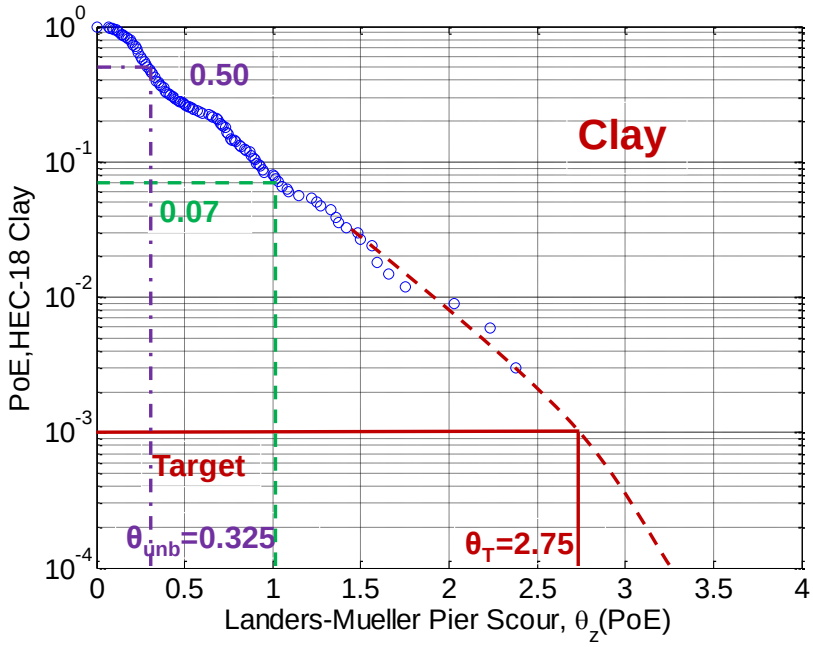

Figure 3-32. Probability of Exceedance Curve with Extension for HEC-18 Clay Using Landers-Mueller Database in a Semilog Scale - $Z_{measured}$ < 2m.

3.5.2 Probabilistic Model Results of TAMU Database

The whole database was analyzed below to find the probabilistic scour depth parameters. Note that Gudavalli and Li performed the experiments mainly in previously defined cohesive soils, and the critical shear stress τ_c was obtained for each type of soil before the experiments by running EFA tests. When using the HEC-18 Clay method to calculate the deterministic scour depth, the critical velocity was calculated using Equation 3-23 (Richardson and Davis, 2001).

Note the Manning's coefficient *n* was assumed to be 0.014.

3.5.2.1 HEC18 Sand Results

Table 3-11 shows the calculated parameters for the HEC-18 Sand method using the Bayesian approach, which will be the inputs for the LRFD calibration of bridge scour depth.

Table 3-11. HEC-18 Sand Calculated Results for TAMU Database.

Parameter	Mean	Standard Deviation	Correlation Coefficient	
			Γ_ζ	σ_ζ
Γ_ζ	-0.4376	0.0468	1	-0.3365
σ_ζ	0.4757	0.0374	-0.3365	1

Figure 3-33 shows the scatter plot of the predicted maximum scour depth using HEC-18 Sand against the measured scour depth in the TAMU Database. From Figure 3-33, it is clear that the prediction is conservative as most of the data points are above the 1:1 line. The correction factor θ_{unb} is determined to be 0.646; in other words, on the average, the prediction is about 1.55 times larger than the measured values. Figure 3-14 shows the regression analysis results. It can be seen that the HEC-18 Sand method is about 1.55 times larger than the measured value.

Figure 3-35 is obtained from Figure 3-33 after applying the correction factor 0.646 to all predicted values. As such, Figure 3-35 shows the unbiased prediction of maximum scour depth for HEC-18 Sand and for the TAMU Database. The Mean Absolute Percentage Error (MAPE) is 43.4%, which means the absolute difference percentage between the unbiased prediction value and the measured scour depth is

43.4%. The R-square value is 0.33. Note that Figure 3-35 also shows the 1 Standard Deviation (68% confidence interval) and the 1.96 Standard Deviation (95% confidence interval) beyond the 1:1 slope line. Most of the unbiased data fall into the 95% confidence interval.

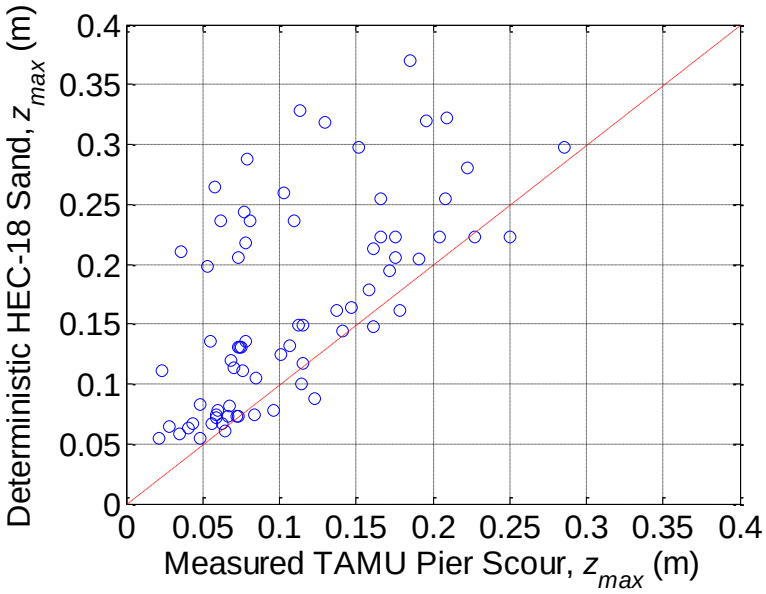

Figure 3-33. Deterministic Prediction of Maximum Scour Depth for HEC-18 Sand Using TAMU Database.

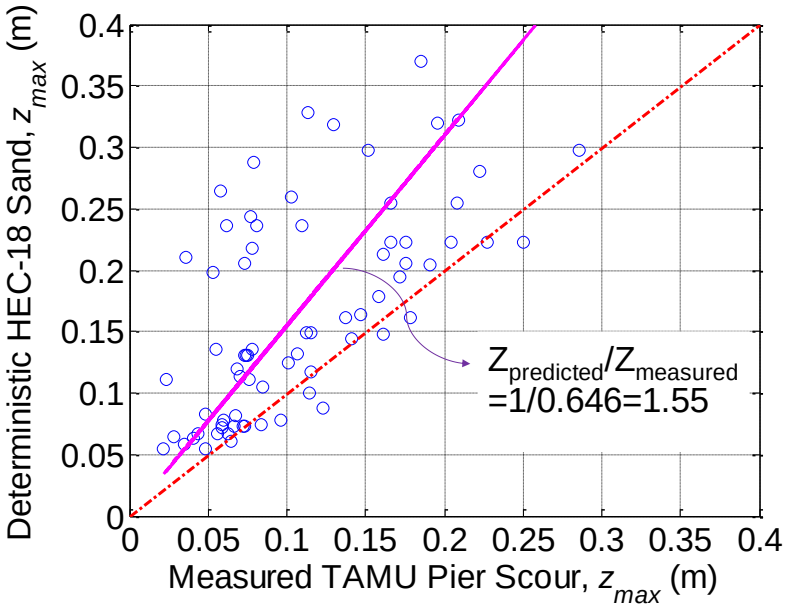

Figure 3-34. Deterministic Prediction of Maximum Scour Depth for HEC-18 Sand Using TAMU Database-Regression Analysis.

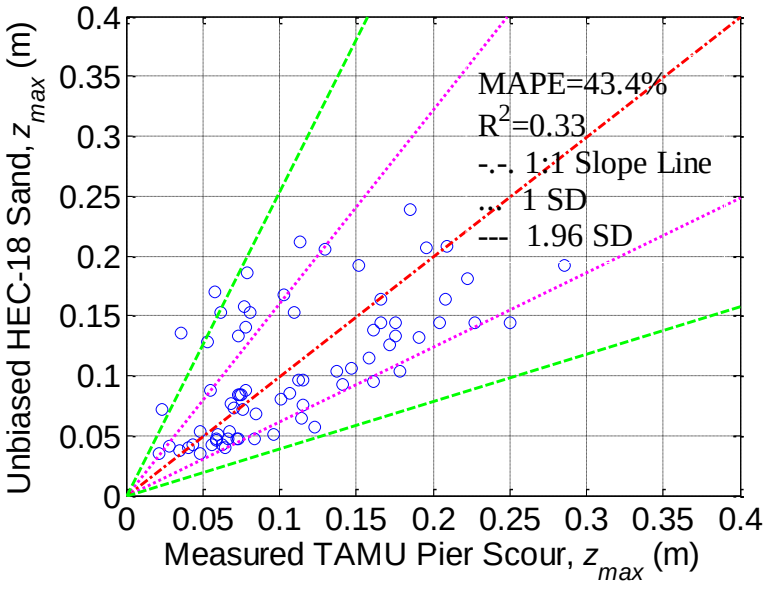

Figure 3-35. Unbiased Prediction of Maximum Scour Depth for HEC-18 Sand Using TAMU Database (1 SD, 68% Confidence Interval; 1.96 SD, 95% Confidence Interval).

Figure 3-36 and Figure 3-37 show the PoE curve for HEC-18 Sand using the TAMU Database in an algorithm scale and semilog scale respectively.

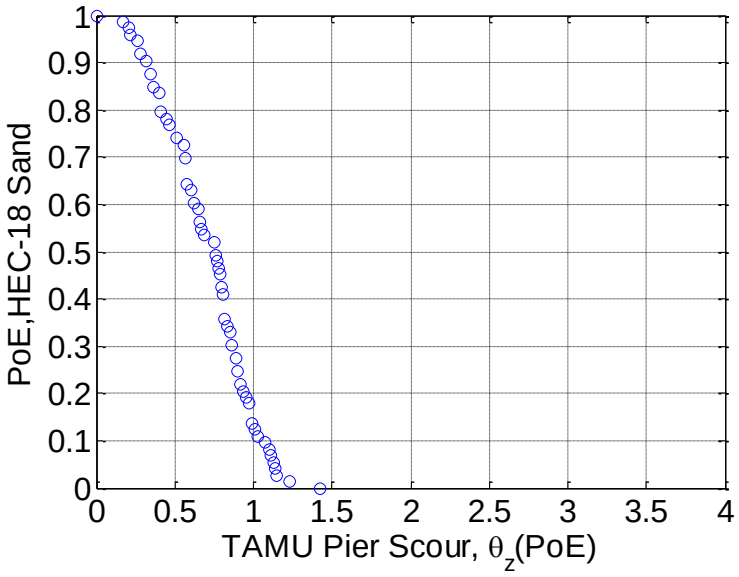

Figure 3-36. Probability of Exceedance Curve for HEC-18 Sand Using TAMU Database in an Algorithm Scale.

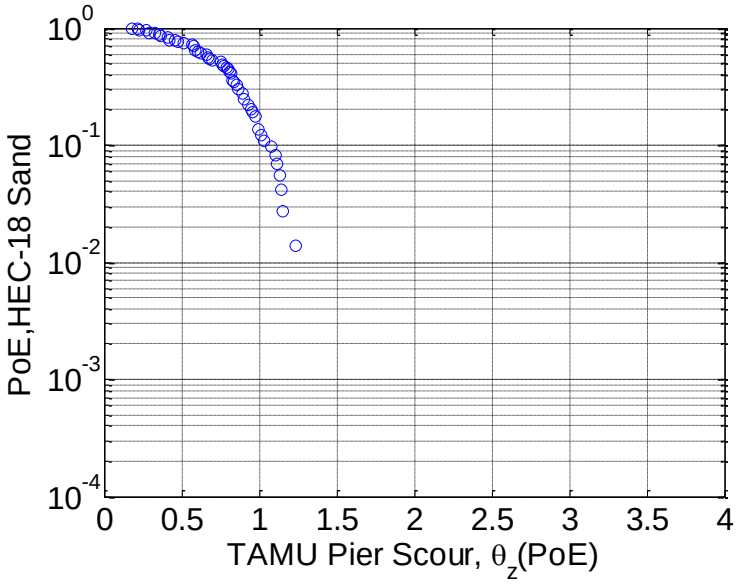

Figure 3-37. Probability of Exceedance Curve for HEC-18 Sand Using TAMU Database in a Semilog Scale.

Figure 3-38 shows the PoE curve with extension line for HEC-18 Sand using the TAMU Database in semilog scale. From the figure, it can be seen that there is an 11% chance that the HEC-18 Sand prediction is smaller than the measured depth. The target value will be explained in Section 4.

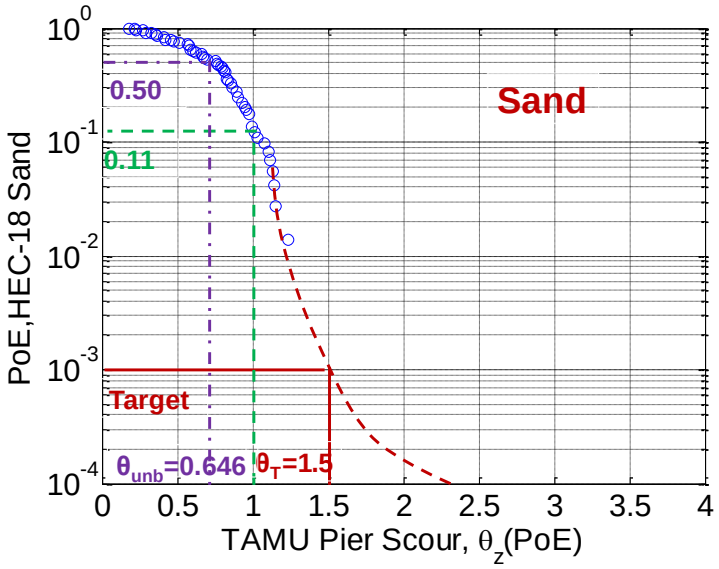

Figure 3-38. Probability of Exceedance Curve with Extension for HEC-18 Sand Using TAMU Database in a Semilog Scale.

3.5.2.2 HEC18 Clay Results

Table 3-12 shows the calculated parameters for the HEC-18 Clay method, which will be the inputs for the LRFD calibration of bridge scour depth.

Table 3-12. HEC-18 Clay Calculated Results for TAMU Database.

Parameter	Mean	Standard Deviation	Correlation Coefficient	
			Γ_ζ	σ_ζ
Γ_ζ	-0.1317	0.0343	1	0.1396
σ_ζ	0.3404	0.0211	0.1396	1

Figure 3-39 shows the scatter plot of the predicted maximum scour depth using HEC-18 Clay against the measured scour depth in the TAMU Database. From Figure 3-39, it is clear that the prediction is conservative as most of the data points are above the 1:1 line. The correction factor θ_{unb} is determined to be 0.877; in other words, on the average, the prediction is about 1.14 times larger than the measured values. Figure 3-40 shows the regression analysis results. It can be seen that the HEC-18 Clay method is about 1.14 times larger than the measured value.

Figure 3-41 is obtained from Figure 3-39 after applying the correction factor 0.877 to all predicted values. As such, Figure 3-41 shows the unbiased prediction of maximum scour depth for HEC-18 Clay and for the TAMU Database. The Mean Absolute Percentage Error (MAPE) is 29.4%, which means that the error on any prediction is on average + or – 29.4%. The R-square value is 0.66. Note that Figure 3-41 also shows the 1 Standard Deviation (68% confidence interval) and the 1.96 Standard Deviation (95% confidence interval) beyond the 1:1 slope line. Most of the unbiased data fall into the 95% confidence interval.

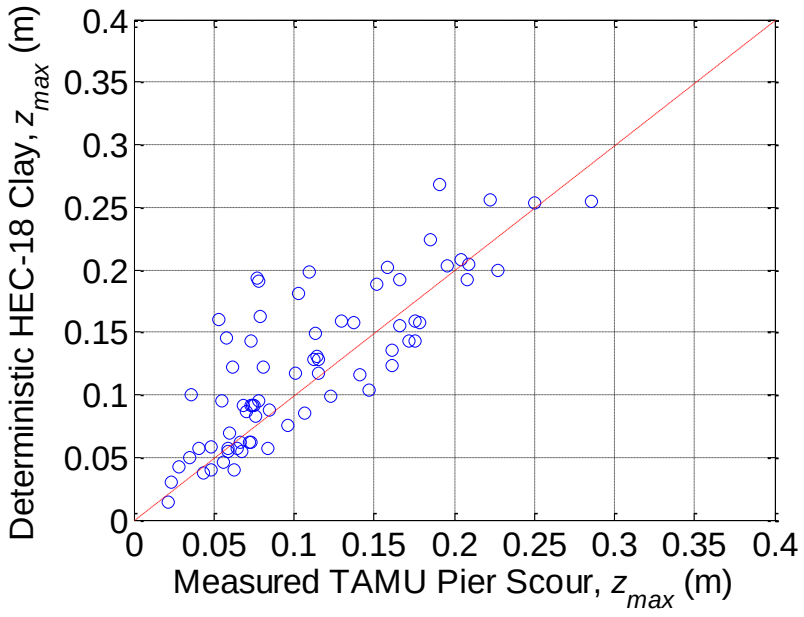

Figure 3-39. Deterministic Prediction of Maximum Scour Depth for HEC-18 Clay Using TAMU Database.

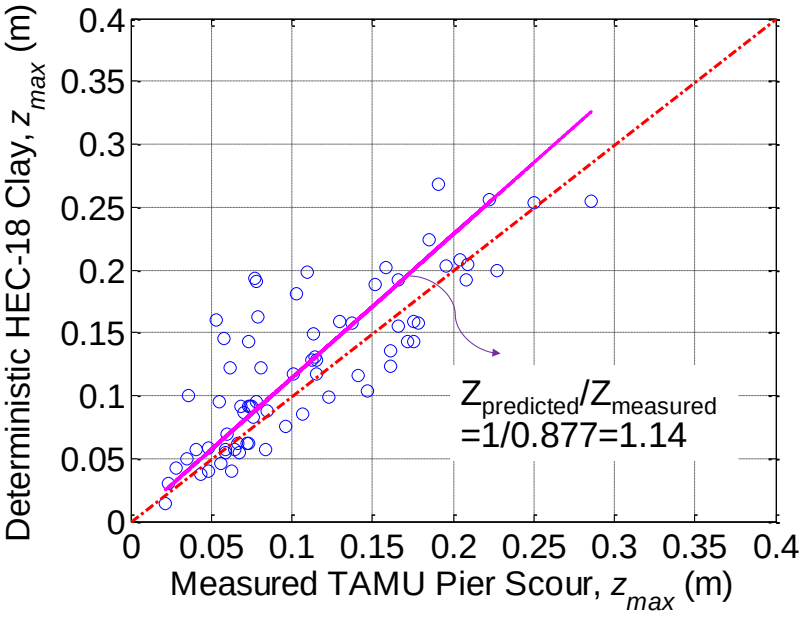

Figure 3-40. Deterministic Prediction of Maximum Scour Depth for HEC-18 Clay Using TAMU Database-Regression Analysis.

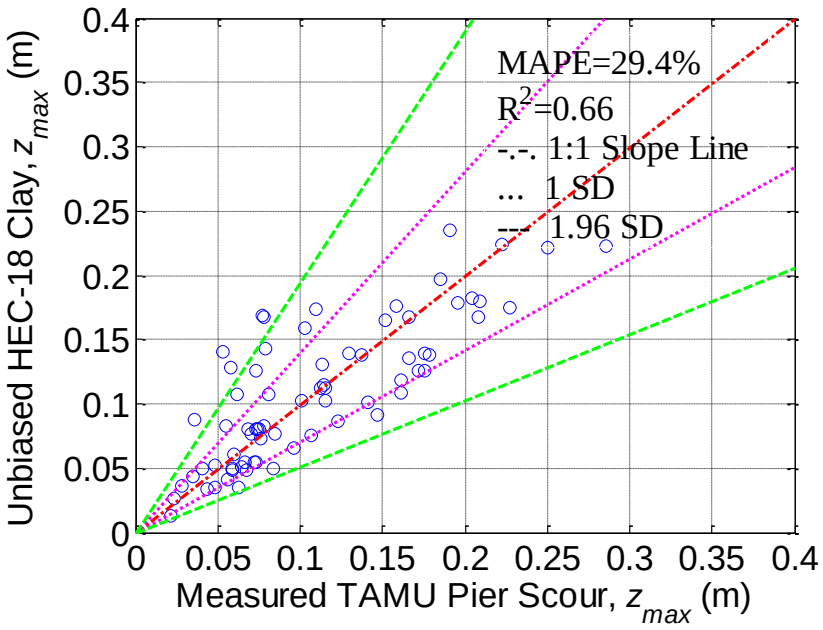

Figure 3-41. Unbiased Prediction of Maximum Scour Depth for HEC-18 Clay Using TAMU Database (1 SD, 68% Confidence Interval; 1.96 SD, 95% Confidence Interval).

Figure 3-42 and Figure 3-43 show the PoE curve for HEC-18 Clay using the TAMU Database in an algorithm scale and semilog scale respectively.

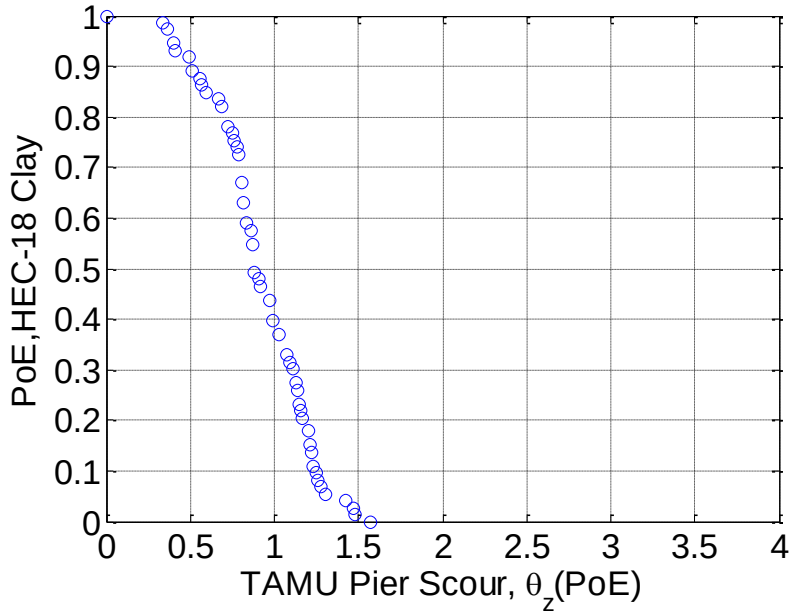

Figure 3-42. Probability of Exceedance Curve for HEC-18 Clay Using TAMU Database in an Algorithm Scale.

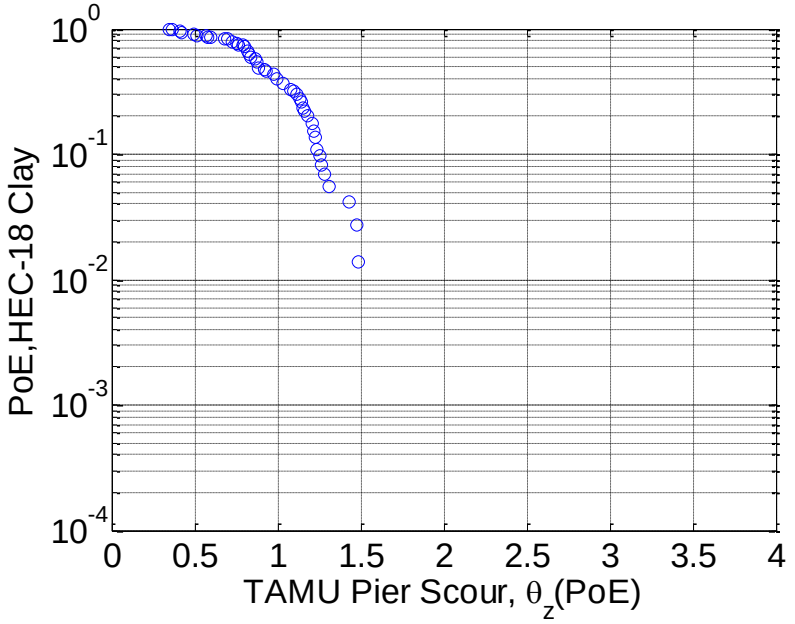

Figure 3-43. Probability of Exceedance Curve for HEC-18 Clay Using TAMU Database in a Semilog Scale.

Figure 3-44 shows the PoE curve with an extension line for HEC-18 Clay using the TAMU Database in a semilog scale. From the figure, it can be seen that there is a 38% chance that the HEC-18 Clay prediction is smaller than the measured depth. The target value will be explained in Section 4.

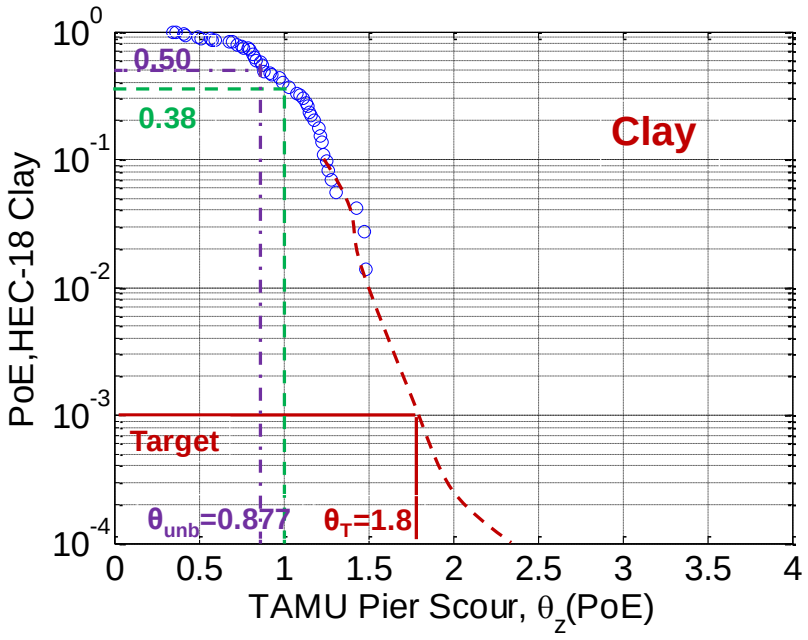

Figure 3-44. Probability of Exceedance Curve with Extension for HEC-18 Clay Using TAMU Database in a Semilog Scale.

3.5.3 Probabilistic Model Results of Froehlich Database

The whole database was analyzed below to find the probabilistic scour depth parameters. Note that the database includes 79 data points, among which 13 experiments were about

cohesive soils. The author used three different equations to compute critical velocity with the HEC-18 Clay method: Equations 3-22, 3-23, and 3-38.

Recall:

$$V_c(\text{m/s}) = 0.35(D_{50}(\text{mm}))^{0.45} \tag{3-22}$$

$$V_c(\text{m/s}) = \sqrt{\frac{\tau_c(\text{Pa})y_1(\text{m})^{0.33}}{\rho(\text{kg/m}^3)g(\text{N/kg})n^2}} \tag{3-23}$$

Equation 3-38 is shown below, which can be referred to Section 2.1.3.

$$V_c(\text{m/s}) = 6.19y_1(\text{m})^{1/6}D_{50}(\text{m})^{1/3} \tag{3-38}$$

Note that V_c in Equation 3-22 is marked as V_{c_Briaud}, V_c in Equation 3-23 is marked as V_{c*}, and V_c in Equation 3-38 is marked as V_{c**} in the future analysis.

Figure 3-45 shows the computed critical shear stress based on Shield's Coefficient versus mean grain size. Regression analysis shows that the critical shear stress is following a linear relationship with D_{50} :

$$\tau_c(\text{N/m}^2) = 0.745D_{50}(\text{mm}) \tag{3-39}$$

Note that Briaud et al. (1999) performed EFA tests on different sands, and found out a relative simple relationship between critical shear stress τ_c and D_{50}, which was shown in Equation 3-28.

It is concluded that for the Froehlich Database, the critical shear stress (Pa) is about ¾ of the mean grain size (mm). The results match the Landers-Mueller Database.

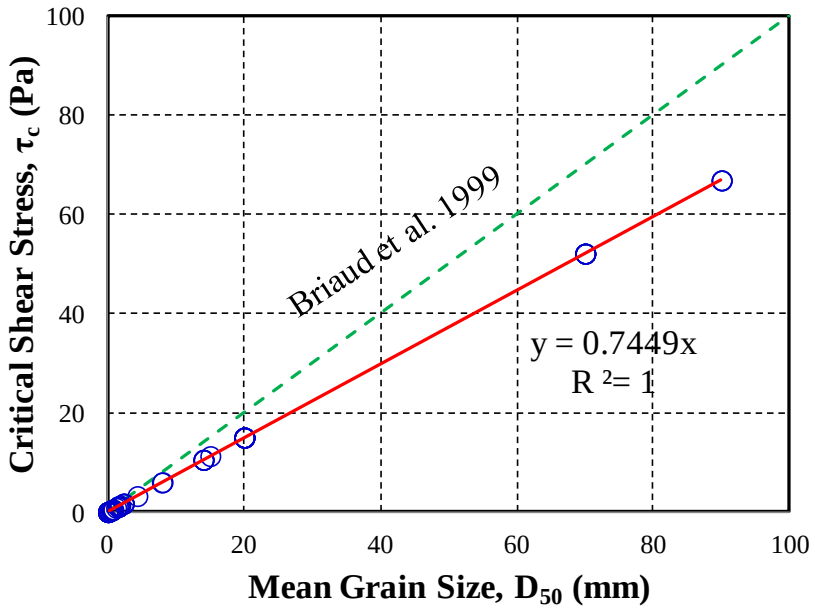

Figure 3-45. Critical Shear Stress Computed using Shields Coefficient vs. Mean Grain Size-Froehlich Database.

Figure 3-46 shows the relationship between critical velocity and mean grain size for the Froehlich Database using different approaches. Note that the critical velocity computed using Equation 3-22 is marked as V_{c_Briaud}, the critical velocity computed using Equation 3-23 is marked as V_{c*}, the critical velocity computed using Equation 3-38 is marked as V_{c**}.

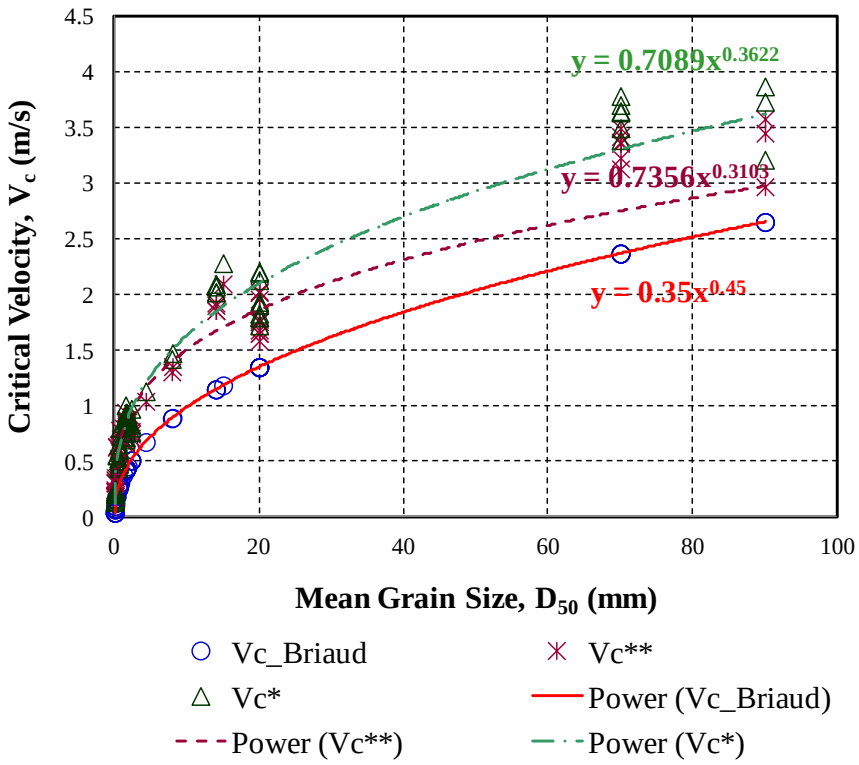

Figure 3-46. Critical Velocity vs. Mean Grain Size for Froehlich Database Using Different Approaches.

The regression analysis based on V_{c*} shows the relationship between critical velocity and D_{50} in Equation 3-40:

$$V_c(\text{m/s}) = 0.71(D_{50}(\text{mm}))^{0.36} \tag{3-40}$$

The regression analysis based on V_{c**} shows the relationship between critical velocity and D_{50} in Equation 3-41:

$$V_c(\text{m/s}) = 0.74(D_{50}(\text{mm}))^{0.31} \tag{3-41}$$

Figure 3-47 shows the deterministic maximum scour depth using V_{c_Briaud} and V_{c*} respectively in the HEC-18 Clay method. From the figure, we can see that the scour depth computed using V_{c_Briaud} is more conservative, but they are very close.

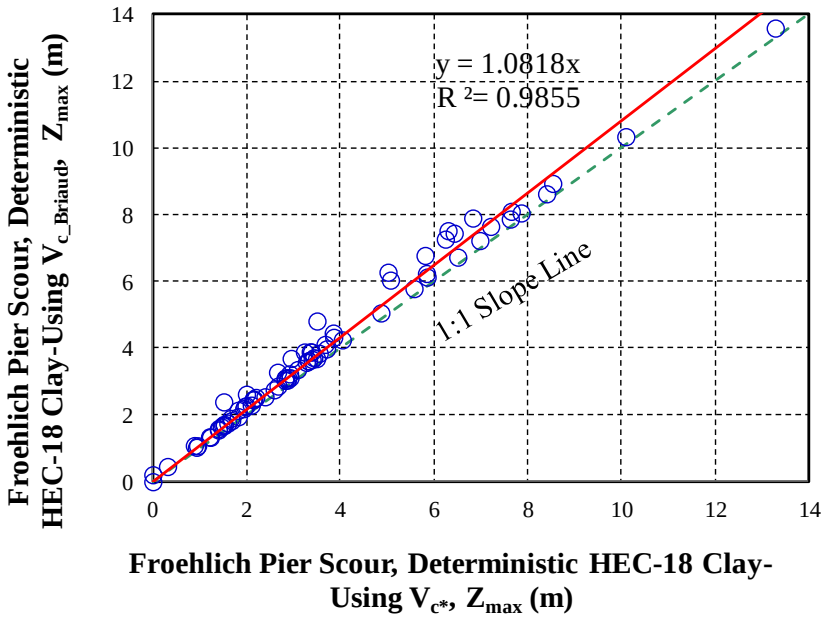

Figure 3-47. Deterministic HEC-18 Clay Using V_{c_Briaud} and V_{c*} Respectively-Froehlich Database.

Figure 3-48 shows the deterministic maximum scour depth using V_{c_Briaud} and V_{c**} respectively in the HEC-18 Clay method. From the figure, we can see that the scour depth computed using V_{c_Briaud} is more conservative, but they are very close.

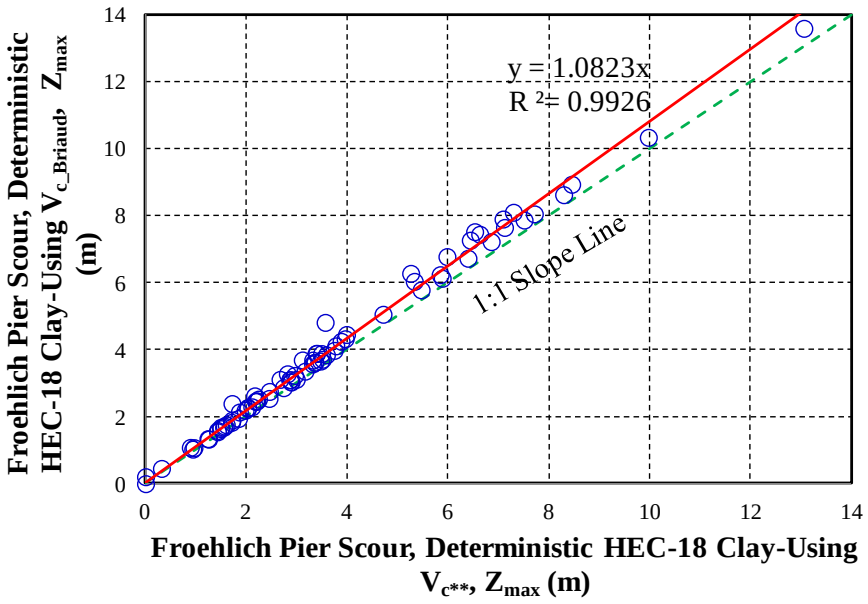

Figure 3-48. Deterministic HEC-18 Clay Using V_{c_Briaud} and V_{c**} Respectively-Froehlich Database.

The following probabilistic analysis for HEC-18 Clay will be based on those three approaches.

3.5.3.1 HEC18 Sand Results

Table 3-13 shows the calculated parameters for the HEC-18 Sand method using the Bayesian approach, which will be the inputs for the LRFD calibration of bridge scour depth.

Table 3-13. HEC-18 Sand Calculated Results for Froehlich Database.

Parameter	Mean	Standard Deviation	Correlation Coefficient	
			Γ_ζ	σ_ζ
Γ_ζ	-1.0116	0.0473	1	-0.1311
σ_ζ	0.5381	0.0351	-0.1311	1

Figure 3-49 shows the scatter plot of the predicted maximum scour depth using HEC-18 Sand against the measured scour depth in the Froehlich Database. From Figure 3-49, it is clear that the prediction is conservative as most of the data points are above the 1:1 line. The correction factor θ_{unb} is determined to be 0.364; in other words, on the average, the prediction is about 2.75 times larger than the measured values. Figure 3-50 shows the regression analysis results. It can be seen that the HEC-18 Sand method is about 2.75 times larger than the measured value.

Figure 3-51 is obtained from Figure 3-49 after applying the correction factor 0.364 to all predicted values. As such, Figure 3-51 shows the unbiased prediction of maximum scour depth for HEC-18 Sand and for the Froehlich Database. The Mean Absolute Percentage Error (MAPE) is 44.9%. The R-square value is 0.57. Note that Figure 3-51 also shows the 1 Standard Deviation (68% confidence interval) and the 1.96 Standard Deviation (95% confidence interval) beyond the 1:1 slope line. Most of the unbiased data fall into the 95% confidence interval.

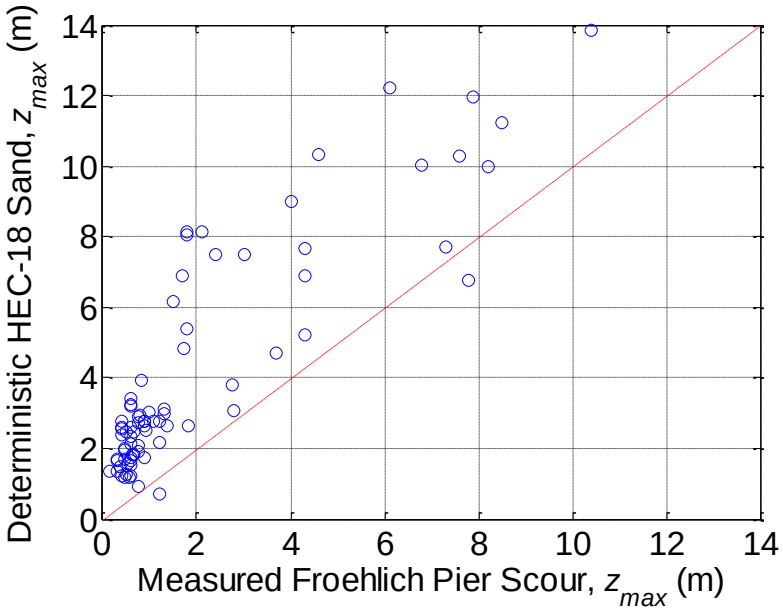

Figure 3-49. Deterministic Prediction of Maximum Scour Depth for HEC-18 Sand Using Froehlich Database.

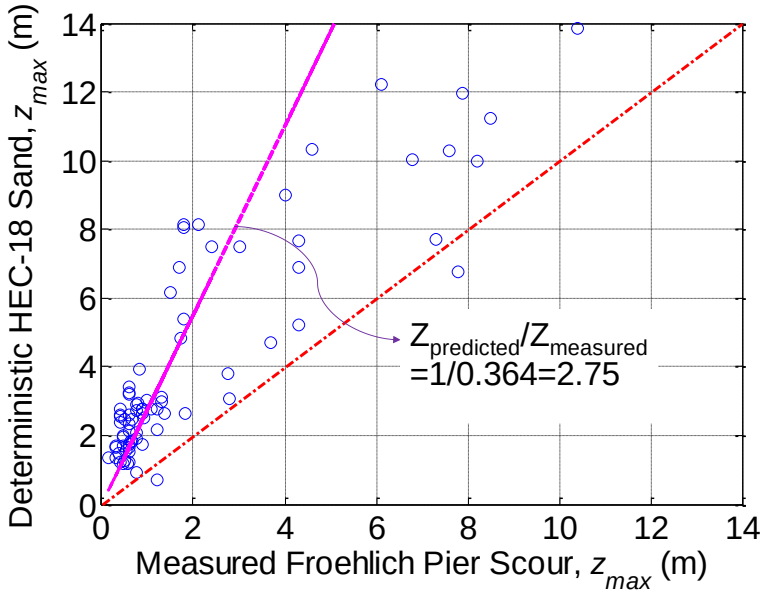

Figure 3-50. Deterministic Prediction of Maximum Scour Depth for HEC-18 Sand Using Froehlich Database-Regression Analysis.

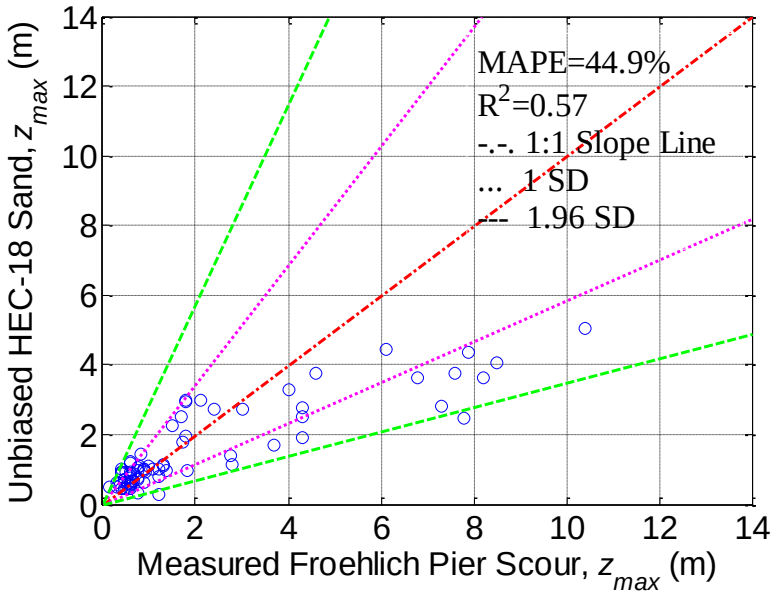

Figure 3-51. Unbiased Prediction of Maximum Scour Depth for HEC-18 Sand Using Froehlich Database (1 SD, 68% Confidence Interval; 1.96 SD, 95% Confidence Interval).

Figure 3-52 and Figure 3-53 show the PoE curve for HEC-18 Sand using the Froehlich Database in an algorithm scale and semilog scale respectively.

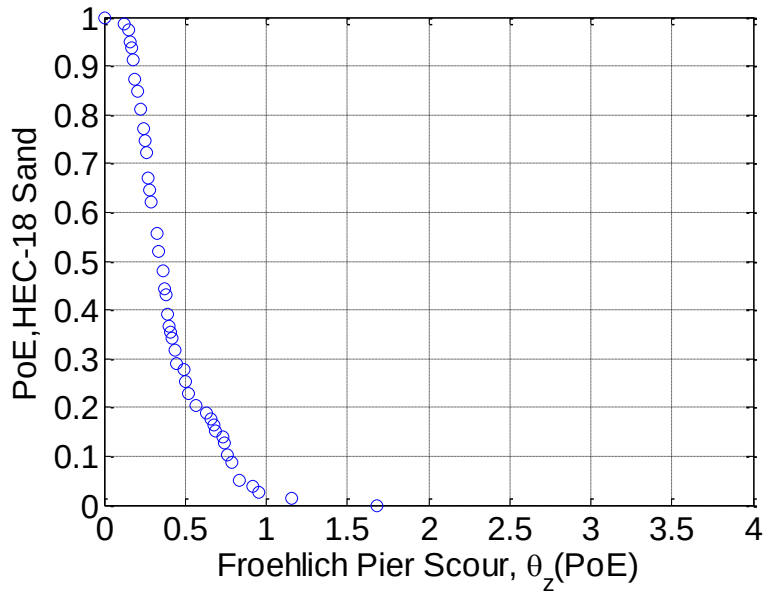

Figure 3-52. Probability of Exceedance Curve for HEC-18 Sand Using Landers-Mueller Database in an Algorithm Scale.

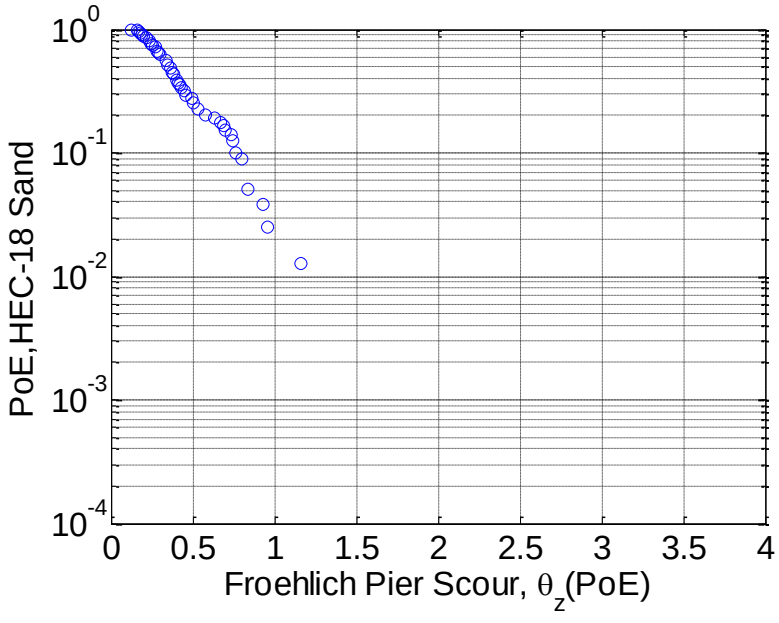

Figure 3-53. Probability of Exceedance Curve for HEC-18 Sand Using Froehlich Database in a Semilog Scale.

Figure 3-54 shows the PoE curve with an extension line for HEC-18 Sand using the Froehlich Database in a semilog scale. From the figure, it can be seen that there is a 2% chance that the HEC-18 Sand prediction is smaller than the measured depth. The target value will be explained in Section 4.

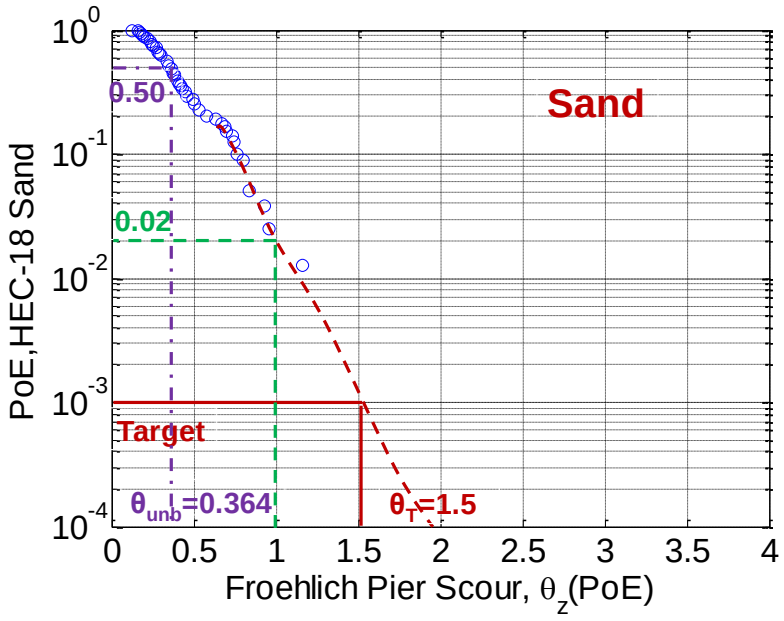

Figure 3-54. Probability of Exceedance Curve with Extension for HEC-18 Sand Using Froehlich Database in a Semilog Scale.

3.5.3.2 HEC18 Clay Results

HEC-18 Clay Using V_{c_Briaud}

Table 3-14 shows the calculated parameters for the HEC-18 Clay method, which will be the inputs for the LRFD calibration of bridge scour depth.

Table 3-14. HEC-18 Clay Calculated Results for Froehlich Database Using V_{c_Briaud}.

Parameter	Mean	Standard Deviation	Correlation Coefficient	
			Γ_ζ	σ_ζ
Γ_ζ	-1.0385	0.0749	1	-0.3427
σ_ζ	0.7709	0.0592	-0.3427	1

Figure 3-55 shows the scatter plot of the predicted maximum scour depth using HEC-18 Clay based on V_{c_Briaud} against the measured scour depth in the Froehlich Database. From Figure 3-55, it is clear that the prediction is conservative as most of the data points are above the 1:1 line. The correction factor θ_{unb} is determined to be 0.354; in other words, on the average the prediction is about 2.82 times larger than the measured values. Figure 3-56 shows the regression analysis results. It can be seen that the HEC-18 Clay method based on V_{c_Briaud} is about 2.82 times larger than the measured value.

Figure 3-57 is obtained from Figure 3-55 after applying the correction factor 0.354 to all predicted values. As such, Figure 3-57 shows the unbiased prediction of maximum scour depth for HEC-18 Clay and for the Froehlich Database. The Mean Absolute Percentage Error (MAPE) is 57.8%. The R-square value is 0.31. Note that Figure 3-57 also shows the 1 Standard Deviation (68% confidence interval) and the 1.96 Standard Deviation (95% confidence interval) beyond the 1:1 slope line. Most of the unbiased data fall into the 95% confidence interval.

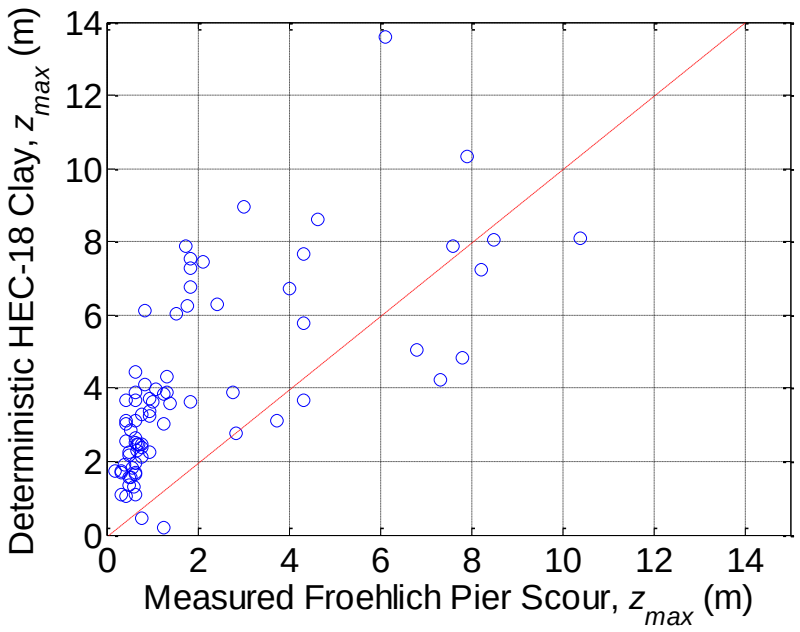

Figure 3-55. Deterministic Prediction of Maximum Scour Depth for HEC-18 Clay Using V_{c_Briaud} for Froehlich Database.

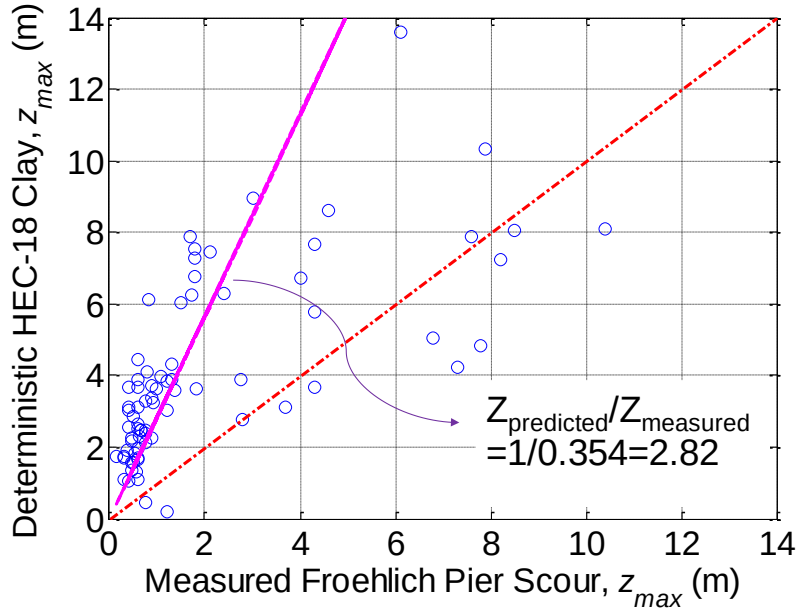

Figure 3-56. Deterministic Prediction of Maximum Scour Depth for HEC-18 Clay Using V_{c_Briaud} for Froehlich Database-Regression Analysis.

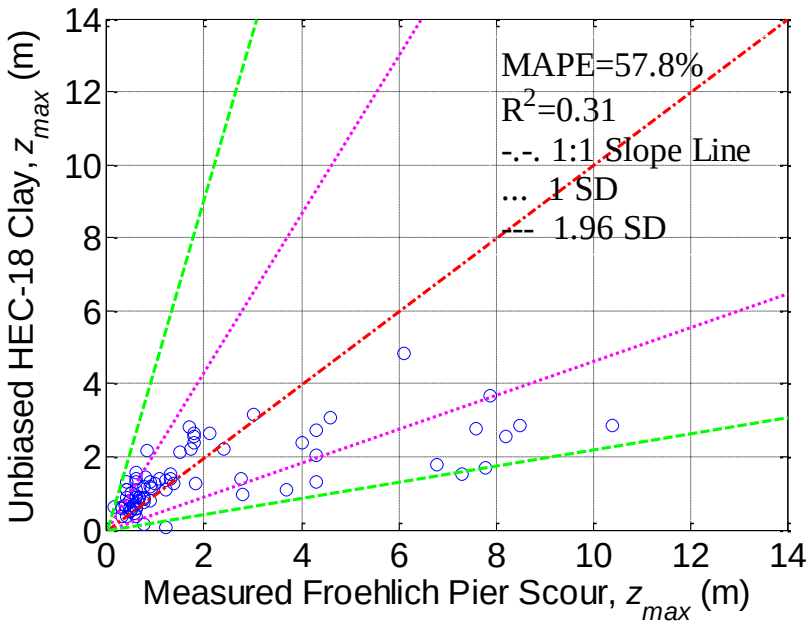

Figure 3-57. Unbiased Prediction of Maximum Scour Depth for HEC-18 Clay Using V_{c_Briaud} for Froehlich Database (1 SD, 68% Confidence Interval; 1.96 SD, 95% Confidence Interval).

Figure 3-58 and Figure 3-59 show the PoE curve for HEC-18 Clay based on V_{c_Briaud} using the Froehlich Database in an algorithm scale and semilog scale respectively.

Figure 3-60 shows the PoE curve with an extension line for HEC-18 Clay based on V_{c_Briaud} using the Froehlich Database in a semilog scale. From the figure, it can be seen that there is an 11% chance that the HEC-18 Clay prediction is smaller than the measured depth. The target value will be explained in Section 4.

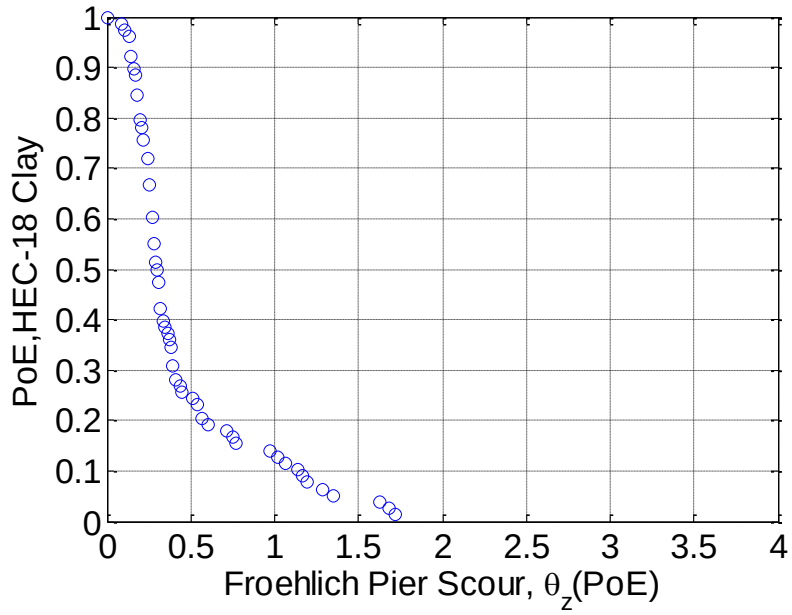

Figure 3-58. Probability of Exceedance Curve for HEC-18 Clay Using V_{c_Briaud} for Froehlich Database in an Algorithm Scale.

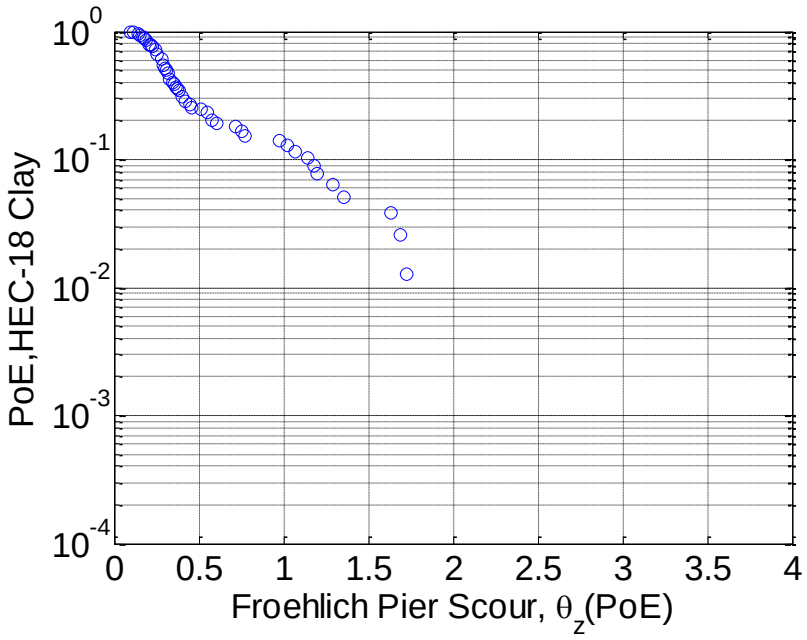

Figure 3-59. Probability of Exceedance Curve for HEC-18 Clay Using V_{c_Briaud} for Froehlich Database in a Semilog Scale.

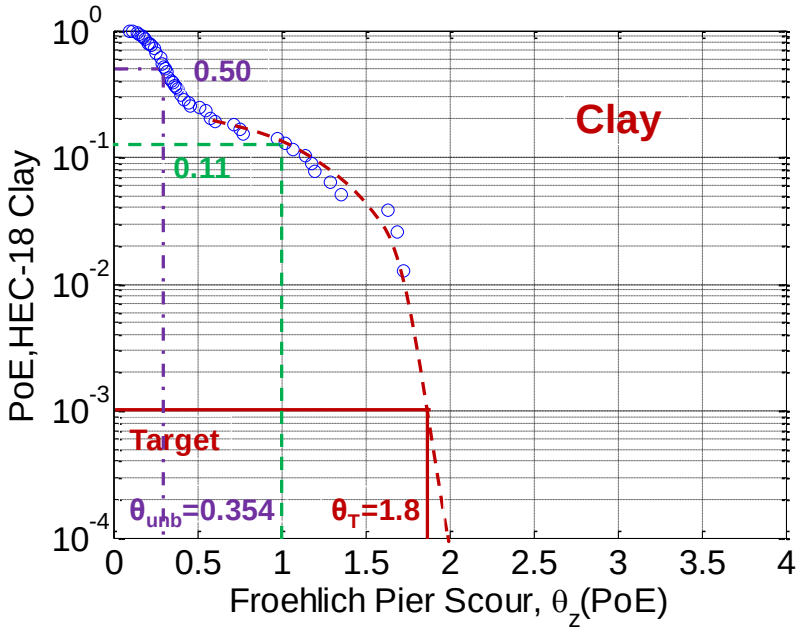

Figure 3-60. Probability of Exceedance Curve for HEC-18 Clay with Extension Using V_{c_Briaud} for Froehlich Database in a Semilog Scale.

HEC-18 Clay Using V_{c*}

Table 3-15 shows the calculated parameters for the HEC-18 Clay method, which will be the inputs for the LRFD calibration of bridge scour depth.

Table 3-15. HEC-18 Clay Calculated Results for Froehlich Database Using V_{c*}.

Parameter	Mean	Standard Deviation	Correlation Coefficient	
			Γ_ζ	σ_ζ
Γ_ζ	-0.9629	0.0650	1	-0.0509
σ_ζ	0.6788	0.0445	-0.0509	1

Figure 3-61 shows the scatter plot of the predicted maximum scour depth using HEC-18 Clay based on V_{c*} against the measured scour depth in the Froehlich Database. From Figure 3-61, it is clear that the prediction is conservative as most of the data points are above the 1:1 line. The correction factor θ_{unb} is determined to be 0.382; in other words, on the average the prediction is about 2.62 times larger than the measured values. Figure 3-62 shows the regression analysis results. It can be seen that the HEC-18 Clay method based on V_{c*} is about 2.62 times larger than the measured value.

Figure 3-63 is obtained from Figure 3-61 after applying the correction factor 0.382 to all predicted values. As such, Figure 3-63 shows the unbiased prediction of maximum scour depth for HEC-18 Clay and for the Froehlich Database. The Mean Absolute Percentage Error (MAPE) is 53.9%. The R-square value is 0.33. Note that Figure 3-63 also shows the 1 Standard Deviation (68% confidence interval) and the 1.96 Standard Deviation (95% confidence interval) beyond the 1:1 slope line. Most of the unbiased data fall into the 95% confidence interval.

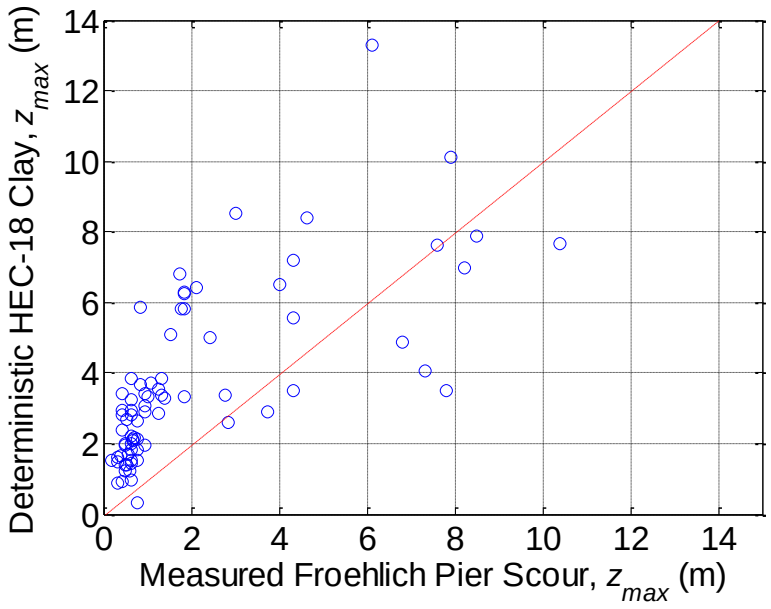

Figure 3-61. Deterministic Prediction of Maximum Scour Depth for HEC-18 Clay Using V_{c*} for Froehlich Database.

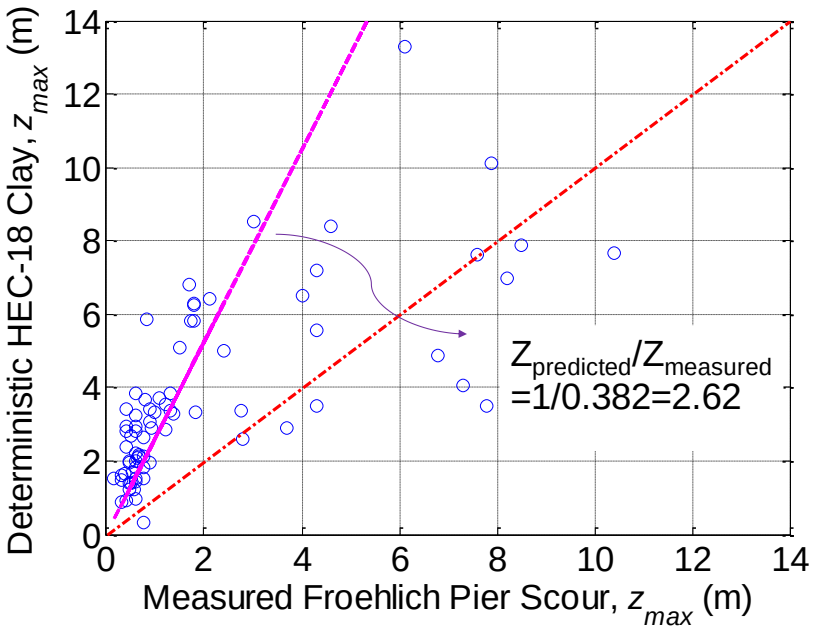

Figure 3-62. Deterministic Prediction of Maximum Scour Depth for HEC-18 Clay Using V_{c*} for Froehlich Database-Regression Analysis.

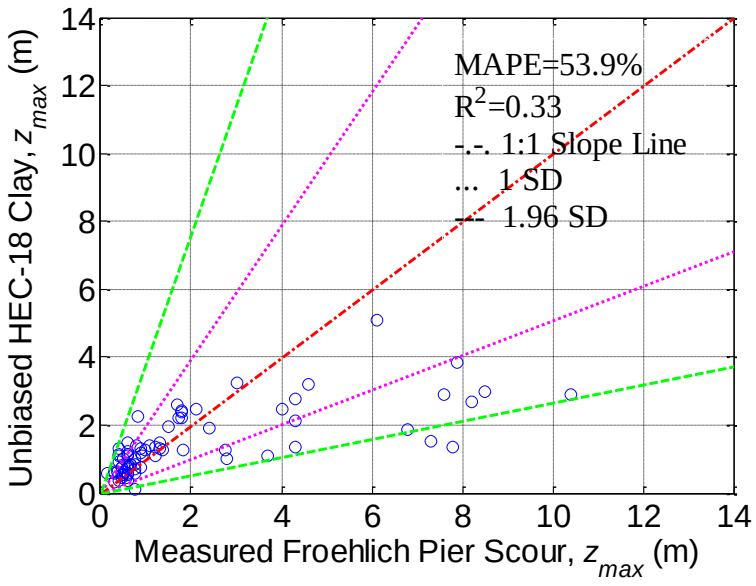

Figure 3-63. Unbiased Prediction of Maximum Scour Depth for HEC-18 Clay Using V_{c*} for Froehlich Database (1 SD, 68% Confidence Interval; 1.96 SD, 95% Confidence Interval).

Figure 3-64 and Figure 3-65 show the PoE curve for HEC-18 Clay based on V_{c*} using the Froehlich Database in an algorithm scale and semilog scale respectively.

Figure 3-66 shows the PoE curve with an extension line for HEC-18 Clay based on V_{c*} using the Froehlich Database in a semilog scale. From the figure, it can be seen that there is an 11% chance that the HEC-18 Clay prediction is smaller than the measured depth. The target value will be explained in Section 4.

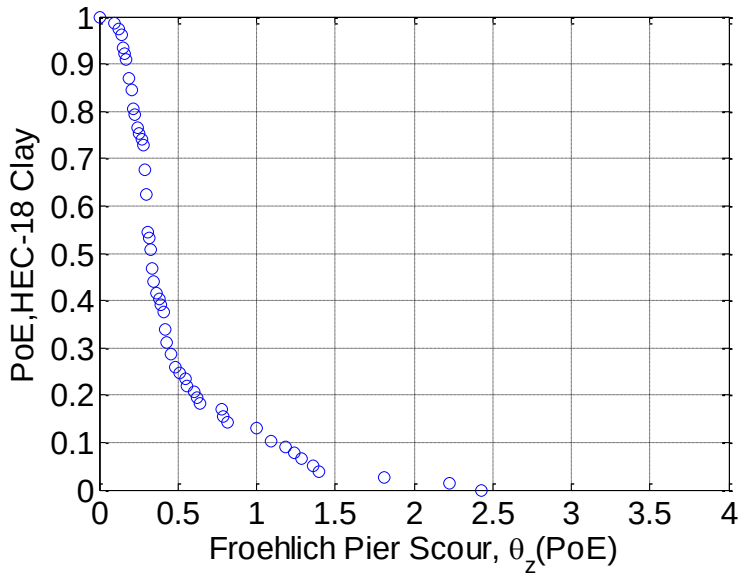

Figure 3-64. Probability of Exceedance Curve for HEC-18 Clay Using V_{c^*} for Froehlich Database in an Algorithm Scale.

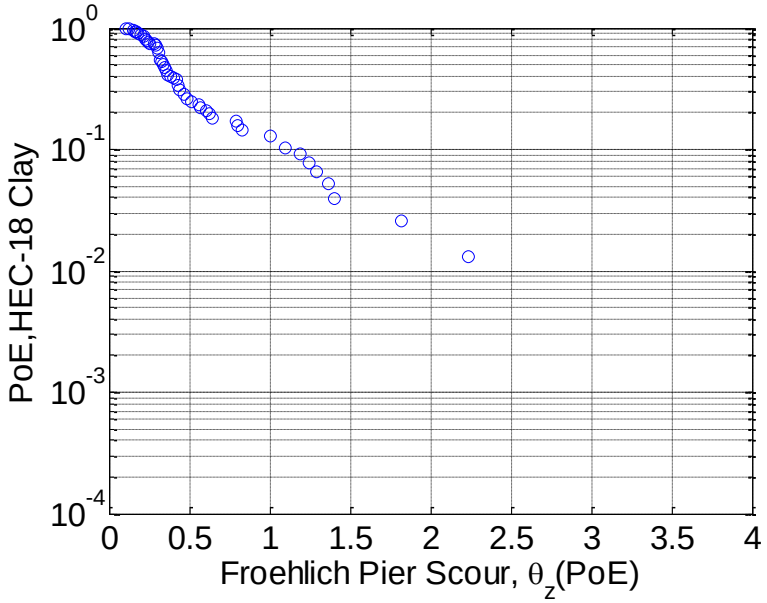

Figure 3-65. Probability of Exceedance Curve for HEC-18 Clay Using V_{c^*} for Froehlich Database in a Semilog Scale.

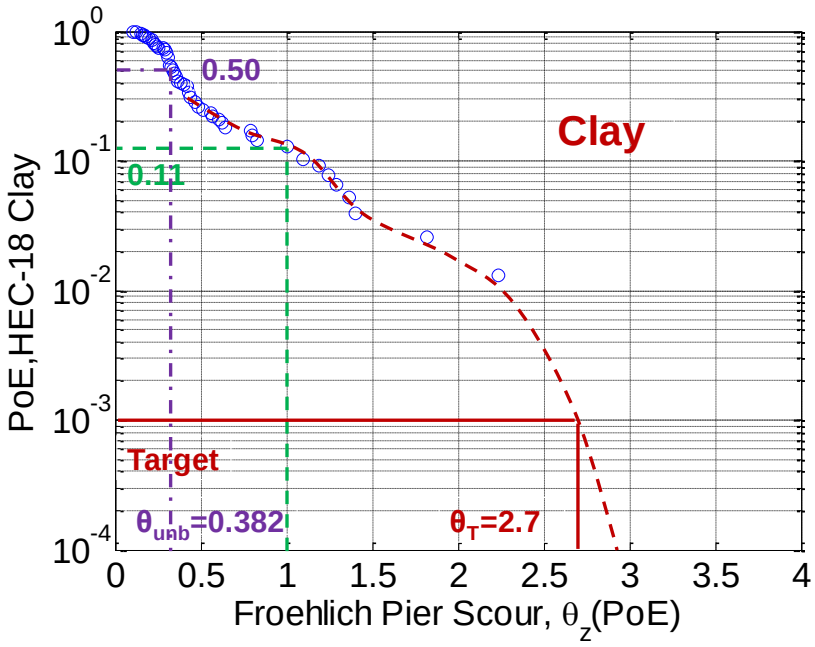

Figure 3-66. Probability of Exceedance Curve with Extension for HEC-18 Clay Using V_{c*} for Froehlich Database in a Semilog Scale.

HEC-18 Clay Using V_{c**}

Table 3-16 shows the calculated parameters for the HEC-18 Clay method, which will be the inputs for the LRFD calibration of bridge scour depth.

Table 3-16. HEC-18 Clay Calculated Results for Froehlich Database Using V_{c**}.

Parameter	Mean	Standard Deviation	Correlation Coefficient	
			Γ_ζ	σ_ζ
Γ_ζ	-0.9368	0.0547	1	0.1994
σ_ζ	0.6865	0.0327	0.1994	1

Figure 3-67 shows the scatter plot of the predicted maximum scour depth using HEC-18 Clay based on $V_{c^{**}}$ against the measured scour depth in the Froehlich Database. From Figure 3-67, it is clear that the prediction is conservative as most of the data points are above the 1:1 line. The correction factor θ_{unb} is determined to be 0.392; in other words, on the average the prediction is about 2.55 times larger than the measured values. Figure 3-68 shows the regression analysis results. It can be seen that the HEC-18 Clay method based on $V_{c^{**}}$ is about 2.55 times larger than the measured value.

Figure 3-69 is obtained from Figure 3-67 after applying the correction factor 0.392 to all predicted values. As such, Figure 3-69 shows the unbiased prediction of maximum scour depth for HEC-18 Clay and for the Froehlich Database. The Mean Absolute Percentage Error (MAPE) is 58.0%. The R-square value is 0.32. Note that Figure 3-69 also shows the 1 Standard Deviation (68% confidence interval) and the 1.96 Standard Deviation (95% confidence interval) beyond the 1:1 slope line. Most of the unbiased data fall into the 95% confidence interval.

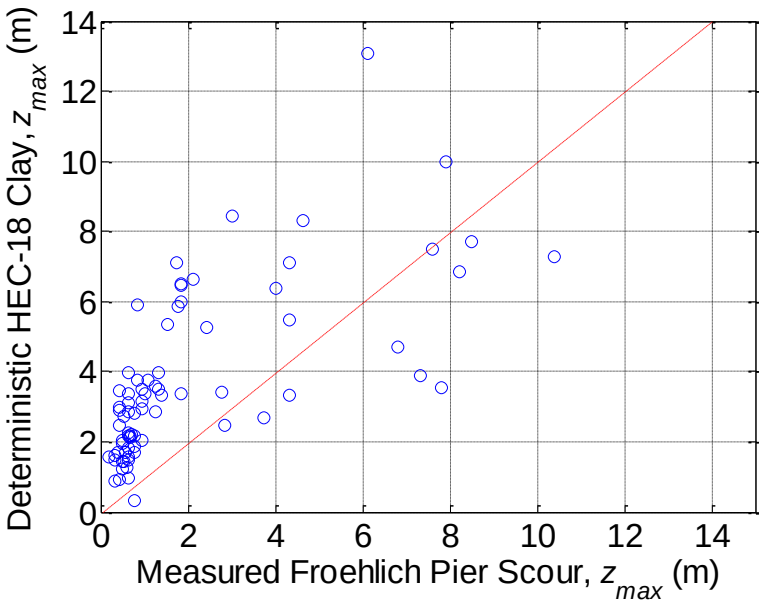

Figure 3-67. Deterministic Prediction of Maximum Scour Depth for HEC-18 Clay Using $V_{c^{**}}$ for Froehlich Database.

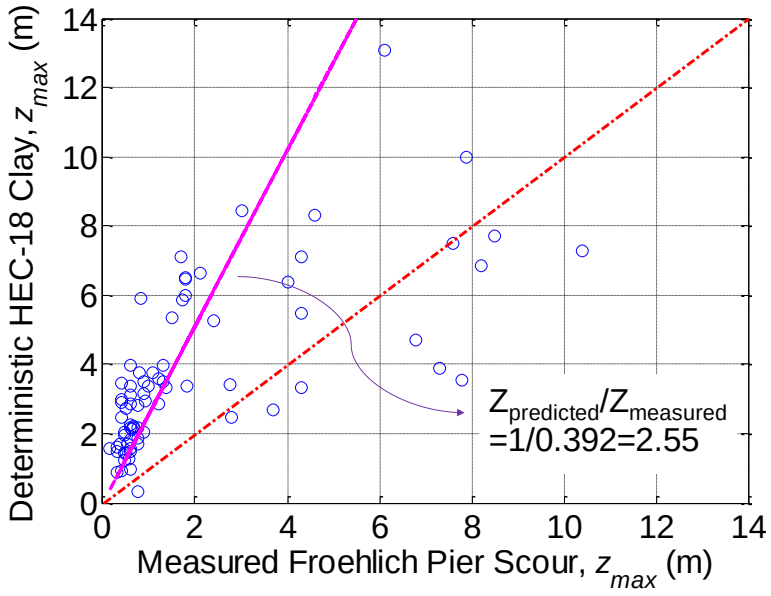

Figure 3-68. Deterministic Prediction of Maximum Scour Depth for HEC-18 Clay Using $V_{c^{**}}$ for Froehlich Database-Regression Analysis.

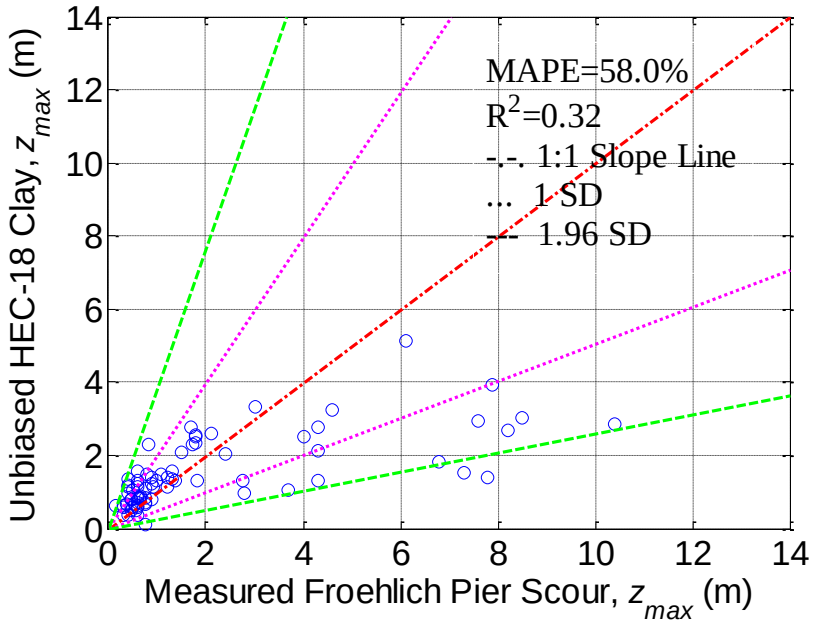

Figure 3-69. Unbiased Prediction of Maximum Scour Depth for HEC-18 Clay Using V_{c**} for Froehlich Database (1 SD, 68% Confidence Interval; 1.96 SD, 95% Confidence Interval).

Figure 3-70 and Figure 3-71 show the PoE curve for HEC-18 Clay based on V_{c**} using the Froehlich Database in an algorithm scale and semilog scale respectively.

Figure 3-72 shows the PoE curve with an extension line for HEC-18 Clay based on V_{c**} using the Froehlich Database in a semilog scale. From the figure, it can be seen that there is a 10% chance that the HEC-18 Clay prediction is smaller than the measured depth. The target value will be explained in Section 4.

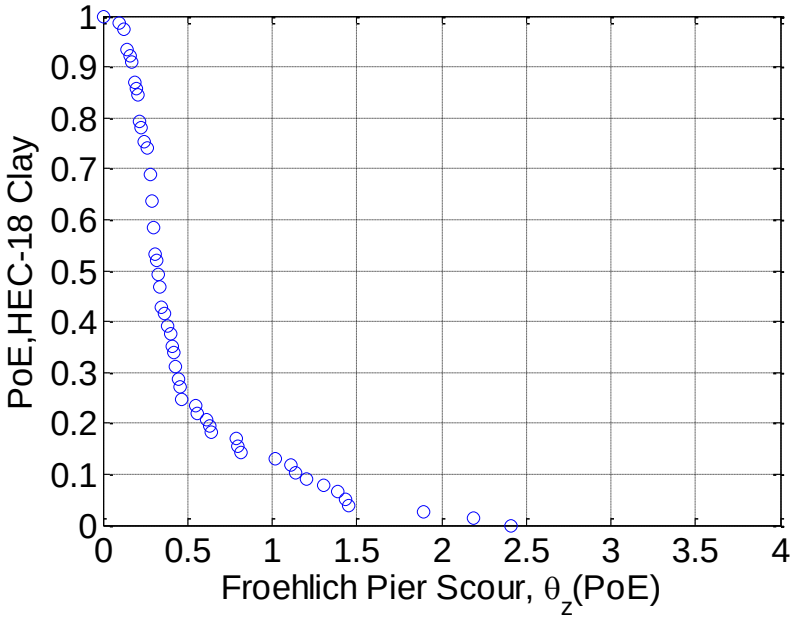

Figure 3-70. Probability of Exceedance Curve for HEC-18 Clay Using V_{c**} for Froehlich Database in an Algorithm Scale.

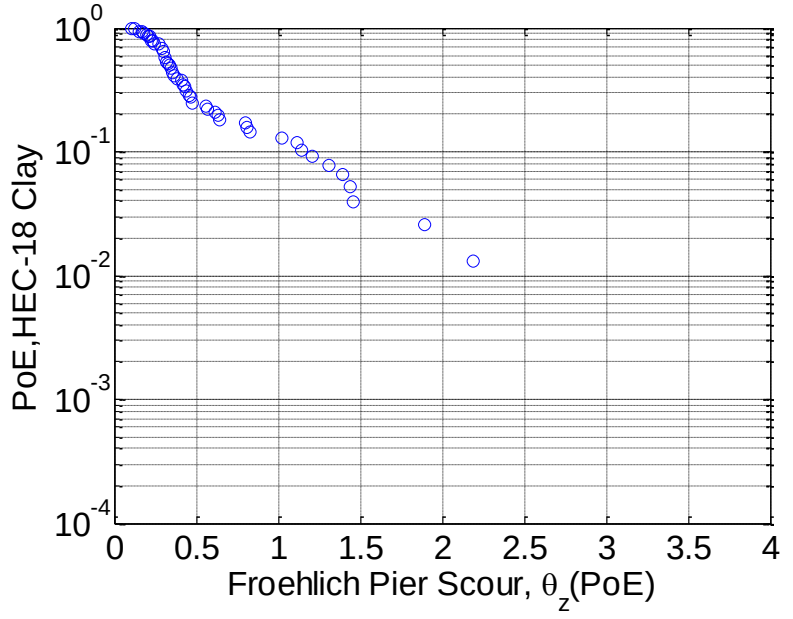

Figure 3-71. Probability of Exceedance Curve for HEC-18 Clay Using V_{c**} for Froehlich Database in a Semilog Scale.

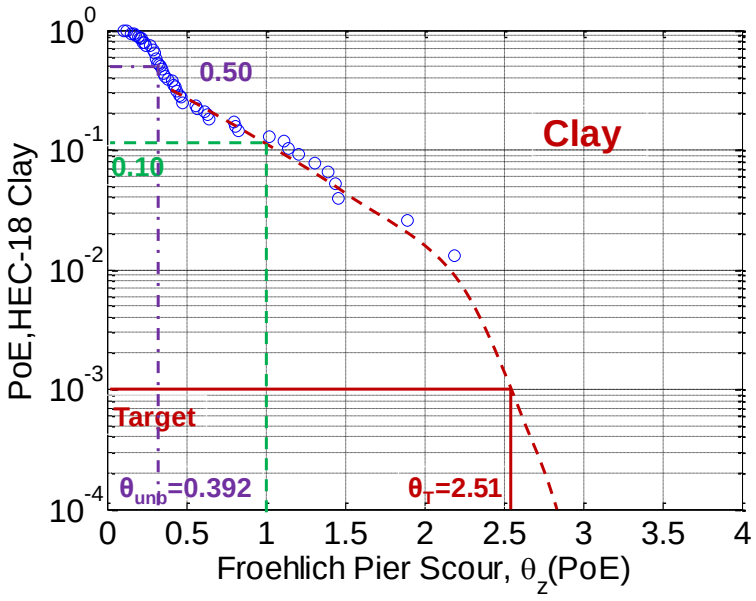

Figure 3-72. Probability of Exceedance Curve with Extension for HEC-18 Clay Using V_{c**} for Froehlich Database in a Semilog Scale.

3.6 CONCLUSIONS ON PROBABILISTIC PIER SCOUR DEPTH PREDICTION MODEL

This section established the probability-based pier scour depth prediction model for three databases: Landers and Mueller Database, TAMU Database, and Froehlich Database. Both HEC-18 Sand and HEC-18 Clay methods were discussed in this section. A different approach to compute critical velocity was also discussed for the three databases. Table 3-17 shows the computed parameters in the probabilistic scour depth prediction model for three databases using both HEC-18 Sand and HEC-18 Clay methods. It can be seen that for those two full scale database (Landers-Mueller Database and Froehlich Database), the computed results do not differ much. For the TAMU database, the computed parameters show a big difference from the full scale database.

Table 3-17. Computed Parameters in the Probabilistic Scour Depth Prediction Model.

Database	Cases	Method	Data Points	Maximum Likelyhood		Bayesian		θ_{unb}	Error (%)	r^2
				Parameter Γ_ζ	Parameter σ_ζ	Parameter Γ_ζ	Parameter σ_ζ			
L&M	Whole Database	HEC-18 Sand	344	-1.179	0.6744	-1.1778	0.6787	**0.3079**	63.6104	0.297
		HEC-18 Clay	366	-1.0876	0.7409	-1.087	0.745	**0.3372**	66.2066	0.5578
TAMU	Whole Database	HEC-18 Sand	73	-0.434	0.4616	-0.4376	0.4757	**0.6456**	43.4108	0.3287
		HEC-18 Clay	73	-0.1323	0.3448	-0.1317	0.3404	**0.8766**	29.4046	0.6607
Froehlich	Whole Database	HEC-18 Sand	79	-1.0095	0.5359	-1.0116	0.5381	**0.3636**	44.8873	0.5725
		HEC-18 Clay using V_{c_Briaud}	78	-1.0333	0.7485	-1.0385	0.7709	**0.354**	57.8235	0.308
		HEC-18 Clay using V_{c*}	77	-0.9559	0.6789	-0.9629	0.6788	**0.3818**	53.8734	0.3256
		HEC-18 Clay using V_{c**}	77	-0.9682	0.695	-0.9368	0.6865	**0.3919**	58.042	0.3211

4 PROPOSED LRFD CALIBRATION FOR BRIDGE SCOUR DEPTH PREDICTIONS: SHALLOW FOUNDATIONS

4.1 INTRODUCTION

This section is the LRFD calibration for shallow foundations in the case of bridge scour. The statistical analysis of the bridge scour databases is shown first. Then the calibration procedure is described.

4.2 LRFD CALIBRATION FOR SHALLOW FOUNDATIONS

For shallow foundations, the issue is the location of the foundation depth and the probability that the scour depth will exceed the foundation depth. Therefore, for shallow foundations, the proposed LRFD calibration is based on the probability of exceedance of the predicted scour depth. However for deep foundations, the issue is the resistance factor associated with the axial capacity of a pile, which will be introduced in the following section. For deep foundations, the proposed LRFD calibration is based on a reliability analysis using First-Order Reliability Method (FORM).

4.3 STATISTICAL ANALYSIS OF BRIDGE SCOUR DEPTH PREDICTIONS

This section is using the distribution fitting analysis to analyze the Landers and Mueller Database, and compare the results with the previous section.

4.3.1 HEC-18 Sand

Note that the bias factor λ is the ratio of mean over predicted value ($\lambda_{Ls} = Z_{unb}/Z_{det} = Z_{measured}/Z_{det}$). Both normal distribution fitting and lognormal distribution fitting using

maximum likelihood methods are analyzed in this section. Figure 4-1 shows the normal distribution fitting using maximum likelihood method for the Landers-Mueller Database using HEC-18 Sand. Figure 4-2 shows the lognormal distribution fitting using the maximum likelihood method for the Landers-Mueller Database using HEC-18 Sand.

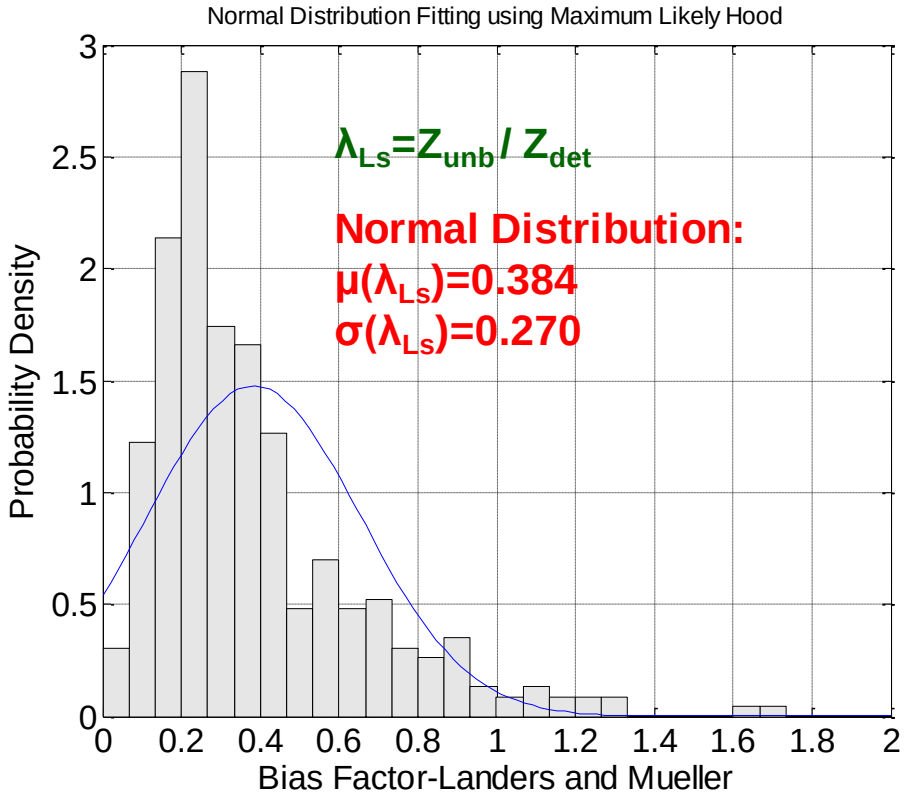

Figure 4-1. Normal Distribution Fitting Using Maximum Likelihood Method for Landers-Mueller Database Using HEC-18 Sand.

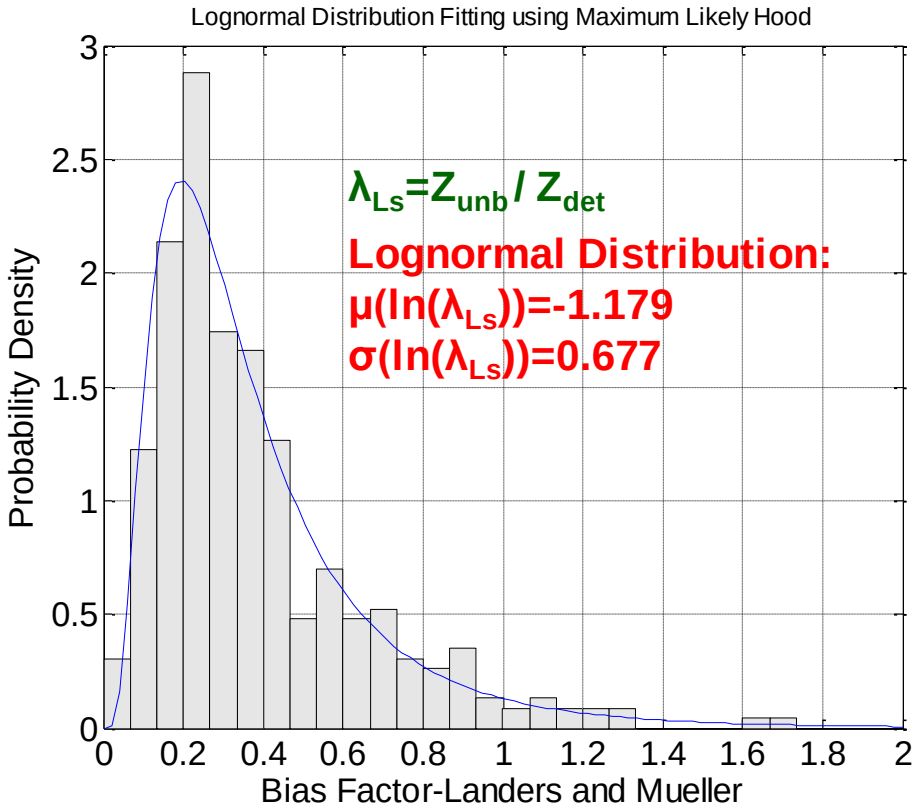

Figure 4-2. Lognormal Distribution Fitting Using Maximum Likelihood Method for Landers-Mueller Database Using HEC-18 Sand.

The comparison analysis is shown below.

The parameters in Figure 4-2 are: μ=-1.179, σ=0.677

Note that if we use $\mu(\ln\lambda_{Ls})$=-1.179, $\sigma(\ln\lambda_{Ls})$=0.677 from the lognormal distribution to back calculate the mean and standard deviation of the normal distribution, we might not get $\mu(\lambda_{Ls})$=0.384, $\sigma(\lambda_{Ls})$==0.270. The explanation is below:

$$\mu(\lambda_{Ls}) = e^{(\mu(\ln\lambda_{Ls})+\frac{1}{2}\sigma^2(\ln\lambda_{Ls}))} = e^{(-1.179+\frac{1}{2}\times 0.677^2)} = 0.387$$

$$\delta(\lambda_{Ls}) = \sqrt{e^{\sigma^2(\ln\lambda_{Ls})}-1} = \sqrt{e^{0.677^2}-1} = 0.763$$

$$\sigma(\lambda_{Ls}) = \mu(\lambda_{Ls}) \times \delta(\lambda_{Ls}) = 0.387 \times 0.763 = 0.295$$.

The reason is that the relationship between the normal distribution parameters and lognormal distribution parameters is based on the probability density function rather than the histogram.

Compare the results from lognormal distribution fitting using maximum likelihood method with the model proposed in Section 3.

In the HEC-18 Sand method, Equation 4-1 shows the unbiased scour depth prediction model.

$$Z_{\text{unb}} = \lambda_{\text{Ls}} \cdot Z_{\text{det}} \tag{4-1}$$

Note that λ_{Ls} includes the uncertainty information, therefore no error term shown in the equation. Equation 4-2 shows the model proposed in Section 3.

$$\ln Z_{\text{unb}} = \theta + \ln Z_{\text{det}} + \sigma\varepsilon \tag{4-2}$$

Hence, $\ln(\lambda_{Ls}) = \theta + \sigma\varepsilon$. Equations 4-3 and 4-4 show the mean and standard deviation of $\ln(\lambda_{\text{Ls}})$.

$$\mu(\ln \lambda_{Ls}) = \mu(\theta) \tag{4-3}$$

$$\sigma(\ln \lambda_{Ls}) = \sqrt{\sigma^2(\theta) + \mu^2(\sigma)} \tag{4-4}$$

From the results obtained from Section 3,

$$\mu(\theta) = -1.1778,\ \sigma(\theta) = 0.0210.$$

$$\mu(\sigma) = 0.6787,\ \sigma(\sigma) = 0.0273$$

Therefore,

$$\mu(\ln \lambda_{Ls}) = \mu(\theta) = -1.178$$

$$\sigma(\ln \lambda_{Ls}) = \sqrt{\sigma^2(\theta) + \mu^2(\sigma)} = \sqrt{0.0210^2 + 0.6787^2} = 0.679$$

Since we obtained the distribution of $ln\lambda_{Ls}$, we can back calculate the parameter of $\mu(ln\lambda_{Ls})$ and $\sigma(ln\lambda_{Ls})$.

$$\mu(\lambda_{L_s}) = e^{(\mu(\ln \lambda_{Ls}) + \frac{1}{2}\sigma^2(\ln \lambda_{Ls}))} = e^{(-1.178 + \frac{1}{2} \times 0.679^2)} = 0.388$$

$$\delta(\lambda_{L_s}) = \sqrt{e^{\sigma^2(\ln \lambda_{Ls})} - 1} = \sqrt{e^{0.679^2} - 1} = 0.765$$

$$\sigma(\lambda_{L_s}) = \mu(\lambda_{L_s}) \times \delta(\lambda_{L_s}) = 0.388 \times 0.765 = 0.297$$

Table 4-1 shows the parameters using both lognormal distribution fitting and model proposed in Section 3. It can be seen that the results match.

Table 4-1. Comparison between Different Approaches-HEC-18 Sand.

Parameters	Normal Fitting Histogram	Lognormal Fitting Histogram	Lognormal → Normal	Model in Section 3 (Lognormal)	Lognormal → Normal
μ	0.384	-1.179	0.387	-1.178	0.388
σ	0.270	0.677	0.295	0.679	0.297

4.3.2 HEC-18 Clay

Both normal distribution fitting and lognormal distribution fitting using maximum likelihood methods are analyzed in this section. Figure 4-3 shows the normal distribution fitting using the maximum likelihood method for the Landers-Mueller Database using HEC-18 Clay. Figure 4-4 shows the lognormal distribution fitting using maximum likelihood method for the Landers-Mueller Database using HEC-18 Clay.

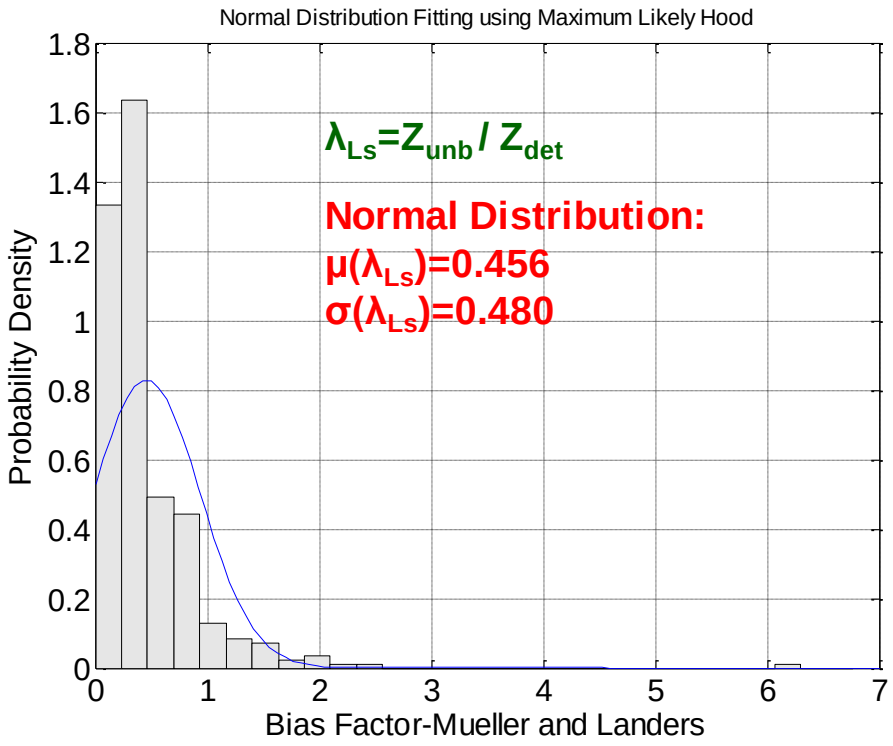

Figure 4-3. Normal Distribution Fitting Using Maximum Likelihood Method for Landers-Mueller Database Using HEC-18 Clay.

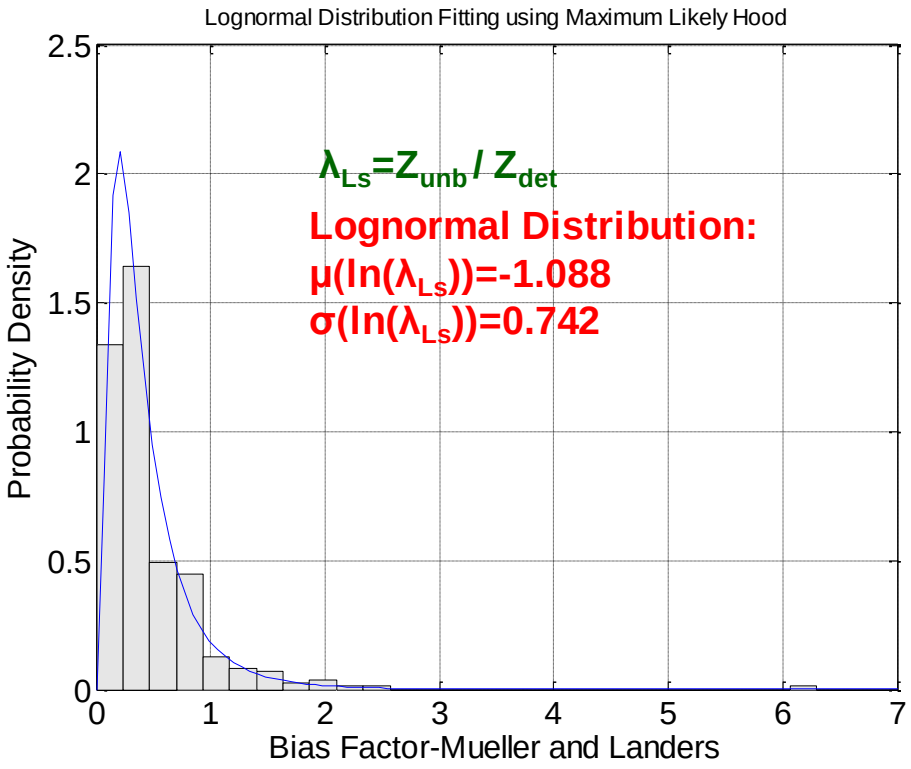

Figure 4-4. Lognormal Distribution Fitting Using Maximum Likelihood Method for Landers-Mueller Database Using HEC-18 Clay.

The comparison analysis is shown below.

The parameters in Figure 4-4 are: μ=-1.088, σ=0.742

Note that if we use $\mu(\ln\lambda_{Ls})$=-1.088, $\sigma(\ln\lambda_{Ls})$=0.742 from the lognormal distribution to back calculate the mean and standard deviation of the normal distribution, we might not get μ=0.456, σ=0.480.

$$\mu(\lambda_{Ls}) = e^{(\mu(\ln\lambda_{Ls})+\frac{1}{2}\sigma^2(\ln\lambda_{Ls}))} = e^{(-1.088+\frac{1}{2}\times 0.742^2)} = 0.444$$

$$\delta(\lambda_{Ls}) = \sqrt{e^{\sigma^2(\ln\lambda_{Ls})}-1} = \sqrt{e^{0.742^2}-1} = 0.857$$

$$\sigma(\lambda_{Ls}) = \mu(\lambda_{Ls}) \times \delta(\lambda_{Ls}) = 0.444 \times 0.857 = 0.381$$

The reason is that the relationship between the normal distribution parameters and lognormal distribution parameters is based on the probability density function rather than the histogram.

Compare the results from the lognormal distribution fitting using the maximum likelihood method with the model proposed in Section 3.

In the HEC-18 Clay method, Equation 4-5 shows the unbiased scour depth prediction model.

$$Z_{\text{unb}} = \lambda_{\text{Ls}} \cdot Z_{\text{det}} \ , \tag{4-5}$$

Note that λ_{Ls} includes the uncertainty information, therefore no error term shown in the equation. Equation 4-6 shows the model proposed in Section 3.

$$\ln Z_{\text{unb}} = \theta + \ln Z_{\text{det}} + \sigma\varepsilon \tag{4-6}$$

Hence, $\ln(\lambda_{Ls}) = \theta + \sigma\varepsilon$. Equations 4-7 and 4-8 show the mean and standard deviation of $\ln(\lambda_{\text{Ls}})$.

$$\mu(\ln \lambda_{Ls}) = \mu(\theta) \tag{4-7}$$

$$\sigma(\ln \lambda_{Ls}) = \sqrt{\sigma^2(\theta) + \mu^2(\sigma)} \tag{4-8}$$

From the results obtained from Section 3,

$$\mu(\theta) = -1.0870 \ , \ \sigma(\theta) = 0.0253 .$$

$$\mu(\sigma) = 0.7450 \ , \ \sigma(\sigma) = 0.0294$$

Therefore,

$$\mu(\ln \lambda_{Ls}) = \mu(\theta) = -1.0870$$

$$\sigma(\ln\lambda_{Ls}) = \sqrt{\sigma^2(\theta) + \mu^2(\sigma)} = \sqrt{0.0253^2 + 0.7450^2} = 0.7454$$

Since we obtained the distribution of $ln\lambda_{Ls}$, we can back calculate the parameter of $\mu(ln\lambda_{Ls})$ and $\sigma(ln\lambda_{Ls})$.

$$\mu(\lambda_{L_s}) = e^{(\mu(\ln\lambda_{Ls}) + \frac{1}{2}\sigma^2(\ln\lambda_{Ls}))} = e^{(-1.0870 + \frac{1}{2}\times 0.7454^2)} = 0.445$$

$$\delta(\lambda_{L_s}) = \sqrt{e^{\sigma^2(\ln\lambda_{Ls})} - 1} = \sqrt{e^{0.7454^2} - 1} = 0.862$$

$$\sigma(\lambda_{L_s}) = \mu(\lambda_{L_s}) \times \delta(\lambda_{L_s}) = 0.445 \times 0.862 = 0.383$$

Table 4-2 shows the parameters using both the lognormal distribution fitting and the model proposed in Section 3. It can be seen that the results match.

Table 4-2. Comparison between Different Approaches-HEC-18 Clay.

Parameters	Normal Fitting Histogram	Lognormal Fitting Histogram	Lognormal → Normal	Model in Section 3 (Lognormal)	Lognormal → Normal
μ	0.456	-1.088	0.444	-1.0870	0.445
σ	0.480	0.742	0.381	0.7454	0.383

4.4 STATISTICAL PARAMETERS OF SCOUR DEPTH

These statistical values are used in the calibration in the following section.

The goal is to match the reliability index β_T associated with a probability of failure typically used in existing probabilistic LRFD codes. Such probabilistic codes have been used for many years by structural engineers, and they are increasingly used by geotechnical engineers worldwide, but scour is still handled in a deterministic fashion.

The probabilistic factors to affect the scour depth are calculated from the data collected while matching the reliability index. Because shallow foundations are typically non-redundant systems, a target reliability index β_T equal to 3 (PoF = 0.001) will be used (Equation 4-9).

$$Z_{LRFD} = \theta_T \times Z_{det} \tag{4-9}$$

where the factor θ_T = the ratio of the probabilistically predicted scour depth Z_{LRFD} to match a target probability of exceedance over the deterministically predicted scour depth by HEC-18 equations (Z_{det}).

More generally, the value of θ can be determined from any chosen value of the probability of exceedance (PoE).

$$Z(PoE) = \theta(PoE) \times Z_{det} \tag{4-10}$$

where the probabilistic factor θ can be plotted against the PoE by using different databases. The following section will aim to obtain θ_T using different databases and different methods.

4.4.1 Statistical Parameters of Landers and Mueller Database

4.4.1.1 Full Database

Figure 4-5 and Figure 4-6 show the values of the factor θ as a function of the probability that the scour depth predicted by HEC-18 will be exceeded. For a given probability of exceedance of 0.001 (i.e. β_T = 3), the target value of θ, θ_T , using HEC-18 Sand and HEC-18 Clay are 2.05 and 2.5 respectively. In other words, even though HEC-18 Sand and HEC-18 Clay are quite conservative already, the predictions need to be multiplied

by 2.05 and 2.5 respectively to ensure that the probability of exceeding the predicted scour depth will be 0.001 or less. The probability of exceeding the predicted scour depth is 3.3% and 7% for HEC-18 Sand and HEC-18 Clay respectively (θ(PoE)=1 in both figures). The correction factor θ_{unb} corresponding to a 50% PoE for HEC-18 Sand and HEC-18 Clay are shown in Figure 4-5 and Figure 4-6 as well and confirm the previous results in Section 3.

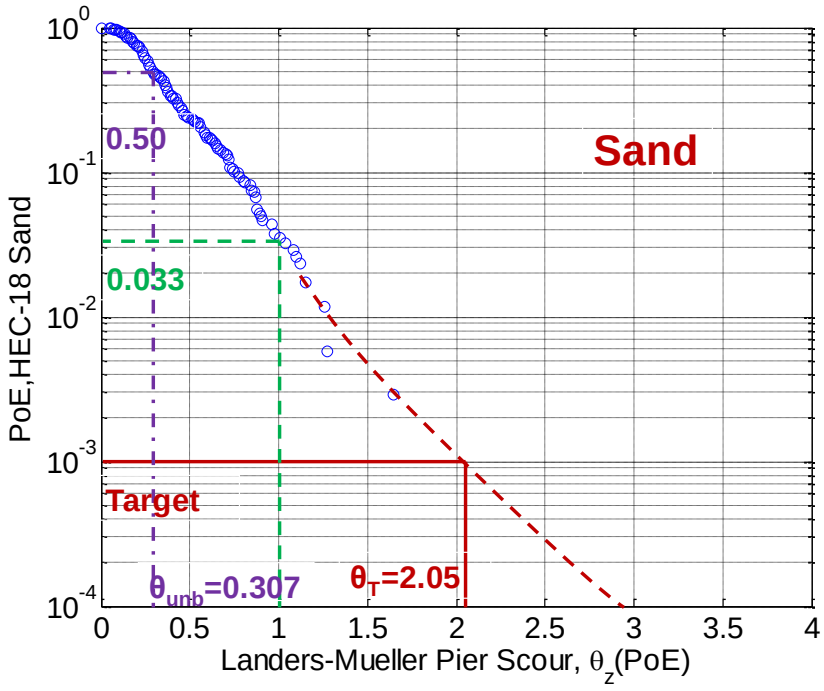

Figure 4-5. LRFD Calibration for HEC-18 Sand Using Landers-Mueller Database in a Semilog Scale.

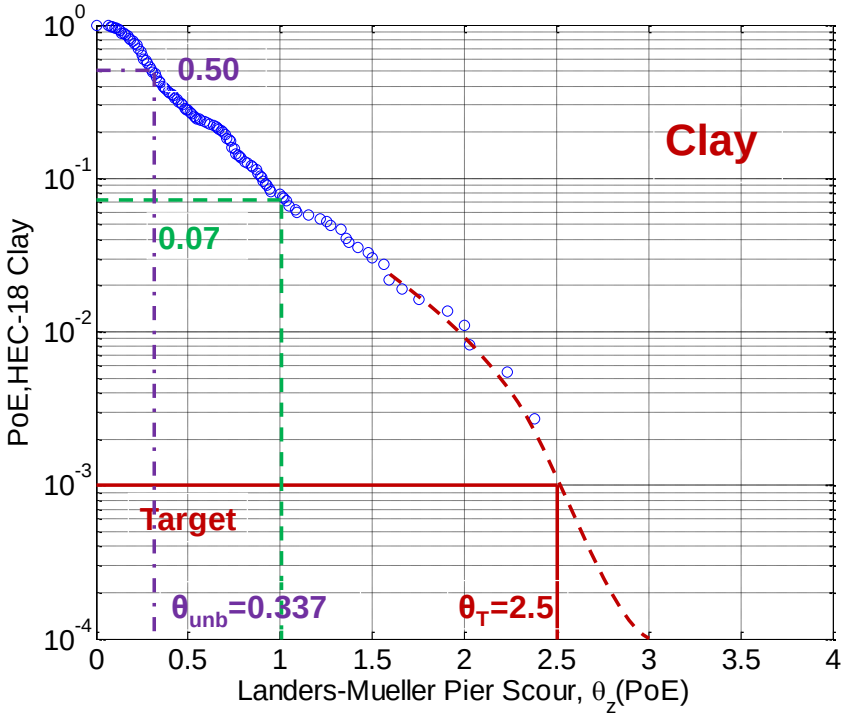

Figure 4-6. LRFD Calibration for HEC-18 Clay Using Landers-Mueller Database in a Semilog Scale.

4.4.1.2 Scour Depth > 2m

Figure 4-7 and Figure 4-8 show the values of the factor θ as a function of the probability that the scour depth predicted by HEC-18 will be exceeded when only the measured scour depth larger than 2m is considered. For a given probability of exceedance of 0.001 (i.e. $\beta_T = 3$), the target value of θ, θ_T , using HEC-18 Sand and HEC-18 Clay are 1.4 and 1.3 respectively. The probability of exceeding the predicted scour depth is 8% and 0.7% for HEC-18 Sand and HEC-18 Clay respectively (θ(PoE)=1 in both figures). The correction factor θ_{unb} corresponding to a 50% PoE for HEC-18 Sand and HEC-18 Clay

are shown in Figure 4-7 and Figure 4-8 as well and confirm the previous results in Section 3.

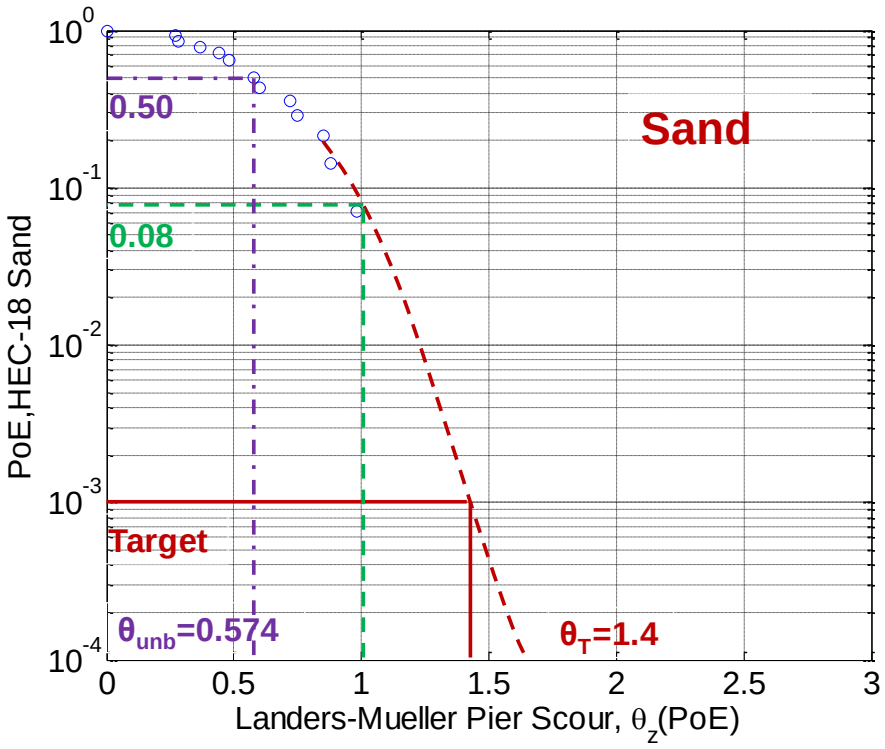

Figure 4-7. LRFD Calibration for HEC-18 Sand Using Landers-Mueller Database in a Semilog Scale - $Z_{measured}$ > 2m.

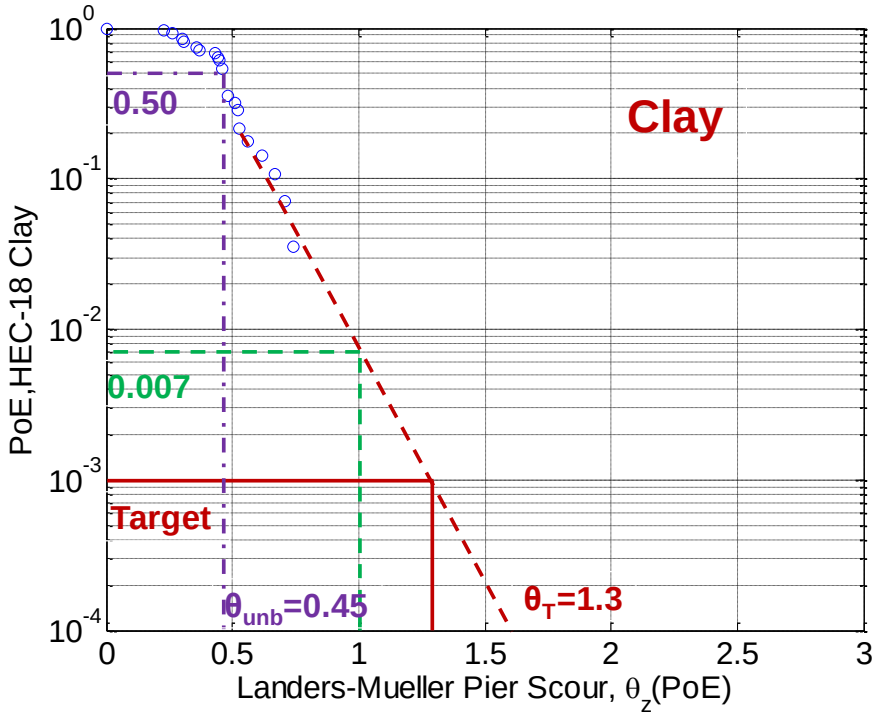

Figure 4-8. LRFD Calibration for HEC-18 Clay Using Landers-Mueller Database in a Semilog Scale - $Z_{measured}$ > 2m.

4.4.1.3 Scour Depth < 2m

Figure 4-9 and Figure 4-10 show the values of the factor θ as a function of the probability that the scour depth predicted by HEC-18 will be exceeded only when the measured scour depth less than 2m is considered. For a given probability of exceedance of 0.001 (i.e. $\beta_T = 3$), the target value of θ, θ_T , using HEC-18 Sand and HEC-18 Clay are 1.95 and 2.75 respectively. The probability of exceeding the predicted scour depth is 2.6% and 7% for HEC-18 Sand and HEC-18 Clay respectively (θ(PoE)=1 in both figures). The correction factor θ_{unb} corresponding to a 50% PoE for HEC-18 Sand and HEC-18

Clay are shown in Figure 4-9 and Figure 4-10 as well and confirm the previous results in Section 3.

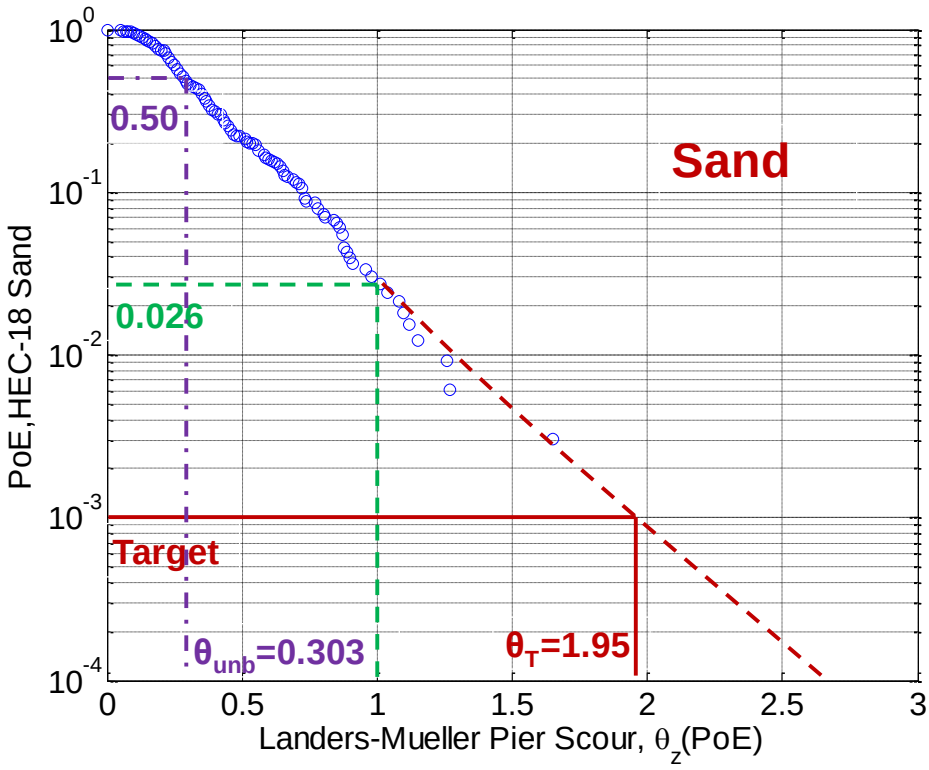

Figure 4-9. LRFD Calibration for HEC-18 Sand Using Landers-Mueller Database in a Semilog Scale - $Z_{measured}$ < 2m.

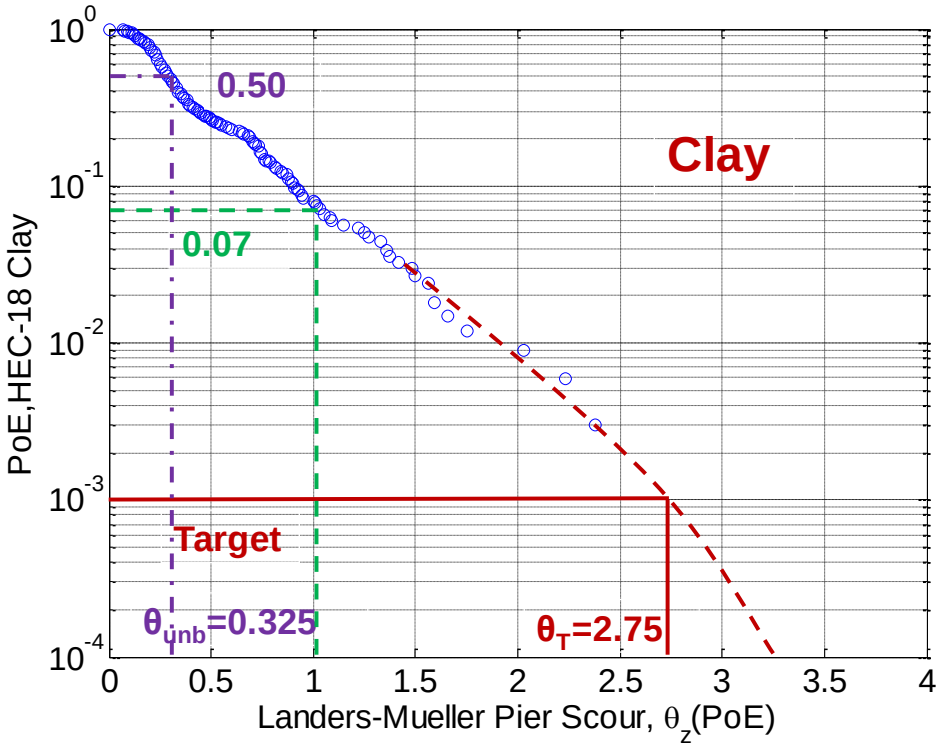

Figure 4-10. LRFD Calibration for HEC-18 Clay Using Landers-Mueller Database in a Semilog Scale - $Z_{measured}$ < 2m.

4.4.2 Statistical Parameters of TAMU Database

Figure 4-11 and Figure 4-12 show the values of the factor θ as a function of the probability that the scour depth predicted by HEC-18 will be exceeded. For a given probability of exceedance of 0.001 (i.e. $\beta_T = 3$), the target value of θ, θ_T , using HEC-18 Sand and HEC-18 Clay are 1.5 and 1.8 respectively. The probability of exceeding the predicted scour depth is 11% and 38% for HEC-18 Sand and HEC-18 Clay respectively (θ(PoE)=1 in both figures). The correction factor θ_{unb} corresponding to a 50% PoE for

HEC-18 Sand and HEC-18 Clay are shown in Figure 4-11 and Figure 4-12 as well and confirm the previous results in Section 3.

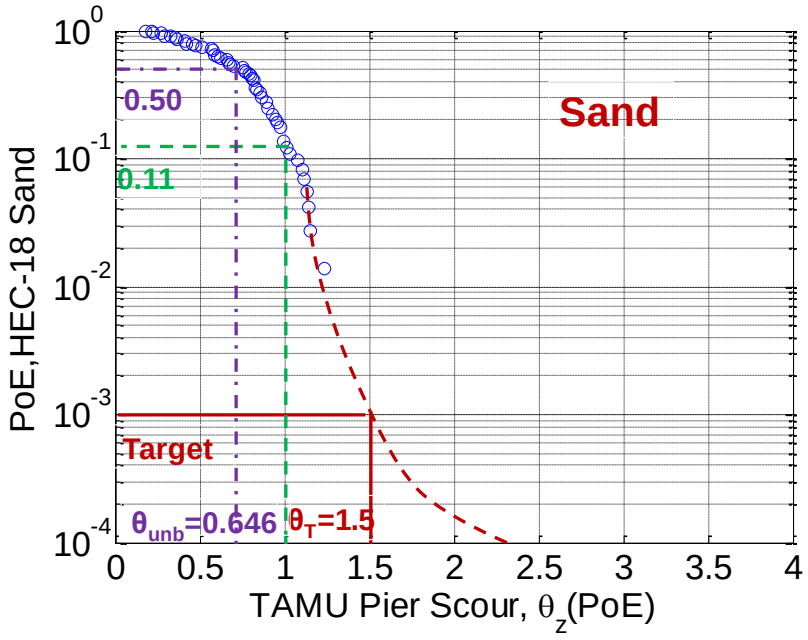

Figure 4-11. LRFD Calibration for HEC-18 Sand Using TAMU Database in a Semilog Scale.

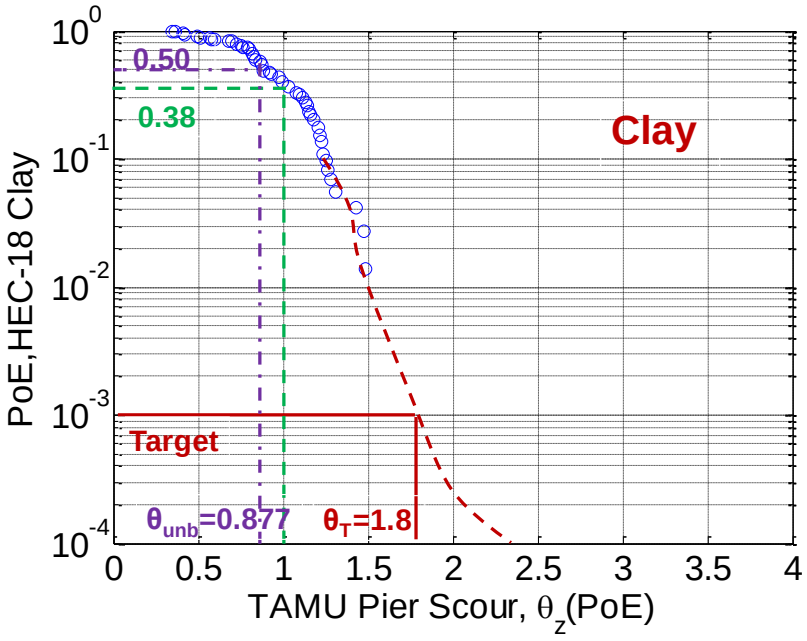

Figure 4-12. LRFD Calibration for HEC-18 Clay Using TAMU Database in a Semilog Scale.

4.4.3 Statistical Parameters of Froehlich Database

Figure 4-13 through Figure 4-16 show the values of the factor θ as a function of the probability that the scour depth predicted by HEC-18 will be exceeded. Note that the HEC-18 Clay method using V_{c_Briaud}, V_{c*} and V_{c**} are discussed respectively. For a given probability of exceedance of 0.001 (i.e. $\beta_T = 3$), the target value of θ, θ_T , using HEC-18 Sand is 1.5. For a given probability of exceedance of 0.001 (i.e. $\beta_T = 3$), the target value of θ, θ_T , using HEC-18 Clay based on V_{c_Briaud} is 1.8. For a given probability of exceedance of 0.001 (i.e. $\beta_T = 3$), the target value of θ, θ_T , using HEC-18 Clay based on V_{c*} is 2.7. For a given probability of exceedance of 0.001 (i.e. $\beta_T = 3$), the target value of θ, θ_T , using HEC-18 Clay based on V_{c**} is 2.51.

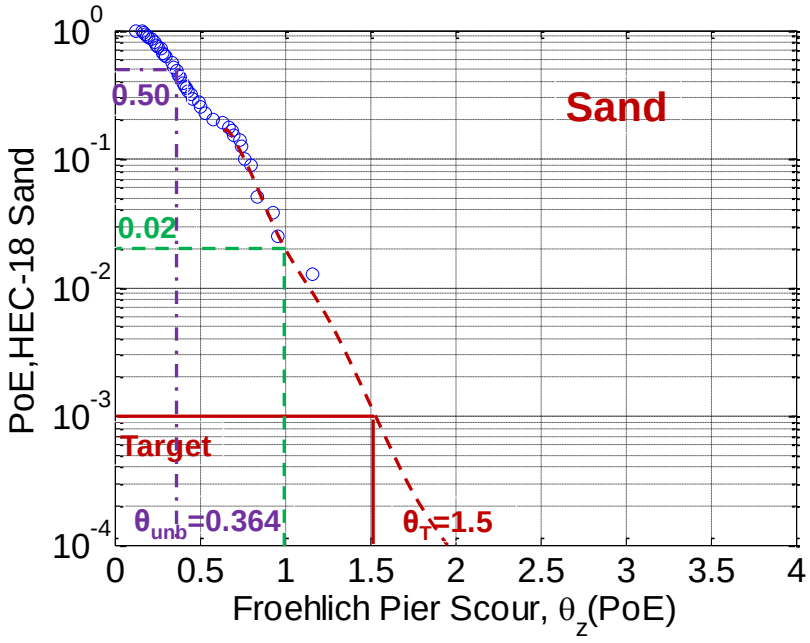

Figure 4-13. LRFD Calibration for HEC-18 Sand Using Froehlich Database in a Semilog Scale.

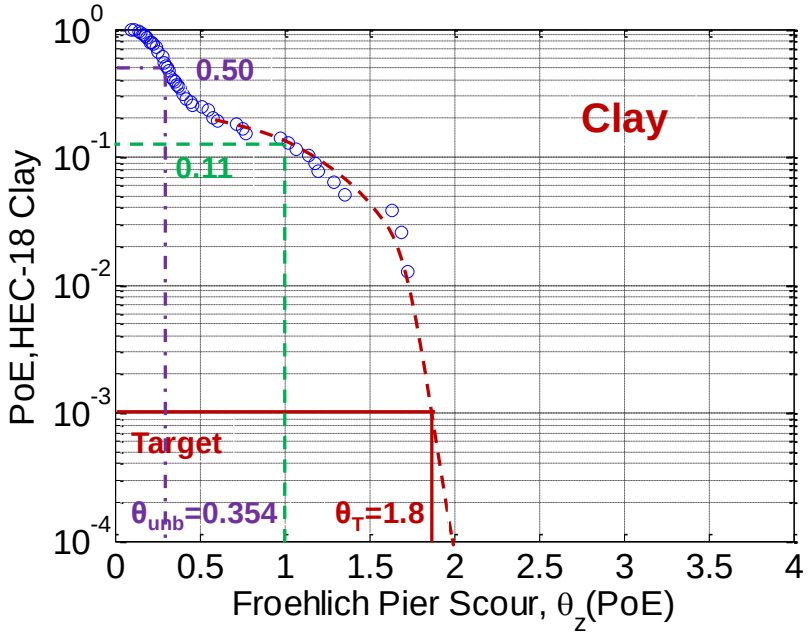

Figure 4-14. LRFD Calibration for HEC-18 Clay Using V_{c_Briaud} for Froehlich Database in a Semilog Scale.

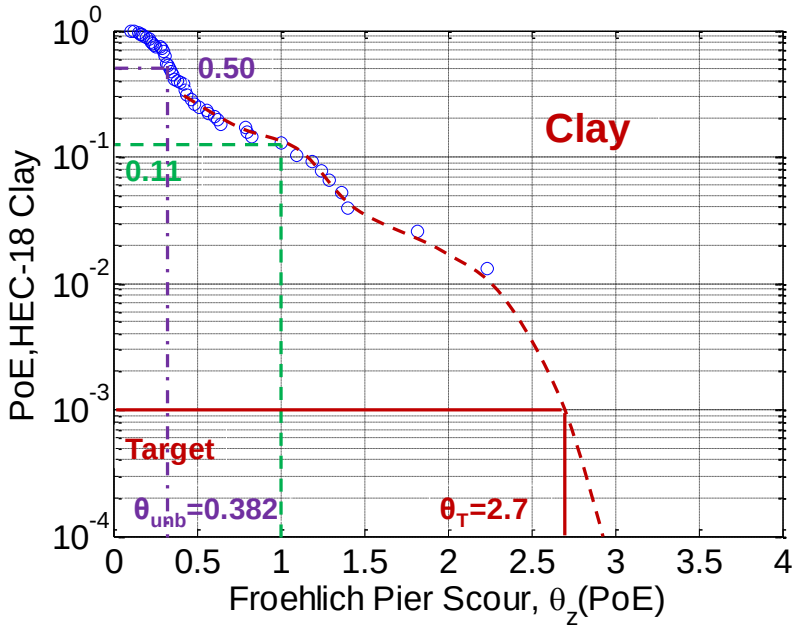

Figure 4-15. LRFD Calibration for HEC-18 Clay Using V_{c*} for Froehlich Database in a Semilog Scale.

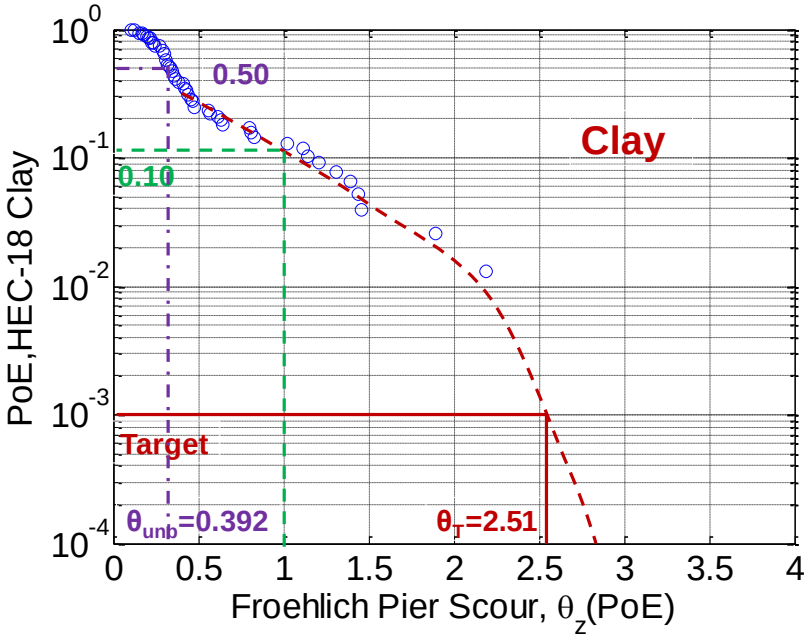

Figure 4-16. LRFD Calibration for HEC-18 Clay Using V_{c**} for Froehlich Database in a Semilog Scale.

The probability of exceeding the predicted scour depth is 2% for HEC-18 Sand (θ(PoE)=1 in Figure 4-13). The probability of exceeding the predicted scour depth is 11% for HEC-18 Clay based on V_{c_Briaud} (θ(PoE)=1 in Figure 4-14). The probability of exceeding the predicted scour depth is 11% for HEC-18 Clay based on V_{c*} (θ(PoE)=1 in Figure 4-15). The probability of exceeding the predicted scour depth is 10% for HEC-18 Clay based on V_{c**} (θ(PoE)=1 in Figure 4-16). The correction factor θ_{unb} corresponding to a 50% PoE for HEC-18 Sand and HEC-18 Clay are shown in Figure 4-13 through Figure 4-16 as well and confirm the previous results in Section 3.

4.5 CONCLUSIONS ON LRFD CALIBRATION FOR SHALLOW FOUNDATIONS IN THE CASE OF SCOUR

This section is about the LRFD calibration for shallow foundations in the case of bridge scour. The statistical analysis of the bridge scour databases was shown first. Then the calibration procedure is described. In order to meet the target probability of exceedance (0.001), the scour depth should be multiplied by a factor θ_T in the design process.

Results based on the Landers-Mueller Database:

- If you want to build shallow foundations in sand, the foundation depth should be 2.05 Z_{det} in order to meet the probability of exceedance of 0.001.
- If you want to build shallow foundations in clay, the foundation depth should be 2.5 Z_{det} in order to meet the probability of exceedance of 0.001.
- If Z_{scour} > 2m, the foundation depth in sand should be 1.4 Z_{det} in order to meet the probability of exceedance of 0.001.

- If Z_{scour} > 2m, the foundation depth in clay should be 1.3 Z_{det} in order to meet the probability of exceedance of 0.001.
- If Z_{scour} < 2m, the foundation depth in sand should be 1.95 Z_{det} in order to meet the probability of exceedance of 0.001.
- If Z_{scour} < 2m, the foundation depth in clay should be 2.75 Z_{det} in order to meet the probability of exceedance of 0.001.

Results based on the TAMU Database:

- If you want to build shallow foundations in sand, the foundation depth should be 1.5 Z_{det} in order to meet the probability of exceedance of 0.001.
- If you want to build shallow foundations in clay, the foundation depth should be 1.8 Z_{det} in order to meet the probability of exceedance of 0.001.

Results based on the Froehlich Database:

- If you want to build shallow foundations in sand, the foundation depth should be 1.5 Z_{det} in order to meet the probability of exceedance of 0.001.
- If you want to build shallow foundations in clay, the foundation depth should be 1.8 Z_{det} in order to meet the probability of exceedance of 0.001.

All in all, if you want to build shallow foundations in sand, the foundation depth should be 1.5 Z_{det} in order to meet the probability of exceedance of 0.001. If you want to build shallow foundations in clay, the foundation depth should be 1.8 Z_{det} in order to meet the probability of exceedance of 0.001.

Table 4-3 shows the Computed θ_T for Different Databases using Different Methods.

Table 4-3. Computed θ_T for Different Databases Using Different Methods.

Database	Cases	Method	Data Points	Maximum Likelyhood		Bayesian		θ_{unb}	θ_T	P_f
				Parameter Γ_ζ	Parameter σ_ζ	Parameter Γ_ζ	Parameter σ_ζ			
L&M	Whole Database	HEC-18 Sand	344	-1.179	0.6744	-1.1778	0.6787	0.3079	2.05	0.001
		HEC-18 Clay	366	-1.0876	0.7409	-1.087	0.745	0.3372	2.5	0.001
TAMU	Whole Database	HEC-18 Sand	73	-0.434	0.4616	-0.4376	0.4757	0.6456	1.5	0.001
		HEC-18 Clay	73	-0.1323	0.3448	-0.1317	0.3404	0.8766	1.8	0.001
Froehlich	Whole Database	HEC-18 Sand	79	-1.0095	0.5359	-1.0116	0.5381	0.3636	1.5	0.001
		HEC-18 Clay using V_{c_Briaud}	78	-1.0333	0.7485	-1.0385	0.7709	0.354	1.8	0.001
		HEC-18 Clay using V_{c*}	77	-0.9559	0.6789	-0.9629	0.6788	0.3818	2.7	0.001
		HEC-18 Clay using V_{c**}	77	-0.9682	0.695	-0.9368	0.6865	0.3919	2.51	0.001

5 PROPOSED LRFD CALIBRATION FOR BRIDGE SCOUR DEPTH PREDICTIONS: DEEP FOUNDATIONS

5.1 INTRODUCTION

This section is about the LRFD calibration for deep foundations in the case of scour. For shallow foundations, the issue is the location of the foundation depth and the probability that the scour depth will exceed the foundation depth. Therefore, for shallow foundations, the proposed LRFD calibration is based on the probability of exceedance of the predicted scour depth. However for deep foundations, the issue is the resistance factor associated with the axial capacity of a pile, which will be introduced in the following section. For deep foundations, the proposed LRFD calibration is based on a reliability analysis using the First-Order Reliability Method (FORM).

This section includes two parts: the duplication of LRFD calibration of deep foundations without scour and the proposed LRFD calibration with scour effect. Due to the fact that most of the literature does not show the details of the LRFD calibration for the deep foundations without scour, the author spent lots of time and effort figuring out the calibration procedure and finally successfully matched the results from the NCHRP 507 Report (Paikowsky 2004). In order to well document the author's work and be beneficial to other researchers, the detailed LRFD calibration procedure for deep foundations without scour effect is also shown in this section. The results match the NCHRP 507 report very well. Following the same concept, the author developed the model to determine the resistance factor for deep foundations in the case of scour for

given dead load factor and live load factor. Different soil types, different design methods and different foundation sizes were considered during the calibration process. The recommendations for deep foundation design to engineers are provided at the end of this section.

5.2 CAPACITY

In the scour depth prediction model, the capacity means the ultimate bearing capacity for piles. For different design methods and different soil types, different pile capacity equations should be adopted.

5.3 DEMAND

In the scour depth prediction model, the demand is the dead and live load. The limit state function is defined in Equation 5-1.

$$g=R-D \tag{5-1}$$

where R = Capacity, and D = Demand.

5.4 GENERAL APPROACH FOR LRFD CALIBRATION

This section is introducing the general approach for LRFD calibration.

5.4.1 Definition of Parameters

Parameters that will be used in this section are shown below.

R_m : The unbiased estimates / best estimates / true values / measured values of the ultimate resistance

L_m : The unbiased estimates / best estimates / true values / measured values of the load

R_p : The nominal values / design values / predicted values of the resistance

L_p : The nominal values / design values / predicted values of the load

$\bar{\gamma}$: The central load factor

$\bar{\varphi}$: The central resistance factor

φ : The nominal resistance factor

γ : The nominal load factor

5.4.2 Procedure

The general approach to obtain the load factor and resistance factor is shown below (Briaud 2013).

1. The unbiased estimates or best estimates or true values or measured values of the ultimate resistance and the load are R_m and L_m. The nominal values or design values or predicted values of the resistance and the load are R_p and L_p

2. Obtain the probability distribution of the load L_m and of the ultimate resistance R_m. Note that L_m and R_m are probabilistic. Each follows a certain distribution (for example lognormal) with specified means (μ_{Rm} and μ_{Lm}) and standard deviation (σ_{Rm} and σ_{Lm}).

3. Write the limit state function as $g = R_m - L_m$. Because R_m and L_m are random, g is also random.

4. Compute using reliability software such as FERUM

a. the probability $P(g \leq 0)$

b. the corresponding value of the generalized reliability index β

c. the coordinates of the design point (R_m*, L_m*)

5. Choose a target reliability index β_T, usually 2.33 for redundant systems and 3 for non-redundant systems

6. Compare the β from Step 3 with the β_T, from Step 4. If the β from Step 3 is equal to the β_T from Step 4, then the central resistance factor $\overline{\varphi}$ and the central load factor $\overline{\gamma}$ can be calculated as ,

a. $\overline{\varphi} = R_m * / \mu_{Rm}$

b. $\overline{\gamma} = L_m * / \mu_{Lm}$

7. Otherwise, increase or decrease μ_{Rm} and repeat Steps 1 through 5.

8. Calculate the nominal resistance factor φ and the nominal load factor γ as follows

a. $$\varphi = \overline{\varphi} \frac{\mu_{Rm}}{\mu_{Rp}}$$

b. $$\gamma = \overline{\gamma} \frac{\mu_{Lm}}{\mu_{Lp}}$$

5.5 LRFD CALIBRATION FOR BRIDGE SCOUR DEPTH PREDICTIONS

Since in this dissertation the load factors are fixed, a different approach to compute resistance factor is used here.

5.5.1 Duplication of LRFD Calibration without Scour

5.5.1.1 Definition of Parameters

Equivalent parameters are defined as follows: measured value is equivalent to actual value or true value; predicted value is equivalent to nominal value, design value, analytical value, or deterministic value.

Load/Demand:

DL represents Dead Load; is a Random Variable.

$DL \sim LN(\mu_{DL}, \sigma_{DL})$

Here, μ_{DL} -- mean value of the measured dead load

σ_{DL} -- standard deviation of the measured dead load

δ_{DL} – coefficient of variation of the measured dead load

λ_{DL} – bias factor of dead load; the ratio of the measured dead load to the predicted dead load; *A Random Variable*.

$DL_{predicted} \sim DL_{nominal}$ – predicted value of dead load ~ nominal value of dead load

$$\lambda_{DL} = \frac{DL_{measured}}{DL_{nominal}} = \frac{DL_{measured}}{DL_{predicted}} \quad (5\text{-}2)$$

$\mu(\lambda_{DL})$ – mean value of the bias factor of dead load, =1.05

$\delta(\lambda_{DL})$ – coefficient of variation of the bias factor of dead load, =0.1

$\sigma(\lambda_{DL})$ – standard deviation of the bias factor of dead load, =0.105

γ_{DL} – dead load factor, =1.25, obtained from NCHRP Report 368 (Nowak 1999).

$$\gamma_{DL} = \mu(\lambda_{DL})(1 + k\delta(\lambda_{DL}))$$

where k=2.

LL—Live Load; A Random Variable

LL ~ LN(μ_{LL}, σ_{LL})

Here, μ_{LL} -- mean value of the measured live load

σ_{LL} -- standard deviation of the measured live load

δ_{LL} – coefficient of variation of the measured live load

λ_{LL} – bias factor of live load; the ratio of the measured live load to the predicted live load; *A Random Variable*.

$LL_{predicted}$ ~ $LL_{nominal}$ – predicted value of live load ~ nominal value of live load

$$\lambda_{LL} = \frac{LL_{measured}}{LL_{nominal}} = \frac{LL_{measured}}{LL_{predicted}} \quad (5\text{-}3)$$

$\mu(\lambda_{LL})$ – mean value of the bias factor of live load, =1.15

$\delta(\lambda_{LL})$ – coefficient of variation of the bias factor of live load, =0.2

$\sigma(\lambda_{LL})$ – standard deviation of the bias factor of live load, =0.23

γ_{LL} – live load factor, =1.75, obtained from NCHRP Report 368 (Nowak, 1999).

$$\gamma_{LL} = \mu(\lambda_{LL})(1 + k\delta(\lambda_{LL}))$$

where k=2.

Resistance/Capacity:

R—Ultimate Bearing Capacity, A Random Variable

R ~ LN(μ_R, σ_R)

Here, μ_R -- mean value of the measured resistance

σ_R -- standard deviation of the measured resistance

δ_R – coefficient of variation of the measured resistance

λ_R – bias factor of resistance; the ratio of the measured resistance to the predicted resistance; *A Random Variable*.

$R_{predicted} \sim R_{analytical} \sim R_{nominal}$ – predicted value of resistance ~ analytical value of resistance (from different design method) ~ nominal value of resistance

$$\lambda_R = \frac{R_{measured}}{R_{nominal}} = \frac{R_{measured}}{R_{analytical}} = \frac{R_{measured}}{R_{predicted}} \quad (5\text{-}4)$$

$\mu(\lambda_R)$ – mean value of the bias factor of resistance, obtained by performing the normal distribution fitting of the database.

$\sigma(\lambda_R)$ – standard deviation of the bias factor of resistance, obtained by performing the normal distribution fitting of the database.

$\delta(\lambda_R)$ – coefficient of variation of the bias factor of resistance, calculated from $\mu(\lambda_R)$ and $\sigma(\lambda_R)$.

φ – resistance factor, can be obtained by performing FORM (First Order Reliability Method) analysis.

5.5.1.2 Distribution Fitting Analysis

Here the author performed the distribution fitting analysis using the data from Appendix C of the NCHRP 507 Report (Paikowsky 2004, p. C-112). The data (Table 5-1) is for the case of pipe piles in cohesionless soils, using the Nordlund, 36,2B,P(5) design method.

Table 5-1. List of Bias Factors (Paikowsky 2004).

Case No.	1	2	3	4	5	6	7	8	9	10
Bias Factor λ	1.09	1.69	1.92	2.54	0.51	0.76	1.74	2.88	2.34	1.43
Case No.	11	12	13	14	15	16	17	18	19	20
Bias Factor λ	0.53	0.45	1.38	3.03	1.03	1.2	1.24	1.11	3.79	1.16

The mean and standard deviation of the bias factor is calculated in Equation 5-5 and Equation 5-6.

$$\mu = \bar{x} = \frac{\sum_{i=1}^{n} x_i}{n} = 1.591 \tag{5-5}$$

$$\sigma = \sqrt{\frac{\sum_{i=1}^{n} (x_i - \bar{x})^2}{n-1}} = 0.9115 \tag{5-6}$$

After eliminating the data out of the range $[\mu - 2\sigma, \mu + 2\sigma]$, the author obtained 19 data points. The histogram is plotted in Figure 5-1.

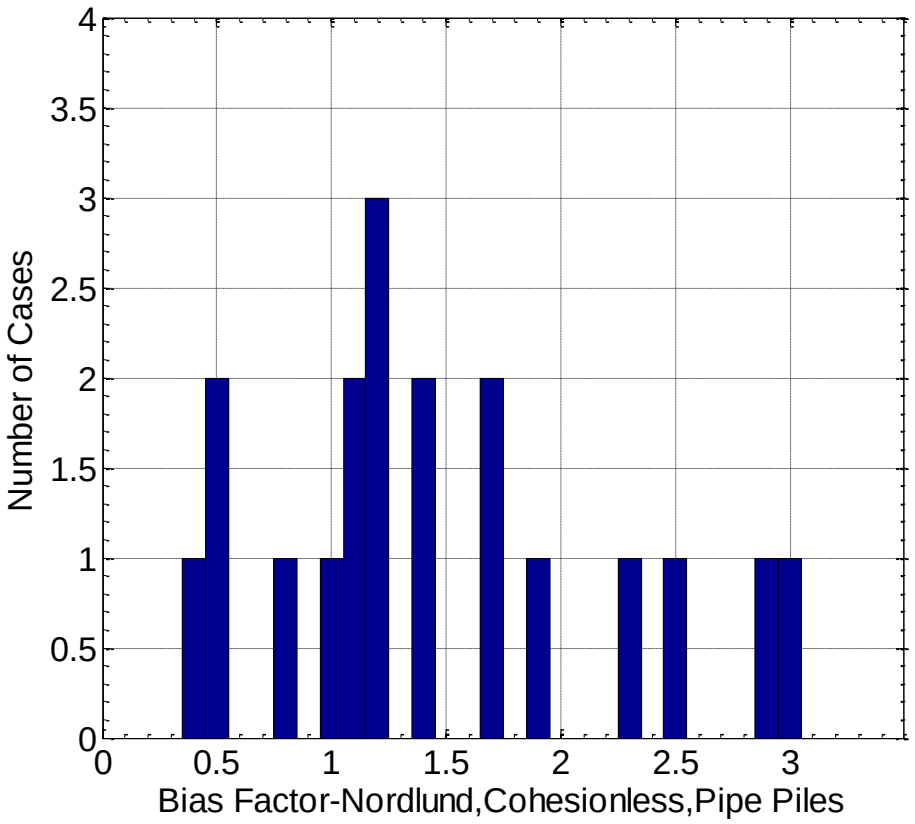

Figure 5-1. Histogram of Bias Factor (Comparable to Figure 22 in the NCHRP 507).

Here the author used two different fitting methods to obtain the distribution fitting: nonlinear least squares and maximum likelihood method.

The nonlinear least squares method is to choose the peaks of the histograms and do the curve fitting using those peaks by performing the least squares. It is a good method for curve fitting; nevertheless, it is not very pleasant for distribution fitting. The maximum likelihood method (MLE) is a better method for distribution fitting. It is applicable to do the distribution fitting for a histogram.

Figure 5-2 and Figure 5-3 below show the normal and lognormal distribution fitting using the nonlinear least square method respectively.

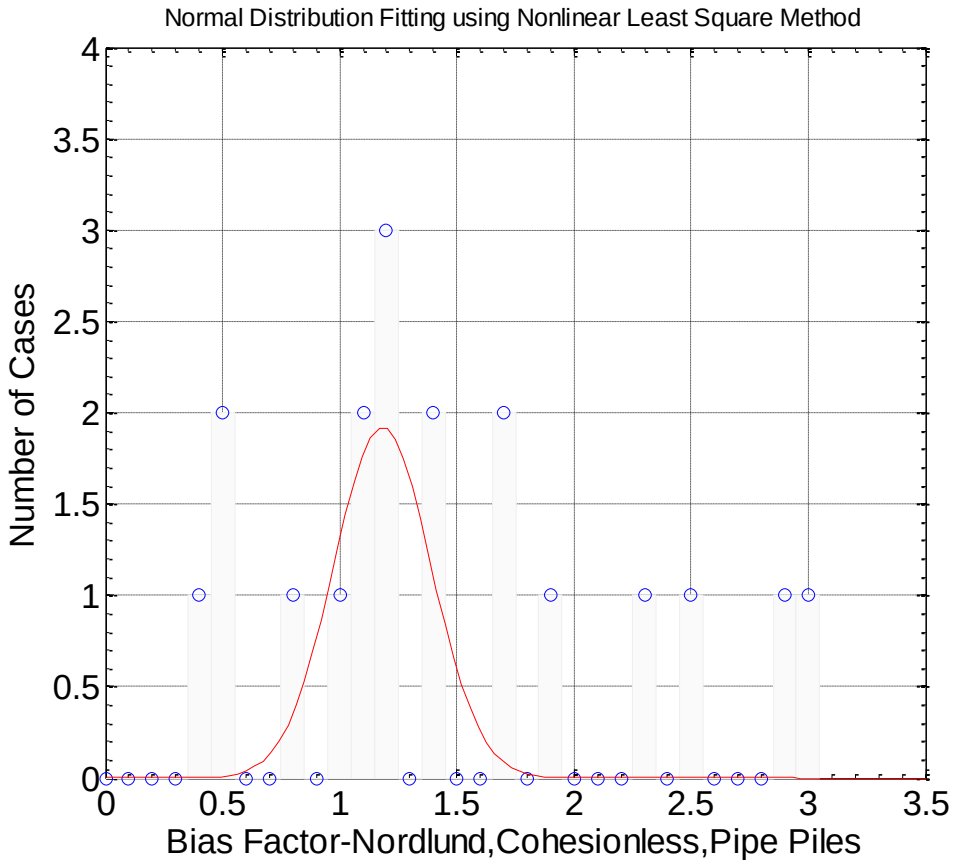

Figure 5-2. Normal Distribution Fitting Using Nonlinear Least Square Method for Nordlund, Cohesionless, Pipe Piles.

The parameters are: μ=1.182, σ=0.208.

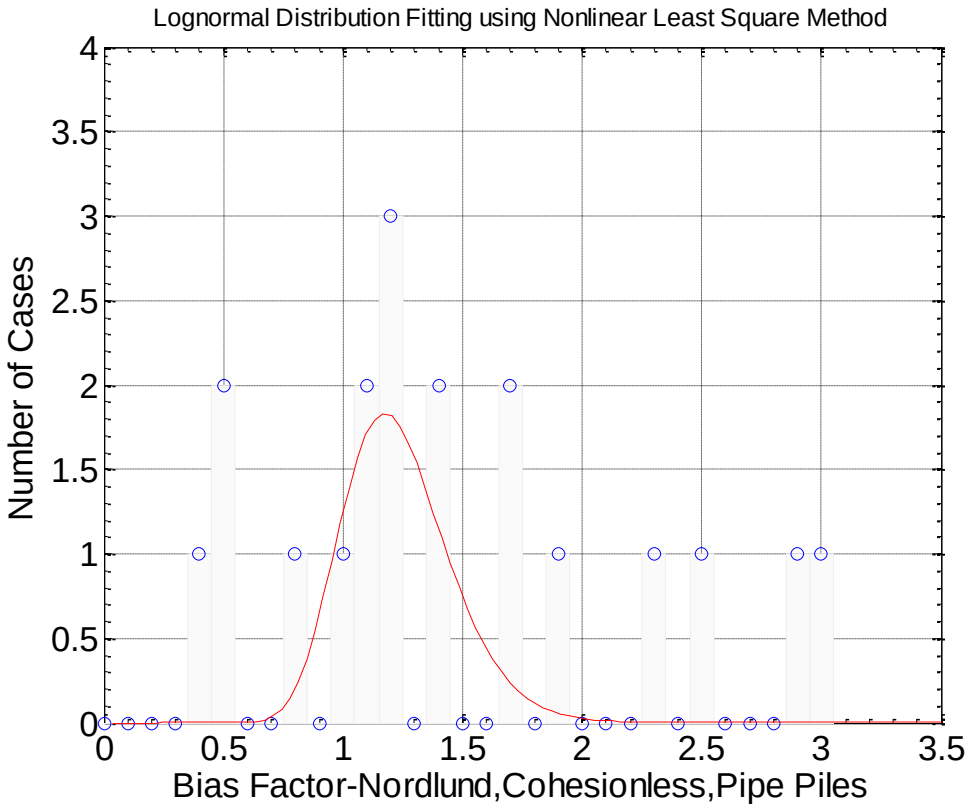

Figure 5-3. Lognormal Distribution Fitting Using Nonlinear Least Square Method for Nordlund, Cohesionless, Pipe Piles.

The parameters are: μ=0.194, σ=0.183

Figure 5-4 and Figure 5-5 below show the normal and lognormal distribution fitting using the maximum likelihood method respectively.

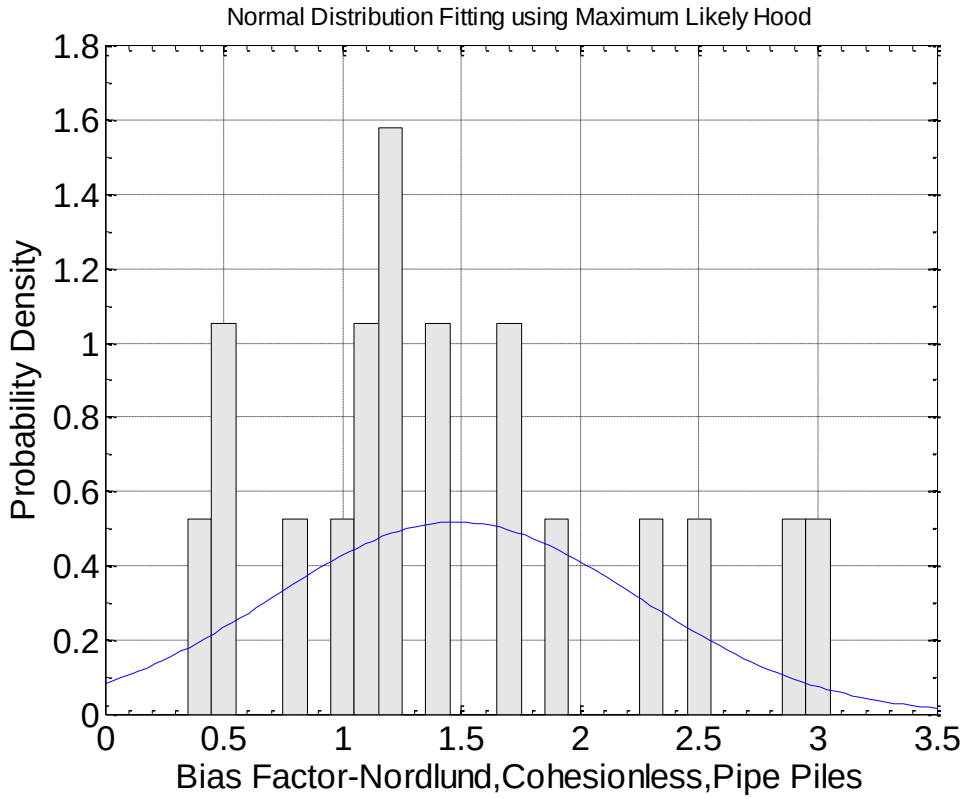

Figure 5-4. Normal Distribution Fitting Using Maximum Likelihood Method for Nordlund, Cohesionless, Pipe Piles.

The parameters are: μ=1.475, σ=0.771.

$$\delta(\lambda_R) = \frac{\sigma(\lambda_R)}{\mu(\lambda_R)} = \frac{0.771}{1.475} = 0.523$$

$$\sigma(\ln \lambda_R) = \sqrt{\ln(1+\delta^2(\lambda_R))} = \sqrt{\ln(1+0.523^2)} = 0.492$$

$$\mu(\ln \lambda_R) = \ln(\mu(\lambda_R)) - \frac{1}{2}\sigma^2(\ln \lambda_R) = \ln 1.475 - \frac{1}{2} \times 0.492^2 = 0.268\,.$$

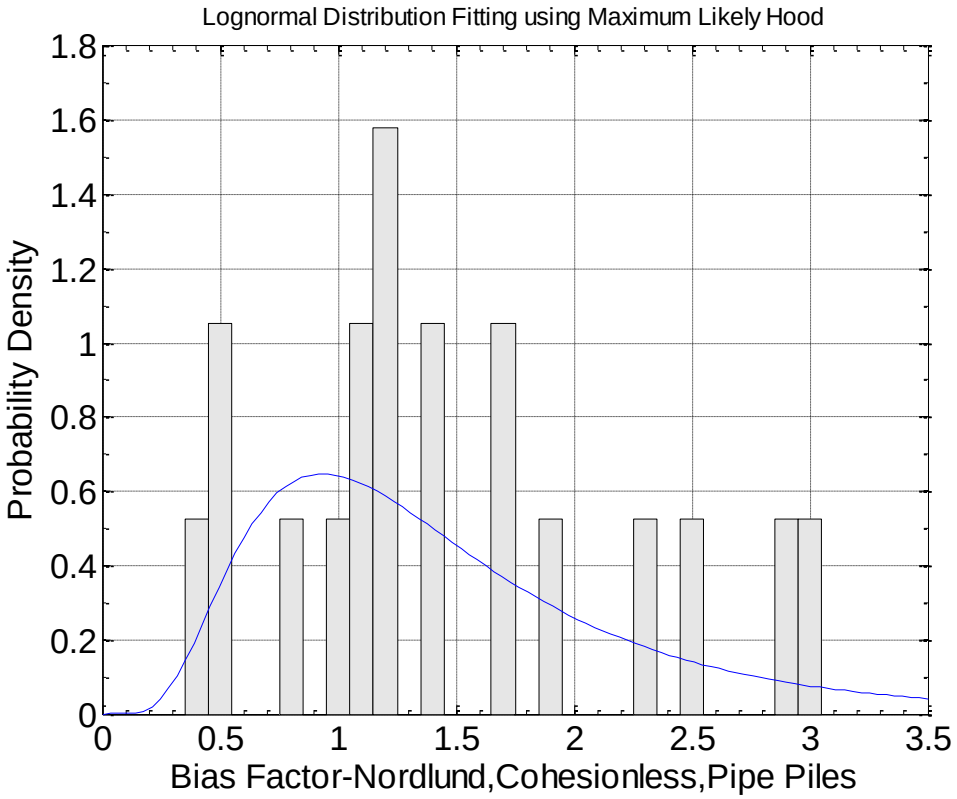

Figure 5-5. Lognormal Distribution Fitting Using Maximum Likelihood Method for Nordlund, Cohesionless, Pipe Piles.

The parameters are: μ=0.250, σ=0.562.

$$\mu(\lambda_R) = e^{(\mu(\ln\lambda_R)+\frac{1}{2}\sigma^2(\ln\lambda_R))} = e^{(0.250+\frac{1}{2}\times 0.562^2)} = 1.504$$

$$\delta(\lambda_R) = \sqrt{e^{\sigma^2(\ln\lambda_R)} - 1} = \sqrt{e^{0.562^2} - 1} = 0.609$$

$$\sigma(\lambda_R) = \mu(\lambda_R) \times \delta(\lambda_R) = 1.504 \times 0.609 = 0.916$$

Conclusion:

The normal distribution curve fitting (maximum likelihood method):

1. Calculate the mean and standard deviation of the sample data points

2. Generate the normal distribution using those parameters

The lognormal distribution curve fitting (maximum likelihood method):

1. Calculate the natural logarithm of the data points

2. Calculate the mean and standard deviation of the logarithm of sample data points

3. Generate the lognormal distribution using those parameters

In the NCHRP Report 507 (Paikowsky 2004), Paikowsky fitted the bias factor of resistance using both normal distribution and lognormal distribution, and discovered that the lognormal distribution shows better agreement with the histogram. Therefore, λ_R is seen as a random variable following lognormal distribution. In the reliability analysis, the mean and standard deviation of λ_R obtained from the normal distribution curve fitting are the inputs since they are easier to be determined. It is believed that the parameters for the lognormal distribution were back-calculated from the normal distribution parameters. Note that the lognormal distribution parameters back-calculated from the normal distribution are slightly different from the results obtained by directly performing lognormal distribution fitting of the raw data. It is easy to understand because the back-calculated lognormal distribution parameters are based on the entire normal distribution curve rather than the limited sample data points. On the other hand, the back-calculated normal distribution parameters from lognormal distribution fitting are different from the results obtained by directly performing normal distribution fitting of the raw data.

5.5.1.3 Step by Step Procedure

Dead Load (DL):

$DL \sim LN(\mu_{DL}, \sigma_{DL})$

$$\mu_{\mathrm{DL}} = \mu(DL_{\mathrm{measured}}) = \mu(\lambda_{\mathrm{DL}}) \times DL_{\mathrm{predicted}}$$

$$\sigma_{\mathrm{DL}} = \sigma(DL_{\mathrm{measured}}) = \sigma(\lambda_{\mathrm{DL}}) \times DL_{\mathrm{predicted}}$$

Here, $\mu(\lambda_{DL})=1.05$, $\delta(\lambda_{DL})=0.1$, $\sigma(\lambda_{DL})=0.105$.

Live Load (LL):

$LL \sim LN(\mu_{LL}, \sigma_{LL})$

$$\mu_{\mathrm{LL}} = \mu(LL_{\mathrm{measured}}) = \mu(\lambda_{\mathrm{LL}}) \times LL_{\mathrm{predicted}}$$

$$\sigma_{\mathrm{LL}} = \sigma(LL_{\mathrm{measured}}) = \sigma(\lambda_{\mathrm{LL}}) \times LL_{\mathrm{predicted}}$$

Here, $\mu(\lambda_{LL})=1.15$, $\delta(\lambda_{LL})=0.2$, $\sigma(\lambda_{LL})=0.23$.

Resistance (Ultimate Bearing Capacity):

$R \sim LN(\mu_R, \sigma_R)$,

$$\mu_{\mathrm{R}} = \mu(R_{\mathrm{measured}}) = \mu(\lambda_{\mathrm{R}}) \times R_{\mathrm{predicted}},$$

$$\sigma_{\mathrm{R}} = \sigma(R_{\mathrm{measured}}) = \sigma(\lambda_{\mathrm{R}}) \times R_{\mathrm{predicted}},$$

Here, $\mu(\lambda_R)$ and $\sigma(\lambda_R)$ are determined by the databases, provided in Table 16 in the NCHRP Report 507.

Limit State Function (unbiased):

$$g = R - DL - LL$$

$$g = \lambda_{\mathrm{R}} \times R_{\mathrm{predicted}} - \lambda_{\mathrm{DL}} \times DL_{\mathrm{predicted}} - \lambda_{\mathrm{LL}} \times LL_{\mathrm{predicted}}$$

$$g' = \lambda_R \times \frac{R_{predicted}}{LL_{predicted}} - \lambda_{DL} \times \frac{DL_{predicted}}{LL_{predicted}} - \lambda_{LL} \times \frac{LL_{predicted}}{LL_{predicted}}$$
$$= \lambda_R \times \frac{R_{predicted}}{LL_{predicted}} - \lambda_{DL} \times \frac{DL_{predicted}}{LL_{predicted}} - \lambda_{LL}$$

Given $\frac{DL_{predicted}}{LL_{predicted}} = 2$,

$$g' = \lambda_R \times \frac{R_{predicted}}{LL_{predicted}} - \lambda_{DL} \times \frac{DL_{predicted}}{LL_{predicted}} - \lambda_{LL} \times \frac{LL_{predicted}}{LL_{predicted}}$$
$$= \lambda_R \times \frac{R_{predicted}}{LL_{predicted}} - \lambda_{DL} \times 2 - \lambda_{LL}$$

Calculate the resistance factor:

Given $\gamma_{DL} \times DL_{predicted} + \gamma_{LL} \times LL_{predicted} = \varphi \times R_{predicted}$,

$\gamma_{DL} = 1.25$, $\gamma_{LL} = 1.75$

$$\varphi = \frac{\gamma_{DL} \times DL_{predicted} + \gamma_{LL} \times LL_{predicted}}{R_{predicted}} = \frac{\gamma_{DL} \times \frac{DL_{predicted}}{LL_{predicted}} + \gamma_{LL} \times 1}{\frac{R_{predicted}}{LL_{predicted}}} = \frac{\gamma_{DL} \times 2 + \gamma_{LL}}{\frac{R_{predicted}}{LL_{predicted}}} = \frac{1.25 \times 2 + 1.75}{\frac{R_{predicted}}{LL_{predicted}}} \quad (5\text{-}7)$$

where, $\frac{R_{predicted}}{LL_{predicted}}$ can be obtained from the FORM analysis.

Figure 5-6 shows the flow chart of the FERUM analysis without scour effect.

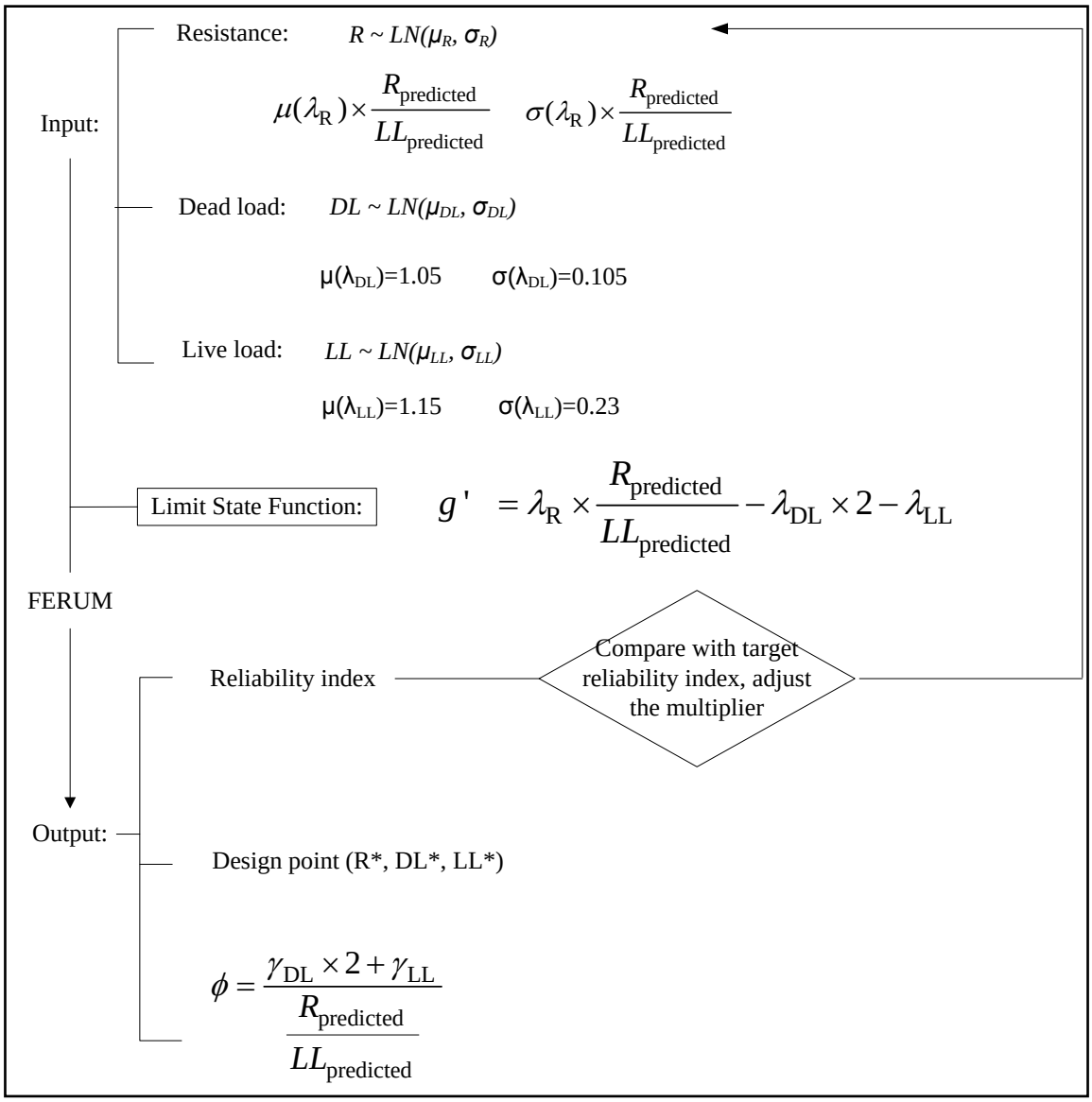

Figure 5-6. Flow Chart of FERUM Analysis without Scour Effect.

The author calculated the resistances factors of the 39 cases in Table 16 in the NCHRP Report 507 for a given reliability index β of 2 (probability of failure equals to 0.02), and compared the results with the results from the report. Figure 5-7 shows the comparison of resistance factors obtained from the code and the resistance factors

provided by Dr. Paikowsky. The linear regression analysis shows that the results match with each other pretty well.

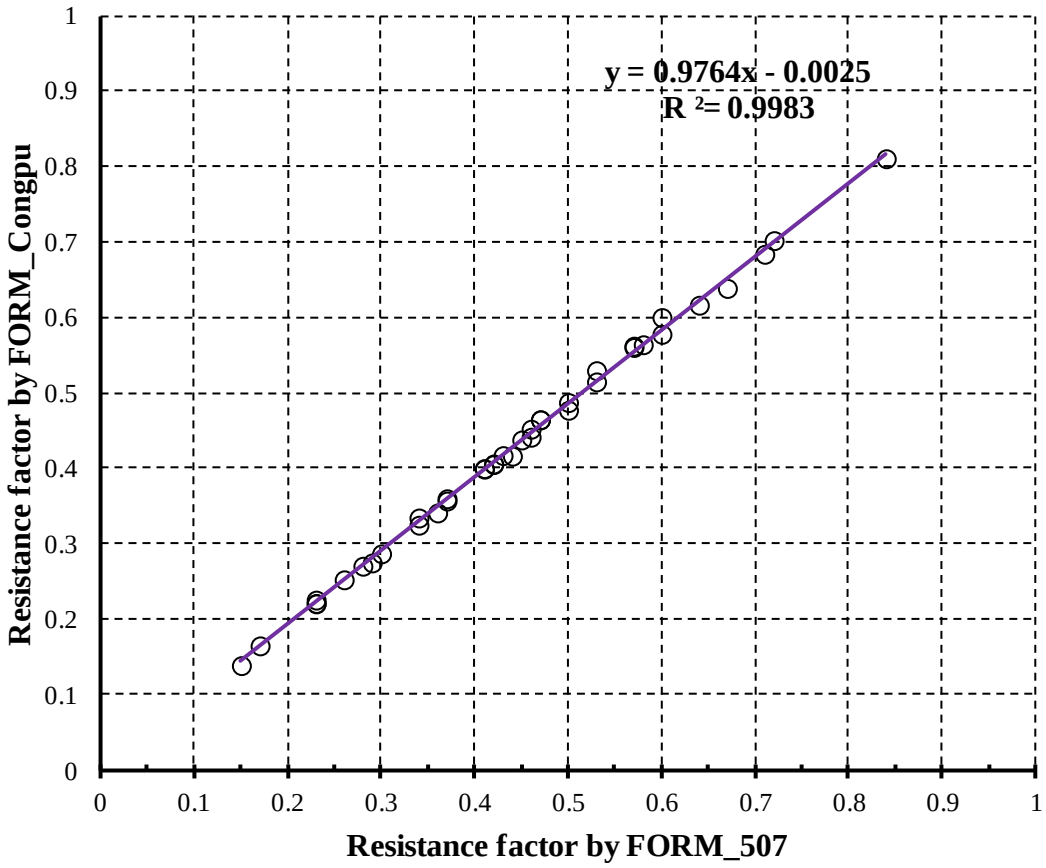

Figure 5-7. Results of FORM Analysis for β_{target} = 2 (Briaud et al. 2012).

5.5.2 Proposed LRFD Calibration with Scour Effect

5.5.2.1 Definition of Parameters

L_s—scour depth, a Random Variable

p_u—coefficient of tip resistance

f_u—coefficient of side resistance

L_p—designed total pile length

$L_{p\_noscour}$ — designed pile length to be able to sustain the design load when no scour is involved

B—designed pile width

S_u—undrained shear strength

λ_{Ls} – bias factor of scour depth; the ratio of the measured scour depth to the predicted scour depth; A Random Variable.

$L_{s\_predicted}$ ~ L_{s_det} – predicted scour depth ~ deterministic value of scour depth

$L_{s\_measured}$ ~ L_{s_unb} – measured scour depth ~ unbiased value of scour depth

$$\lambda_{Ls} = \frac{L_{s\_measured}}{L_{s\_predicted}} = \frac{L_{s\_unb}}{L_{s\_det}}$$

$\mu(\lambda_{Ls})$ – mean value of the bias factor of scour depth, obtained by performing the lognormal distribution fitting of the database first, then back-calculating the mean value of the bias factor of scour depth based on the relationship between the lognormal distribution parameters and normal distribution parameters.

$\delta(\lambda_{Ls})$ – coefficient of variation of the bias factor of scour depth, obtained by performing the lognormal distribution fitting of the database first, then back-calculating the standard deviation of the bias factor of scour depth based on the relationship between the lognormal distribution parameters and normal distribution parameters.

$\sigma(\lambda_{Ls})$ – standard deviation of the bias factor of scour depth, calculated from $\mu(\lambda_{Ls})$ and $\delta(\lambda_{Ls})$.

5.5.2.2 Distribution Fitting Analysis

Section 4.3 shows the distribution fitting analysis for bias factor of scour depth λ_{Ls} using the Landers and Mueller Database. The statistical parameters of bias factor of scour depth λ_{Ls} is the input to the limit state function.

5.5.2.3 Step by Step Procedure

Since there are so many different soil conditions, pile types, and design methods in geotechnical engineering, it is not easy to propose a single number of resistance factor in the scour condition. In order to better resolve this problem, a simple case is analyzed first here. Figure 5-8 shows the flow chart of the FERUM analysis in the case of scour.

5.6 CASE STUDIES

Several case studies are shown in this section in order to propose the LRFD design of bridge foundations in the case of scour.

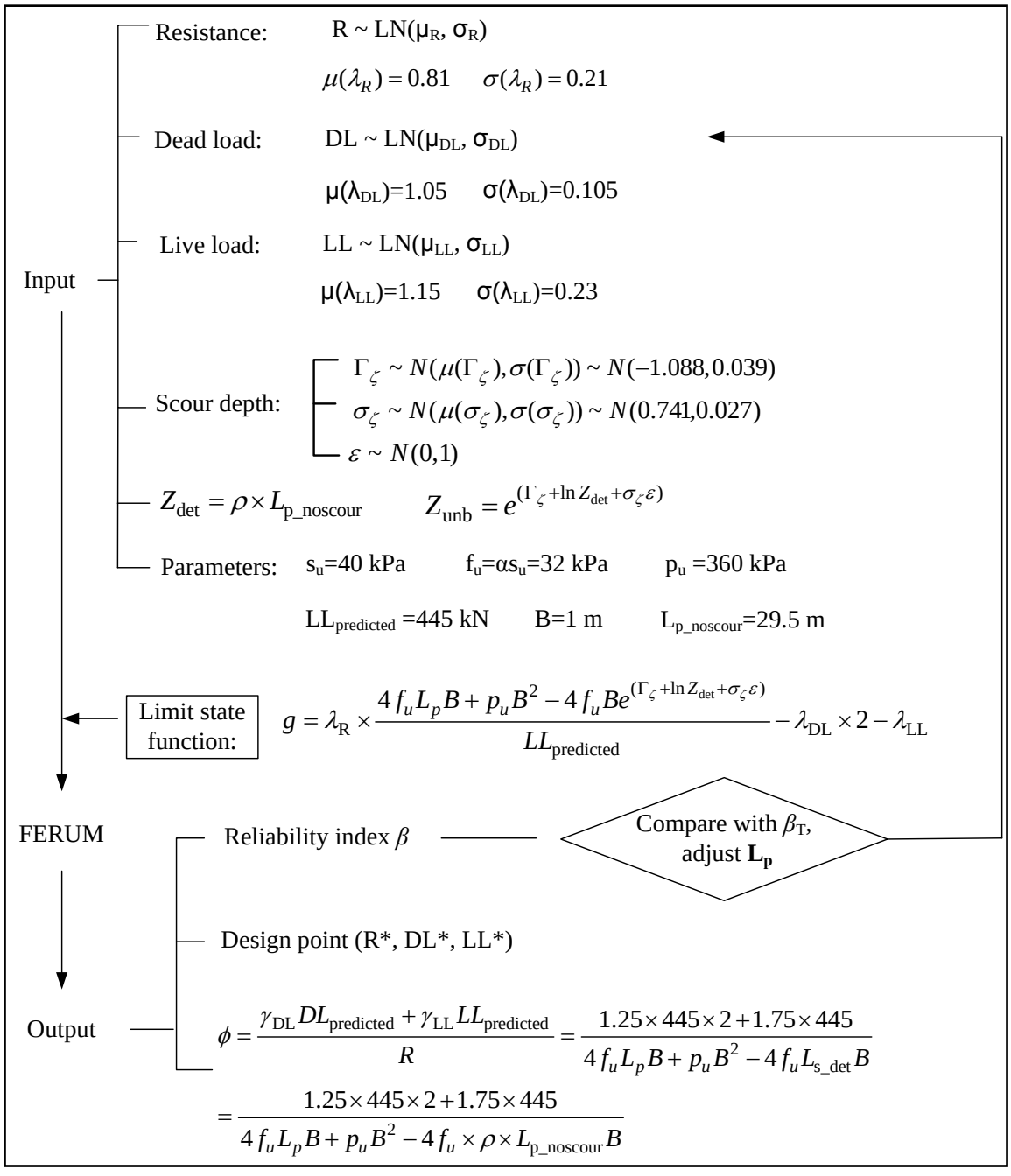

Figure 5-8. Flow Chart of FERUM Analysis in the Case of Scour.

5.6.1 Case Studies in Clay, α-API Design

Since there are several different soil types, pile types, and design methods in geotechnical engineering, it is not easy to propose a single resistance factor in the case of scour. In this section a square concrete pile with a width *B* in clay designed using the α-API method is adopted as an example. Based on the NCHRP Report 507 (Paikowsky 2004, p. 34), which is the basis for the AASHTO LRFD (2007), in the case of no scour, the mean of the resistance bias factor is $\mu(\lambda_R) = 0.81$, the standard deviation of the resistance bias factor is $\sigma(\lambda_R) = 0.21$, and the coefficient of variation of the resistance bias factor is $\delta(\lambda_R) = 0.26$. For a target reliability index of 3 ($\beta_T = 3$, PoF = 0.001), the AASHTO LRFD resistance factor is 0.44 ($\varphi = 0.44$). The objective is to revise this "no scour" resistance factor when scour occurs.

First, the no scour case is analyzed to choose a reasonable diameter and length for the pile (B and $L_{p\_noscour}$) to meet the target reliability index of 3 (β_T=3, PoF=0.001). Note that $L_{p\_noscour}$ is the pile length required by design to sustain the design load with β_T=3 when no scour is involved. For the analysis, an undrained shear strength s_u equal to 40kPa is selected (i.e. s_u=40kPa). The pile ultimate resistance is given as Equation 5-8.

$$R_u = f_u A_f + p_u A_p = \alpha s_u A_f + 9 s_u A_p \ , \qquad (5\text{-}8)$$

where the coefficient α for the ultimate side friction f_u is determined to be 0.8, (i.e., $f_u = \alpha s_u = 0.8 \times 40 = 32\ kPa$), and the ultimate point pressure p_u is determined to be 360kPa (i.e., $p_u = 9 s_u = 9 \times 40 = 360\ kPa$). The live load model is an HS-20-44 truck

(Paikowsky 2004), which gives $LL_{predicted}$=445kN. In order to keep a consistency with the NCHRP Report 507, the dead load and live load ratio is chosen to be 2, therefore, $DL_{\text{predicted}} = 2 \times LL_{\text{predicted}} = 2 \times 445 = 890\,kN$. The limit state function can be written in Equation 5-9.

$$g = R - DL - LL \tag{5-9}$$

where, *R*, *DL* and *LL* are the unbiased values of the resistance, the dead load and the live load respectively.

$$g = \lambda_{\text{R}} \times R_{\text{predicted}} - \lambda_{\text{DL}} \times DL_{\text{predicted}} - \lambda_{\text{LL}} \times LL_{\text{predicted}} \tag{5-10}$$

$$g' = \lambda_{\text{R}} \times \frac{R_{\text{predicted}}}{LL_{\text{predicted}}} - \lambda_{\text{DL}} \times \frac{DL_{\text{predicted}}}{LL_{\text{predicted}}} - \lambda_{\text{LL}} \tag{5-11}$$

given $\frac{DL_{\text{predicted}}}{LL_{\text{predicted}}} = 2$,

$$g' = \lambda_{\text{R}} \times \frac{R_{\text{predicted}}}{LL_{\text{predicted}}} - \lambda_{\text{DL}} \times 2 - \lambda_{\text{LL}} \tag{5-12}$$

Then a FORM analysis was performed using the software package FERUM (FERUM 2001) for a target reliability index β_T equal to 3. The statistical parameters of λ_R, λ_{DL} and λ_{LL} are given in the previous section. In Equation 5-12, for g'=0, the only unknown is $R_{predicted}/LL_{predicted}$. FERUM gives $R_{predicted}/LL_{predicted}$=9.2913, therefore, according to Equation 5-7, φ=4.25/9.2913=0.457. Now the pile length L_p in the no scour case can be related to the pile diameter B to satisfy β_T=3. $\frac{R_{\text{predicted}}}{LL_{\text{predicted}}} = \frac{4 f_u L_p B + p_u B^2}{445} = 9.2913$, which gives $L_p = -2.8125B + \frac{32.30}{B}$.

Figure 5-9 shows the combination of L_p and B that provide the same target reliability index β_T=3 (PoF=0.001). For example, the width B of the pile is chosen to be 1m, while the corresponding length of pile $L_{p\_noscour}$, which is the pile length when there is no scour, is 29. 5m.

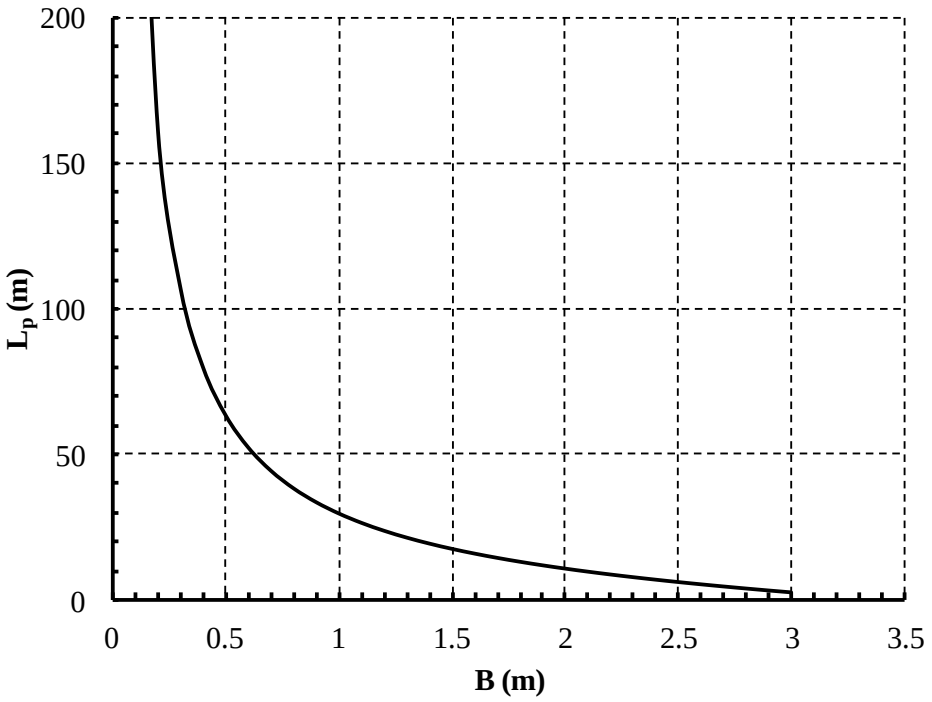

Figure 5-9. Required Combination $L_{p\_noscour}$ vs. B for No Scour, β_T = 3, and in the Case of Clay.

To incorporate the effects of scour, Equation 5-8 needs to be modified to Equation 5-13.

$$R_u = 4 f_u L_p B + p_u B^2 - 4 f_u Z B \tag{5-13}$$

Then the limit state function becomes (Equation 5-14):

$$g' = \lambda_R \times \frac{R_{\text{predicted}}}{LL_{\text{predicted}}} - \lambda_{DL} \times 2 - \lambda_{LL} = \lambda_R \times \frac{4 f_u L_p B + p_u B^2 - 4 f_u Z B}{LL_{\text{predicted}}} - \lambda_{DL} \times 2 - \lambda_{LL} \quad (5\text{-}14)$$

where, λ_R, λ_{LL}, λ_{DL}, are random variables, ratio of measured over predicted values and Z is the unbiased scour depth, also a random variable. Based on the probabilistic model of scour depth prediction, Z can be replaced with Equation 5-15.

$$Z_{\text{unb}} = e^{\Gamma_\zeta + \ln Z_{\text{det}} + \sigma_\zeta \varepsilon} \quad (5\text{-}15)$$

Using the statistics results in Section 3.5.1.1 (HEC-18 Clay method), Γ_ζ follows a normal distribution, i.e. $\Gamma_\zeta \sim N(-1.0870, 0.0253)$, while σ_ζ follows a normal distribution, i.e. $\sigma_\zeta \sim N(0.7450, 0.0294)$. These are the inputs for the FORM analysis. The limit function Equation 5-14 can be rewritten as Equation 5-16:

$$g' = \lambda_R \times \frac{4 f_u L_p B + p_u B^2 - 4 f_u B e^{(\Gamma_\zeta + \ln Z_{\text{det}} + \sigma_\zeta \varepsilon)}}{LL_{\text{predicted}}} - \lambda_{DL} \times 2 - \lambda_{LL} \quad (5\text{-}16)$$

where the values of the parameters can be found in the previous sections. For different values of Z_{det}, different values of L_p (total length of pile in the scour condition) are obtained for β_T=3 (PoF=0.001). The resistance factor φ can be obtained using Equation 5-17 below.

$$\phi = \frac{\gamma_{DL} DL_{\text{predicted}} + \gamma_{LL} LL_{\text{predicted}}}{R} = \frac{1.25 \times 445 \times 2 + 1.75 \times 445}{4 f_u L_p B + p_u B^2 - 4 f_u Z_{\text{det}} B} \quad (5\text{-}17)$$

Figure 5-10 shows the resistance factor for different ratios of Z_{det} to $L_{p\_noscour}$ for this specific case. It shows that the resistance factor φ first increases with an increase in

scour depth, then decreases. This trend is explained as follows. The predicted scour depth Z_{det} has two characteristics: it is very conservative and it is very scattered. When Z_{det} is small compared to the LRFD required pile length in the case of no scour $L_{p\_noscour}$, the conservatism dominates in the reliability calculations and it is possible to use a less conservative (higher) value of φ for calculating the global pile length L_p including scour. When Z_{det} is large compared to $L_{p\_noscour}$, the scatter dominates in the reliability calculations and it is necessary to use a more conservative (lower) value of φ for L_p including scour. Thus the shape of the φ vs. $Z_{det}/L_{p\_noscour}$ curve shows a peak.

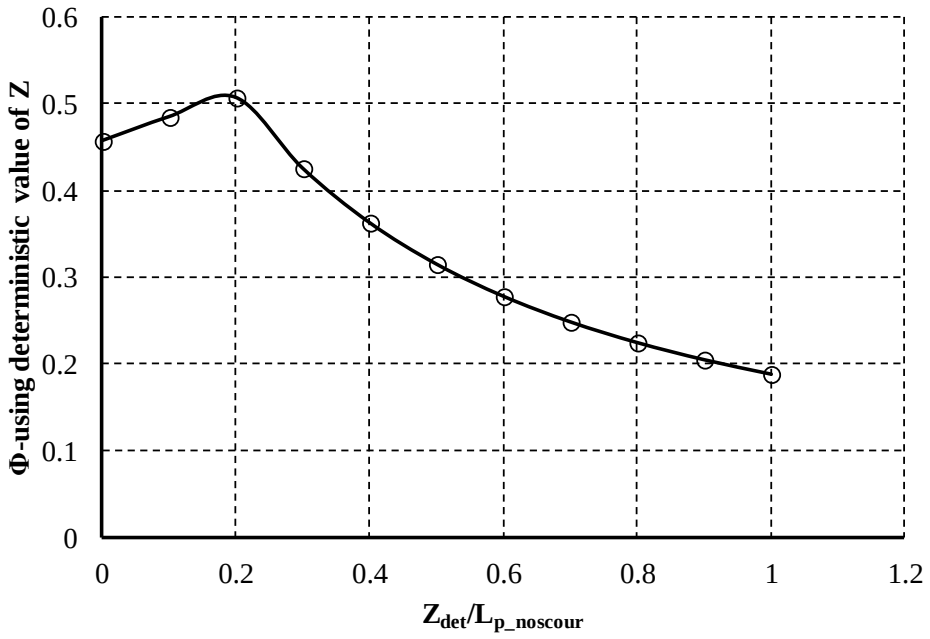

Figure 5-10. The Relationship between the Ratio of Deterministic Scour Depth over the Pile Length without Scour Effect and the Resistance Factor.

Further study was done to isolate the effects of the conservatism (bias) and the scatter of the scour depth on the resistance factor φ. Figure 5-11 shows how the resistance factor φ varies as a function of the ratio of Z_{det} over $L_{p\_noscour}$ when considering only the effect of the scatter (uncertainty). The only difference here is that the resistance factor φ was calculated using the unbiased scour depth prediction instead of the deterministic prediction, i.e. in Equation 5-17 Z_{det} is replaced with Z_{unb}. The resistance factor φ is relatively unchanged until $Z_{det}/L_{p\_noscour}$ is equal to 0.2 and then it decreases more rapidly.

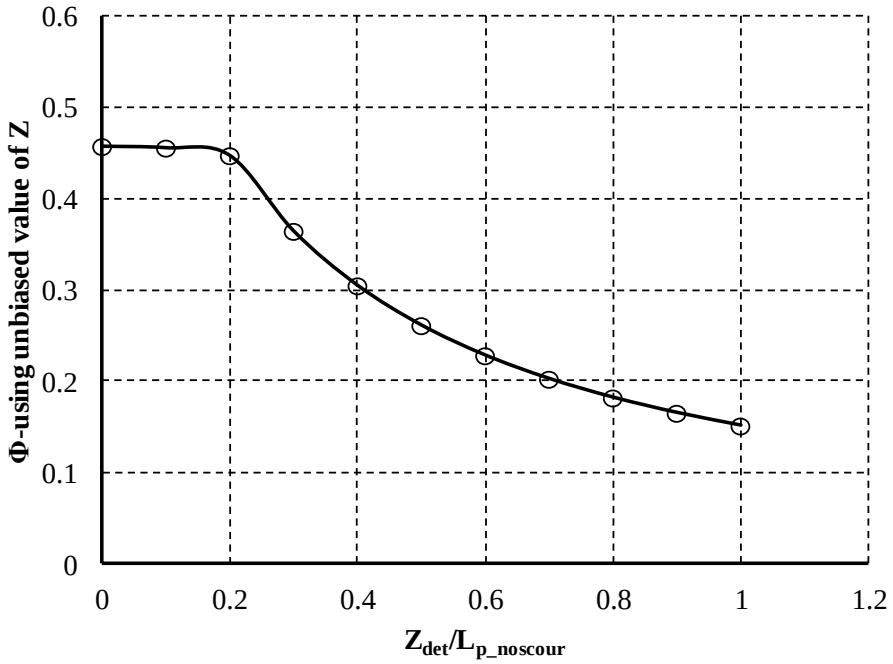

Figure 5-11. The Relationship between the Ratio of Deterministic Scour Depth over the Pile Length without Scour Effect and the Resistance Factor, when only the Effect of Uncertainty is Considered.

In order to analyze the effect of conservatism (bias) only, in the reliability analysis, σ_ζ is defined to be 0 in Equation 5-16, and the resistance factor φ is calculated using Equation 5-17. Figure 5-12 shows that the resistance factor φ is increasing significantly with the scour depth when considering only the effect of conservatism (bias).

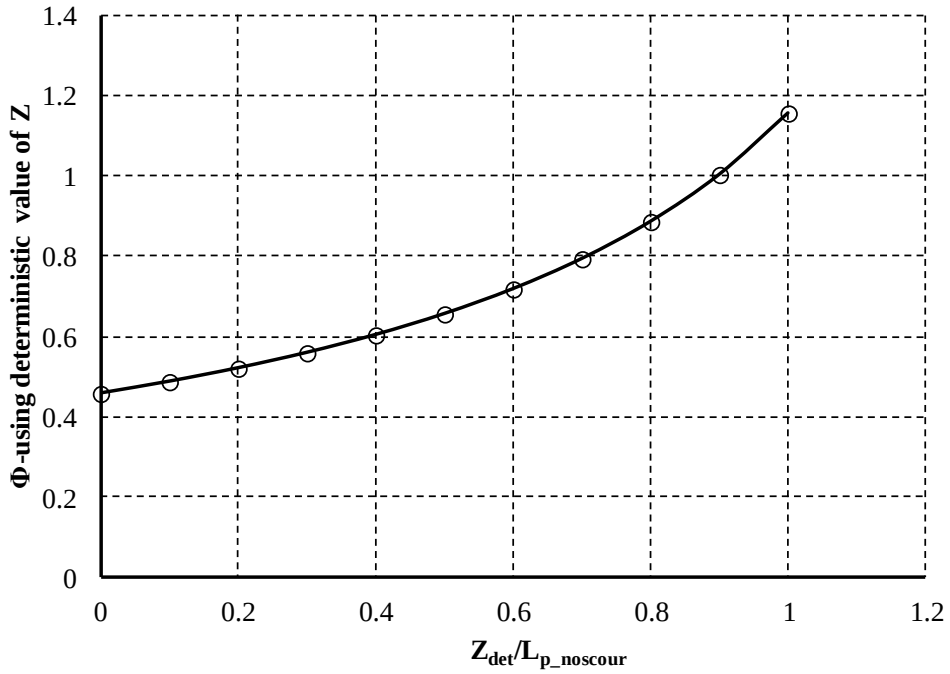

Figure 5-12. The Relationship between the Ratio of Deterministic Scour Depth over the Pile Length without Scour Effect and the Resistance Factor, when only the Effect of Bias is Considered.

Adopting the same methodology, the author analyzed four more cases with different pile dimensions. According to Figure 5-9, the author chose the pile width, B = 0.2 m. Correspondingly the pile length required by design to sustain the design load

with β_T = 3 when no scour is involved, $L_{p\_noscour}$ is read to be 160.9 m. For different values of scour depth (ρ=0, 0.1, 0.2, …, 1.0), the resistance factor in the case of scour is calculated by performing FORM analysis. Note ρ is defined to be the ratio of deterministic scour depth Z_{det} over the pile length without scour effect $L_{p\_noscour}$. The relationship between the ratio of deterministic scour depth over the pile length without scour effect and the resistance factor is shown in Figure 5-13 (diamond line).

Repeat the same procedure for different conditions of pile width (B = 0.6 m, B = 1.4 m, and B = 2 m). Figure 5-13 shows the relationship between the ratio of revised resistance factor in the case of scour over the resistance factor without scour effect ($\varphi_{scour}/\varphi_{noscour}$) and the ratio of the deterministic scour depth over the pile length without scour effect ($Z_{det}/L_{p\_noscour}$) in clay.

Figure 5-14 shows the required combination of L_p and B for different values of ρ (ratio of Z_{det} over $L_{p\_noscour}$) to meet a target reliability index β_T of 3 (PoF=0.001). It is a different way of expression from Figure 5-13. As can be expected for a given diameter B, a larger scour depth requires longer piles to be able to maintain the same target probability of failure.

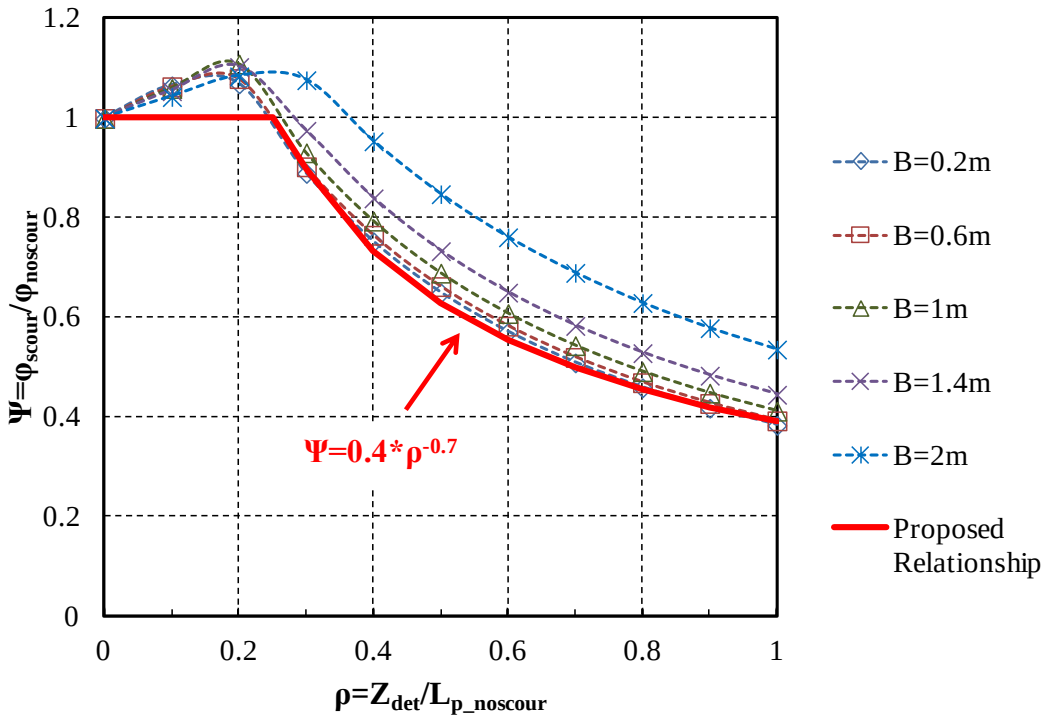

Figure 5-13. Relationship between the Ratio of Revised Resistance Factor in the Case of Scour over the Resistance Factor without Scour Effect ($\varphi_{scour}/\varphi_{noscour}$) and the Ratio of the Deterministic Scour Depth over the Pile Length without Scour Effect ($Z_{det}/L_{p\_noscour}$) in Clay.

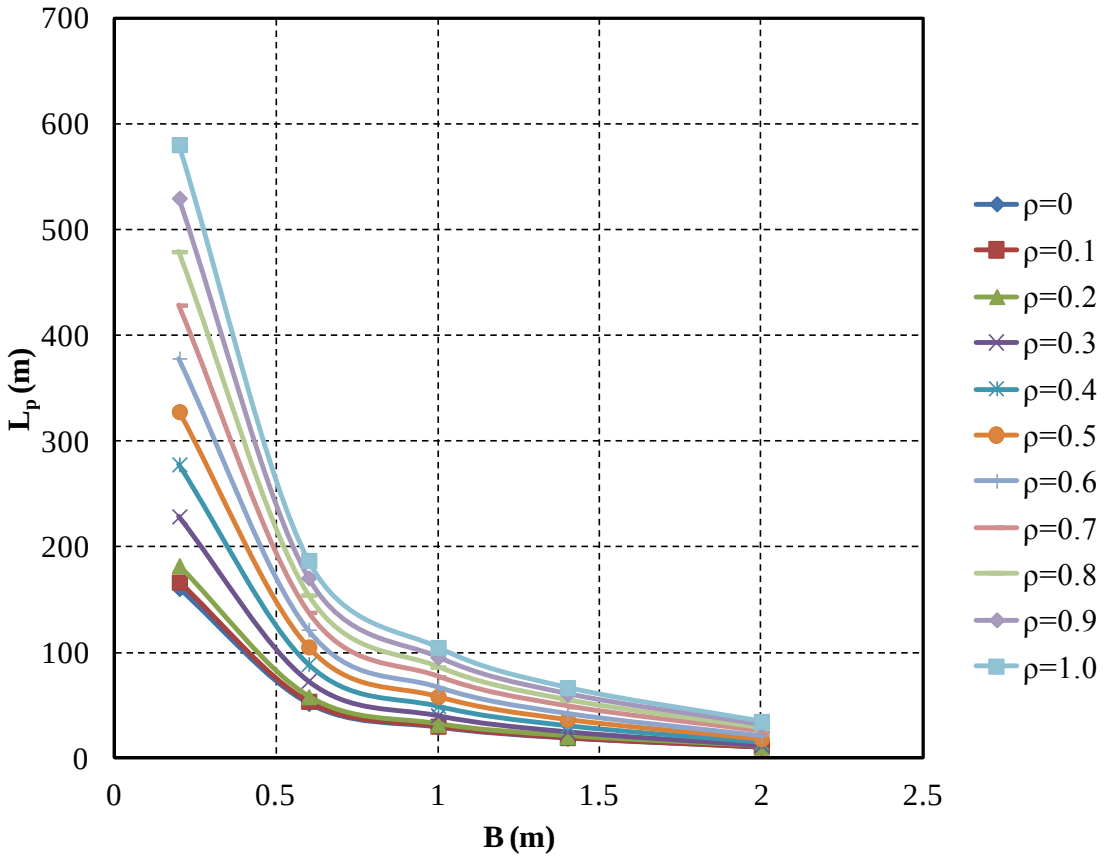

Figure 5-14. Relationship between L_p and B for Different Values of ρ (ratio of Z_{det} over $L_{p\_noscour}$) to Meet a Target Reliability Index β_T of 3 (PoF = 0.001).

According to the results in Figure 5-13, the author proposed the LRFD calibration of resistance factor in the case of scour in clay as follows:

If the deterministic scour depth is less than 25% of the pile length without scour effect in clay, the resistance factor for foundation design remains the same as AASHTO (2007).

If the deterministic scour depth is larger than 25% of the pile length without scour effect in clay, the resistance factor for foundation design reduces. The relationship

between the ratio of revised resistance factor in the case of scour over the resistance factor without scour effect ($\varphi_{scour}/\varphi_{noscour}$) and the ratio of the deterministic scour depth over the pile length without scour effect ($Z_{det}/L_{p\_noscour}$) follows:

$$\frac{\varphi_{scour}}{\varphi_{noscour}} = 0.4\left(\frac{Z_{det}}{L_{p\_noscour}}\right)^{-0.7} \tag{5-18}$$

where φ_{scour} = the resistance factor for foundation design in the case of scour; $\varphi_{noscour}$ = the resistance factor for foundation design without considering scour; Z_{det} = deterministic scour depth prediction; $L_{p\_noscour}$ = the pile length required by design to sustain the design load in the no scour case.

5.6.2 Case Studies in Sand, SPT Design Method

In this section, the case studies in sand are addressed. A square concrete pile with a width B in sand designed using SPT method is discussed. Based on the NCHRP Report 507 (Paikowsky 2004, p. 34), which is the basis for the AASHTO LRFD (2007), in the case of no scour, the mean of the resistance bias factor is $\mu(\lambda_R) = 1.21$, the standard deviation of the resistance bias factor is $\sigma(\lambda_R) = 0.57$, and the coefficient of variation of the resistance bias factor is $\delta(\lambda_R) = 0.47$. For a target reliability index of 3 (β_T=3, PoF=0.001), the AASHTO LRFD resistance factor is 0.38 (φ=0.38). The objective is to revise this "no scour" resistance factor when scour occurs.

First, the no scour case is analyzed to choose a reasonable diameter and length for the pile (B and $L_{p\_noscour}$) to meet the target reliability index of 3 (β_T=3, PoF=0.001). Note that $L_{p\_noscour}$ is the pile length required by design to sustain the design load with

β_T=3 when no scour is involved. For the analysis, an N equal to 20 blows/ft is selected (i.e. N = 20 blows/ft). The pile ultimate resistance is given as Equation 5-19.

$$R_u = f_u A_f + p_u A_p = 5N^{0.7} A_f + 1000N^{0.5} A_p \quad (5\text{-}19)$$

where the ultimate side friction f_u is determined to be 40 kPa, (i.e., $f_u = 5N^{0.7} = 5 \times 20^{0.7} = 40\,kPa$), and the ultimate point pressure p_u is determined to be 4500 kPa (i.e., $p_u = 1000N^{0.5} = 1000 \times 20^{0.5} = 4500\,kPa$). The live load model is an HS-20-44 truck (Paikowsky 2004), which gives $LL_{predicted}$=445kN. In order to keep a consistency with NCHRP Report 507, the dead load and live load ratio is chosen to be 2, therefore, $DL_{predicted} = 2 \times LL_{predicted} = 2 \times 445 = 890\,kN$.

Then a FORM analysis was performed using the software package FERUM (FERUM 2001) for a target reliability index β_T equal to 3. The statistical parameters of λ_R, λ_{DL} and λ_{LL} are given in the previous section. FERUM gives $R_{predicted}/LL_{predicted}$=11.604, therefore, according to Equation 5-7, φ=4.25/11.604=0.366. Now the pile length L_p in no scour case can be related to the pile diameter B to satisfy β_T=3. $\frac{R_{predicted}}{LL_{predicted}} = \frac{4 f_u L_p B + p_u B^2}{445} = 11.604$, which gives $L_p = -28.125B + \frac{32.274}{B}$.

Figure 5-15 shows the combination of L_p and B that provide the same target reliability index β_T=3 (PoF=0.001). For example, the width B of the pile is chosen to be 1 m, while the corresponding length of pile $L_{p\_noscour}$, which is the pile length when there is no scour, is 4.149 m.

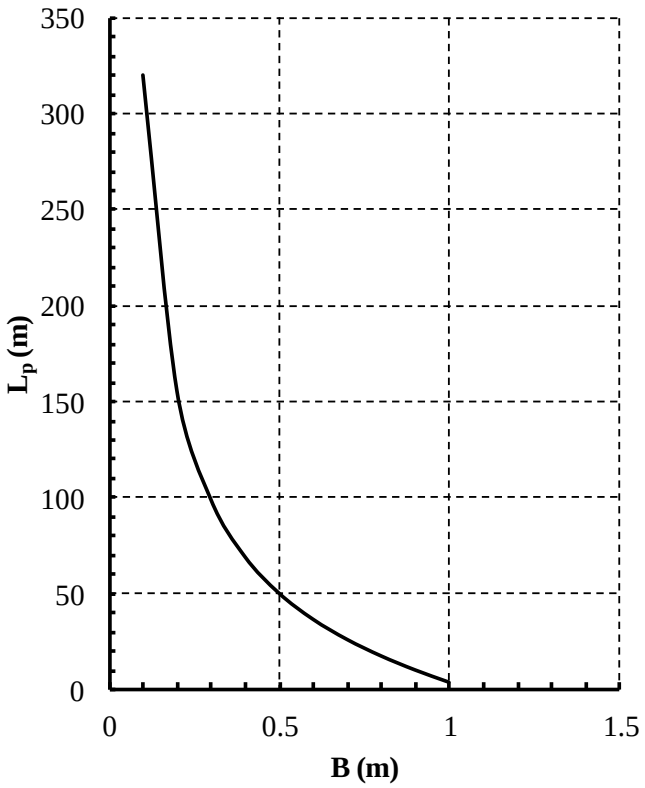

Figure 5-15. Required Combination $L_{p\_noscour}$ vs. B for No Scour, $\beta_T = 3$, and in the Case of Sand.

The author analyzes the different conditions of pile width (B = 1 m, B = 0.8 m, and B = 0.5 m). Figure 5-16 shows the relationship between the ratio of the revised resistance factor in the case of scour over the resistance factor without scour effect ($\varphi_{scour}/\varphi_{noscour}$) and the ratio of the deterministic scour depth over the pile length without scour effect ($Z_{det}/L_{p\_noscour}$) in sand.

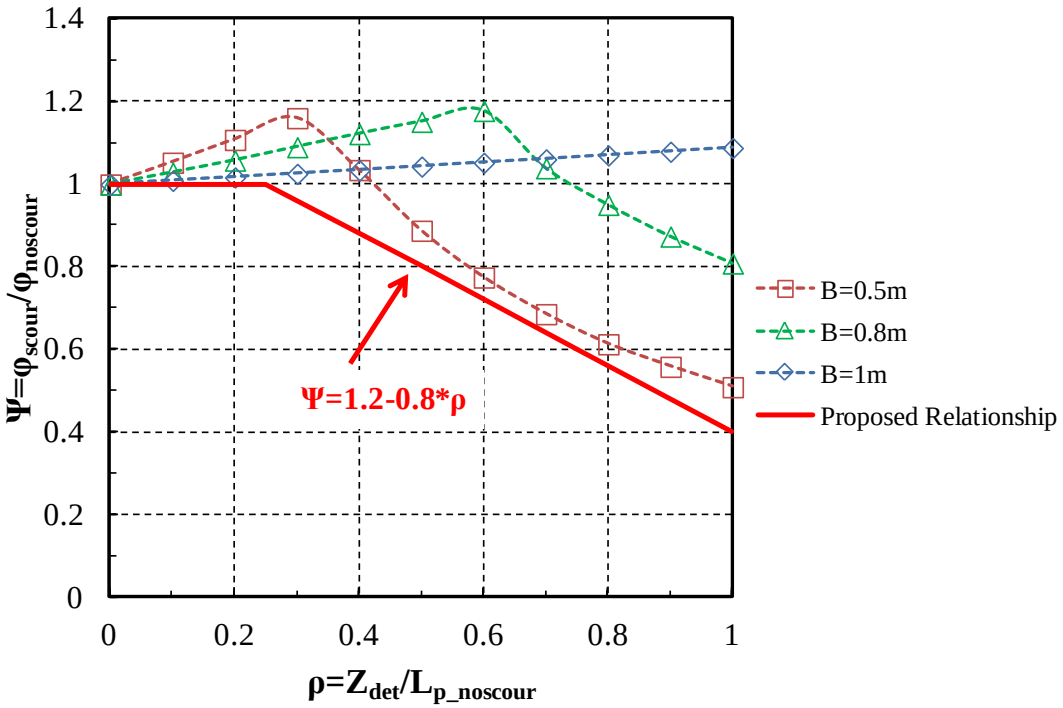

Figure 5-16. Relationship between the Ratio of Revised Resistance Factor in the Case of Scour over the Resistance Factor without Scour Effect ($\varphi_{scour}/\varphi_{noscour}$) and the Ratio of the Deterministic Scour Depth over the Pile Length without Scour Effect ($Z_{det}/L_{p\_noscour}$) in Sand.

According to the results in Figure 5-16, the author proposed the LRFD calibration of resistance factor in the case of scour in sand as follows:

If the deterministic scour depth is less than 25% of the pile length without scour effect in sand, the resistance factor for foundation design remains the same as AASHTO (2007).

If the deterministic scour depth is larger than 25% of the pile length without scour effect in sand, the resistance factor for foundation design reduces. The relationship between the ratio of revised resistance factor in the case of scour over the

resistance factor without scour effect (φ_{scour}/ $\varphi_{noscour}$) and the ratio of the deterministic scour depth over the pile length without scour effect ($Z_{det}/L_{p\_noscour}$) follows:

$$\frac{\varphi_{scour}}{\varphi_{noscour}} = 1.2 - 0.8\frac{Z_{det}}{L_{p\_noscour}} \tag{5-20}$$

where φ_{scour} = the resistance factor for foundation design in the case of scour; $\varphi_{noscour}$ = the resistance factor for foundation design without considering scour; Z_{det} = deterministic scour depth prediction; $L_{p\_noscour}$ = the pile length required by design to sustain the design load in no scour case.

5.7 CONCLUSIONS AND RECOMMENDATIONS ON LRFD CALIBRATION FOR DEEP FOUNDATIONS IN THE CASE OF SCOUR

5.7.1 Conclusions on LRFD Calibration for Deep Foundations in the Case of Scour

This section is about the LRFD calibration for deep foundations in the case of scour. Firstly, the general approach to compute load factor and resistance factor is shown. Secondly, the author duplicated the work in NCHRP Report 507, which is the LRFD calibration of deep foundation design without scour effect. Then the step by step procedure of computing the resistance factor given the load factors in the case of scour is shown. Several case studies are performed in order to achieve the LRFD calibration code for the foundation design in the case of scour.

5.7.2 Recommendations for Design

Use the same load factor and resistance factor for common situations (scour depth less than 25% of the pile length corresponding to no scour). For a larger percent of scour depth, the resistance factor decreases significantly.

In clay, the relationship between the ratio of revised resistance factor in the case of scour over the resistance factor without scour effect ($\varphi_{scour}/\varphi_{noscour}$) and the ratio of the deterministic scour depth over the pile length without scour effect ($Z_{det}/L_{p\_noscour}$) follows (if $Z_{det}/L_{p\_noscour} > 0.25$):

$$\frac{\varphi_{scour}}{\varphi_{noscour}} = 0.4\left(\frac{Z_{det}}{L_{p\_noscour}}\right)^{-0.7} \tag{5-18}$$

where φ_{scour} = the resistance factor for foundation design in the case of scour; $\varphi_{noscour}$ = the resistance factor for foundation design without considering scour; Z_{det} = deterministic scour depth prediction; $L_{p\_noscour}$ = the pile length required by design to sustain the design load in the no scour case.

In sand, the relationship between the ratio of the revised resistance factor in the case of scour over the resistance factor without scour effect ($\varphi_{scour}/\varphi_{noscour}$) and the ratio of the deterministic scour depth over the pile length without scour effect ($Z_{det}/L_{p\_noscour}$) follows (if $Z_{det}/L_{p\_noscour} > 0.25$):

$$\frac{\varphi_{scour}}{\varphi_{noscour}} = 1.2 - 0.8\frac{Z_{det}}{L_{p\_noscour}} \tag{5-20}$$

6 SCOUR RISK

6.1 INTRODUCTION

By definition, "risk' means the possibility of loss, injury, disease, or death (Merriam-Webster). It actually includes two parts, the probability of loss, injury or death, and the corresponding outcomes if loss, injury or death happens. It is important for people to gauge the risk level of the events that they are engaged in, not only the probability of loss, but also the consequences of the loss. It usually is a tradeoff between the economic investment and the potential loss that the party can handle. It is not wise to pursue a very low probability of failure or loss with an unacceptably huge investment. On the other hand, it is not safe enough if the structure has a very high probability of failure with limited investment.

In this section, firstly the author referred to the work of Baecher and Christian (2003), which shows the risk of common civil engineering structures in the F-N Chart. Note that F means frequency, and N means the consequences. Thereafter the acceptable risk level, medium risk level, and unacceptable risk level is defined. Secondly, the author analyzed several societal risks, including cancer, heart attacks, car accidents, plane crashes, Hurricane Katrina and offshore structures. The results were also plotted in the F-N Chart as comparisons. Thirdly, the author made use of two databases: NYSDOT Bridge Failure Database and FDOT Unknown Foundation Bridge Database to quantify the bridge scour risk, which was plotted in the F-N Chart as well. The

conclusion was drawn based on all previous results. The risk level for bridge scour failure is determined.

6.2 CIVIL ENGINEERING RISK

Risk is defined as the product of the probability of occurrence times the value of the consequence. The probability of exceedance is the probability that an event will be exceeded. The annual probability of exceedance is the probability that an event will be exceeded in any given one year.

Figure 6-1 is called the F-N Chart, showing the risk in various fields of civil engineering (Baecher and Christian 2003). Note that F means frequency, and N means the consequences. Therefore, the F-N Chart includes two parameters: the annual probability of failure and consequences (dollars loss and fatalities loss). The annual probability of failure is on the vertical axis and the value of the consequence is on the horizontal axis. Two horizontal axes are presented: one for economic loss in dollars (lower axis) and one for fatalities (upper axis) (Briaud et al. 2012). On the vertical axis, the F-N Chart contains, F, the probability of incremental loss of life or incremental economic loss exceeding the value N. The F-N Chart of risk is associated with the events. The ellipses in the diagram below show what risk is associated with various fields of engineering.

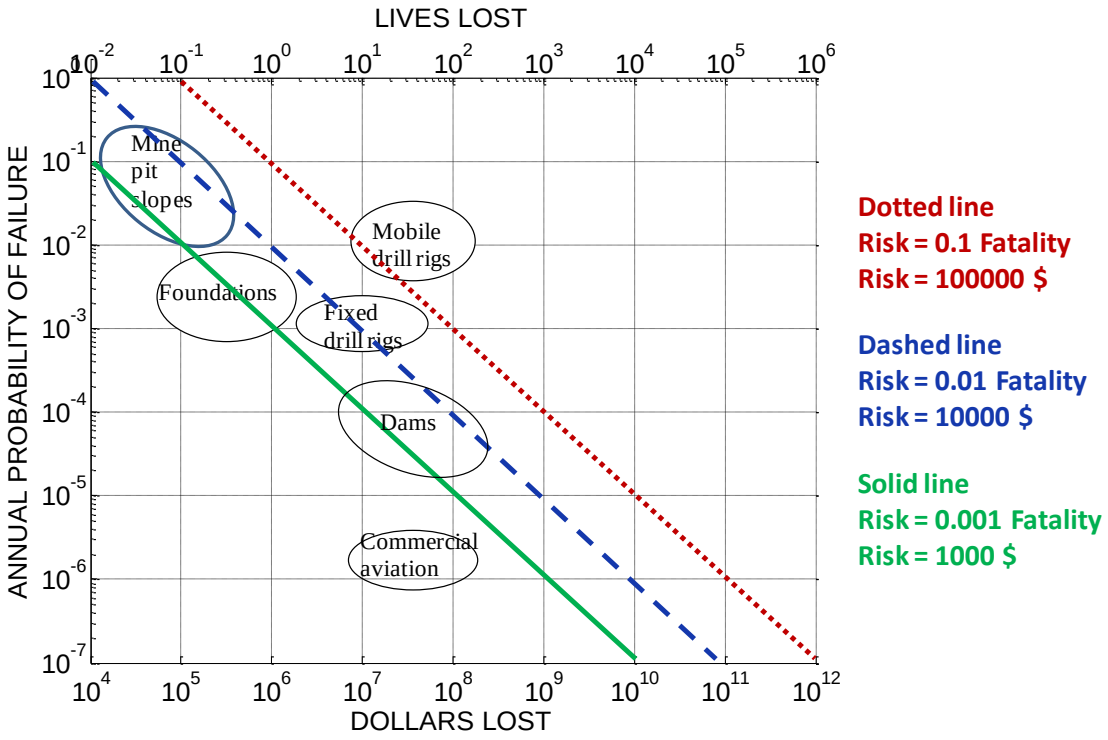

Figure 6-1. Civil Engineering Risk (after Baecher and Christian, 2003).

Note that Figure 6-1 is based on data accumulated in the United States. The annual risk R is the annual probability of failure PoF times the value of the consequence C (Equation 6-1).

$$R = PoF \times C \tag{6-1}$$

Therefore, the solid, dashed, and dotted diagonals on Figure 6-1 represent lines of equal risk, which are also called risk tolerance curves. For example, the solid line corresponds to an annual risk of $1,000/yr and 0.001 fatalities/yr and the dotted line to an annual risk of $100,000/yr and 0.1 fatalities/yr. Since most of the ellipses for civil engineering structures are located above the solid line, the solid line defines an

acceptable risk in practice. Conversely the dotted line defines an unacceptable risk (Briaud et al. 2012).

Note that the risk tolerance curve does not have to be a one to one slope line. It may have a steeper slope than one to one. A steeper slope means that the tolerable expected consequence in fatalities or dollars per year decreases as the consequence increases (Gilbert et al. 2008). "Steeper curves reflect an aversion to more catastrophic events" (Gilbert et al. 2008, p. 200). Correspondingly, the tolerance curve may not even be a straight line; it can be a curved envelope. In this dissertation, I am analyzing the equal risk lines.

Table 6-1 summarizes the target risk levels; these data indicate that acceptable target risks for civil engineering structures in the United States are $1,000/yr and 0.001 fatalities/yr (Briaud et al. 2012).

Table 6-1. Target Risk Levels for the United States (Briaud et al. 2012).

Risk Level	Risk ($/yr)	Risk (fatalities/yr)
Acceptable	1,000	0.001
Medium	10,000	0.01
Unacceptable	100,000	0.1

6.3 SOCIETAL RISKS

In order to compare the risk levels among civil engineering structures and daily events related to human beings, the author also analyzed the risks associated with cancer, heart

attacks, car accidents, plane crashes, and Hurricane Katrina. The risk level for each event will be explained clearly below.

6.3.1 Cancer

Cancer is the second most-common cause of death in the United States, exceeded only by heart disease (Briaud 2013). In the United States, cancer accounts for 23% of the deaths (Briaud 2013). According to the statistics from the American Cancer Society (2011), there were 300,430 men and 271,520 women who died of cancer in the United States in 2011. Hence, an average of 571,950 people die of cancer in the United States, corresponding to 1,500 deaths per day. There were 311,000,000 people in 2011 in the United States (U.S. Census Bureau). Therefore, the annual probability of failure associated with cancer is calculated as 1.8×10^{-3} ($571{,}950/311{,}000{,}000=1.8\times10^{-3}$), and the life lost is 1. Note that if the average life expectancy of American people is 78.24 years (World Bank 2010), the possibility that a person will die of cancer during his or her lifetime is 13% ($1-(1-1.8\times10^{-3})^{78.24}=13\%$).

According to American Cancer Society (2011) report, "the National Institute of Health estimates overall costs of cancer in 2010 at $263.8 billion: $102.8 billion for direct medical costs (total of all health expenditures); $20.9 billion for indirect morbidity costs (costs of lost productivity due to illness); and $140.1 billion for indirect mortality costs (cost of lost productivity due to premature death)" (p.3). For an individual, the economic loss is calculated to be $461,229 ($\$263.8\times10^{9}/571{,}950=\$461{,}229$). The data associated with cancer is located on Figure 6-2.

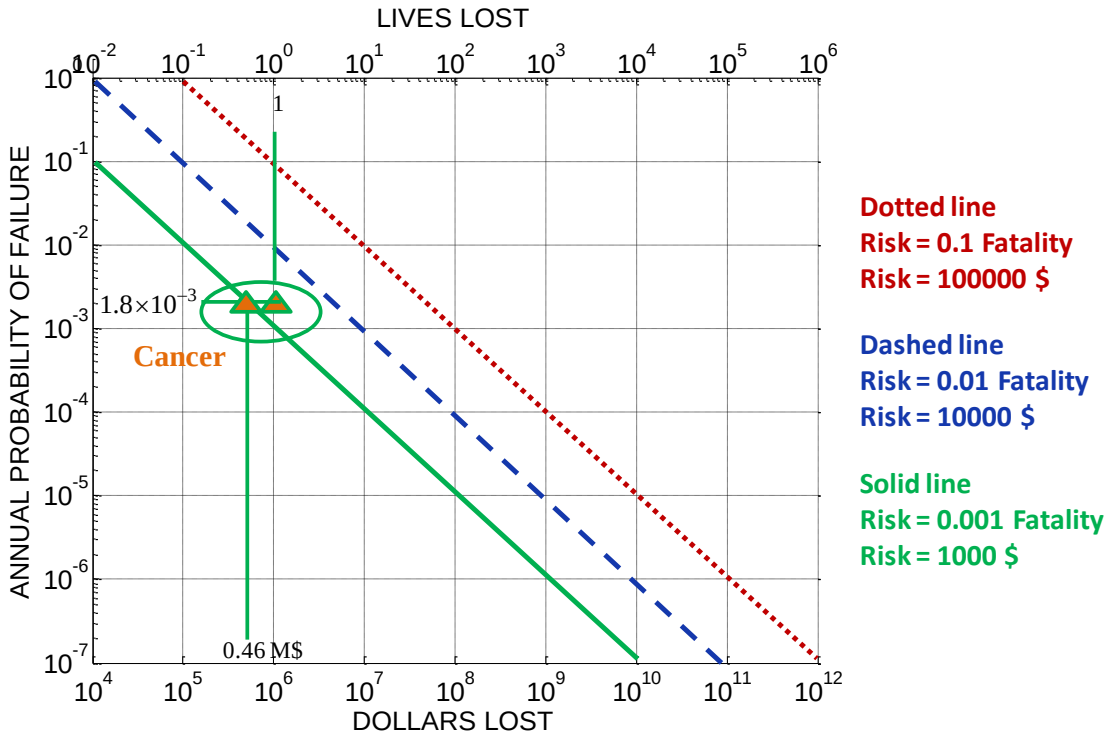

Figure 6-2. Risk of Cancer.

6.3.2 Heart Disease

Heart disease, which counts for 25% of the total deaths, is the number one cause of death in the United States (Briaud 2013).

According to the Heart Foundation (2012), there are about 1 million lives lost due to heart disease annually in the United States. It means that every 32 seconds someone in the United States dies from heart disease. There were 311,000,000 people in 2011 in the United States (U.S. Census Bureau). Therefore, the annual probability of failure associated with heart disease is calculated as 3.2×10^{-3} ($1{,}000{,}000/311{,}000{,}000=3.2\times10^{-3}$), and the life lost is 1. Note that if the average life

expectancy of American people is 78.24 years (World Bank 2010), the possibility that a person will die of heart disease during his or her lifetime is 22% ($1-(1-3.2\times10^{-3})^{78.24}=22\%$).

According to the Heart Foundation (2012), "In 2008, the total cost of heart disease in the United States was estimated at $448.5 billion. Note that this includes direct costs such as costs of doctors, hospital services, medications, etc., and indirect costs such as lost productivity". For an individual, the economic loss is calculated to be $448,500 ($\$448.5\times10^{9}/1{,}000{,}000=\$448{,}500$). The data associated with heart disease is located on Figure 6-3.

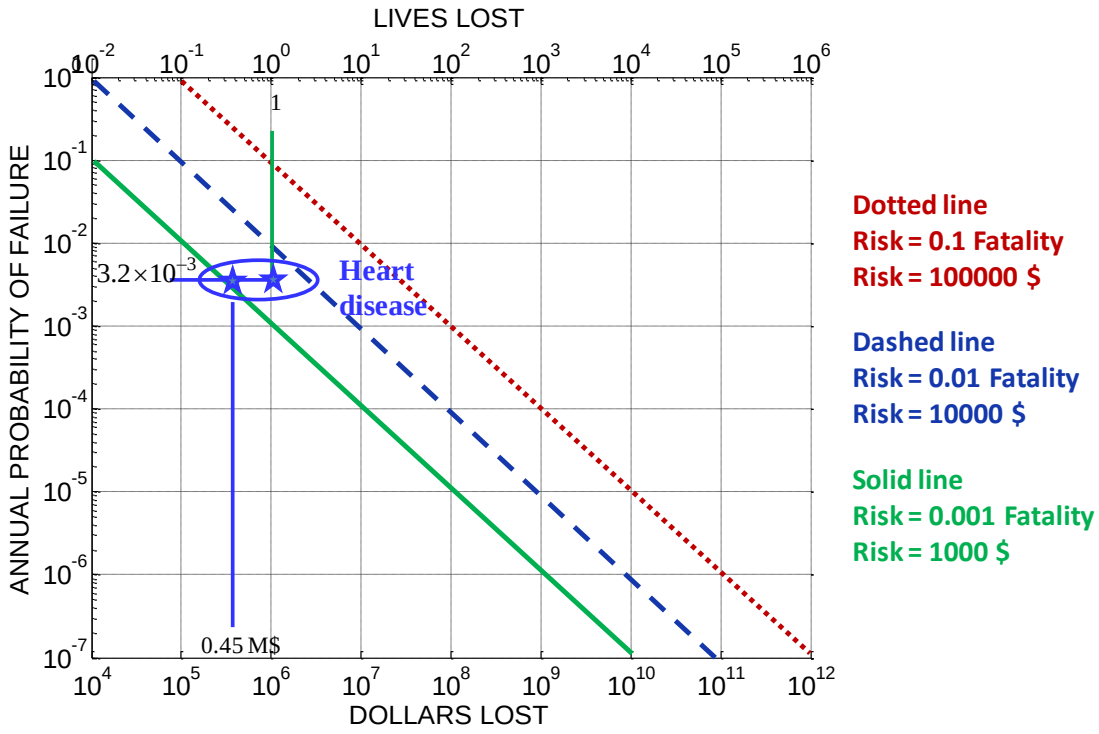

Figure 6-3. Risk of Heart Disease.

6.3.3 Car Accident

A car accident is the fourth most-common cause of death in the United States, which accounts for 1.2% of total deaths (Briaud 2013).

Table 6-2 shows the fatal crash statistics by year (National Highway Traffic Safety Administration, [NHTSA] 2012). From Table 6-2 it is concluded that on the average every year about 42,616 people died from car accidents. This indicates that about 117 people die every day in vehicle crashes in the United States, i.e. one death every 13 minutes.

Table 6-2. Fatal Crash Statistics by Year (after NHTSA 2012).

Year	2,005	2,004	2,003	2,002	2,001	2,000	1,999	1,998	1,997
Fatal Vehicle Crashes	39,189	38,444	38,477	38,491	38,862	37,526	37,140	37,107	37,324
Fatality Totals:									
Drivers	27,472	28,871	26,779	26,659	25,869	25,567	25,257	24,743	24,667
Passengers	10,036	10,355	10,458	10,604	10,469	10,695	10,521	10,530	10,944
Other	86	78	104	112	102	86	97	109	114
Sub-total	37,594	39,304	37,341	37,375	36,440	36,348	35,875	35,382	35,725
Pedestrians	4,881	4,675	4,774	4,851	4,901	4,763	4,939	5,228	5,321
Bicyclists	784	727	629	665	732	693	754	760	814
Other	184	130	140	114	123	141	149	131	153
Total Killed	43,443	44,836	42,884	43,005	42,196	41,945	41,717	41,501	42,013
Average Fatality	42,616								

There were 311,000,000 people in 2011 in the United States (U.S. Census Bureau). Therefore, the annual probability of death associated with car accidents is 1.4×10^{-4} ($42,616/311,000,000=1.4\times10^{-4}$), and the life lost is 1. Note that if the average life expectancy of American people is 78.24 years (World Bank 2010), the possibility that a person will die in a car accident during his or her lifetime is 1% ($1-(1-1.4\times10^{-4})^{78.24}=1\%$). Since the average occupancy for a running vehicle is 1.63 persons (Stein and Sedmera 2006), therefore the annual probability of a fatal car accident is 8.6×10^{-5} ($1.4\times10^{-4}/1.63=8.6\times10^{-5}$) corresponding to 1.63 lives lost. The reason for doing that is because the F-N Chart links the annual probability of failure to the corresponding dollars loss and fatalities loss due to one failure. The yearly economic loss of car accidents is $230 billion (CAS 2012). The economic loss corresponding to one fatality is calculated to be $5.4 million ($\$230\times10^{9}/42,616=\$5,397,034$). For a fatal car accident, the economic loss is calculated to be $9 million ($\$230\times10^{9}/42,616\times1.63=\$8,797,165$). The data associated with dying in a car accident and probability of a fatal car accident is located on Figure 6-4.

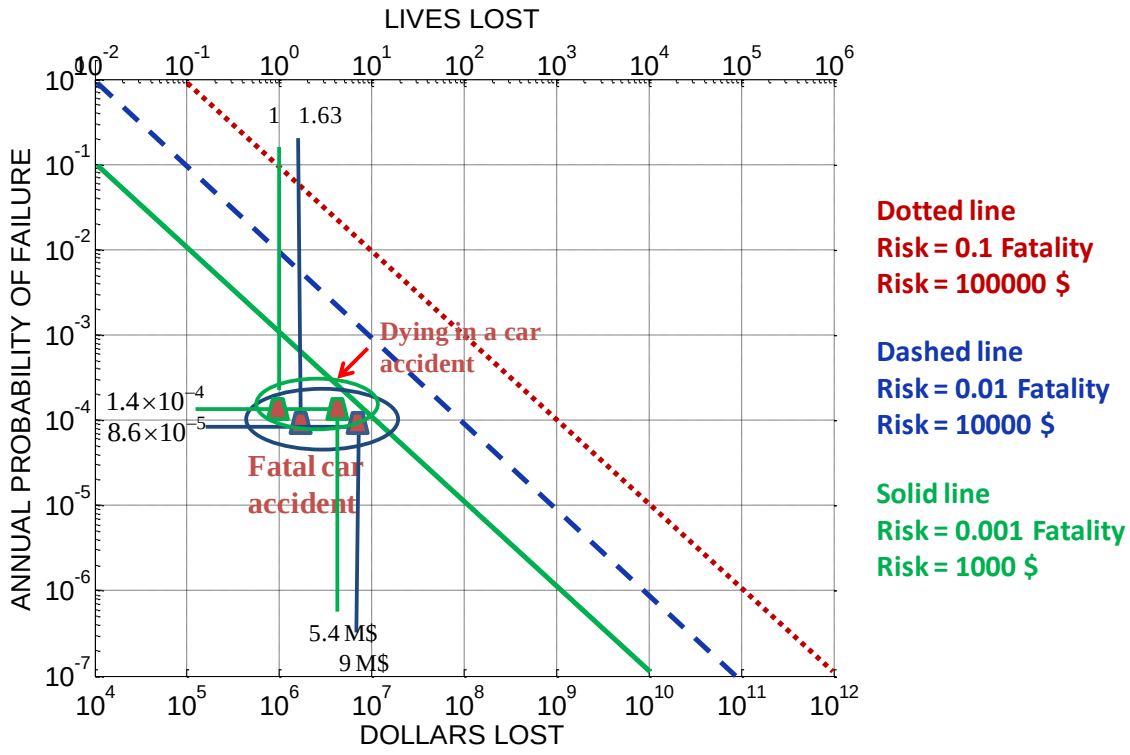

Figure 6-4. Risk Associated with Car Accident.

6.3.4 General Aviation Failure

The risk of plane crashes is analyzed in this section as well. There are several ways to calculate the probability of failure for plane crashes. One approach is to divide the number of people who die in a plane crash into the population at that time, which reflects the risk for the average person. The second approach is to divide the number of planes which crash into the total number of flights during the same period of time, which reflects the risk for the average plane crash accident. The third approach is to divide the number of fatal accidents into the total flight hours, which provides the risk of a plane crash per hour.

Data source1 (Approach 1):

Ropeik, D. (2006) stated that the statistics from the Department of Transportation show that, on an average of 5 years (from 1999 till 2003), 138 people died from plane crashes, excluding the fatalities in the 9/11 terrorist attack in 2001. There were 311,000,000 people in 2011 in the United States (U.S. Census Bureau). Therefore, the annual probability of death associated with car accidents is 4.4×10^{-7} ($138/311,000,000 = 4.4\times10^{-7}$), and the life lost is 1.

Data source2 (Approach 2):

The National Transportation Safety Board (NTSB) releases an annual review of aircraft accident data every year. In NTSB (2006), 1,523 general aviation accidents occurred, involving 1,535 aircraft. Among those 1,523 accidents, there were 308 fatal ones. General aviation includes both private aviation and commercial aviation. NTSB (2006) states "General aviation operations employ a wide range of aircraft, including airplanes, rotorcraft, gliders, balloons and blimps, and registered experimental or amateur-built aircraft". In NTSB (2006), "an accident is defined in 49 Code of Federal Regulations (CFR) 830.2 as, an occurrence associated with the operation of an aircraft which takes place between the time any person boards the aircraft with the intention of flight and all such persons have disembarked, and in which any person suffers death or serious injury, or in which the aircraft receives substantial damage." (p. 51).

According to NTSB (2006), the active general aviation fleet was 221,943 aircraft in 2006. Therefore, according to the second approach, the annual probability of plane accidents, related to the average plane crash rate, is determined to be 6.9×10^{-3}

($1{,}535/221{,}943 = 6.9\times10^{-3}$). The general aviation accidents caused 706 total fatalities. This gives the number of lives lost as 0.46 every time a plane has an accident (706/1,535=0.46). The author also analyzed the latest report from the NTSB (2011), which described the civil aircraft accidents in the United States between January 1, 2007 and December 31, 2009. Record showed that there were 5,019 U.S. –registered civil aircraft involved in 4,958 accidents during those three years (Table 6-3).

Table 6-3. Total Accidents, Fatal Accidents, and Fatalities for All Sectors of U.S. Civil Aviation, 2007-2009 (NTSB 2011).

Sector	2007			2008			2009		
	Number of Accidents			Number of Accidents			Number of Accidents		
	Total	Fatal	Fatalities	Total	Fatal	Fatalities	Total	Fatal	Fatalities
Total U.S. Civil Aviation	1745	303	540	1659	297	566	1554	276	535
Part 121	28	1	1	28	2	3	30	2	52
Part 135 Scheduled	3	0	0	7	0	0	2	0	0
Part 135 On Demand	62	14	43	58	20	69	47	2	17
Part 91-General Aviation	1652	288	496	1567	275	494	1477	273	475
Unregulated/Foreign Registration	27	7	10	13	5	8	16	4	4

On the average, 1,673 aircraft had accidents per year, which is fairly close to the 2006 Report statistics. It means that the estimated probability of failure for aviation as 6.9×10^{-3} is very reasonable. The total fatality number is 1,641 during those three years, which gives 547 fatalities per year. It means that the estimated 706 fatalities in year 2006 are fairly reasonable and representative.

The NTSB (2006) also shows the general aviation accident rate from the point of view of flight hours is 6.35 accidents per 100,000 hours. The general aviation hours flown in every year is about 23,963,000 hours. The average number of general aviation accidents per year is 1,522 ($6.35/100{,}000 \times 23{,}963{,}000 = 1{,}522$). The number of fatal accidents per year is 307 ($1.28/100{,}000 \times 23{,}963{,}000 = 307$).

In order to compare the risk of driving and flying, the author recalculated the probability of dying in a plane crash using the data obtained from the 2006 NTSB Report. The general aviation accidents in 2006 caused 706 total fatalities. There were 311,000,000 people in 2011 in the United States (U.S. Census Bureau). Therefore, the annual probability of death associated with plane crashes is 2.3×10^{-6} ($706/311{,}000{,}000 = 2.3\times10^{-6}$), and the life lost is 1. Note that the probability of dying in a car accident is 1.4×10^{-4}. It is obvious that it tends to be more dangerous to ride in a car than fly in an airplane.

There have not been many studies estimating the costs caused by aviation crashes. Scuffham et al. (2012) analyzed the direct and indirect costs and general aviation crashes in New Zealand using human capital (HC) and willingness-to-pay (WTP) approaches. These two approaches were used to quantify the indirect cost caused by aviation crashes, which included the medical care, repair of the aircraft and cost of investigation. The conclusion of Scuffham et al. (2012) is the annual average cost of general aviation crashes in New Zealand was between $22.6 million and $58.4 million. However Scuffham et al. (2012) did not mention how many aviation crashes happened each year; therefore, the results could not be directly used in this research.

King, E. and Smith, J. analyzed the economic loss in aviation accidents in their book which was published in 1988 (King and Smith 1988). They analyzed the 56 aviation crashes during the years 1964 to 1979 in the United States. The estimated cost of aircraft loss is $2.5 billion, and the total societal loss is $13.7 billion. Therefore for each crash, the total economic loss is $244 million ($\$13.7\times10^{9}/56=\$2.4\times10^{8}$). According to the study of the NTSB (2006), on average, 0.46 people die in one airplane accident. Therefore, the economic loss for one person dying in an airplane accident is $530 million ($\$2.4\times10^{8}/0.46=\$5.3\times10^{8}$).

The risk data associated with general aviation accidents is located on Figure 6-5. The risk associated with dying in a plane crash is also located on Figure 6-5.

6.3.5 Hurricane Katrina

Hurricane Katrina hit the Gulf of Mexico on August 29, 2005. More than 1,000 people died from the storm. The risk associated with the 2005 Hurricane Katrina protection system is located on Figure 6-6. The annual probability of occurrence of a Katrina hurricane is estimated at 5×10^{-3} as the recurrence interval of that hurricane is between 100 and 300 years. This disaster led to approximately 1500 lives lost and about $100 billion in economic loss by Dr. Jean-Louis Briaud's estimation (Briaud, personal communication, March 23, 2012).

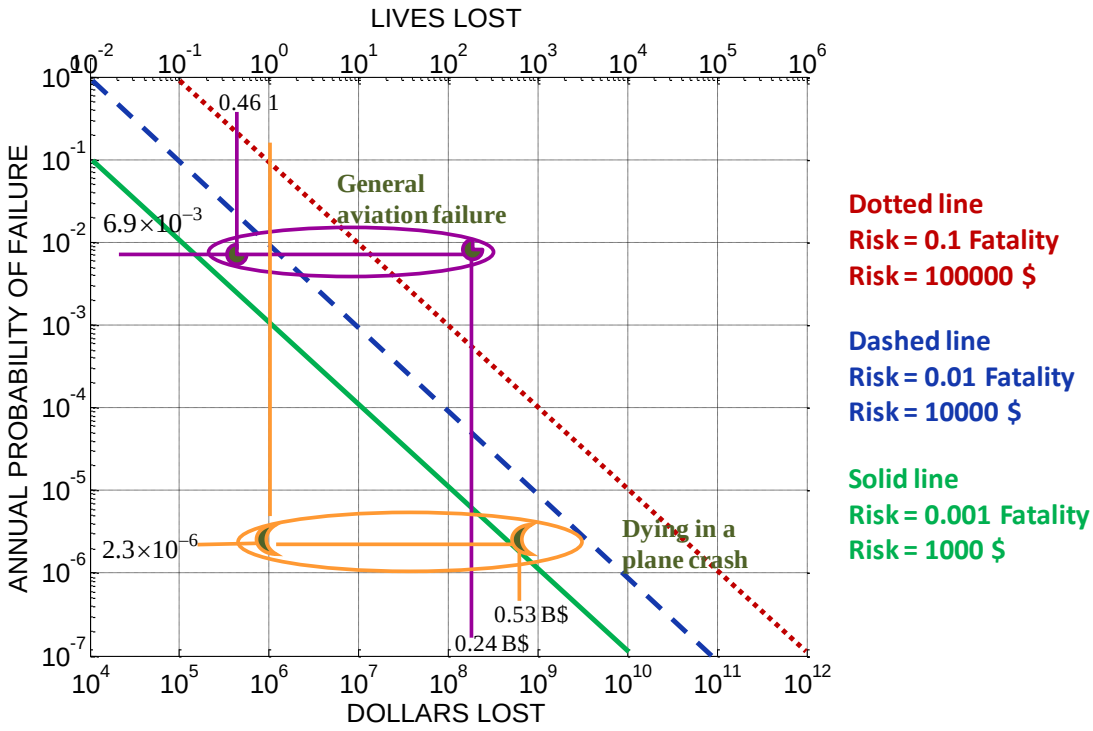

Figure 6-5. Risk Associated with General Aviation.

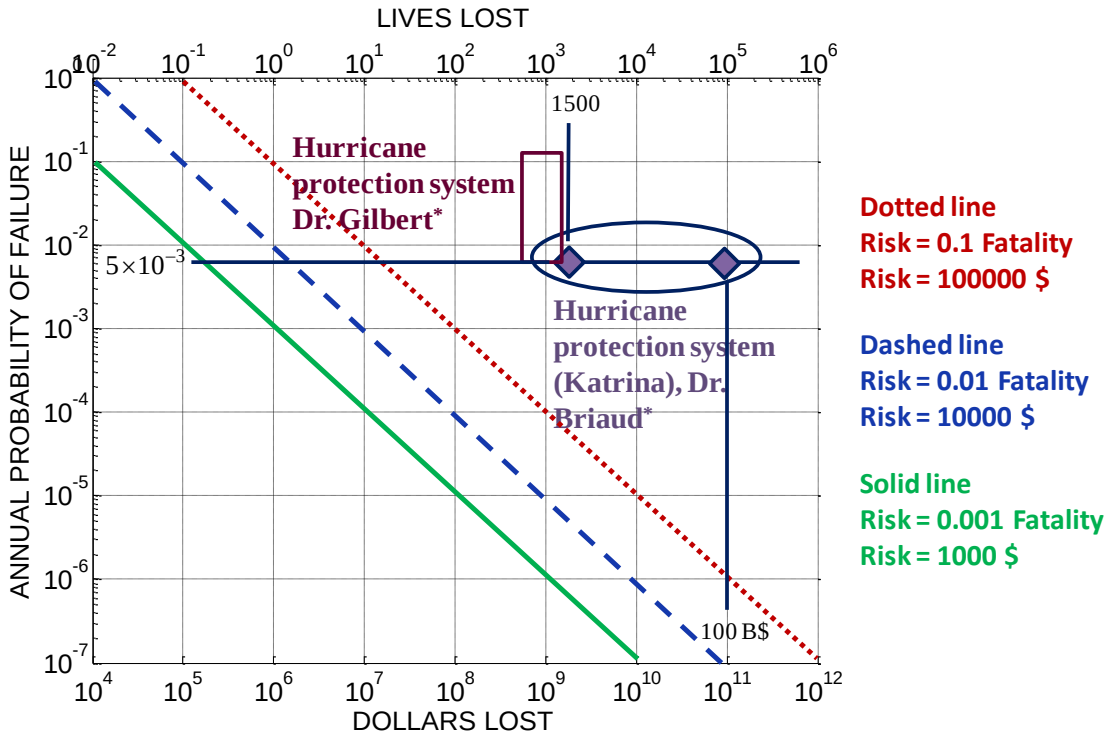

Figure 6-6. Risk Associated with Hurricane.

Figure 6-7 is obtained from a presentation delivered by Professor Robert Gilbert at the University of Texas at Austin, which shows the estimated risk of Hurricane Katrina (Gilbert 2012; Gilbert et al. 2011). A hurricane like Katrina is considered as an occurrence of every 10 years or 100 years event. Therefore, the annual probability of Hurricane Katrina is between 0.1 and 0.01. The fatality is estimated as 1,000 by Professor Gilbert. The red area in Figure 6-7 represents the risk of Hurricane Katrina based on Professor Gilbert's estimation. In his presentation, he also set up two thresholds (blue lines in Figure 6-7): one threshold for justification to take expedited action to reduce risk (Risk = 0.01 fatality), and one threshold for diminishing justification to take action to reduce risk (Risk =0.001 fatality). From the figure, it is

very obvious that Hurricane Katrina is an unacceptable risk, and people should take expedited action to reduce risk.

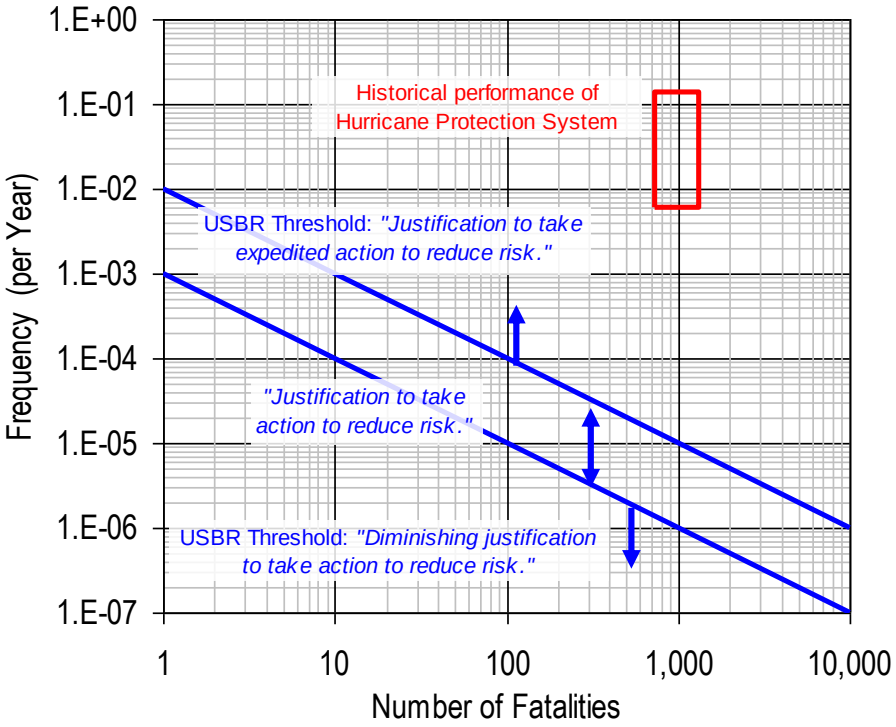

Figure 6-7. Risk of Hurricane Katrina (Gilbert 2012; Gilbert et al. 2011).

6.3.6 Dam Failure

In Professor Gilbert's presentation (Gilbert 2012), the risk associated with Teton Dam was also analyzed. The Teton Dam, 44 miles northeast of Idaho Falls in southeastern Idaho, failed abruptly on June 5, 1976. It caused loss of 14 lives, direct or indirect, cost of nearly $1 billion. Figure 6-8 shows the illustration of the failure of the Teton Dam. Figure 6-9 shows the relationship between the annual probability of failure and the

length of system. It gives us the basic idea of the risk related with dam failure. The annual probability of dam failure is estimated to be 10^{-4}; the lives lost is estimated to be 15 per failure. The results match the bubble related to dam failure in Figure 6-1.

Figure 6-8. Failure of Teton Dam (Gilbert 2012).

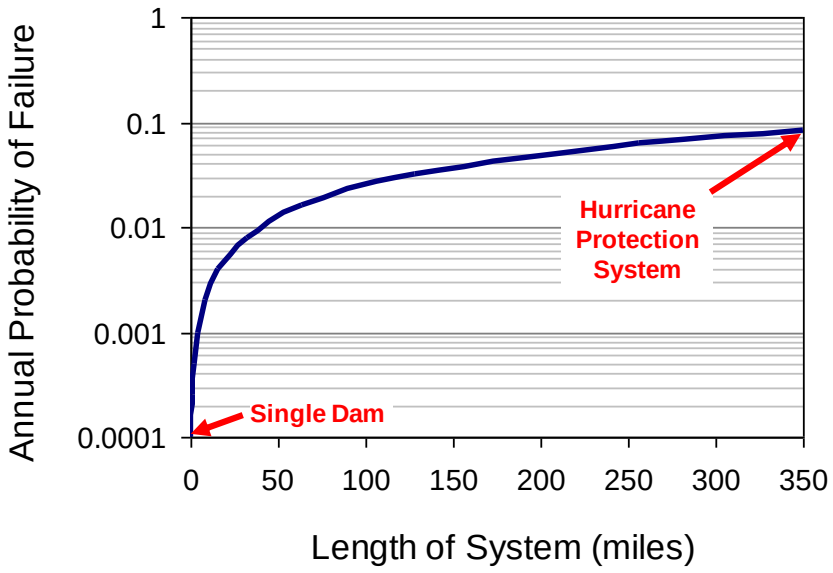

Figure 6-9. Annual Probability of Failure vs. Length of System (Gilbert 2012).

6.3.7 Offshore Structures

Gilbert et al (2008) analyzed the potential risk of offshore structures. Two types of structures were considered in the paper: fixed jacket platforms and floating production systems. Both structures provide a platform for the production and processing of oil and gas offshore. The paper showed the target risk area for offshore structures in the F-N Chart. The annual probability of failure for offshore structures is between 10^{-3} and 10^{-4}, while the number of fatalities is between 10 and 100 (Gilbert et al. 2008, p. 199). The risk associated with offshore structure failure is also located on Figure 6-10.

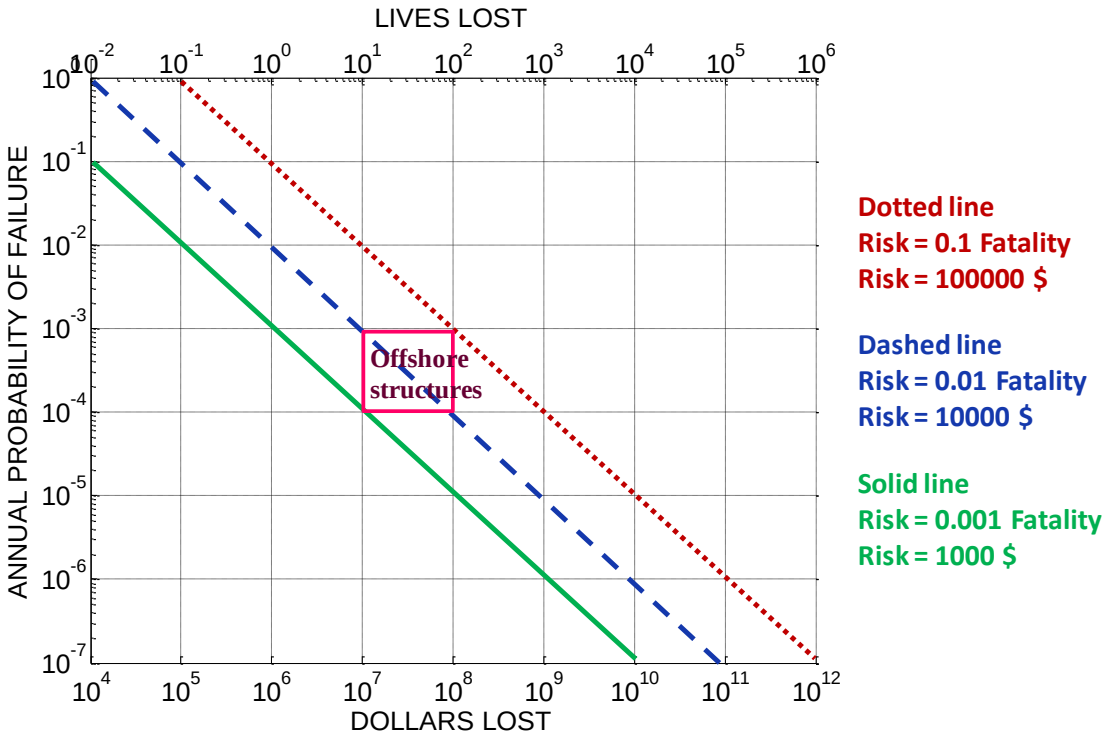

Figure 6-10. Risk Associated with Offshore Structures.

Figure 6-11 shows all societal risks analyzed in this section, from which we can see that most of the societal risks are at medium level.

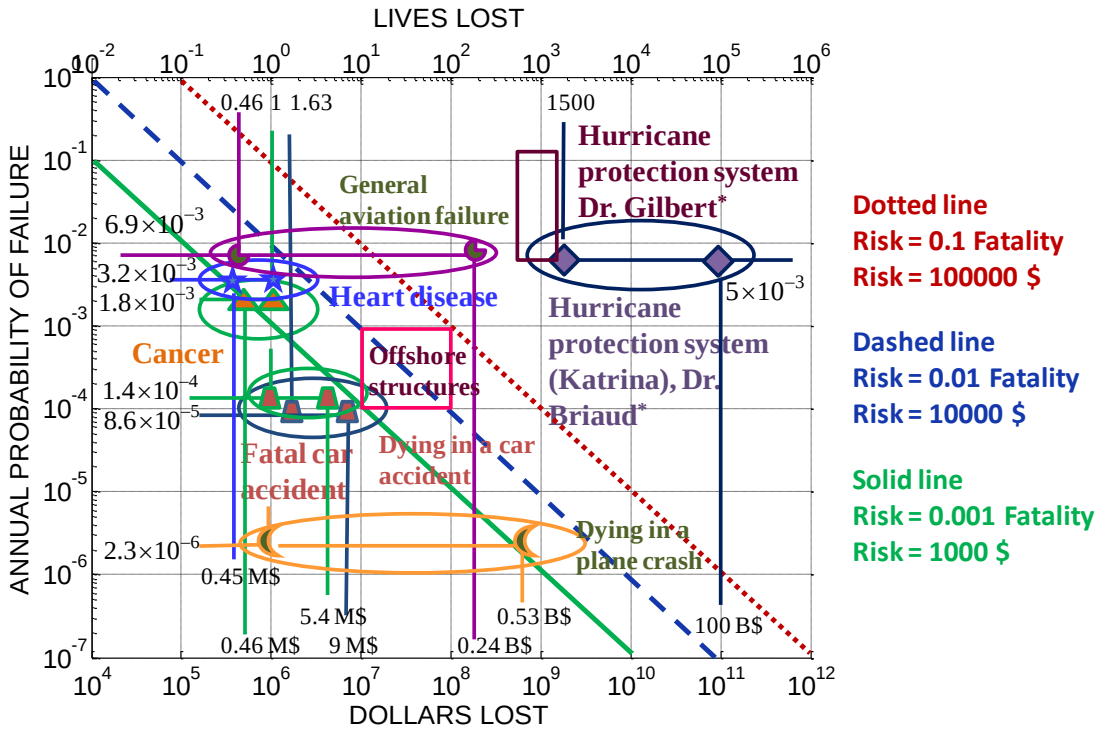

Figure 6-11. Selected Societal Risks.

6.4 SCOUR RISK BASED ON TWO DATABASES

To locate the data associated with bridge scour on Figure 6-11, two databases are used: the New York State Department of Transportation (NYSDOT) Bridge Failure Database (Sullivan 2005a) and the Florida Department of Transportation (FDOT) Unknown Foundation Bridge Database (FDOT 2009; 2010). The annual probability of scour failure, the corresponding dollars lost and fatalities are analyzed to calculate the risk of scour in dollar and fatality units.

6.4.1 NYSDOT Database (Sullivan 2005a)

6.4.1.1 Introduction to NYSDOT Database

The NYSDOT has compiled a database of bridge failures in the United States since 1966. It recorded the bridge failure types, failure time, location, reason to fail and number of fatalities in different states during 1966 and 2005 (Sullivan 2005a). Two types of failure are analyzed in the database: total collapse (TC) and partial collapse (PC). TC means structures on which all primary members of a span or several spans have undergone severe deformation such that no travel lanes are passable. PC means structures on which all or some of the primary structural members of a span or multiple spans have undergone severe deformation such that the lives of those traveling on or under the structure would be in danger (Auyeung, Winchell, personal communication, June 16, 2011). The eleven reasons which caused bridge failure in the database are shown below in detail.

A. Fire—It means the fire caused by collision, explosion, car crash, arson, and so on.

B. Collision—It means the collision of the trucks, cars, vehicles, barge, and ship with bridges. There is one case for a plane crash.

C. Concrete----It means the deterioration of concrete as a cause of bridge failure. There are only seven cases of a "concrete" cause.

D. Deterioration---- Here it mostly means the deterioration of timber (decay), deterioration of cables, and deterioration of abutments. There are 13 cases in this category.

E. Construction—Here it means the bridge failure during construction, possibly during the maintenance or extension of the bridge. The failure can be caused by hydraulic jack failure or inadequate bracing. There is one case where the failure happened during the first stage construction of a bridge on October 11, 2002.

F. Earthquake—Here it means the bridge failures caused by earthquake. All the 15 cases occurred in California.

G. Hydraulic—Here it means the bridge failures caused by flood, scour, and so on. In the northern part of the United States, floods were mostly caused by snowmelt in a short period.

H. Natural--- Here it means the bridge failures caused by tornado, avalanche, sinkhole, wind, volcano, and tree fall. Bridge failures caused by volcano usually happened in Washington State.

I. Overload—Here it means bridge failures due to overloading of vehicles, mostly of trucks. There are several cases also involved with timber deterioration.

J. Steel—Here it mostly refers to steel bridges. It refers to bridge failures due to steel corrosion (deterioration) and fatigue.

K. Miscellaneous—Here it probably means bridge failures caused by multiple reasons. The reasons could be the combination of deterioration, deck collapse, scour, traffic damage, construction failure and so on. If the failure cause is "Miscellaneous", it is usually followed by a description such as "falsework", "deterioration", "soil", etc. If it just says "Miscellaneous", then the cause is unknown.

Figure 6-12 shows the weights of the eleven causes of bridge failure based on the database. It is shown that the scour accounts for about 58% of the bridge failures in the United States (Briaud 2006). The second most common reason of bridge failure is collisions caused by ship, truck, or train impact. The third most common reason of bridge failure is overload.

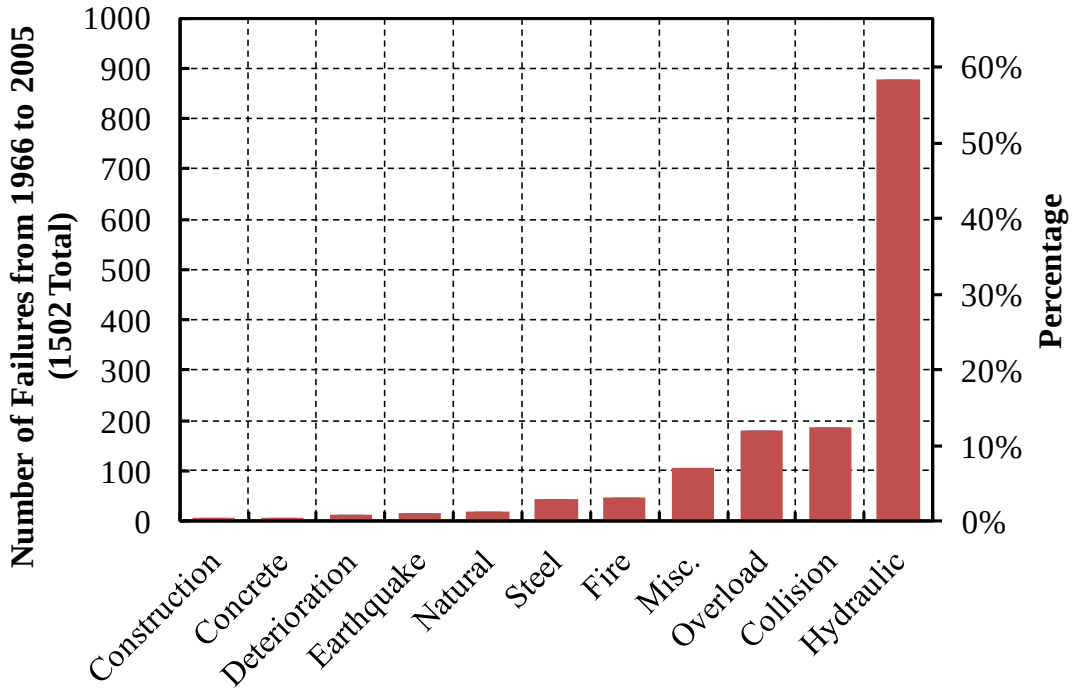

Figure 6-12. NYSDOT Bridge Failure Database Study-Causes of Bridge Failure (1966–2005) (after Briaud 2006).

Figure 6-13 shows the number of bridge failures vary with time. From the figure we can see that the bridge failures have significantly dropped since 2001. The reason is

that the number of bridge failures caused by scour was significantly reduced since 2001 (Figure 6-14).

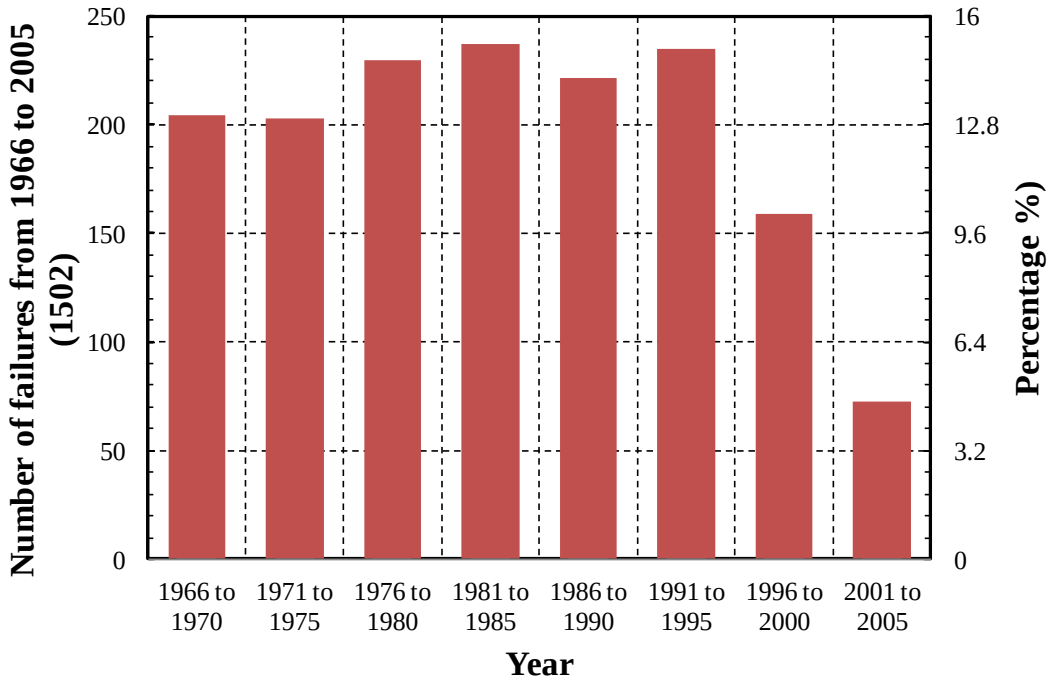

Figure 6-13. The Number of Failures Varies with Time.

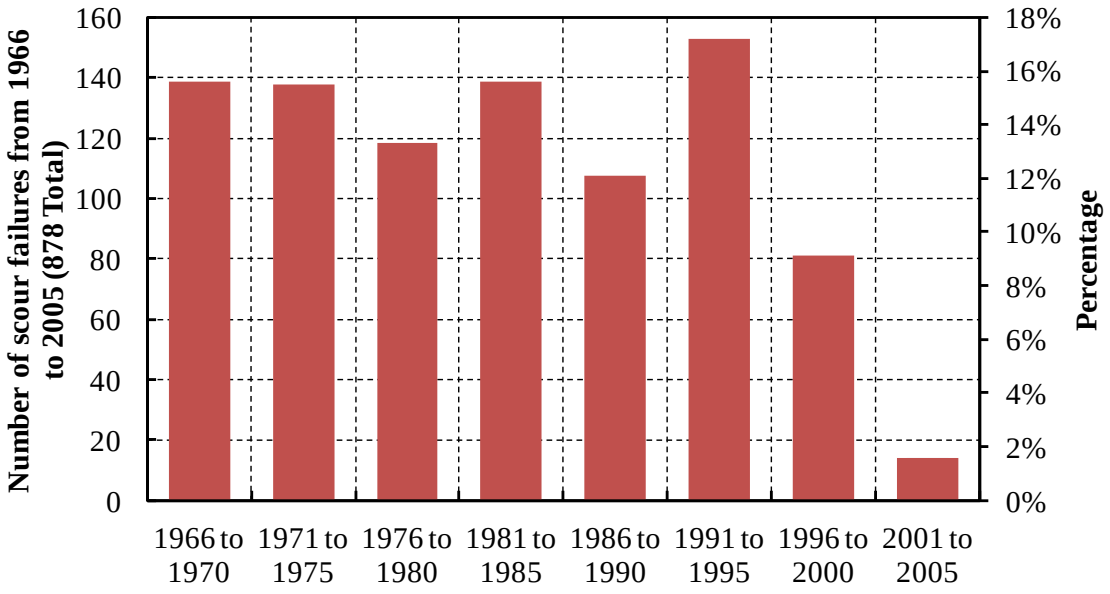

Figure 6-14. Number of Scour Failures Varies with Time (after Briaud 2006).

Figure 6-15 and Figure 6-16 show the number of bridge failures due to different causes between 1966 and 2005.

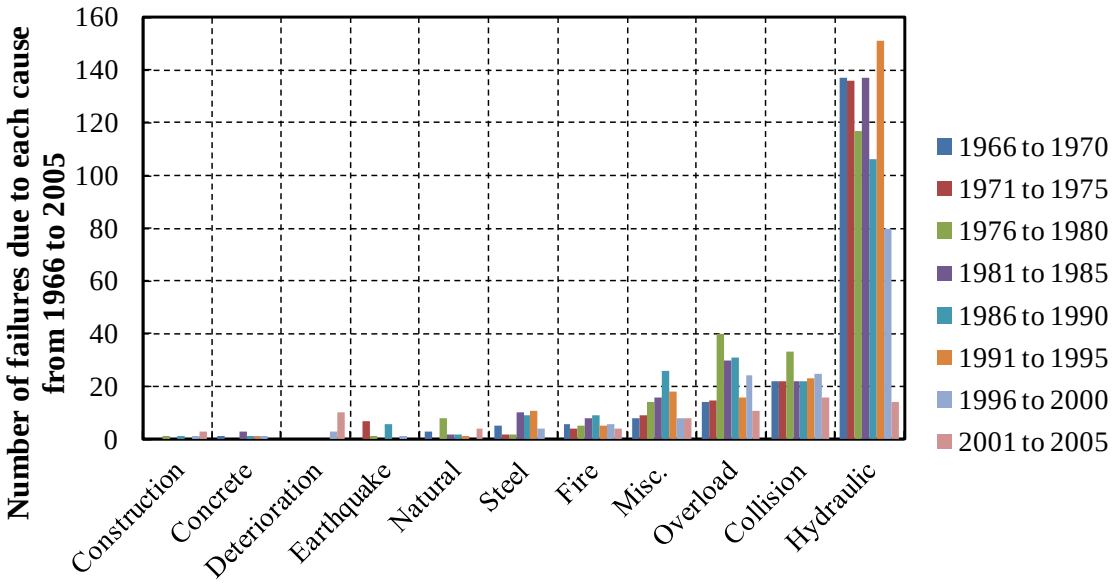

Figure 6-15. Number of Bridge Failures due to Different Causes-in Terms of Causes (Briaud et al. 2012).

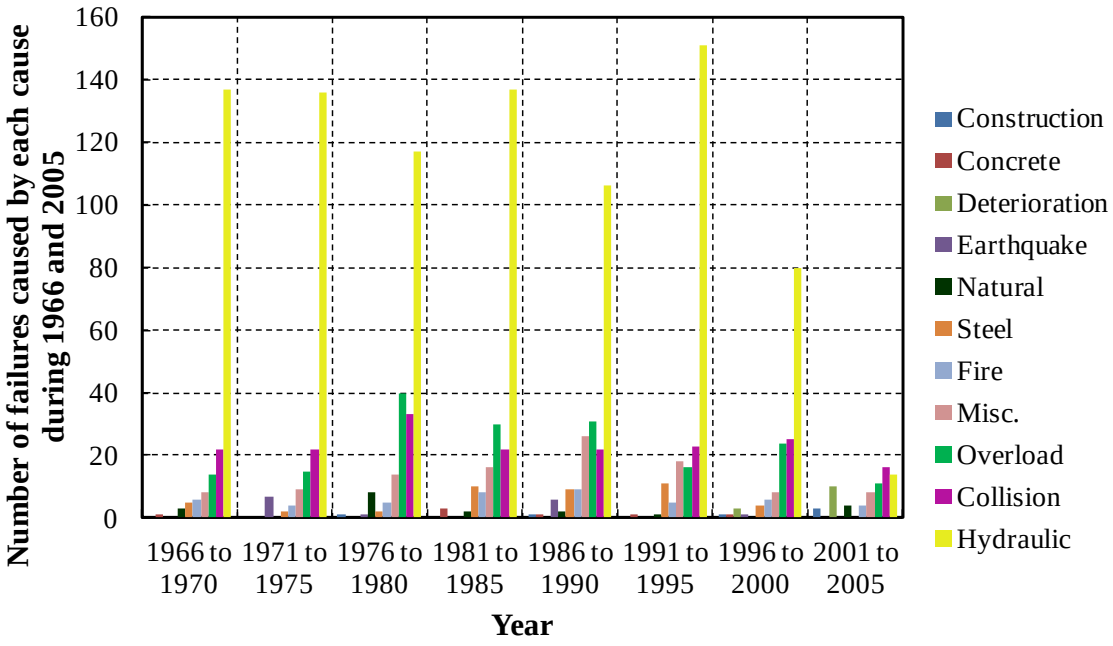

Figure 6-16. Number of Bridge Failures due to Different Causes-in Terms of Years.

Figure 6-17 shows the number of fatalities caused by bridge failure. Collisions caused by ship, trucks, and cars are the most possible reasons to cause the death of people. Deterioration and fatigue of steel is the second possible reason to cause the death of people. Scour is the third most possible reason to cause deaths. It is understood that scour is the number one cause of bridge failure, while it does not always cause fatalities. It is probably because most of the scour failure happens with hurricanes, during which period traffic is restricted.

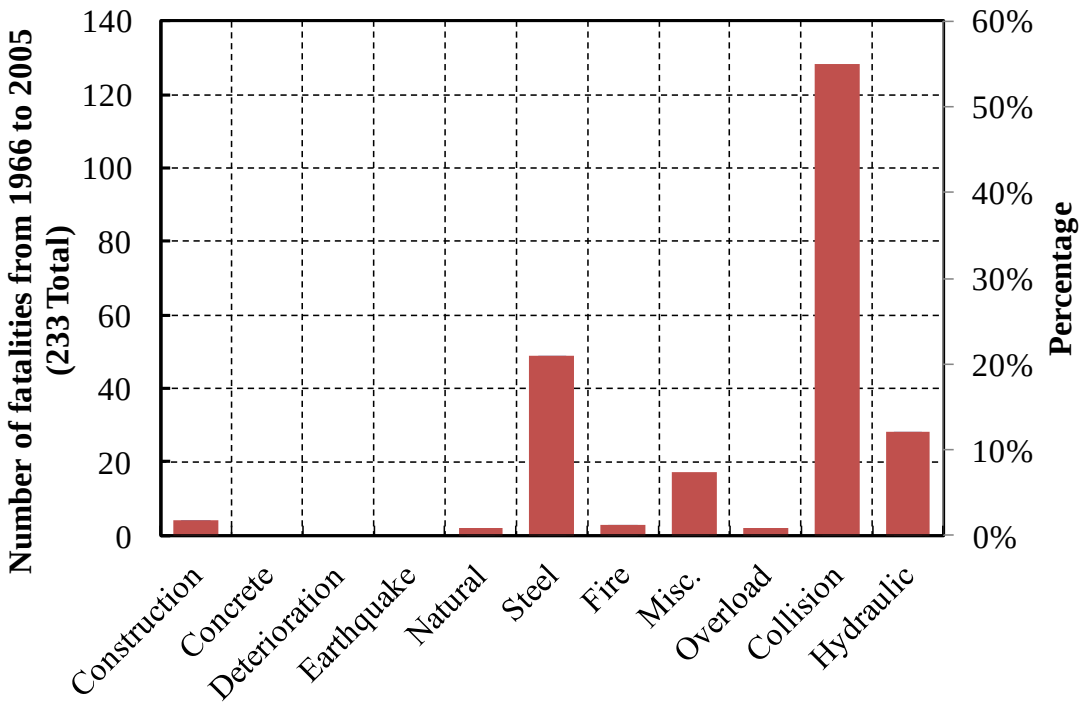

Figure 6-17. Number of Fatalities Caused by Different Reasons of Bridge Failure.

Figure 6-18 shows the fatality and injury data caused by bridge failure due to any reason from 1966 till 2005. It can be seen that the fatality number and injury number does not vary too much with time except the injury data from Year 1996 to Year 2000.

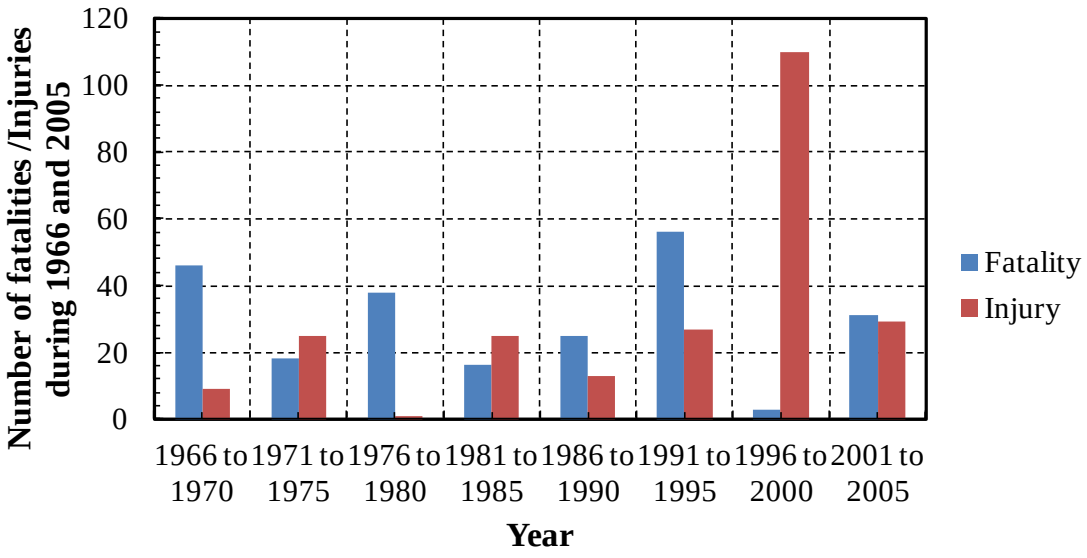

Figure 6-18. Fatalities & Injuries with Time for All Causes.

Figure 6-19 and Figure 6-20 show the fatality data caused by bridge failure due to different reasons within those 40 years. Compared with Figure 6-17 (Number of fatalities caused by different reasons of bridge failure), these two figures show "three-dimensional" analysis of the bridge failure. They show the number of fatalities caused by bridge failure due to each reason in different years.

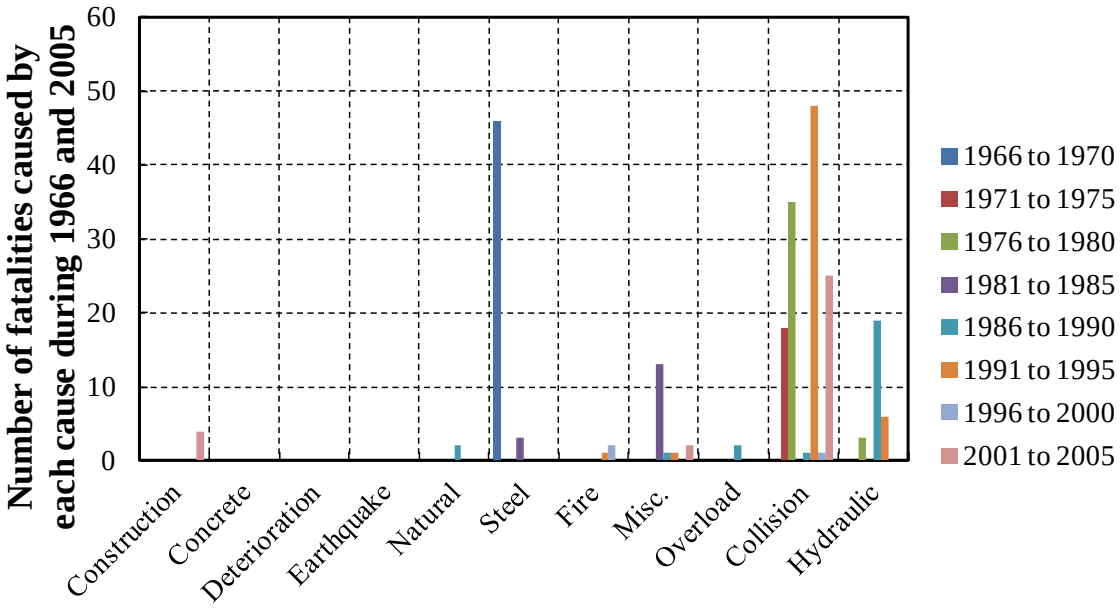

Figure 6-19. Fatality Data Caused by Each Cause in Different Yeas (Cause Oriented).

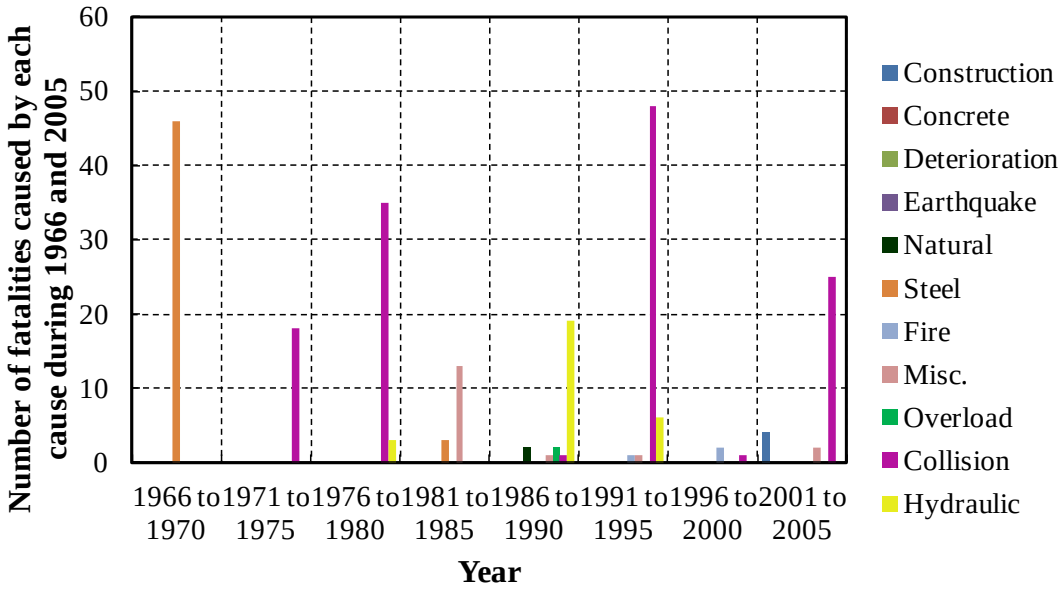

Figure 6-20. Fatality Data Caused by Each Cause in Different Yeas (Time Oriented).

Figure 6-21 and Figure 6-22 show the injury data caused by bridge failure due to different reasons within those 40 years. Compared with Figure 6-18 (Number of injuries caused by different reasons of bridge failure), these two figures show "three-dimensional" analysis of the bridge failure. They show the number of injuries caused by bridge failure due to each reason in different years.

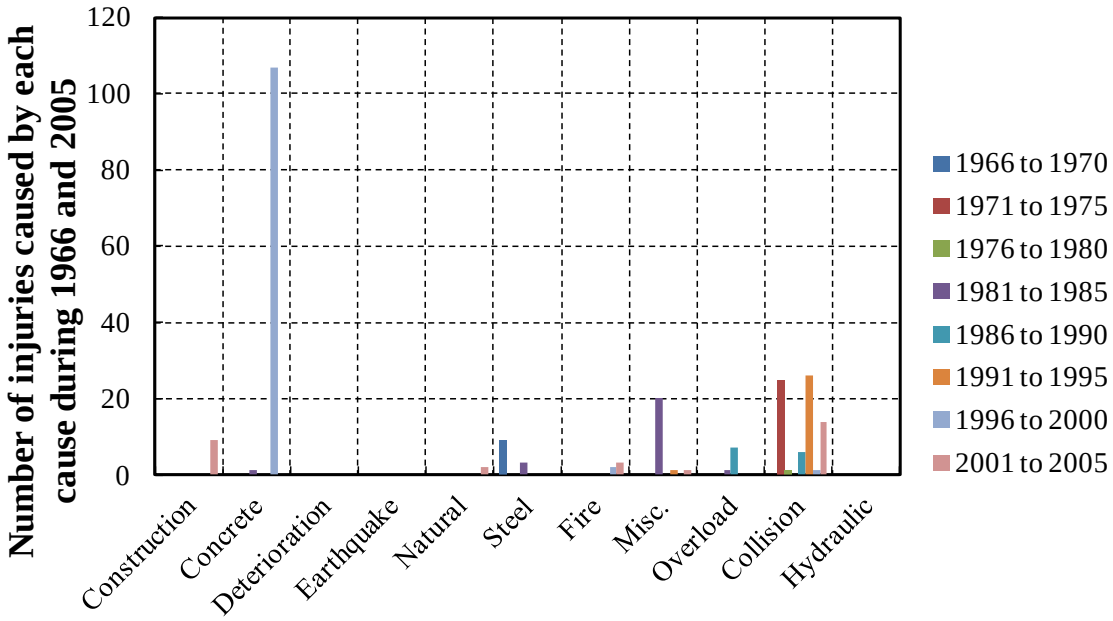

Figure 6-21. Injury Data Caused by Each Cause in Different Years (Cause Oriented).

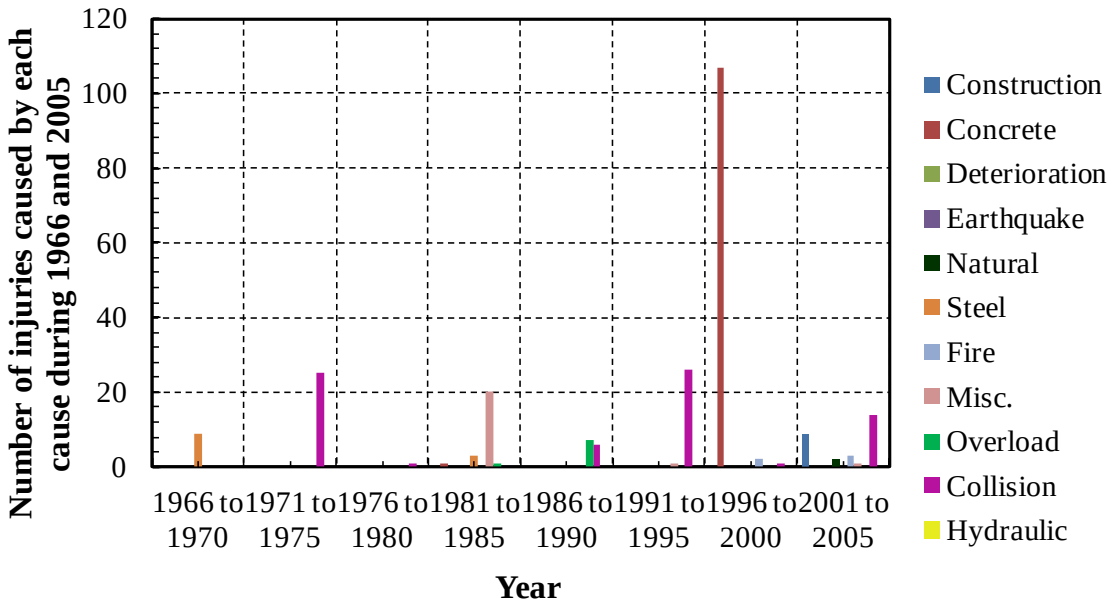

Figure 6-22. Injury Data Caused by Each Cause in Different Years (Time Oriented).

Figure 6-23 shows the fatality and injury data caused by bridge failure due to scour. It can be seen that 28 people died in the bridge failures caused by scour during these 40 years, while no injury occurred.

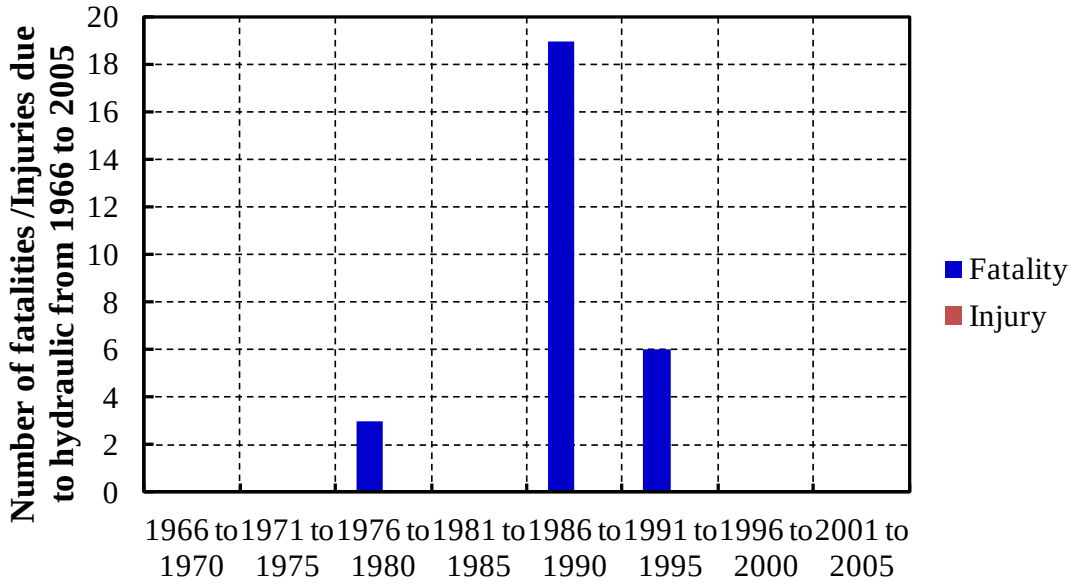

Figure 6-23. Fatality and Injury Data Caused by Bridge Failure due to Scour (Briaud et al. 2012).

6.4.1.2 Risk Analysis

The annual probability of failure is the average number of bridge failures per year over a given period divided by the total number of bridges that exist during that same period. According to the NYSDOT database, 1502 bridges failed between 1966 and 2005 in the United States; that is one bridge failure every 10 days on the average. Within those 1502 failures, 878 failures were due to scour (hydraulic reason). Therefore, 22 bridge failures due to scour per year or one bridge failure due to scour every 17 days is the statistic for the United States. According to the US National Bridge Inventory (NBI), about 500,000 bridges over water were in existence during that 40 year period. Therefore the annual probability of bridge failure due to scour is 4.4×10^{-5} (878/40/500,000). The database

shows that the number of fatalities due to bridge scour failures from 1966 to 2005 is 28. This gives the number of lives lost as 0.03 every time a bridge fails (28/878=0.03).

According to the Caltrans Bridge Square Foot Cost Summary (Caltrans, 2011), the average cost of a bridge in 2011 was \$1,867/m^2 of bridge deck. It is the analysis based on three different types of bridges: reinforced concrete bridges, prestressed concrete bridges and steel bridges. The statistics are obtained according to 76 bridges, and they only include the bridge cost.

A typical bridge may have a span of 50m and a width of 12m. If it is assumed that a bridge failure corresponds to the loss of one span, an estimate of the financial loss per year is $\$1,867 \times 50 \times 12 = \$1,120,200 / \text{yr}$.

Stein and Sedmera (2006) proposed a way to quantify the risk due to bridge failure. They included the cost of replacement of the failed portion of the bridge, and the cost of lost time and detours. They proposed the following equation:

$$Cost = \{C_1 eWL\}_1 + \{[C_2(1-\frac{T}{100}) + C_3\frac{T}{100}]DAd + [C_4 O(1-\frac{T}{100}) + C_5\frac{T}{100}]\frac{DAd}{S}\}_2 + \{C_6 X\}_3 \quad (6\text{-}2)$$

where *Cost* = the total cost of bridge failure (\$), C_1 = the unit building cost (\$/m^2), *e* = the cost multiplier for early replacement based on Average Daily Traffic (ADT), *W* = the bridge width (m), *L* = the bridge length (m), C_2 = the cost of operating a running automobile (\$0.28/km), *T* = the average daily truck traffic (percentage of ADT), *D* = the detour length (km), *A* = the Average Daily Traffic (ADT), *d* = the duration of the detour based on ADT (days), C_3 = the cost of operating a running truck (\$0.808/km), C_4 = the value of time per adult in passenger car (\$/hr), *O* = the average occupancy rate (1.63 usually), C_5 = the value of time for truck (\$22.01/h), *S* = the average detour speed

(65km/h), C_6 = the cost for each life loss (typically $500,000, in Stein and Sedmera 2006), X=the number of fatalities from the failure. Note that the first part in the equation (subscript as 1) is the cost of replacing the bridge, the second part in the equation (subscript as 2) is the detour cost and the time cost due to bridge failure, and the last term (subscript as 3) is the cost of fatalities.

In order to determine the location of the ellipse for bridge scour in Figure 6-11, the lives lost need to be separated from the total cost. Therefore, only the first two terms are used in Equation 6-2 for the economic loss (Equation 6-3), while the number of fatalities is considered independently.

$$Cost = \{C_1 eWL\}_1 + \{[C_2(1-\frac{T}{100}) + C_3\frac{T}{100}]DAd + [C_4 O(1-\frac{T}{100}) + C_5\frac{T}{100}]\frac{DAd}{S}\}_2 \ , \qquad (6\text{-}3)$$

The parameters for a typical bridge are shown in Table 6-4.

Note that the value of average daily traffic (A = 6635 vehicles/day) is according to the bridge plan of US59 over the Guadalupe River. The value of cost multiplier for early replacement (e = 2) and duration of detour (d = 183 days) is chosen based on the average daily traffic (Stein and Sedmera 2006). The unit building cost is $1,867/m^2 according to the Caltrans Bridge Square Foot Cost Summary (Caltrans 2011), the average daily truck traffic T is assumed to be 30%, and the detour length D is also assumed to be 15 km in this case study. The value of time per adult in passenger cars is $6.96/hr according to the statistic in Texas (Stein and Sedmera 2006).

Using Equation 6-3 the economic loss for one bridge failure is determined to be

$$C_1 eWL + [C_2(1-\frac{T}{100}) + C_3\frac{T}{100}]DAd + [C_4 O(1-\frac{T}{100}) + C_5\frac{T}{100}]\frac{DAd}{S}$$

$$\$14{,}300{,}358\ (= 1{,}867\times 2\times 12\times 50 + (0.28\times(1-\frac{30}{100}) + 0.808\times\frac{30}{100})\times 15\times 6{,}635\times 183 +$$

$$(6.96\times 1.63\times(1-\frac{30}{100}) + 22.01\times\frac{30}{100})\times\frac{15\times 6635\times 183}{65} = 14{,}300{,}358$$

Note that the cost of replacing the bridge is only about 16% of the total economic cost. Therefore, the estimated risk is 0.03 fatalities/yr, $1.1 M/yr (cost of bridge repair only), and $14 M/yr (bridge repair cost, detour cost and time cost). These numbers are used to locate the bridge scour ellipse on Figure 6-24 labeled as "Scour-NY".

Table 6-4. Parameters to Calculate Risk for a Typical Bridge (after Stein and Sedmera 2006).

Parameters		Values
Unit building cost ($/m^2)	C_1	1867
cost multiplier for early replacement based on ADT	e	2
Bridge width (m)	W	12
Bridge length (m)	L	50
Cost of running automobile ($.28/km)	C_2	0.28
Average daily truck traffic (%)	T	30
detour length (km)	D	15
Average daily traffic (vehicles/day)	A	6635
Duration of detour based on ADT (days)	d	183
Cost of running truck ($0.808/km)	C_3	0.808
Value of time per adult in passenger car ($/hr)	C_4	6.96
Average occupancy rate (1.63 people)	O	1.63
Value of time for truck ($22.01/hr)	C_5	22.01
Average detour speed (65km/h)	S	65

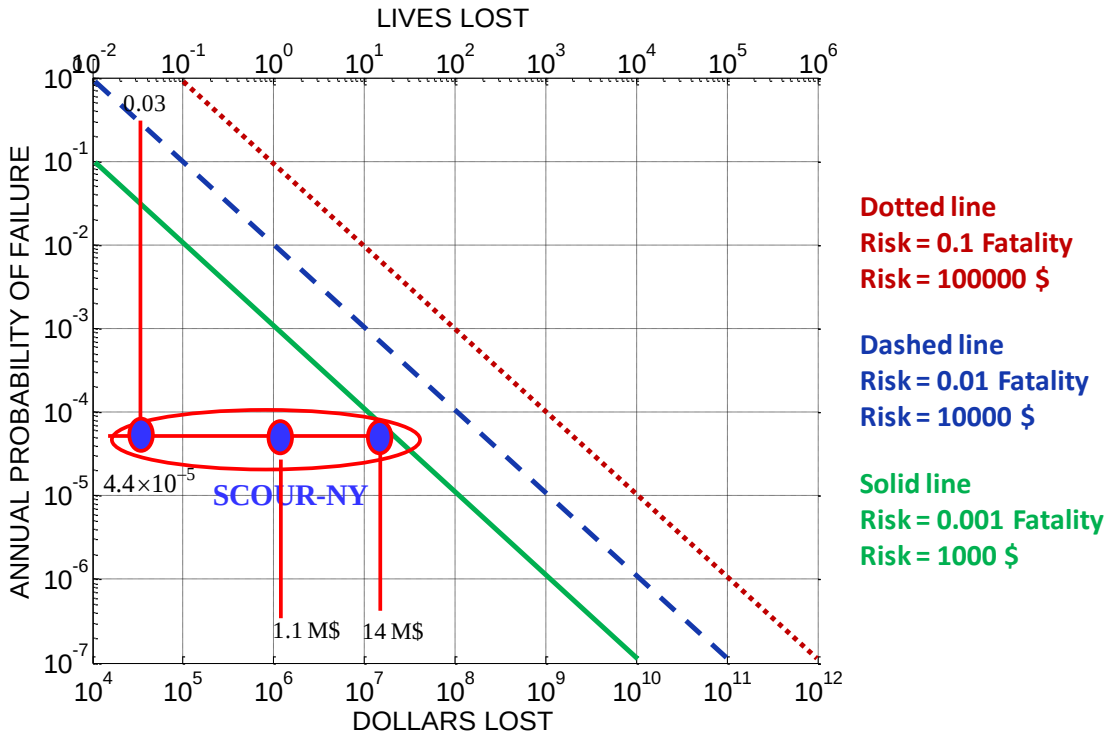

Figure 6-24. Bridge Scour Risk Based on NYSDOT Database.

If all the reasons that contribute to bridge failure are taken into consideration, the bubble location will be slightly different, but not too much. The annual probability of failure is calculated to be 7.5×10^{-5} (1502/40/500,000). The database shows that the number of fatalities from 1966 to 2005 is 233. This gives the number of lives lost as 0.16 every time a bridge fails (233/1502=0.16). The economic loss due to bridge failure is the same as above, i.e. $1.1 M/yr (cost of bridge repair only), and $14 M/yr (bridge repair cost, detour cost and time cost). These numbers are used to locate the bridge failure ellipse on Figure 6-25 labeled as "Bridge failure-NY". It is easy to see that these two ellipses are very close to each other.

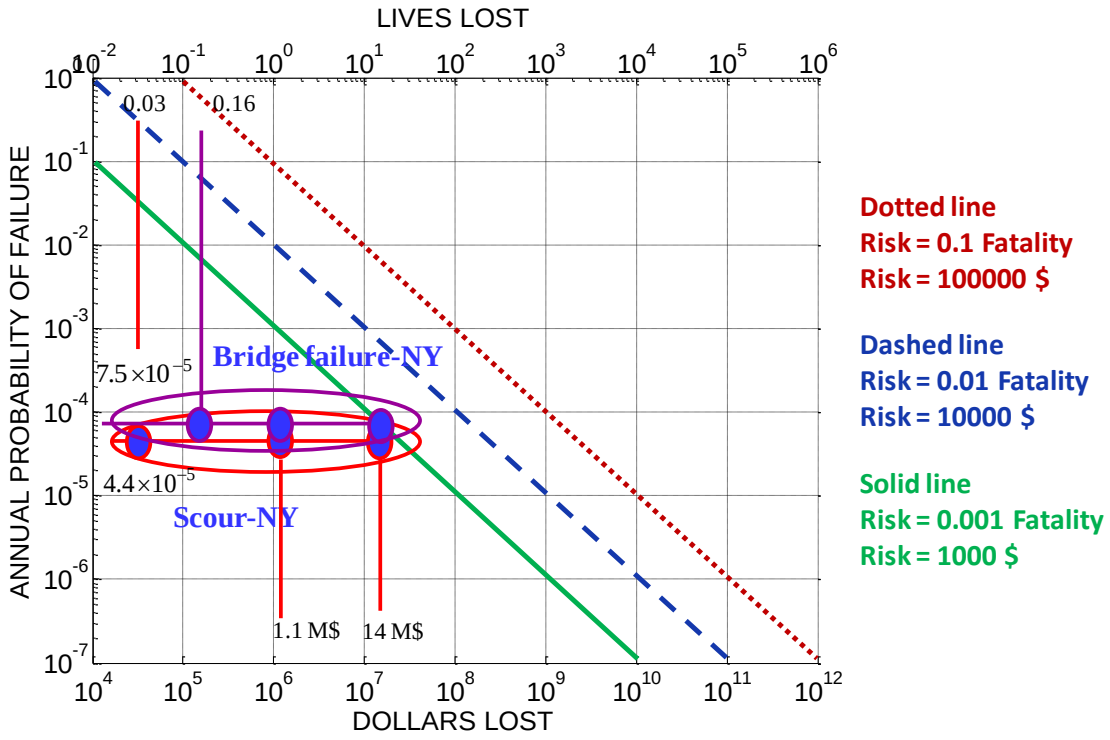

Figure 6-25. Bridge Failure Risk Based on NYSDOT.

6.4.2 FDOT Unknown Foundation Bridges Database (FDOT 2009; 2010)

6.4.2.1 Introduction to FDOT Database

The Florida Department of Transportation (FDOT) launched a research project investigating the potential risk of scour failure for unknown foundation bridges in Florida (FDOT 2009; 2010). Florida has approximately 8,200 bridges over water, and approximately 2,500 bridges are classified as having unknown foundations, at about 30% of all bridges.

The FDOT set up the database recording those 2,482 bridges with unknown foundations over water. The potential failure cost for each bridge is calculated using

Stein's method, which includes rebuilding cost, detour cost and time cost (Equation 6-2). Note that some changes in parameters are made to make the cost calculation adaptable for Florida. In this study, the detour cost was not very accurate due to the fact that it was out of the scope of the study.

The annual probability of failure is calculated using a modified HYRISK method, which is revised according to the original HYRISK method.

The FDOT database recorded the bridge replacement cost, detour cost, loss of life cost, total cost of failure, annual probability of failure, lifetime probability of failure, annual risk and annual lifetime risk for 2482 bridges.

6.4.2.2 Risk Analysis

This section is to locate the risk of bridge scour failure on the F-N Chart using the FDOT database, and compare it with the results from the NYSDOT database.

Since in the database the cost of failure includes the bridge replacement cost, detour cost, loss of life cost, the first step would be to isolate the fatalities from the total economic loss. Here an average cost of a life is estimated to be $576,750 (FDOT 2010). The annual probability of failure, fatalities, and dollars lost are plotted in Figure 6-26. Note that the blue dots represent the data related to dollar loss, while the green stars represent the fatalities.

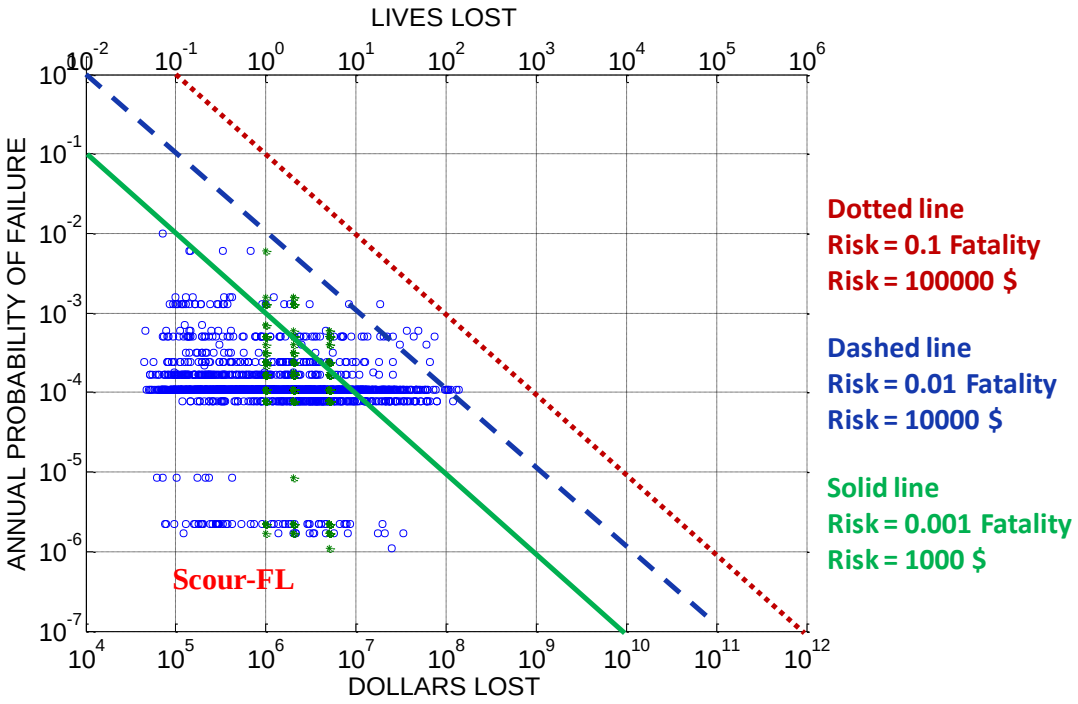

Figure 6-26. Bridge Scour Risk Based on FDOT Database (Scatter Plot).

Since the scatter plot is covering a large area in the F-N Chart and hard to compare with the results obtained from the NYSDOT database, the accumulated plot is drawn below. First, the average probability of failure is calculated by the mean of all probabilities, which gives 1.6×10^{-4}. The risk per bridge failure is calculated as \$591 from the perspective of economic loss, and 0.0003 fatalities. The concept is to maintain the equal risk from the database. Hence, the dollar loss is calculated to be \$3.7 M ($= 591/(1.6\times10^{-4})$), and the fatalities are calculated to be 1.75 ($=0.0003/(1.6\times10^{-4})$). The accumulated plot is shown in Figure 6-27.

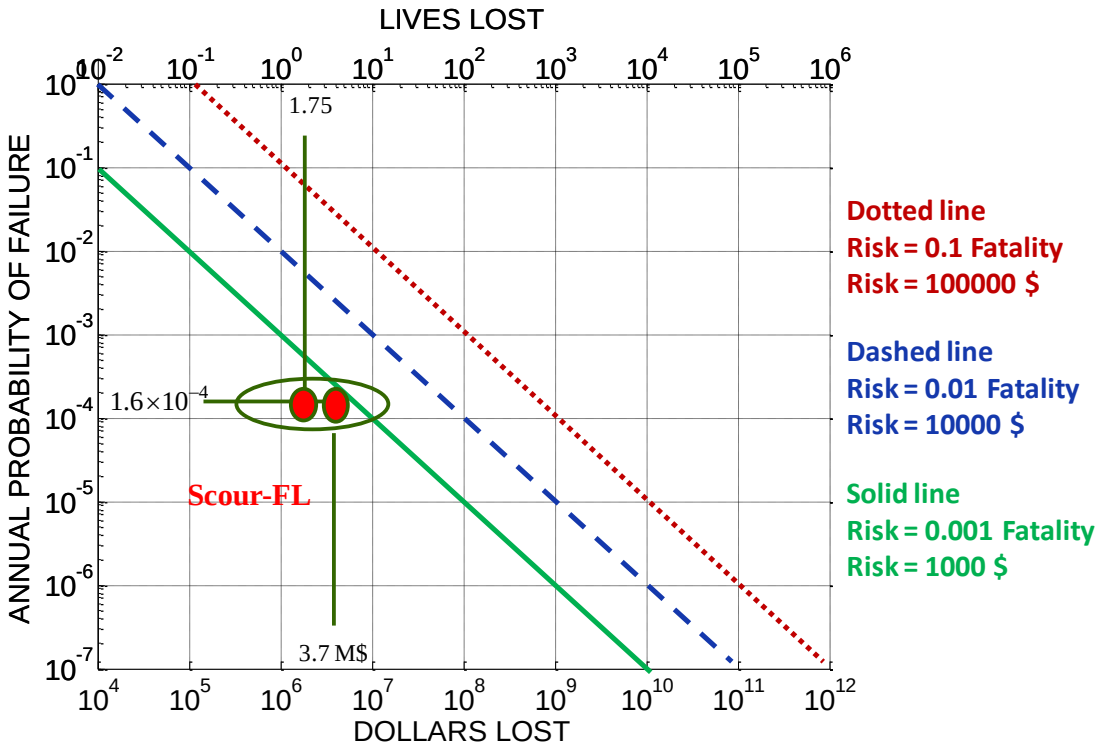

Figure 6-27. Bridge Scour Risk Based on FDOT Database (Accumulated Plot).

Figure 6-28 shows the bridge scour risk obtained from both the NYSDOT database and FDOT database. It is clear that the scour risk is within the acceptable limit.

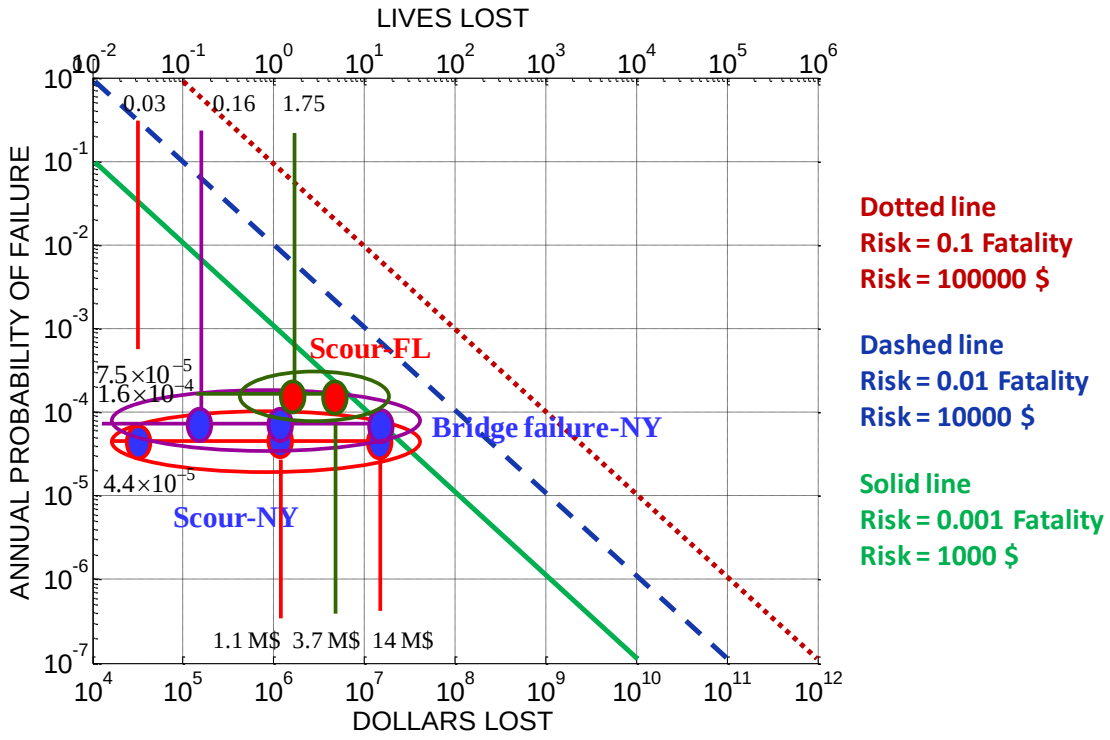

Figure 6-28. Bridge Scour Risk.

6.5 CONCLUSIONS ON SCOUR RISK

Risk is the probability of failure times the value of the consequence. Figure 6-29 shows the risk of all events mentioned in this section. Acceptable risk criterion is dependent on the definition of the economic loss for each given event, the cultural factors, and the probability of failure. From the study in this section, the accepted risk values are defined to be $1,000/yr and 0.001 fatalities/yr for most civil engineering structures and societal events based on the United States data. However, bridge scour risk is within acceptable limits when compared to other risks.

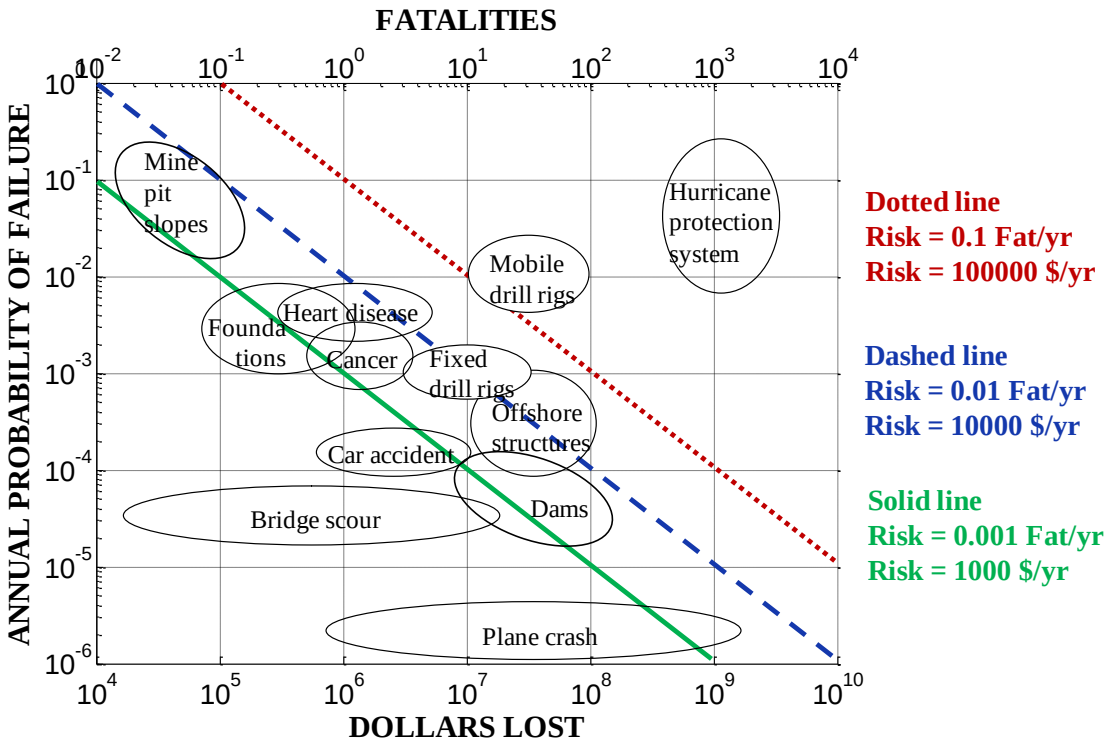

Figure 6-29. Risk Plot.

It is very important to point out that risk is a very subjective topic. The economic loss is hard to define sometimes. It is based on local experience and former data. In this section, the vulnerability analysis is not included, which could be a future research area. For the bridge scour risk, different failure modes will cause a different probability of failure and different economic loss and fatalities. If the vulnerability analysis is conducted, the risk of bridge scour failure would be different. It could be a future research topic.

7 CONCLUSIONS

The dissertation fulfills three objectives: develop a probabilistic approach for prediction of scour depth; develop a reliability-based LRFD calibration of bridge foundations in the case of scour; and quantify bridge scour risks.

7.1 STATISTICAL ANALYSIS

The author established the probability-based pier scour depth prediction model for three databases: Landers and Mueller Database (1996), TAMU Database (Gudavalli 1997; Li 2002), and Froehlich Database (1988). Both HEC-18 Sand and HEC-18 Clay methods were discussed in this dissertation. A different approach to compute critical velocity was also discussed for the three databases. Table 7-1 shows the Bayesian analysis results for the probabilistic scour depth prediction models using three databases and both HEC-18 Sand and HEC-18 Clay methods. It can be seen that for those two full scale database (Landers-Mueller Database and Froehlich Database), the computed results do not differ much. For the TAMU database, which is the experimental results, the computed parameters show a big difference from the full scale database.

Table 7-1. Bayesian Analysis Results for the Probabilistic Scour Depth Prediction Models Using Different Databases and Different Methods.

Database	Cases	Method	Data Points	Maximum Likelyhood		Bayesian		θ_{unb}	$1/\theta_{unb}$
				Parameter Γ_ζ	Parameter σ_ζ	Parameter Γ_ζ	Parameter σ_ζ		
L&M	Whole Database	HEC-18 Sand	344	-1.179	0.6744	-1.1778	0.6787	0.3079	3.2478
		HEC-18 Clay	366	-1.0876	0.7409	-1.087	0.745	0.3372	2.9656
TAMU	Whole Database	HEC-18 Sand	73	-0.434	0.4616	-0.4376	0.4757	0.6456	1.5489
		HEC-18 Clay	73	-0.1323	0.3448	-0.1317	0.3404	0.8766	1.1408
Froehlich	Whole Database	HEC-18 Sand	79	-1.0095	0.5359	-1.0116	0.5381	0.3636	2.7503
		HEC-18 Clay using V_{c_Briaud}	78	-1.0333	0.7485	-1.0385	0.7709	0.354	2.8249
		HEC-18 Clay using V_{c^*}	77	-0.9559	0.6789	-0.9629	0.6788	0.3818	2.6192
		HEC-18 Clay using $V_{c^{**}}$	77	-0.9682	0.695	-0.9368	0.6865	0.3919	2.5517

7.2 LRFD-SHALLOW FOUNDATIONS

In order to meet the target probability of exceedance (0.001), the scour depth should be multiplied by a factor θ_T in the design process.

Results based on the Landers-Mueller Database:

- If you want to build shallow foundations in sand, the foundation depth should be 2.05 Z_{det} in order to meet the probability of exceedance of 0.001.
- If you want to build shallow foundations in clay, the foundation depth should be 2.5 Z_{det} in order to meet the probability of exceedance of 0.001.
- If Z_{scour} > 2m, the foundation depth in sand should be 1.4 Z_{det} in order to meet the probability of exceedance of 0.001.
- If Z_{scour} > 2m, the foundation depth in clay should be 1.3 Z_{det} in order to meet the probability of exceedance of 0.001.
- If Z_{scour} < 2m, the foundation depth in sand should be 1.95 Z_{det} in order to meet the probability of exceedance of 0.001.
- If Z_{scour} < 2m, the foundation depth in clay should be 2.75 Z_{det} in order to meet the probability of exceedance of 0.001.

Results based on the TAMU Database:

- If you want to build shallow foundations in sand, the foundation depth should be 1.5 Z_{det} in order to meet the probability of exceedance of 0.001.
- If you want to build shallow foundations in clay, the foundation depth should be 1.8 Z_{det} in order to meet the probability of exceedance of 0.001.

Results based on the Froehlich Database:

- If you want to build shallow foundations in sand, the foundation depth should be 1.5 Z_{det} in order to meet the probability of exceedance of 0.001.
- If you want to build shallow foundations in clay, the foundation depth should be 1.8 Z_{det} in order to meet the probability of exceedance of 0.001.

All in all, if you want to build shallow foundations in sand, the foundation depth should be 1.5 Z_{det} in order to meet the probability of exceedance of 0.001. If you want to build shallow foundations in clay, the foundation depth should be 1.8 Z_{det} in order to meet the probability of exceedance of 0.001.

Table 7-2 shows proposed LRFD calibration for shallow foundation design using different databases and different methods (β_T=3).

7.3 LRFD-DEEP FOUNDATIONS

The dissertation provided a step by step procedure of computing the resistance factor given the load factors in the case of scour. Several case studies are performed in order to achieve the LRFD calibration code for the foundation design in the case of scour.

Table 7-2. Proposed LRFD Calibration for Shallow Foundation Design Using Different Databases and Different Methods ($\beta_T = 3$).

Database	Cases	Method	Data Points	Maximum Likelyhood		Bayesian		θ_{unb}	$1/\theta_{unb}$	θ_T
				Parameter Γ_ζ	Parameter σ_ζ	Parameter Γ_ζ	Parameter σ_ζ			
L&M	Whole Database	HEC-18 Sand	344	-1.179	0.6744	-1.1778	0.6787	0.3079	3.2478	2.05
		HEC-18 Clay	366	-1.0876	0.7409	-1.087	0.745	0.3372	2.9656	2.5
TAMU	Whole Database	HEC-18 Sand	73	-0.434	0.4616	-0.4376	0.4757	0.6456	1.5489	1.5
		HEC-18 Clay	73	-0.1323	0.3448	-0.1317	0.3404	0.8766	1.1408	1.8
Froehlich	Whole Database	HEC-18 Sand	79	-1.0095	0.5359	-1.0116	0.5381	0.3636	2.7503	1.5
		HEC-18 Clay using V_{c_Briaud}	78	-1.0333	0.7485	-1.0385	0.7709	0.354	2.8249	1.8
		HEC-18 Clay using V_{c*}	77	-0.9559	0.6789	-0.9629	0.6788	0.3818	2.6192	2.7
		HEC-18 Clay using V_{c**}	77	-0.9682	0.695	-0.9368	0.6865	0.3919	2.5517	2.51

The LRFD recommendations for deep foundations are proposed by the author as follows. Use same load factor and resistance factor for common situations (scour depth less than 25% of the pile length corresponding to no scour). For a larger percent of scour depth, the resistance factor decreases significantly.

In clay, the relationship between the ratio of revised resistance factor in the case of scour over the resistance factor without scour effect ($\varphi_{scour}/\varphi_{noscour}$) and the ratio of the deterministic scour depth over the pile length without scour effect ($Z_{det}/L_{p\_noscour}$) follows (if $Z_{det}/L_{p\_noscour} > 0.25$):

$$\frac{\varphi_{scour}}{\varphi_{noscour}} = 0.4\left(\frac{Z_{det}}{L_{p\_noscour}}\right)^{-0.7} \tag{7-1}$$

where φ_{scour} = the resistance factor for foundation design in the case of scour; $\varphi_{noscour}$ = the resistance factor for foundation design without considering scour; Z_{det} = deterministic scour depth prediction; $L_{p\_noscour}$ = the pile length required by design to sustain the design load in a no scour case.

Figure 7-1 shows the proposed LRFD calibration for deep foundation design in the case of scour in clay.

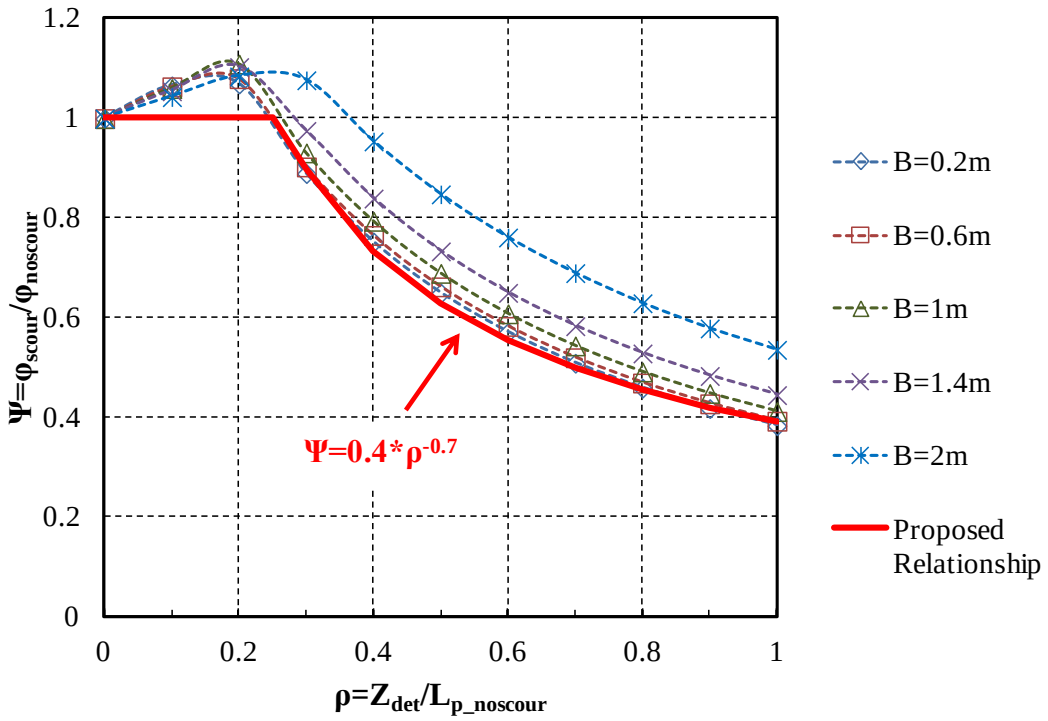

Figure 7-1. Proposed LRFD Calibration for Deep Foundation Design in the Case of Scour in Clay.

In sand, the relationship between the ratio of revised resistance factor in the case of scour over the resistance factor without scour effect ($\varphi_{scour}/\varphi_{noscour}$) and the ratio of the deterministic scour depth over the pile length without scour effect ($Z_{det}/L_{p\_noscour}$) follows (if $Z_{det}/L_{p\_noscour} > 0.25$):

$$\frac{\varphi_{scour}}{\varphi_{noscour}} = 1.2 - 0.8\frac{Z_{det}}{L_{p\_noscour}} \qquad (7\text{-}2)$$

Figure 7-2 shows the proposed LRFD calibration for deep foundation design in the case of scour in sand.

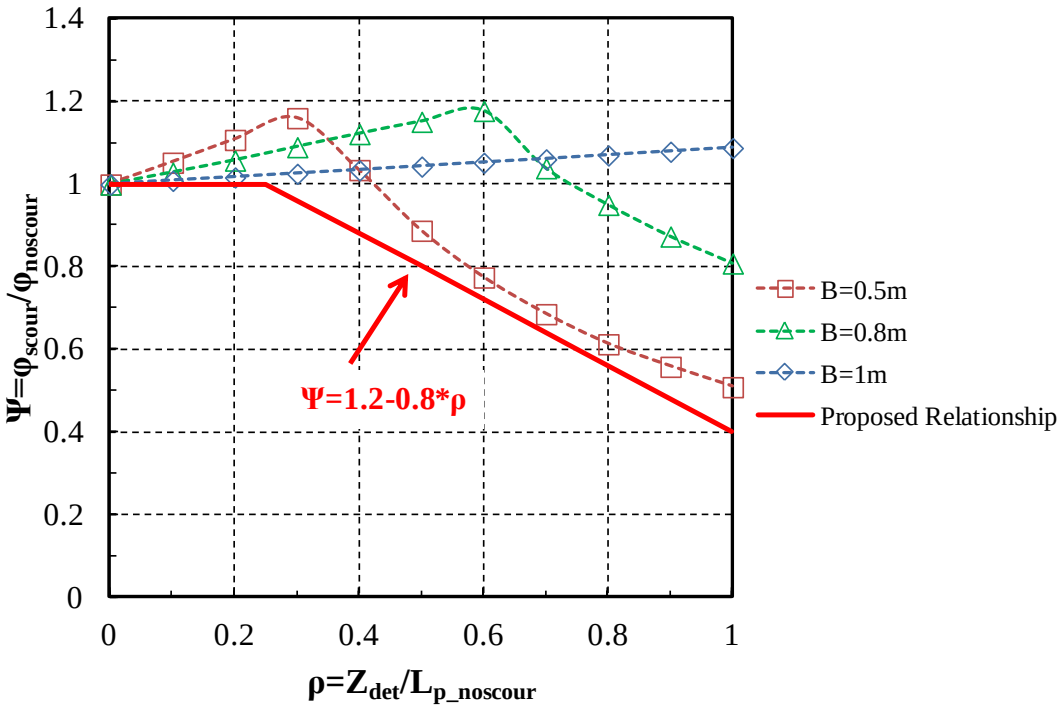

Figure 7-2. Proposed LRFD Calibration for Deep Foundation Design in the Case of Scour in Sand.

The foundation design procedure in the case of scour is proposed by the author as follows:

- Step 1: compute the pile length designed to be able to sustain the given loading condition in no scour case, $L_{p\_noscour}$;
- Step2: compute the deterministic scour depth L_{s_det} using HEC-18 Clay;
- Step 3: compute the ratio of deterministic scour depth over the pile length without considering scour, $L_{s\_det}/L_{p\_no\ scour}$;
- Step 4: choose resistance factor reduction factor Ψ from ρ-Ψ curve (Figure 7-1 and Figure 7-2)

- Step 5: calculate L_p using $\gamma L=\varphi_{scour}R_{scour}$, for fixed $L_{s\_det.}$ Here φ_{scour} is the reduced resistance factor in the case of scour, R_{scour} is the pile capacity considering scour effect as a function of L_p.

7.4 BRIDGE SCOUR RISK

Risk is the probability of failure times the value of the consequence. Figure 7-3 shows the common societal risks, bridge scour risk and the recommendation on acceptable risk level. Acceptable risk criterion is dependent on the definition of the economic loss for each given event, the cultural factors, and the probability of failure. According to the case studies in this dissertation, the accepted risk values are defined to be $1,000/yr and 0.001 fatalities/yr for most of the civil engineering structures and societal events based on the United States data. However, bridge scour risk is within acceptable limits when compared to other risks.

7.5 FUTURE RESEARCH DIRECTIONS

It is very important to point out that risk is a very subjective topic. The economic loss is hard to define sometimes. It is based on local experience and former data. In this dissertation, the vulnerability analysis is not included, which could be the future research directions. For the bridge scour risk, different failure modes will cause different probability of failure and different economic loss and fatalities. If the vulnerability analysis is conducted, the risk of bridge scour failure would be different. It could be a future research topic.

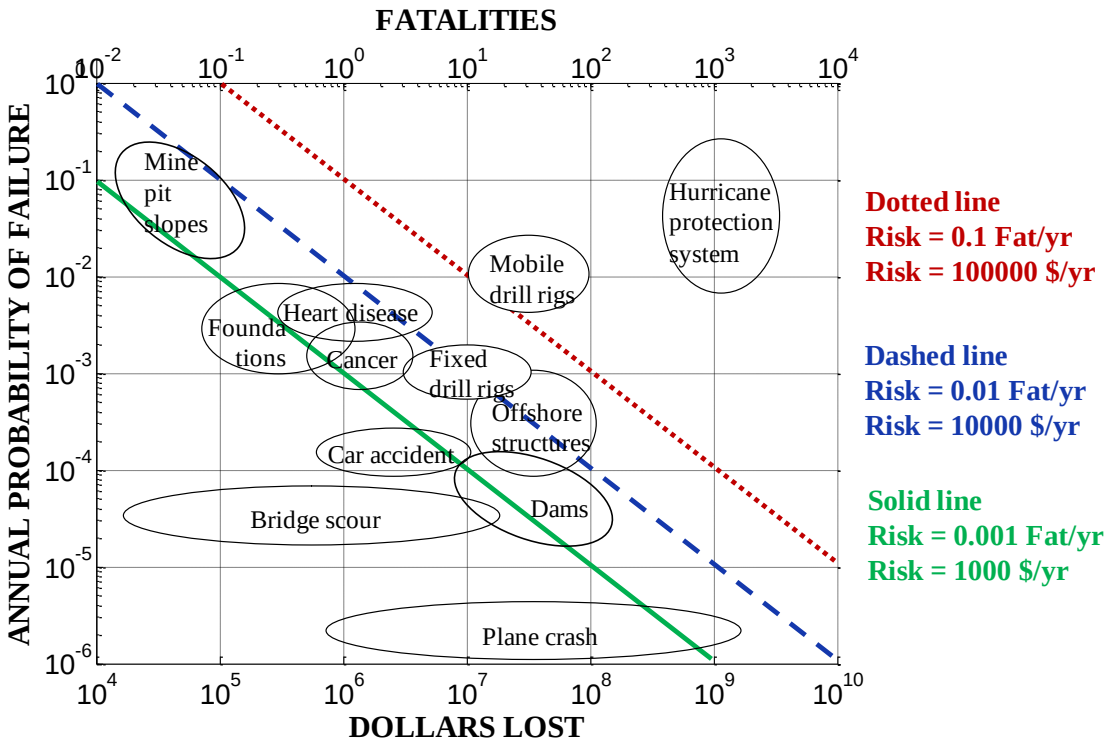

Figure 7-3. Recommendations on Acceptable Risk Level.

Besides the different approach of calculating the scour risk, the future research regarding LRFD calibration in bridge scour could also be conducted in abutment scour and contraction scour as well.

Local scour includes pier scour, abutment scour, and contraction scour. The abutment scour database includes Benedict et al. (2006), Ettema et al. (2008), Froehlich (1989), Sturm (2004), TAMU (Chen 2008; Oh 2009):

- Benedict et al. (2006): field data on abutment scour in South Carolina with more than 140 data points.

- Ettema et al. (2008): larger scale laboratory data in cohesionless soils with 30 points.
- Froehlich (1989): full scale field data with 80 data points.
- Sturm (2004): laboratory data in cohesionless soils with 80 points.
- TAMU (Chen 2008; Oh 2009): laboratory data in cohesive soils with 18 data points.

The contraction scour database includes Gill (1981), Komura (1966) and TAMU (Chen 2008; Oh 2009):

- Gill (1981): laboratory data in cohesionless soils with 20 points.
- Komura (1966): 12 data points.
- TAMU (Chen 2008; Oh 2009): 30 data points.

The contraction scour database and abutment scour database could be analyzed in future research to enhance the scour study, hence enhance the LRFD calibration in the case of scour considering all types of local scour.

In this dissertation, only a few case studies were performed to propose LRFD calibration for foundation design in the case of scour. In the future research, more case studies could be performed to validate the proposed model using the step by step procedure described in the dissertation.

REFERENCES

AASHTO (1994). *AASHTO LRFD Bridge Design Specifications*, 1st edition, American Association of State Highway and Transportation Officials (AASHTO), Customary U.S. Units, Washington, D.C.

AASHTO (2007). *AASHTO LRFD Bridge Design Specifications*, 4th edition, American Association of State Highway and Transportation Officials (AASHTO), Customary U.S. Units, Washington, D.C.

AASHTO (2002). *Standard Specifications for Highway Bridges*, 17th edition, American Association of State Highway and Transportation Officials (AASHTO), Inc., Washington, D.C.

American Cancer Society (2011). "Cancer facts & figures." URL: http://www.cancer.org/Research/CancerFactsFigures/CancerFactsFigures/cancer-facts-figures-2011(2011)

Arneson, L.A., Zevenbergen, L.W., Lagasse, P.F., Clopper, P.E. (2012). "Evaluating scour at bridges." *Hydraulic Engineering Circular No. 18*, FHWA-HIF-12-003, 5th Ed. US DOT, Washington, D.C.

Baecher, G.B., Christian J.T. (2003). *Reliability and Statistics in Geotechnical Engineering*. New York, John Wiley & Sons.

Benedict, S.T., Deshpande, N., Aziz N.M., and Conrads, P.A. (2006). "Trends of abutment scour prediction equations applied to 144 field sites in South Carolina." Open-file Rep. 2003-295, *U.S. Geology Survey*, Washington, D.C.

Bolduc, L.C., Gardoni, P., and Briaud, J.-L. (2008). "Probability of Exceedance Estimates for Scour Depth around Bridge Piers." *Journal of Geotechnical and Geoenvironmental Engineering*, Vol. 134, No. 2, February 2008, ASCE, Reston, Virginia, USA. pp. 175-184.

Brandimarte, L., Montanari, A., Briaud, J.-L., D'Odorico, P. (2006). " Stochastic flow analysis for predicting scour of cohesive soils," *Journal of Hydraulic Engineering*, Vol. 132, No. 5, May 2006, ASCE, Reston, Virginia, USA.

Briaud, J.-L. (2013). *Introduction to the Geotechnical Engineering: Unsaturated and Saturated Soils*. John Wiley & Sons, Inc. (under press).

Briaud, J.-L. (2008). "Case histories in soil and rock erosion: Woodrow Wilson Bridge, Brazos River Meander, Normandy Cliffs, and New Orleans Levees." *Journal of Geotechnical and Geoenvironmental Engineering*. 2008 October. 1425-1447.

Briaud J.-L., (2006), "Bridge Scour," *Geotechnical News*, Vol. 24, No.3, September, BiTech Publishers Ltd.

Briaud, J.-L., Brandimarte, L., Wang, J., D'Odorico, P. (2007). "Probability of scour depth exceedance due to hydrologic uncertainty," *Georisk Journal for Assessment and Management of Risk for Engineered Systems and Geohazards*, Vol 1 No.2, March 2007, page 77-88, Taylor and Francis publishers, UK.

Briaud, J.-L., Chen, H.-C., Chang, K.-A., Oh, S.J., Chen, S., Wang, J., Li, Y., Kwak, K., Nartjaho, P., Gudavalli, R., Wei, W., Pergu, S., Cao, Y.W., and Ting, F. (2011a). "The SRICOS-EFA Method." *Summary Report*, Texas A&M University. URL:

https://ceprofs.civil.tamu.edu/briaud/SRICOS-EFA/Summary%20of%20SRICOS-EFA%20Method.pdf

Briaud, J.-L., Chen, H.-C., Li, Y., Nurtjahyo, P., and Wang, J. (2004). "Pier and contraction scour in cohesive soils." *NCHRP Report 516*. Transportation Research Board, Washington, D.C.

Briaud, J.-L., Gardoni, P., Yao, C. (2012). "Keynote Lecture: Bridge Scour Risk." *6th International Conference on Scour and Erosion (ICSE6)*. Paris, August 27-31, 2012.

Briaud, J.-L., Hurlebaus, S., Chang, K.-A., Yao, C., Hrishikesh, S., Yu, O.-Y., Darby, C., Hunt, B., Price, G.R. (2011b). "*Realtime Monitoring of Bridge Scour Using Remote Monitoring Technology*", Research Project: Realtime Monitoring of Scour Events Using Remote Monitoring Technology, Funded by TxDOT and Federal Highway Administration. URL: http://tti.tamu.edu/documents/0-6060-1.pdf (2011).

Briaud, J.-L., Ting, F.C.K., Chen, H.C., Cao, Y, Han, S.W., Kwak, K.W. (2001). "Erosion function apparatus for scour rate predictions." *Journal of Geotechnical and Geoenvironmental Engineering*. ASCE, Vol. 127, No. 2, 2001, pp. 105-113.

Briaud, J.-L., Ting, F.C.K., Chen, H.C., Gudavalli, R., Perugu, S., and Wei, G. (1999). "SRICOS: prediction of scour rate in cohesive soils at bridge piers." *Journal of Geotechnical and Geoenvironmental Engineering*, ASCE, 125(4), pp. 237-246.

Caltrans, (2011). "Construction statistics," compiled by the Division of Engineering Services of California Department of Transportation, USA. URL: http://www.dot.ca.gov/hq/esc/estimates/Construction_Stats_2011.pdf (2011).

CAS. (2012). "Car accident statistic." URL: http://www.car-accidents.com/pages/stats.html(2012).

Chee, R.K.W. (1982). "Live-bed scour at bridge piers." *Report No. 209*, School of Engineering, University of Auckland, Auckland, New Zealand.

Chen, X. (2008). "Numerical study of abutment scour in cohesive soils." Ph.D. Dissertation. Texas A&M University, College Station, TX, USA.

Chiew, Y.M. (1984). "Local scour at bridge piers." *Report No. 355*, School of Engineering, University of Auckland, Auckland, New Zealand.

Elias, V. (1994). Strategies for Managing Unknown Bridge Foundations. *FHWA Report No. FHWA-RD-92-030*. U.S. Department of Transportation, Federal Highway Administration, Research and Development, Turner-Fairbank Highway Research Center. McLean, VA.

Ettema, R., Nakato, T., and Muste, M. (2008). "Estimation of scour depth at bridge abutment." *NCHRP Report No. 24-20*. Transportation Research Board, Washington, D.C.

FERUM (Finite Element Reliability Using Matlab) Version 3.0 (2001). Developed by University of California, Berkeley. URL: http://www.ce.berkeley.edu/projects/ferum/index.html.

Florida Department of Transportation (2010). *Unknown Foundation Bridges Pilot Study*, USA, Federal Highway Administration, URL: http://www.dot.state.fl.us/statemaintenanceoffice/Final%20UF%20Study%20Report%20%282-26-10%29.pdf (2010).

Florida Department of Transportation (2009). *Procedural Manual: Reclassify Unknown Foundation Bridges*, Federal Highway Administration, USA, URL: http://www.dot.state.fl.us/statemaintenanceoffice/Final%20UF%20Procedure%20Manual%20%2811-20-09%29.pdf (2009).

Froehlich, D.C. (1989). "Local Scour at Bridge Abutments." *Proceedings of the 1989 National Conference on Hydraulic Engineering*, New York, 13-18.

Froehlich, D. C. (1988). "Analysis of Onsite Measurement of Scour at Piers." *Proceedings of the 1988 National Conference on Hydraulic Engineering*, Colorado Springs, CO. pp 534-539.

Gardoni, P. (2010). CVEN655 Class notes. 2010.

Gardoni, P., Kiureghian, A.D., and Mosalam, K.M. (2002). "Probabilistic capacity models and fragility estimates for reinforced concrete columns based on experimental observations." *Journal of Engineering Mechanics*. 2002 October. 1024-1038.

Gilbert R.B. (2012). "Risk and reliability- a path forward". Presentation.

Gilbert, R.B., Murff J.D., and Clukey, E.C. (2011). "Risk and reliability on the frontier of offshore geotechnics." *Frontiers in Offshore Geotechnics II*. Taylor & Francis

Group, London. URL: http://www.crcnetbase.com/doi/pdfplus/10.1201/b10132-9 (2011).

Gilbert, R.B., Najjar, S.S., Choi, Y., and Gambino, S.J. (2008) "Practical application of reliability-based design in decision-making." *Reliability-Based Design in Geotechnical Engineering – Computations and Applications*, edited by Phoon, K.K. London and New York, Taylor & Francis Group. 192-223.

Gill, M.A. (1981). "Bed erosion in rectangular long contraction." *Journal of the Hydraulics Division*, Vol. 107, No. 3, pp. 273-284.

Govindasamy, A.V. (2009). "Simplified method for estimating future scour depth at existing bridges." Ph.D. Dissertation, Texas A&M University. College Station, TX, USA.

Gudavalli, S. R. (1997). "Prediction model for scour rate around bridge piers in cohesive soils on the basis of flume tests." Ph. D. Dissertation. Texas A&M University, College Station, TX, USA.

Haldar, A. and Mahadevan, S. (2000). *Probability, Reliability, and Statistical Methods in Engineering Design*. John Wiley & Sons, Inc.

Hueste, M.B., Adil, M.S., Adnan, M., and Keating, P.B. (2006). "Impact of LRFD specifications on design of Texas bridges – Volume 1: Parametric Study." *Research Project: Impact of LRFD Specifications on the Design of Texas Bridges*. URL: http://tti.tamu.edu/documents/0-4751-1-V1.pdf (2011).

Independent Levee Investigation Team (2006). "Erosion test results on New Orleans levee samples." *New Orleans Systems*. URL: www.ce.berkeley.edu/~new_orleans/report/I.pdf (2011).

Johnson, P. (1992). "Reliability-based pier scour engineering." *Journal of Hydraulic Engineering*. 1344-1358.

Johnson, P. and Dock, D. (1998). "Probabilistic bridge scour estimates." *Journal of Hydraulic Engineering*. 750-754.

King, E., Smith, J.(1988). *Economic Loss and Compensation in Aviation Accidents*. Published by the RAND Corporation, Santa Monica, CA.

Komura, S. (1966). "Equilibrium depth of scour in long constrictions." *Journal of the Hydraulics Division*, Vol. 92, No. 5, 17–37.

Kulicki, J.M. (2012). "Developing a probability based limit states bridge specification-U.S. experience." URL: http://www.google.com/url?sa=t&rct=j&q=&esrc=s&source=web&cd=1&cad=rja&ved=0CDMQFjAA&url=http%3A%2F%2Fwww.modjeski.com%2Ffile.ashx%3Fid%3Dd536e4bd-843d-4de5-a801-6e23bcf06c38&ei=GNU4Uc3cJeas2wXx34DgBw&usg=AFQjCNEy3Ao2HzaiI_M8O5KVDhtlE3-URA&bvm=bv.43287494,d.b2I (2012).

Kwak, K. (2000). "Prediction of scour depth versus time for bridge piers in cohesive soils in the case of multi-flood and soil systems." Ph.D. Dissertation. Texas A&M University, College Station, TX, USA.

Landers, M.N. and Mueller, D.S. (1996). “Channel Scour at Bridges in the United States.” *Federal Highway Administration Report FHWA-RD-95-184*, Washington, DC.

Li, Y. (2002). "Bridge pier scour and contraction scour in cohesive soils on the basis of flume tests," Ph.D. Dissertation. Texas A&M University, College Station, TX, USA.

Montana Department of Transportation (2008). “MDT Geotechnical Manual - bridge design.” URL: http://www.mdt.mt.gov/other/materials/external/geotech_manual/chapter16.pdf

Moses, F., and Verma, D. (1987). *NCHRP Report 301*: “Load capacity evaluation of existing bridges.” Transportation Research Board, Washington, D.C.

National Highway Traffic Safety Administration (NHTSA). (2012). “Fatal car accident statistics.” URL: http://www.car-accidents.com/pages/fatal-accident-statistics.html (2012).

National Transportation Safety Board. (2011). Review of U.S. Civil Aviation Accidents, 2007-2009. *Annual Review NTSB/ARA-11/01*. Washington, DC. URL: http://www.ntsb.gov/doclib/reports/2011/ARA1101.pdf (2011).

National Transportation Safety Board (2006). *National Annual Review of Aircraft Accident Data*. Washington, D.C. URL: http://libraryonline.erau.edu/online-full-text/ntsb/aircraft-accident-data/ARC10-01.pdf (2011).

National Transportation Safety Board. (1987). “Highway accident reports – collapse of New York Thruway (I-90) Bridge over the Schoharie Creek, near Amsterdam, New York, April 5, 1987.” Washington, D.C. 20594.

Nowak, A. (1995). "Calibration of LRFD bridge code." *Journal of Structural Engineering*, Vol. 121, No. 8, August, 1995. pp. 1245-1251.

Nowak, A. (1999). "Calibration of LRFD bridge design code." *NCHRP Report 368*, Transportation Research Board, Washington, D.C.

Oh, S.J. (2009). "Experimental study of bridge scour in cohesive soil." Ph.D. Dissertation, Texas A&M University. College Station, TX, USA.

Orr, T.L.L and Breysse, D. (2008). "Eurocode 7 and reliability-based design." *Reliability-Based Design in Geotechnical Engineering – Computations and Applications*, edited by Phoon, K.K. London and New York, Taylor & Francis Group. 298-343.

Paikowsky, S.G. (2004). "Load and resistance factor design (LRFD) for deep foundations." *NCHRP Report 507*, Transportation Research Board, Washington, D.C.

Pearson, D., Stein, S., and Jones, J.S. (2002). *HYRISK Methodology and User Guide*. Federal Highway Administration.

Resource Consultants, Inc. and Colorado State University (1987). *Hydraulic, Erosion, and Channel Stability Analysis of the Schoharie Creek Bridge Failure, New York.* Fort Collins, Colorado. December, 1987.

Richardson, E.V. and Davis, S.R. (2001). "Evaluating scour at bridges." *Hydraulic Engineering Circular No. 18, FHWA NHI 01-001*, 4th Ed. US DOT, Washington, D.C.

Ropeik, D. (2006). “How risky is flying?” URL: http://www.pbs.org/wgbh/nova/space/how-risky-is-flying.html (2006).

Scuffham, P., Chalmers, D., O'Hare, D., and Wilson, E. (2012). “Direct and indirect cost of general aviation crashes.” York Health Economics Consortium, University of York, Heslington, England. URL: http://www.ncbi.nlm.nih.gov/pubmed/12234034(2012).

Shields, A. (1936). “Application of similarity principles and turbulence research to bed-load movement.” *Hydrodynamics Laboratory Publ. No. 167*, W.P.Ott, and J.C. van Uchelen, translation, United States Department of Agriculture, Soil Conservation Service, Cooperative Laboratory, California Institute of Technology, Pasadena, Calif.

Stein, S. and Sedmera, K. (2006). “Risk-based management guidelines for scour at bridges with unknown foundations.” *NCHRP Web Only Document 107*, Contractor’s Final Report for NCHRP Project 24-25. National Cooperative Highway Research Program, Transportation Research Board of the National Academies. URL: http://onlinepubs.trb.org/onlinepubs/nchrp/nchrp_w107.pdf(2011).

Sturm, T.W. (2004). “Enhanced abutment scour studies for compound channels.” *Report No. FHWA-RD-99-156*, Georgia Institute of Technology, School of Civil and Environmental Engineering, Atlanta, GA.

Sullivan M. (2005a). “NYDOT national bridge failure database.” compiled by the Structures Division of the New York State Department of Transportation, USA.

Sullivan M. (2005b). “FHWA item 113 and plans of action for scour critical bridges.” Presentation.

The Heart Foundation. (2012). “Heart Disease Facts.” URL: http://www.theheartfoundation.org/heart-disease-facts/heart-disease-statistics/ (2012)

Vanoni, V.A., ed. (1975). “Sedimentation engineering.” *ASCE-manuals and reports on engineering practice-No. 54*, ASCE, New York.

White, C.M. (1940). “The equilibrium of grains on the bed of a stream.” *Proceedings of the Royal Society of London*, London, Series A, No. 958, Vol. 174, pp.322-338.

Wiss, Janney, Elstner Associates, Inc. and Mueser Rutledge Consulting Engineers. (1987). “Collapse of the Thruway Bridge at Schoharie Creek for New York State Thruway Authority.” November 1987.

World Bank. (2010). “Life expectancy.” URL: http://www.google.com/publicdata/explore?ds=d5bncppjof8f9_&met_y=sp_dyn_le00_in&idim=country:USA&dl=en&hl=en&q=life+expectancy (2010).

Yao, C., Gardoni, P., Briaud, J.-L. (2011). “Probability-based pier scour depth predictions: a database study” Texas Section ASCE Spring 2011 Meeting. College Station, Texas. April 27-30, 2011.

Zhang, L. (2008). “Reliability verification using pile load tests.” *Reliability-Based Design in Geotechnical Engineering – Computations and Applications*, edited by Phoon, K.K. London and New York, Taylor & Francis Group. 385-412.